Analysis of HIV-1 Assembly on Intracellular Plasma Membrane-connected Compartments of Primary Human Macrophages

David Onalenna Nkwe

PhD Supervisor: Prof. Mark Marsh

A thesis submitted for the degree of
Doctor of Philosophy (Molecular Cell Biology)
University College London

November 2014

Declaration

I, David Onalenna Nkwe, confirm that the work presented in this thesis is my own. Where information has been derived from other sources, I confirm that this has been indicated in the thesis.

_____

David O. Nkwe

Statement of collaboration

For electron microscopy (EM), I collaborated with Dr Annegret Pelchen-Matthews (Senior Investigator Scientist in Prof Mark Marsh's research group, Laboratory for Molecular Cell Biology [LMCB], University College London [UCL]) and Dr Jemima Burden (Head of the EM Unit, LMCB, UCL). I transfected or infected all cells used for EM. In Chapter 4, Annegret and Jemima imaged the cell profiles in Figures 4.2 and 4.3, respectively. In Chapter 5, correlative and light and electron microscopy was set up by Annegret with the data shown in Figure 5.12. We carried out all other EM work together, and I was involved in all the steps apart from the cryosectioning. I performed all of the data analysis for the EM work presented in this thesis.

Abstract

In primary human monocyte-derived macrophages (MDM), HIV assembles on complex intracellular plasma membrane-connected compartments (IPMCs). Currently, it is unclear whether, in addition to assembly at IPMCs, HIV uses the cell surface of MDM, as viruses that bud at the cell surface may dissociate and be lost from the samples. As the endosomal sorting complex required for transport (ESCRT) machinery is required for the final scission events that release assembled virus from the plasma membrane, this question was addressed by depleting the ESCRT components Tsg101 and ALIX, or generating mutant HIV-1 strains defective in recruiting the ESCRT machinery, to arrest HIV budding and visualise all budding events.

Using siRNA, ALIX and Tsg101 were depleted efficiently in MDM. Although the effects on virus release were minimal, Tsg101 had a greater effect than ALIX for HIV release in MDM. In the second approach, I generated mutants (HIV-1 PTAP^{-}, YP^{-}, PTAP^{-}YP^{-}, Δp6) defective in recruiting the ESCRT machinery, by mutating the sequences that bind Tsg101 and ALIX. The mutants were characterised on HEK 293T cells, and the release of PTAP^{-}, PTAP^{-}YP^{-} and Δp6 was inhibited. Analysis by electron microscopy (EM) showed that the mutants indeed produced arrested viruses. As the mutants are defective in release, I developed a method to rescue HIV-1 PTAP^{-} and PTAP^{-}YP^{-} viruses for infecting MDM. The cells were infected with the rescued mutants, and analysed using immunofluorescence and EM. By confocal microscopy, 77% of the cells had viruses in the IPMCs. Using EM, immature viruses were found predominantly (97%) in the IPMCs. Estimates of membrane area revealed enrichment of HIV in the IPMCs.

This study provides the first conclusive evidence that HIV is targeted to IPMCs in MDM. This may shield the virus from immune surveillance during virus assembly, with potential impact on cell-to-cell transmission and disease progression.

Acknowledgements

I am greatly indebted to Mark Marsh for affording me the opportunity to do a PhD under his mentorship. I am thankful for his critical scientific guidance in my pursuit of good science.

My deepest and sincere gratitude goes to Annegret Pelchen-Matthews who has been constantly supportive throughout my studies. I also thank her and Scott Lawrence for critically reading my thesis. I am grateful to Steffy Cziezo and her predecessor Jane Turner, who excellently prepared the macrophages used in this thesis, weekly. For the work on electron microscopy (EM), I am thankful to Jemima Burden and Annegret for training me, and contributing some of the EM images shown in this thesis. I also thank Janos Kriston-Vizi and Ricardo Henriques, Group Leaders at the LMCB, for teaching me how to use ImageJ for quantitating fluorescence data.

I would like also to thank past and present members of the Marsh group (in addition to Annegret, Scott, Jane and Steffy) who also played pivotal roles in many respects, to create the research environment where I could realise my potential and develop as a young scientist, and these are Petra Mlcochova, Joe Grove, Lucie Goueslain, Komla Sobo, Sebastian Giese, Stuart Weston, Michela Mazzon and Sara Hammoudi. I also thank my office mates and the rest of the LMCB community for the friendly and inclusive atmosphere. The LMCB cocktails were the best unwinding events.

My thesis committee, Stephen Nurrish, Ari Fassati and Adrian Isaacs, also deserve a word of gratitude for their support and guidance. They were a wonderful trio!

Above all, I would like to thank the Government of Botswana and the Botswana International University of Science and Technology for the PhD fellowship, which allowed me to advance academically. In addition, I thank the MRC-LMCB for the excellent laboratory support.

Finally, I wish to thank my family and friends who have been very supportive in many ways to ensure that I achieve my dreams!

The end of a matter is better than its beginning...

Ecclesiastes 7:8, The Holy Bible, New International Version

Table of Contents

List of figures

List of tables

Abbreviations

A-(488,568, 594, 647)	alexa-(488,568, 594, 647)
2D	two-dimensional
3D	three-dimensional
AAA ATPase	ATPases Associated with diverse cellular Activities ATPase
ADP	adenosine diphosphate
AIDS	acquired immunodeficiency syndrome
ALIX	apoptosis linked gene-2 (ALG-2)-interacting protein X
AP-(1, 2, 3)	adaptor protein complex (1, 2, 3)
APC	allophycocyanin
ART	anti-retroviral therapy
ATP	adenosine triphosphate
ATPase	adenosine triphosphatase
bp	base pair
C1-5	constant domains 1 to 5
CA	capsid
CCR5	C-C chemokine receptor 5
CD (e.g. CD4, CD184)	cluster of differentiation
cDNA	complementary DNA
CEP55	centrosome protein 55
CHMP	charged MVB proteins
CLEM	correlative light and electron microscopy
CNS	central nervous system
CRFs	circulating recombinant forms
CT	cytoplasmic tail
CXCR4	C-X-C chemokine receptor type 4
DC-SIGN	dendritic cell-specific intercellular adhesion molecule-3-grabbing non-integrin
DCs	dendritic cells
DMEM	Dulbecco's Modified Eagle's Medium
DMSO	dimethylsulfoxide
DNA	Deoxyribonucleic Acid
dNTPs	deoxynucleoside triphosphates
EDTA	ethylenediaminetetraacetic acid
EEA-1	early endosome antigen 1
EM	electron microscopy
Env	envelope
ER	endoplasmic reticulum
ESCRT	endosomal sorting complex required for transport
FACS	fluorescence-activated cell sorting
FBS	foetal bovine serum
FcR	Fc receptor
FFU	focus forming units
FITC	fluorescein isothiocyanate
FSGS	focal segmental glomerulosclerosis
Gag	group-specific antigen

GALT	gut-associated lymphoid tissue
GFP	green flourescence protein
gp(41/120/160)	glycoprotein (41/120/160)
GTPase	guanosine triphosphatase
HA	haemagglutinin
HAART	highly active retroviral therapy
HAND	HIV-1 associated neurological disorders
HBR	highly basic region
HEK 293T cells	human embryonic kidney 293T cells
HIV	human immunodeficiency virus
HRP	horseradish peroxidase
Hrs	hepatocyte growth factor receptor substrate
HS	human serum
ICAM-1	intracellular adhesion molecule 1
IF	immunofluorescence
IL-2	interleukin-2
IN	integrase
IPMCs	intracellular plasma membrane-connected compartments
KD	knockdown
kDa	kilo Dalton
L domain	late domain
LAMP-1	lysosomal-associated membrane protein 1
LB agar or broth	Luria-Bertani agar or broth
LFA-1	lymphocyte function associated antigen 1
LIP5	lysosomal trafficking regulator interacting protein-5
LTR	long terminal repeat
M-CSF	macrophage-colony stimulating factor
MA	matrix
mCh	monomeric cherry
MDM	monocyte-derived macrophages
MHC (I/II)	major histocompatibility complex (class I/II)
MIP	macrophage inflammatory proteins
mRNA	messenger RNA
MVB	multivesicular bodies
Mvb12	multivesicular body protein 12
myrMA	myristoylated MA
NACA	national AIDS coodinating agency
NC	nucleocapsid
Nef	negative factor
P-TEFb	positive transcription elongation factor b
PAG	protein A-gold
PBMCs	peripheral blood mononuclear cells
PBS	phosphate buffered saline
PCR	polymerase chain reaction
PE	phycoerythrin
PerCP	peridinin chlorophyll protein

$PI(4,5)P_2$	phosphatidylinositol-4,5-bisphosphate
PM	plasma membrane
Pol	polymerase
PR	protease
PVDF	polyvinylidene diflouride membrane
RANTES	regulated-on-activation, normal T cell expressed and secreted
RER	rough endoplasmic reticulum
Rev	regulator of expression of virion proteins
RLU	relative light units
RNA	ribonucleic acid
RNAi	RNA interference
RPMI 1640	Roswell Park Memorial Institute 1640 medium
RR	ruthenium red
RRE	Rev response element
RT	reverse transcriptase
RTC	reverse transcription complex
SAMHD1	sterile alpha motif and HD domain-containing protein-1
SDS-PAGE	sodium dodecyl sulphate polyacrylamide gels electrophoresis
siRNA	small interfering RNA
SIV	simian immunodeficiency viruses
SOC	Super Optimal broth with Catabolite repression
SP	spacer peptide
SU	surface unit
TAR	trans-activation response
Tat	trans-activator
TM	transmembrane
tRNA	transfer RNA
Tsg10l	tumour susceptibility gene 101
UBAP1	ubiquitin-associated protein 1
UEV	ubiquitin-E2-like variant
UNAIDS	United Nations AIDS
URF	unique recombinant forms
UTR	untranslated region
V1-5	variable domains 1-5
V3	variable loop 3
VDAC-1	voltage-dependent anion-selective channel protein 1
Vif	Viral infectivity factor
VLPs	virus-like particles
Vpr	Viral Protein R
Vps/VPS	vacuolar protein sorting
Vpu	Virus protein U
VS	virologic synapse
WHO	World Health Organisation
WT	wild-type

1. General Introduction

The Human Immunodeficiency Virus (HIV) is the causative agent of acquired immunodeficiency syndrome (AIDS), and T cells and macrophages are the main target cells for HIV infection *in vivo*. Although both cell types are infected *in vivo*, infection manifests significant differences in each cell type, and the relative contribution of each to pathogenesis remains unclear. One of the main differences is that macrophages can live for weeks, if not months, following infection (Watters et al., 2013). By contrast, productively infected T cells usually die within 48 hrs (Perelson et al., 1996). This had given rise to the view that macrophages may serve as viral reservoirs, a property that may be linked to the observation that HIV assembles on intracellular membranes in macrophages, but at the cell surface in T cells. The idea of HIV assembling in intracellular structures in macrophages has been evolving for more than two decades. Initially, the structures were thought to be part of the Golgi apparatus (Orenstein et al., 1988), and later considered to be late endosomes (Raposo et al., 2002; Pelchen-Matthews et al., 2003). The current view is that these structures are internally sequestered plasma membrane (PM) compartments that maintain contact with the cell surface (Deneka et al., 2007; Welsch et al., 2007; Bennett et al., 2009; Welsch et al., 2011; Koppensteiner et al., 2012b; Pelchen-Matthews et al., 2012). However, it remains unclear whether HIV also buds at the cell surface, as any viruses budding at the cell surface would dissociate from cells and be lost from samples. To address this question, I established a system to arrest virus assembly during the budding process so that all budding events could be visualised. I then carried out detailed light and electron microscopy analyses to determine where HIV assembly occurs in infected macrophages.

This chapter gives an overview of HIV/AIDS, currently one of the major global health issues, especially in developing countries, and particularly in Africa. The biology of HIV is reviewed in the context of its structure and the replication cycle. I have described in detail the cell machinery that HIV exploits to dissociate from host cells, the endosomal sorting complex required for transport (ESCRT), as this was the main tool used in this thesis to study HIV assembly in macrophages. An overview of the main target cells for HIV is given, with a detailed description of the compartments where

HIV assembles in macrophages. Finally, I describe the general pathogenesis of HIV in infected individuals.

1.1 HIV epidemiology

Globally, the number of people living with HIV was about 35.3 million in 2012, with an estimated 2.3 million new infections, showing a 33% decline in incidence from 2001 (UNAIDS, November 2013). Sub-Saharan Africa is the epicentre of the HIV pandemic (Figure 1.1) (UNAIDS, 2014). In 2009, the region accounted for 68% of new infections, and 72% (1.3 million) of mortality from AIDS (UNAIDS, December 2010). Although southern Africa has only 2% of the world's population, the sub-region has one-third of the global HIV infections (Novitsky and Essex, 2012), which has significantly lowered the life expectancy in the sub-region. Some countries in southern Africa have recorded very high HIV prevalence amongst pregnant women. For instance, in my home country Botswana, HIV prevalence amongst pregnant women was hovering around 33% between 2005 and 2009 (NACA, 2010).

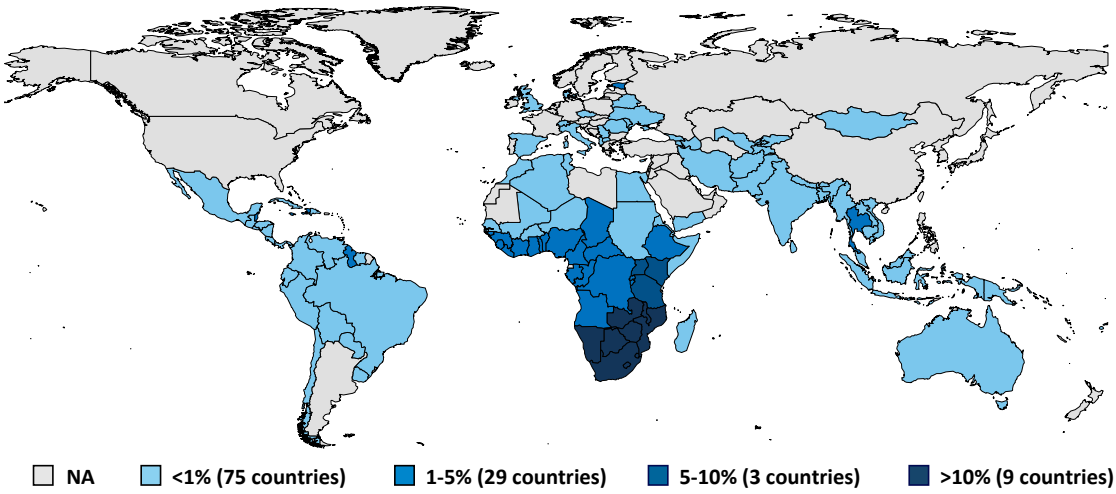

Figure 1.1: Global adult HIV prevalence in 2013.
Taken from Kaiser Family Foundation, based on UNAIDS, The Gap Report, 2014.

Unprotected heterosexual transmission is responsible for the majority of HIV cases, especially in sub-Saharan Africa. In Europe and America, the main route of transmission is unprotected homosexual sex between men, and needle sharing between intravenous drug users. In the absence of anti-retroviral therapy (ART), vertical transmission can also occur from infected mother to the unborn child, and during

delivery or breast-feeding. High viral load in body fluids, as well as sexually transmitted diseases, increase the risk of HIV transmission (Maartens et al., 2014).

1.2 The origin and phylogenetic classification of HIV

HIV is a retrovirus that belongs to the *Lentivirus* genus. Its genome is composed of two copies of single-stranded RNA. During replication, a retroviral genome is reverse transcribed by the viral enzyme, reverse transcriptase (RT), to a double-stranded DNA, hence the family name *Retroviridae*. Currently, there are two types of HIVs: HIV-1 and HIV-2. These exhibit distinct biologic and epidemiologic attributes. HIV-1 has worldwide distributions whilst HIV-2 is mainly confined to West Africa (Gilbert et al., 2003). The two types are believed to have entered the human host independently from different primate sources (Figure 1.2). Phylogenetic analysis has shown that HIV-1 is closely related to simian immunodeficiency viruses (SIVs) from chimpanzee (SIVcpz) and gorilla (SIVgor), whilst HIV-2 is related to SIV from sooty mangabeys (SIVsm) (Heeney et al., 2006; Hemelaar et al., 2011; Tebit and Arts, 2011; Peeters et al., 2014).

Four classes of HIV-1 are recognised, namely M (major), O (outlying), N (new) and P, indicative of viruses having crossed into humans independently at least four times (Figure 1.2) (Renjifo and Essex, 2002; Ndung'u and Weiss, 2012; Peeters et al., 2014). HIV-2 on the other hand, crossed into humans at least nine times (Peeters et al., 2014). The HIV-1 M class is further sub-classified into nine major clades or subtypes: A-D, F-H, J and K; plus viruses derived from the recombination of different clades, to generate what are known as circulating recombinant forms (CRFs) such as AE and AG, as well as the unique recombinant forms (URFs). A URF is found in only one individual, and becomes a CRF when it is transmitted to numerous people. CRFs are continually increasing as HIVs recombine and diversify. As of 2013, 58 CRFs and several URFs had been reported worldwide and they are responsible for 20% of all HIV infections globally (Lau and Wong, 2013). More than 90% of HIV-1 infections in the world are attributed to class M, with HIV-1C being the most predominant subtype, accounting for 50% or more of all infections, particularly in Southern Africa, South America and India (Hemelaar et al., 2011; Lau and Wong, 2013). Classification of subtypes is based to a large extent on the 20-50% difference between envelope (*env*) nucleotide sequences (Wainberg, 2004). The high degree of HIV-1 diversity is partially linked to the lack of a

proofreading mechanism by the RT of the virus, which contributes to viral evolution. However, nucleotide sequences that code for inflexible core proteins, such as Gag, are relatively stable (Wainberg, 2004; Novitsky et al., 2010b).

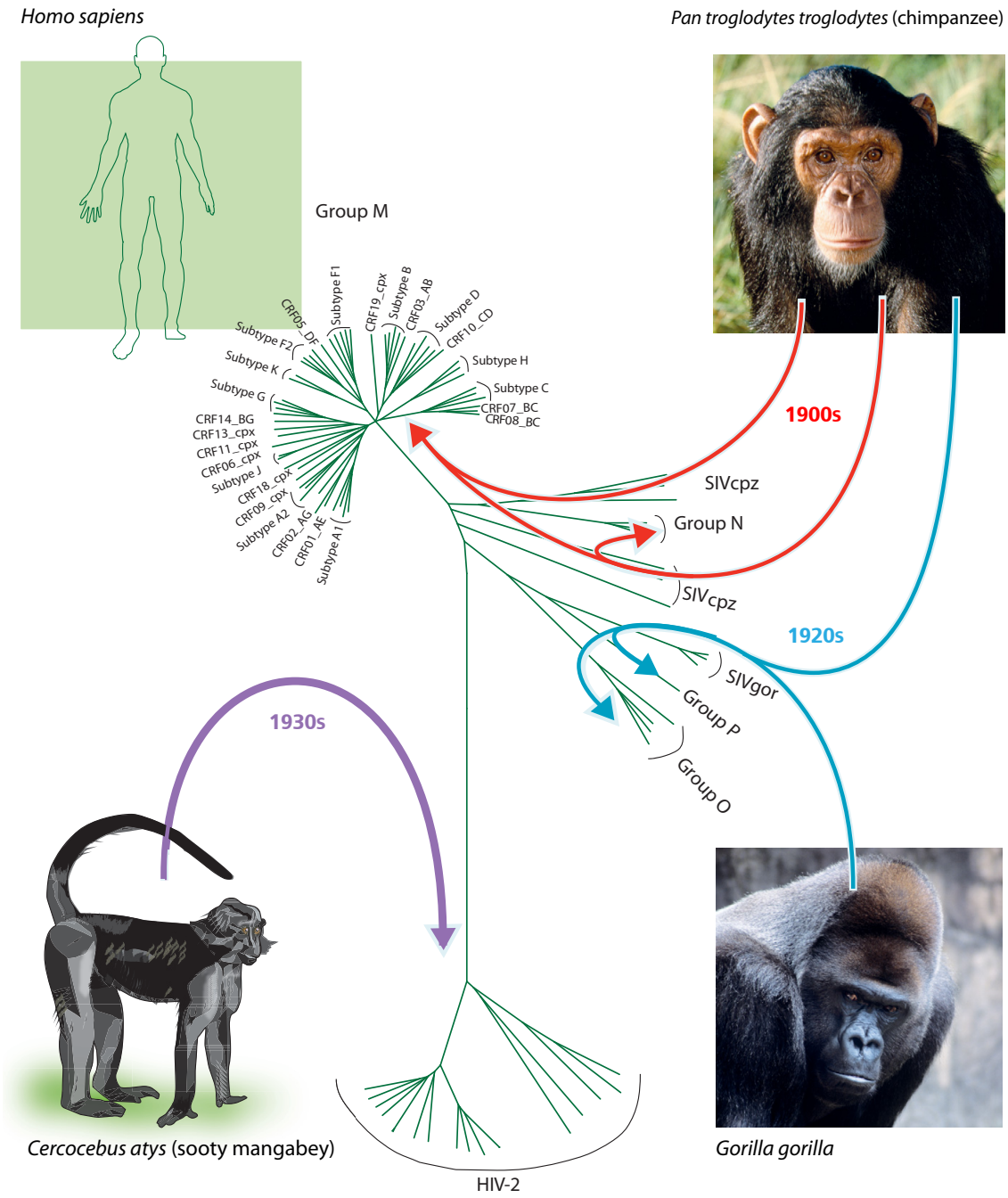

Figure 1.2: Phylogenetic relationships of SIVs to HIVs.

SIVs (SIVcpz, SIVgor, and SIVsm) crossed species from chimpanzees (cpz), gorillas (gor) and sooty mangabeys (sm) into the human population. Adapted from Tebit and Arts (2011).

1.3 HIV-1 structure

HIV-1 is a double stranded RNA enveloped virus, with a genome composed of nine genes: *gag, pol* and *env* – for the structural proteins and essential enzymes; *tat* and *rev* – for the regulatory proteins; *vif*, *vpr*, *vpu* and *nef* – for the auxiliary proteins (Figure 1.3A) (Watts et al., 2009). In total, the nine genes encode 15 viral proteins.

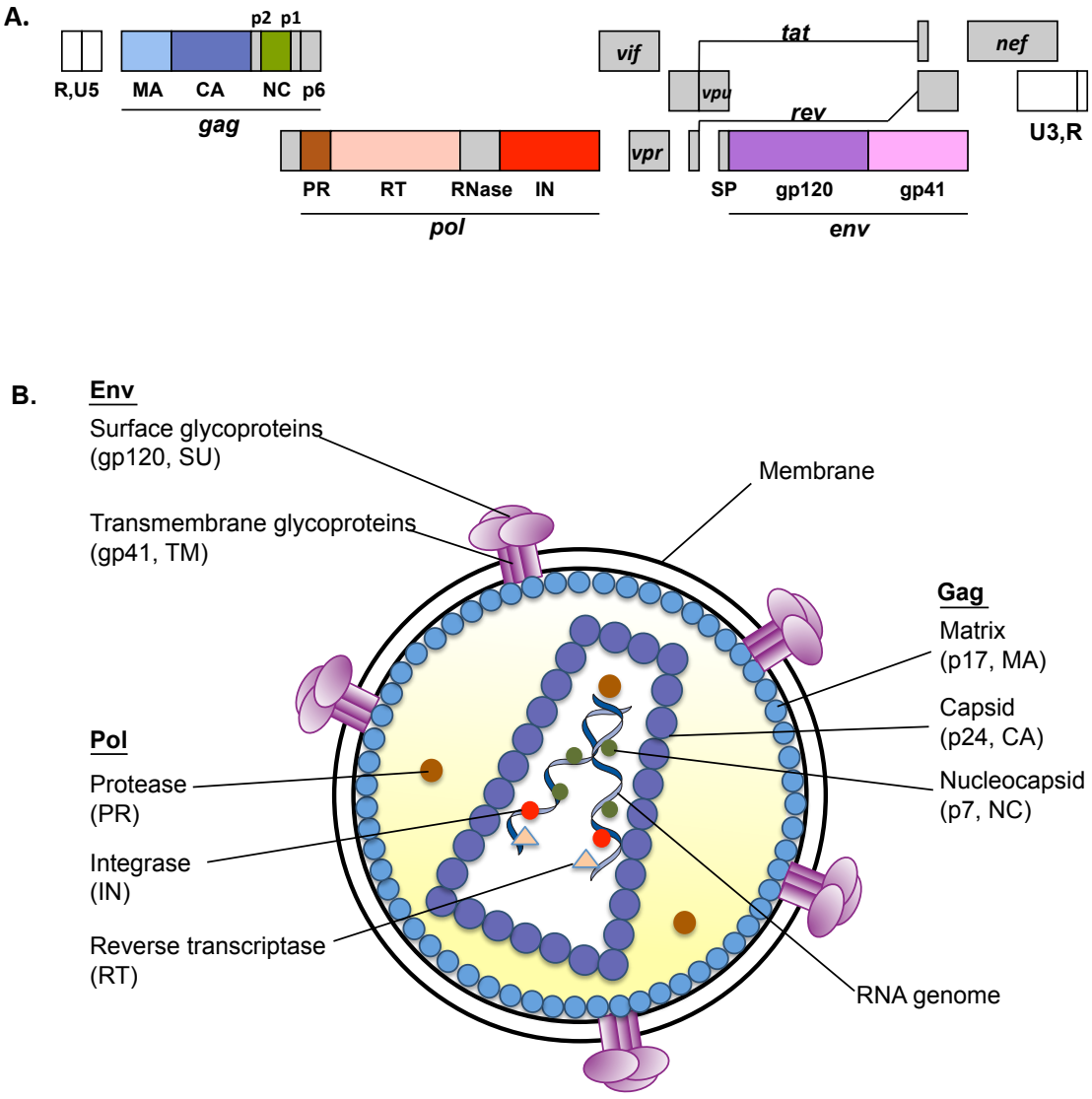

Figure 1.3: Organisation of the HIV-1 genome and mature particle.

(A) Organisation of the HIV-1 genome. Protein coding regions are shown in different colours. CA, capsid; IN, integrase; MA, matrix; NC, nucleocapsid, PR, protease; RT, reverse transcriptase; SP, signal peptide. **(B)** The schematic representation of the mature HIV-1 particle. The location of the viral proteins and genome are indicated.

A mature HIV-1 particle is about 130 nm in diameter (Briggs et al., 2004), and contains two copies of the viral RNA (~10,000 nucleotides in length) encapsulated in a conical capsid (p24) (Figure 1.3B). The virus has a lipid outer membrane derived from the host cell during virus assembly and budding. The inner leaflet of the lipid membrane is lined with the matrix protein (p17). The viral envelope glycoproteins are anchored into the lipid membrane of the virus. These glycoproteins are made up of a receptor binding subunit (gp120) that initiates viral entry into target cells, and a trans-membrane subunit (gp41) responsible for mediating fusion of the viral envelope with the host cell membrane.

1.4 HIV-1 replication cycle

Briefly (details are in later sections), HIV enters a cell through initial interactions between viral surface glycoproteins and cellular receptors, and subsequent fusion of the viral membrane with the host cell plasma membrane (PM). The viral core is then released into the host cytoplasm, where the viral genome undergoes reverse transcription and is eventually integrated into the host genome as a provirus. The integrated viral genome is transcribed upon transcription of the host genome. The mRNAs and genomic RNA are transported to the cytoplasm where mRNAs are translated into viral proteins. The virus assembles on the PM and becomes enwrapped in the membrane. The resulting "lollipop"-like structures dissociate from the plasma membrane to release new virions and complete the replication cycle. The HIV replication cycle can be interrupted at different stages using anti-retroviral drugs. The current classes of ART approved by the United States of America Food and Drug Administration include 25 drugs that target virus entry, membrane fusion, reverse transcription, integration, and maturation (Figure 1.4) (Maartens et al., 2014). Although these drugs cover many facets of the virus life, there remain stages that offer opportunities as new targets for development of novel therapeutic interventions.

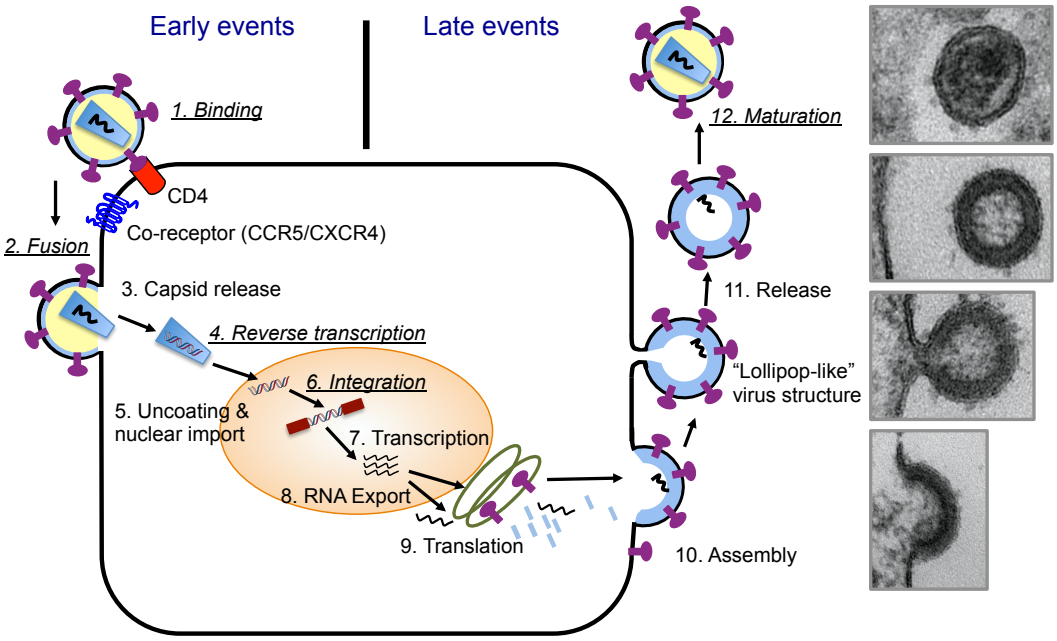

Figure 1.4: Schematic representation of the HIV-1 replication cycle.
HIV binds to receptor (CD4) and co-receptor (CCR5 or CXCR4) molecules on the plasma membrane. The virus and plasma membranes fuse, releasing the virus core into the host cell, where it is reverse transcribed and the DNA is imported into the nucleus for integration into the host genome (brown boxes). Viral transcripts are produced from the integrated genome and exported out of the nucleus, to be translated on the endoplasmic reticulum or free ribosomes. Viral proteins (Gag in blue; Env in purple) and RNA are assembled at the plasma membrane. Finally, the Gag recruits host proteins (shown later in Figure 1.9) to facilitate the dissociation of virus particles from the host cell. EM images (J. Burden, LMCB) on the left depict different stages of virus assembly and maturation. The replication cycle stages that can currently be inhibited by approved anti-retroviral drugs are in italics and underlined.

1.4.1 Virus entry

Viruses are obligate intracellular parasites that completely depend on host cells for their reproduction. HIV-1 typically has about 14 Env spikes on its surface (Cosson, 1996). It is believed that HIV-1 redistributes Env into clusters during maturation, to compensate for the low Env content, which ultimately increases virus entry efficiency (Chojnacki et al., 2012). Virions with truncated Env C-terminal tail (CT) domain do not display Env clustering on mature virions, thereby reducing virus fusion and infectivity. HIV entry into target cells is partially mediated by hijacking cluster of differentiation 4 (CD4) molecules, co-receptors with the T cell receptor for recognising peptides bound to major histocompatibility complex class II (MHC-II) molecules on antigen presenting cells.

The virus attaches to CD4 on host cells through its Env subunit, gp120 (Figure 1.5). Structurally, gp120 is made up of five variable domains (V1-5) interspersed with five constant domains (C1-5) (Checkley et al., 2011). Three of the conserved domains (C1, C3 and C4) are the main determinants of binding to CD4. CD4 binding causes conformational changes in Env that favour exposure of a co-receptor binding surface, at the base of the V3 loop of gp120.

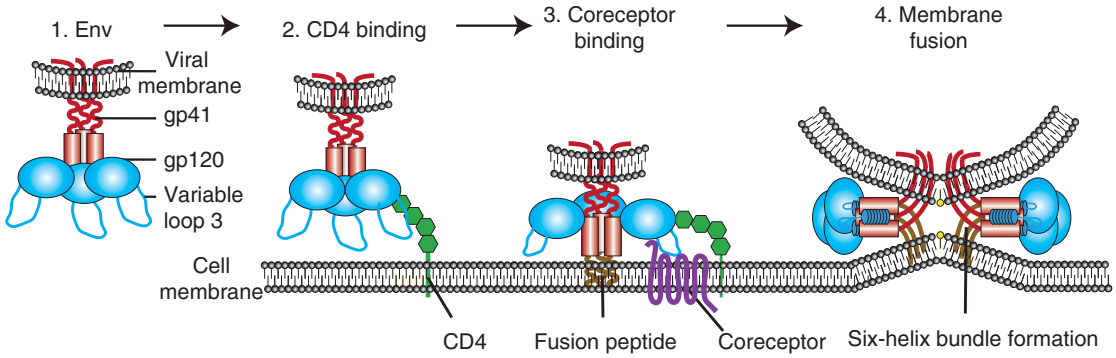

Figure 1.5: Schematic representation of HIV binding and fusion.
During HIV entry, the viral Env binds CD4 molecules on the plasma membrane of target cells. Conformational changes in Env result in the engagement of the co-receptor, insertion of the fusion peptide and ultimately membrane fusion. Taken from Wilen et al. (2012).

HIV-1 uses two chemokine receptors on the cell surface, as coreceptors: CCR5 (CD195) and/or CXCR4 (CD184) depending on the virus strain. CCR5 and CXCR4 are seven-transmembrane G-protein coupled receptors involved in cell signalling (Alkhatib, 2009). The natural ligand for CXCR4 is stromal-derived-factor-1 (Ghanem et al., 2014), whilst natural ligands for CCR5 include macrophage inflammatory proteins (MIP)-1α, MIP-1β, and RANTES (for Regulated-on-Activation, Normal T cell Expressed and Secreted) (Alkhatib et al., 1996). HIV strains are generally divided according to their co-receptor usage: X4 viruses use CXCR4, R5 viruses use CCR5, and R5X4 use both co-receptors (Wilen et al., 2012). An increase in the net positive charge of the V3 loop, favouring binding to the negatively charged CXCR4 surface, results in virus tropism change from R5 to X4 (Checkley et al., 2011). R5 viruses dominate early during infection, but a change to X4 viruses may occur late in the course of infection, in about 50% of infected individuals (Regoes and Bonhoeffer, 2005). A switch from R5 tropism is very rare in HIV-1C infections compared to HIV-1B (Ndung'u et al., 2006; Lin et al., 2011). The reasons for co-receptor switch are not entirely understood.

When gp120 is bound to the co-receptor, further conformational changes in gp41 release the fusion peptide, allowing it to insert into the cell membrane, and forming a pre-hairpin structure. gp120 and gp41 then dissociate, and the pre-hairpin structure is transformed into a six-helix bundle, thereby promoting fusion of the viral and cell membranes and subsequent release of the viral core into the cytoplasm (Gallo et al., 2003; Melikyan, 2008; Wilen et al., 2012).

1.4.2 Transcription and nuclear export

It is still debatable when uncoating of viral genome occurs; and uncoating, or at least partially, may be required for the formation of reverse transcription complex (RTC) (Arhel, 2010; Fassati, 2012; Ambrose and Aiken, 2014). The composition of this complex is not entirely clear, but in addition to viral components (Vpr, p24, IN, RT), the RTC contains host proteins believed to stabilise the complex (Konig et al., 2008; Fassati, 2012; Gaudin et al., 2013b). During reverse transcription, single-stranded positive sense RNA is converted to double-stranded DNA. Reverse transcription is primed by lysyl tRNA. The RTC contains RNA or RNA-DNA intermediates of reverse transcription. Subsequently, the RTC is converted to pre-integration complex that no longer contains the viral RNA, but provirus. The pre-integration complex is translocated to the nucleus where the provirus is integrated into the host DNA using the virus-encoded enzyme, IN (Arhel, 2010).

The productive phase of the HIV replication cycle, described as “late events” in Figure 1.4, begins with the transcription of the integrated viral DNA. Transcription of the provirus is initiated at the 5’LTR by cellular RNA polymerase II, and is activated by HIV-1 Tat that binds to the bulge of TAR RNA, and recruits positive transcription elongation factor b (P-TEFb) [composed of cyclin T1 and cyclin- dependent kinase 9 (Bres et al., 2008)], as well as other transcription factors (Karn and Stoltzfus, 2012). The generated transcripts fall into three major classes: 1) unspliced mRNAs for the Gag and GagPol polyproteins; 2) partially spliced mRNAs which are translated into the Env, Vif, Vpu and Vpr proteins; 3) multiply spliced mRNAs encoding the Rev, Tat and Nef proteins. Before transport to the cytoplasm, intron-containing viral mRNAs are first bound to Rev. Rev binds to a *cis*-acting RNA element, the Rev response element (RRE), which is found in the *env* gene of all unspliced and partially spliced HIV-1

RNAs (Freed, 2001; Freed, 2002). Then mRNA-bound Rev complexes with cellular chromatin maintenance-1 nuclear export receptor to form the viral ribonucleoprotein transport complex. The complex is then transported to the cytoplasm for translation into proteins.

1.4.3 Translation

Translation takes place on the endoplasmic reticulum and on free ribosomes in the cytosol, leading to the synthesis of the viral accessory proteins, as well as the structural and enzyme polyprotein precursors. The Gag polyprotein precursor is synthesized on free ribosomes in the cytosol. The 3' end of *gag* overlaps with the 5' end of *pol*. During translation, a -1 frameshift signalled by UUUUUUA slippery sequence or ribosomal frameshift stimulatory signal, results in the production of a fused GagPol protein, and ultimately a Gag:GagPol ratio of 20:1 (Jacks et al., 1988; Pettit et al., 2005; Bell and Lever, 2013). The viral enzymes (protease, integrase and reverse transcriptase) are produced from the Pol polyprotein.

Env is synthesised on the rough endoplasmic reticulum (RER) as a polyprotein precursor, gp160 (Checkley et al., 2011). Targeting of gp160 to the endoplasmic reticulum (ER) membrane is mediated by a signal sequence at the N-terminus of unprocessed Env. In the ER, gp160 is glycosylated with *N*-linked oligosaccharide side chains (Allan et al., 1985), and oligomerises mostly into trimers before it traffics to the Golgi and trans-Golgi network (Checkley et al., 2011). Addition of O-linked glycans occurs post-translationally during transport of Env through the Golgi. Earlier studies indicate that gp160 is proteolytically cleaved by host cell proteases (furin or furin-like enzymes) in the Golgi, into gp120 and gp41, the subunits found in the mature fusion-competent virions (Hallenberger et al., 1992; Checkley et al., 2011). However, it has been shown that depletion of Rab7a impairs gp160 processing. As Rab7a is involved in membrane trafficking through late endosomes (Brighouse et al., 2010), this suggests that either Env, or a protease, must traffic through late endosomes for gp160 processing (Caillet et al., 2011). Ultimately, the mature trimeric Env is trafficked to the PM to be incorporated into virions by mechanism(s) that are still poorly understood (Checkley et al., 2011; Tedbury and Freed, 2014).

1.5 HIV assembly

HIV-1 Gag is the main structural protein that orchestrates the assembly and egress of virus or virus-like particles (VLPs) in cells. Gag is the only HIV-encoded protein that, when expressed alone, is able to produce non-infectious VLPs with the appearance of immature particles (Bieniasz, 2009). After synthesis, HIV-1 proteins and the full-length genome of the virus are trafficked to the PM where they are assembled into new virus particles. The assembly of HIV is driven primarily by elements within the Gag polyprotein, which include the membrane-targeting (M) domain found at the N-terminus of Gag; the Gag-Gag interaction residues − the majority of which are found in the CA, with some in the NC; and the late assembly (L) domain, or p6, required for the dissociation of nascent virions from the host cell membrane (Fujii et al., 2007; Klein et al., 2007; Pincetic and Leis, 2009; Watts et al., 2009; Maldonado et al., 2014). These interactions will be discussed in more detail below.

1.5.1 Gag assembly at the plasma membrane

The MA domain of Gag (Figure 1.3) is co-translationally modified at the C-terminal end, by the addition of a myristoyl group. The myristoylated Gag is trafficked to the inner leaflet of the PM. Several host proteins, such as ATP binding cassette E1 ATPase, microtubule motor proteins, AP-3 adaptor complex, and small GTPases called ADP-ribosylation factors, are implicated in the trafficking of Gag to the PM. The N-terminal myristoyl moiety and residues 17-31 on the highly basic region of the MA domain of Gag facilitate binding of the Gag polyprotein to phosphatidylinositol-4,5-bisphosphate [$PI(4,5)P_2$]-rich PM (Yuan et al., 1993; Zhou et al., 1994; Ono et al., 2004; Saad et al., 2006b; Chukkapalli et al., 2010). Upon binding of myristoylated MA domain (myrMA) to the $PI(4,5)P_2$, a "myristoyl switch" occurs, whereby the myristoyl moiety, sequestered or concealed in a hydrophobic pocket in the MA domain of Gag, is exposed and inserted into the lipid bilayer. The inositol head group of $PI(4,5)P_2$ also becomes exposed and the 2' unsaturated fatty acid chain of the lipid molecule fits into the "empty" hydrophobic pocket of the MA domain. This leads to the formation of salt bridges with basic residues in the MA (Saad et al., 2006b). Therefore, $PI(4,5)P_2$ performs at least two functions in HIV-1 assembly: (i) triggering the myristoyl switch, and (ii) acting as an anchor for Gag polyprotein in the lipid bilayer.

The Gag polyprotein that accumulates at the PM induces membrane curvature, subsequently forming a spherical Gag shells with two-thirds complete Gag lattice before membrane scission and virus release (Carlson et al., 2008). Viruses with complete Gag lattice are not dissociated from the host cell. Virus release is discussed in detail in Section 1.5.4.

1.5.2 Packaging of viral RNA

The 5' untranslated region (5' UTR) of the HIV-1 genome has determinants for viral genome dimerization, and packaging of two copies of the full-length 9-kb viral RNA into the virions (Laughrea and Jette, 1994; Skripkin et al., 1994; Pallesen, 2011; Jalalirad et al., 2012; Seif et al., 2013). This region is composed of elements that include: the 5' repeated region (5'R) made up of the trans-activator region (TAR) and 5' polyadenylation signal [poly(A)]; the unique 5' region (U5); the primer biding site (PBS), part of which is within the U5; the dimerisation initiation site (DIS); the splice donor (SD) and the packaging signal (PSI) (Pallesen, 2011; Seif et al., 2013). The PSI sequences are made up of a series of stem-loops (SL1 to SL4). Dimerisation is fascilitated by the SL1 (Laughrea and Jette, 1994; Skripkin et al., 1994; Jalalirad et al., 2012).

The initial interaction of the HIV genome and Gag, mediated through the highly basic region of MA and the zinc finger structure of the NC, occurs in the cytoplasm (Lu et al., 2011; Sundquist and Krausslich, 2012; Chukkapalli et al., 2013). The zinc fingers are responsible for selecting unspliced viral genome (Lu et al., 2011). The HIV genome is recruited to the PM as a preformed dimer (Jouvenet et al., 2009). At the PM, the viral genome is encapsidated in the developing buds upon multimerisation of Gag. There are suggestions that binding of the viral RNA to Gag may also serve to regulate the interaction of Gag with the PM and targeting to the assembly site (Chukkapalli et al., 2010; Chukkapalli et al., 2013; Kerviel et al., 2013). In addition to full-length viral genome, tRNA for reverse transcription initiation is also packaged, whilst other RNAs such as 28S rRNA may be packaged due to its abundance in the cytosol (Sundquist and Krausslich, 2012).

1.5.3 Incorporation of Env into virions

The HIV-1 Env protein is trafficked through the secretory pathway to the PM independently of Gag. At the PM, Env has two fates: incorporation into virions by mechanism(s) that are poorly understood, or rapid internalisation in clathrin-coated pits through interactions with the clathrin adaptor protein AP2. Endocytosis may regulate the amount of Env that is exposed at the cell surface. On the cytoplasmic tail (CT) of Env gp41, two internalization motifs, di-leucine and GYxxØ motifs (where x is any amino acid; Ø is an amino acid with a bulky hydrophobic side chain) have been identified in HIV-1 and SIV (Sauter et al., 1996; Berlioz-Torrent et al., 1999; Bowers et al., 2000; Byland et al., 2007; Affranchino and Gonzalez, 2014). Although the full function of the GYxxØ motif is yet to be understood, experiments in a rhesus macaque simian model suggest it is crucial for pathogenesis. In this system, ΔGY viruses, in which the GY codons in the cytoplasmic domain of SIVmac239 were removed, virus levels became undetectable, and no pathogenesis was seen up to 140 weeks post-inoculation with the virus (Fultz et al., 2001). In a recent study, ΔGY-infected macaques showed a decline in peripheral blood CD4+ T cells, but at a slower rate compared to the SIVmac239-infected animals (Breed et al., 2013). Although the animals progressed to AIDS, the ΔGY mutation affected disease pathogenesis as there was no infection of macrophages or the central nervous system, and only transient infection of lamina propria[1]. Also, there was no evidence of microbial translocation.

The CT of Env is thought to interact with the Gag in virions and restrict movement of Env on the surface of the virions (Muranyi et al., 2013; Roy et al., 2013). These two independent studies employed a form of super-resolution microscopy, stochastic optical reconstruction microscopy (STORM), to assess clustering of HIV Env on HeLa cells transfected with wild-type (WT) and mutant (ΔCT Env) proviruses. Analysis of the distribution of Gag and Env proteins revealed that Env lacking the cytoplasmic tail clustered indiscriminately throughout the PM, whilst WT Env primarily colocalised with Gag (Muranyi et al., 2013; Roy et al., 2013). These observations support a model

[1] A thin layer of loose connective tissue, or dense irregular connective tissue that lies beneath the epithelium, and together with the epithelium constitutes the mucosa.

for specific incorporation of Env into virions, mediated by interaction between Gag and Env (Cosson, 1996). Outside of Gag assembly sites, ΔCT Env formed larger clusters compared to WT Env clusters at similar sites, suggesting that the cytoplasmic domain may be modulating Env clustering. In addition to this model, other models have been proposed, which include passive incorporation, Gag-Env co-targeting, and indirect Env interaction (see Checkley et al., 2011; Tedbury and Freed, 2014, for reviews).

1.5.4 Virus release

Gag multimerises on the inner leaflet of the PM, hence forming a Gag shell and driving remodelling of the membrane. The time it takes to assemble an HIV particle has been estimated in HeLa cells, transfected with fluorescently labelled Gag, and analysed using wide-field and total internal reflection fluorescence microscopy (TIR-FM). By these methods, it was seen that on average it takes 8-9 min to assemble about 90% of VLPs, but this can vary from 4 to 20 min (Ivanchenko et al., 2009; Jouvenet et al., 2011). Nascent viral particles are separated from the plasma membrane by severing the membrane stalk that links them to the host cells. To accomplish this, retroviruses and other families of enveloped viruses (filoviruses, rhabdoviruses, and arenaviruses) have specific late (L) domain motifs to recruit host cell proteins that mediate topologically similar membrane scission processes, and these proteins are part of the endosomal sorting complex required for transport (ESCRT) machinery. Three such motifs have been identified: PPXY, P(T/S)AP and YPXnL [where X is any residue, and Xn is any sequence of n = 1–3 residues] (Freed, 2002). These motifs can appear in viruses as a single motif or in combinations (Figure 1.6). HIV-1 has two such motifs, PTAP and YPXnL, in the p6 subdomain of Gag (Figure 1.7).

The ESCRT proteins were initially identified through a detailed morphological analysis of the data from several yeast genetic screens, that aimed at identifying the machinery involved in trafficking proteins to the vacuole, and including the vacuolar protein sorting (Vps) screen. One group of mutants gave similar morphology, dilate endosomal organelles that were subsequently termed class E mutants (Raymond et al., 1992). Members of this class were subsequently found conserved from archea to higher animals (Fujii et al., 2007; Samson and Bell, 2009). They function in various cellular processes such as the biogenesis of multivesicular bodies (MVBs), transcription

regulation, cytoskeletal dynamics, cytokinesis, and formation of microvesicles (Kamura et al., 2001; Slagsvold et al., 2006; Bieniasz, 2009; Samson and Bell, 2009; Wollert et al., 2009; Roxrud et al., 2010; Nabhan et al., 2012; Lin et al., 2013; Choudhuri et al., 2014). Early in the new millennium, work from several laboratories simultaneously found that human homologues of several of these class E proteins are required for HIV formation (Garrus et al., 2001; Demirov et al., 2002a; Martin-Serrano et al., 2003; von Schwedler et al., 2003; Stuchell et al., 2004).

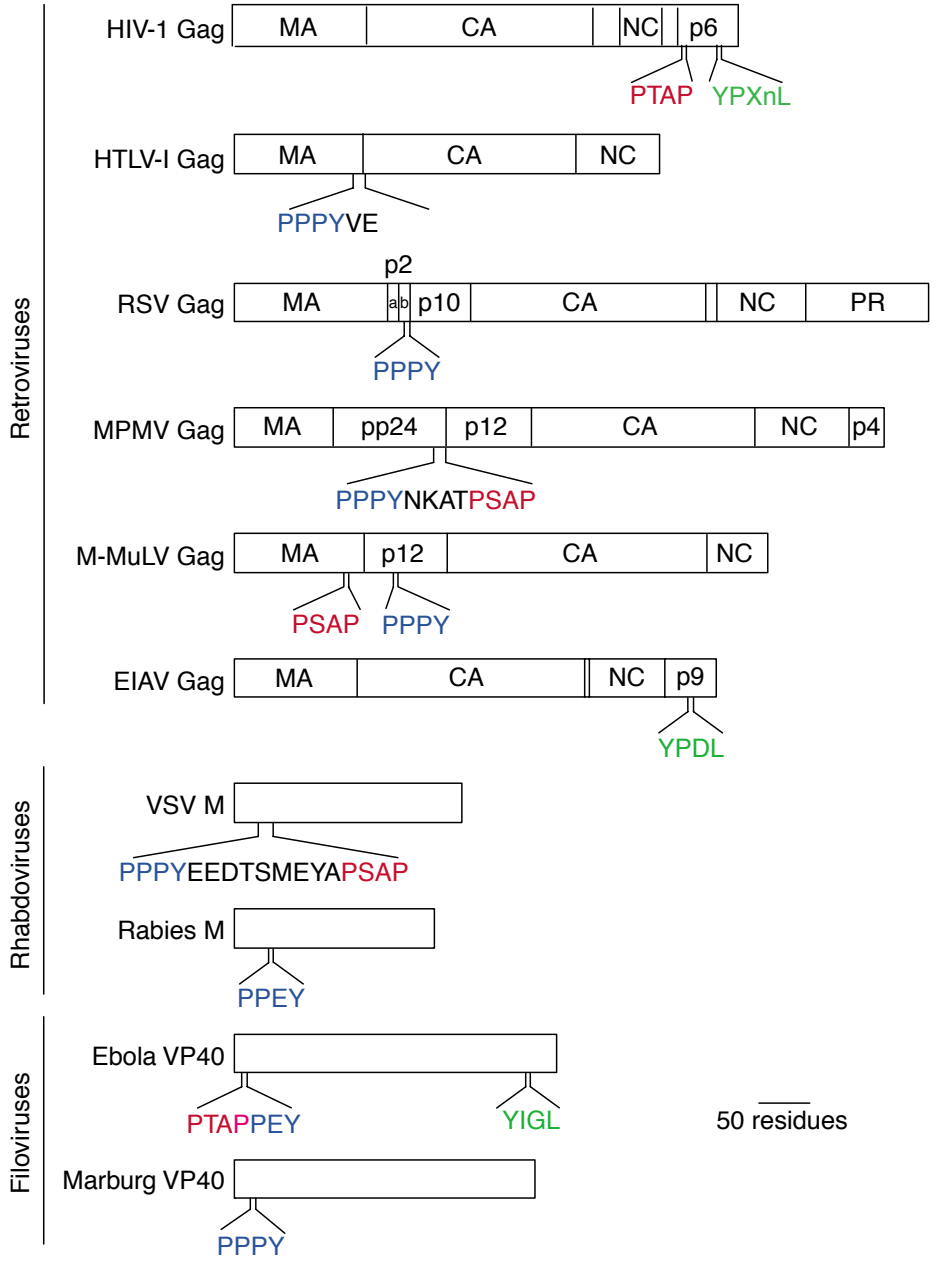

Figure 1.6: Viral late domain motifs found in membrane-associated structural proteins of enveloped viruses.

Motifs are coloured as follows: PT/SAP, red; PPXY, blue; YXXnL, green. From Pornillos et al. (2002).

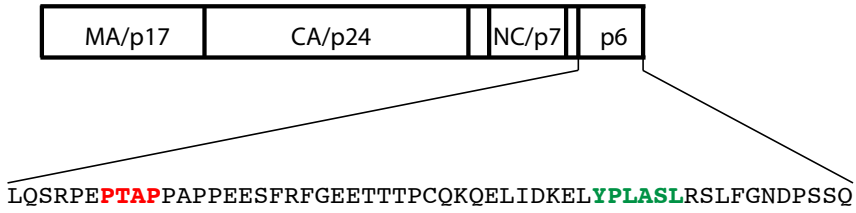

Figure 1.7: HIV-1 Gag organisation.

Amino acids sequence of the p6 subdomain of HIV-1 BaL strain.

1.5.5 The ESCRT machinery and HIV budding

Virus budding is topologically equivalent to abscission during cytokinesis and the formation of intralumenal vesicles in multivesicular bodies (MVB) biogenesis (Figure 1.8). (Balasubramaniam and Freed, 2011; Henne et al., 2013). Other topologically equivalent processes recently identified, and that require the ESCRT machinery, include the arrestin domain containing protein-1 mediated formation and release of microvesicles at the plasma membrane (Nabhan et al., 2012), the release of T cell receptor enriched microvesicles at immunological synapses (Choudhuri et al., 2014), and PM wound repair (Jimenez et al., 2014). In these processes, the membrane scission machinery acts within the membrane neck, in contrast to the dynamin-mediated scission that facilitates the formation of clathrin-coated vesicles, whereby the scission machinery acts outside the membrane neck.

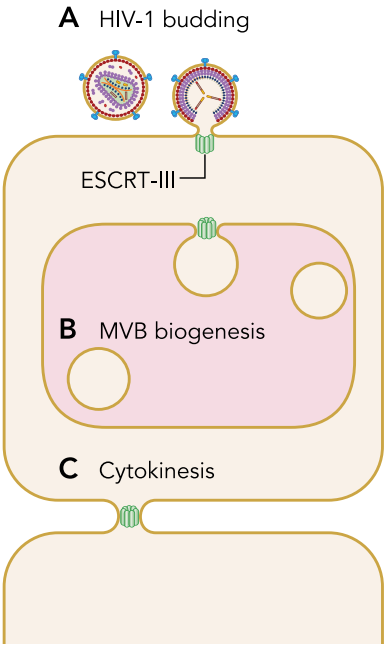

Figure 1.8: Topologically equivalent membrane fission processes.

Taken from Balasubramaniam and Freed, 2011.

The ESCRT proteins are organised into five complexes (Table 1.1) that are recruited sequentially to sites where membrane scission processes occur (Votteler and Sundquist, 2013; Van Engelenburg et al., 2014). In addition, there are a number of ESCRT-associated proteins. The first three complexes, ESCRT-0, -I and -II, exist as preformed complexes in the cytosol, and they primarily interact with cargo or scaffolding proteins. These complexes recruit the fourth complex, ESCRT-III, which polymerises at membrane sites to constrict the membrane. The fifth complex is the AAA ATPase VPS4 and its co-factor lysosomal trafficking regulator interacting protein-5 (LIP5), which together further constrict the vesicle/bud neck, and/or disassemble ESCRT-III.

Table 1.1: A list of ESCRT/ESCRT-associated proteins that have been identified in yeast and their human homologues

	Yeast	**Human**
ESCRT-0	Vps27	Hrs
	Hse1	STAM1/2
ESCRT-I	Vps23	Tsg101
	Vps28	Vps28
	Vps37	Vps37A-D
	Mvb12	Mvb12A, B
	—	UBAP1
ESCRT-II	Vps36	EAP45
	Vps22	EAP30
	Vps25	EAP20
ESCRT-III	Vps20	CHMP6
	Snf7	CHMP4A-D
	Vps24	CHMP3
	Vps2	CHMP2A, B
	Vps60	CHMP5
	Ist1	IST1
	Did2	CHMP1
AAA ATPases	Vps4	Vps4A and B
	—	Spastin
ESCRT-associated proteins	Vta1	LIP5
	Bro1	ALIX
	—	CEP55
	—	AuroraB

Studies of MVB biogenesis and cytokinesis have helped in the understanding of the membrane fission reactions that occur during the assembly of viruses, and *vice versa*. In MVB formation, the hepatocyte growth factor receptor substrate (Hrs) and signal transducing adaptor molecule (STAM), ESCRT-0 components, are recruited by ubiquitinated membrane proteins such as epidermal growth factor receptor, and cholesterol (Du et al., 2012; Schmidt and Teis, 2012). A PSAP motif in Hrs interacts directly with the ubiquitin-E2-like variant (UEV) domain of tumour susceptibility gene 101 (Tsg10l), an ESCRT-I component (Pornillos et al., 2002). In cytokinesis, the centrosome protein 55 (CEP55) recruits Tsg101 (Carlton and Martin-Serrano, 2007). During virus budding, HIV-1 mimics Hrs or CEP55 by recruiting Tsg101. Tsg101 (Vps23 in yeasts) exists with Vps28, Vps37 and Mvb12 as a stable cytosolic multi-protein ESCRT-I complex (Martin-Serrano, 2007; Hurley and Hanson, 2010). However, an endosome specific ESCRT-I complex consisting of Tsg101, Vps37A, Vps28 and ubiquitin-associated protein 1 (UBAP1), has been identified (Stefani et al., 2011; Agromayor et al., 2012). Although UBAP1 plays a role in MVB sorting, it has no function in HIV budding or cytokinesis (Agromayor et al., 2012). A recent study suggests that Tsgl01 is recruited with Gag during VLP assembly, whilst the ESCRT components downstream in the pathway are recruited later and transiently (Bleck et al., 2014). Mutations in the HIV-1 Gag PTAP motif, or the depletion of Tsg101 using RNA interference (RNAi), inhibit virus release and budding viruses remain tethered to the plasma membrane (Huang et al., 1995; Garrus et al., 2001).

In HIV budding, the Gag p6-associated ESCRT-I is capable of directly engaging the ESCRT-III complex to catalyse membrane scission, without the ESCRT-II bridge. Although ESCRT-II is required for MVB formation, it is dispensable for HIV budding (Teis et al., 2010). ESCRT-III is also a multi-protein complex with at least 12 distinct but related subunits in mammals (Votteler and Sundquist, 2013). It is made up of the following core components of charged MVB proteins (CHMP) in humans, existing as monomers in the cytosol: CHMP6, CHMP4A-D, CHMP3, CHMP2A-B and CHMP5. In HIV-1 budding, some components of ESCRT-III are dispensable, except CHMP2 and CHMP4 (Morita et al., 2011; Weiss and Gottlinger, 2011) (Figure 1.9). Based on studies in yeast, the assembly of ESCRT-III is initiated by CHMP6, which nucleates the polymerisation of CHMP4. The CHMP4 polymer recruits CHMP3 to cap the complex

and engage CHMP2 that completes the assembly of ESCRT-III (Hurley and Hanson, 2010; Schmidt and Teis, 2012). Although depleting CHMP6 does not inhibit HIV-1 release (Morita et al., 2011), later work using purified proteins and giant unilamellar vesicles suggests that CHMP6 is required for recruiting downstream components of the ESCRT-III complex (Carlson and Hurley, 2012). Taken together, these studies suggest functional redundancy of ESCRT-III proteins under physiological conditions.

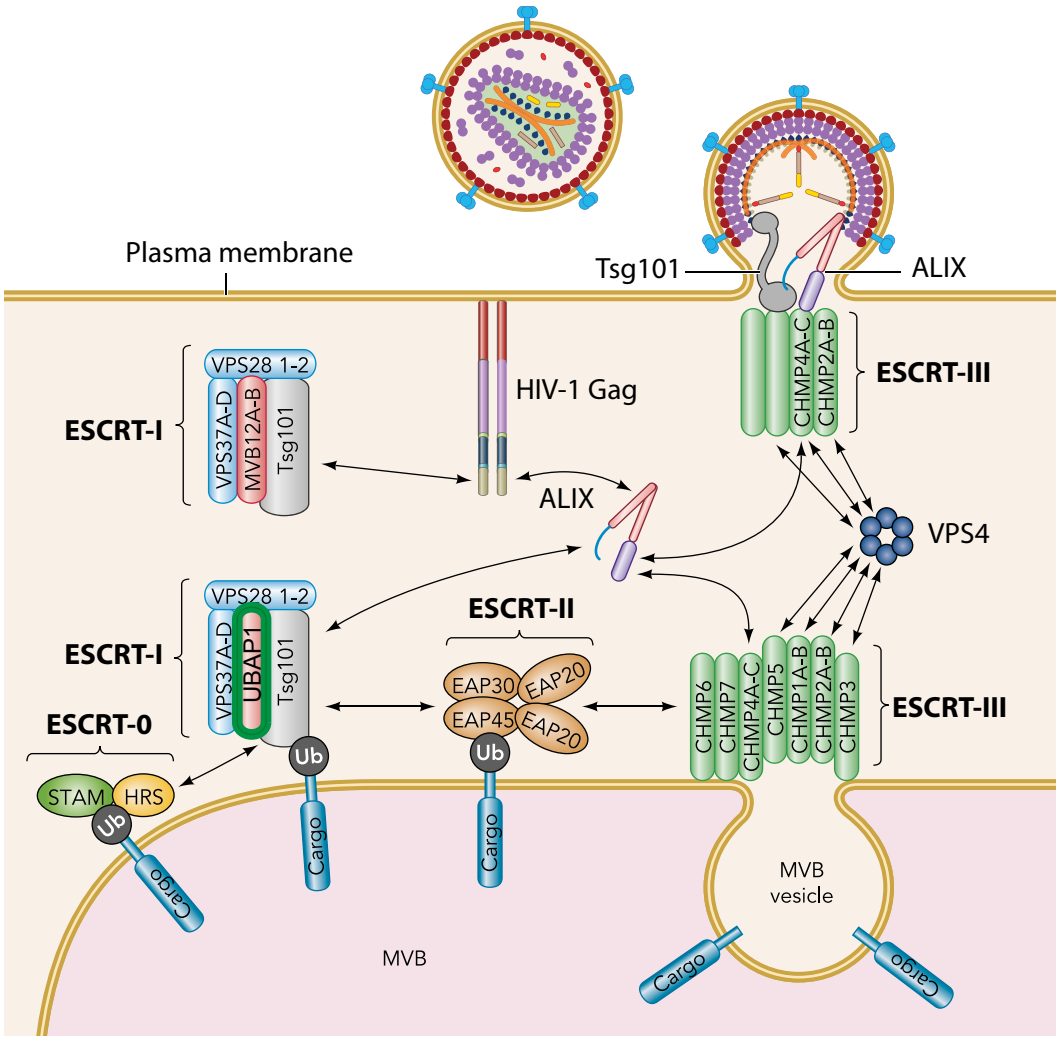

Figure 1.9: Schematic representation of the functions of ESCRT proteins in HIV budding and MVB formation.

Components of the ESCRT pathway are recruited sequentially. Double-headed arrows indicate direct protein-protein interactions. STAM, signal transducing adaptor molecule; Ub, ubiquitin. EAP, ELL (for 11-19 lysine-rich leukaemia gene)-associated protein. Adapted from Balasubramaniam and Freed, 2011.

Several models, reviewed by Henne et al. (2013), have been proposed for the events that occur at the site of ESCRT-III polymerisation. A common feature for these models is that ESCRT-III accumulates at the neck outside of the bud or vesicle head, possibly forming filaments that assemble into helices or spirals (Hanson et al., 2008; Buchkovich et al., 2013). However, a diametrically opposite model has recently been proposed for HIV budding, where it was suggested that ESCRT-III and VPS4 accumulate in the virus bud (Van Engelenburg et al., 2014). Whilst this study provides an attractive model, it is unclear how much of what is observed is due to overexpression of the fluorescently tagged ESCRT proteins. On the contrary, when fluorescently tagged ESCRT-III proteins and VPS4 were stably expressed at endogenous levels, they were transiently recruited to the neck of the assembling particles prior to virus release (Bleck et al., 2014), consistent with the previously proposed models.

Understanding of the mechanism of membrane scission still remains elusive. Overall, it is believed that the electrostatic interactions of ESCRT-III filaments with the membrane of the virus/vesicle neck constrict the aperture. As the neck narrows to ~3 nm, a scission intermediate is spontaneously formed. Then VPS4 is rapidly and transiently recruited by CHMP2 to the scission complex, where it hydrolyses ATP thereby catalyzing membrane scission, and ultimately ESCRT components are disassembled and recycled (Hurley and Hanson, 2010; Adell and Teis, 2011; Jouvenet et al., 2011; Bleck et al., 2014). The disassembly is the only known energy-requiring step in the ESCRT pathway, where ATP is hydrolysed to ADP and inorganic phosphate. Although VPS4 has been suggested to act late during budding/vesiculation, new data suggest that it may also be involved early in the remodelling of membranes during MVB biogenesis and HIV budding (Adell et al., 2014; Cashikar et al., 2014). More studies are required to clarify aspects of the ESCRT pathway that are still obscure.

Mutation of glutamate (E) to glutamine (Q) at position 228 of VPS4 generates a dominant negative VPS4, which is able to bind substrates but fails to hydrolyse ATP, thereby abolishing the catalytic activity of VPS4 (Babst et al., 1998). Overexpression of dominant negative VPS4 EQ in model cell lines results in the formation of enlarged endosomes, with cargo trapped at the surfaces of endosomes (Bishop and Woodman, 2000). When overexpressed in HIV-1 infected cells, VPS4 EQ inhibits virus release

(Garrus et al., 2001). Collectively, these reports demonstrate the importance of VPS4 in these topologically related processes.

Apoptosis linked gene-2 (ALG-2)-interacting protein X (ALIX) is an accessory protein that works in concert with other ESCRT components to mediate HIV release (Strack et al., 2003), and other membrane fission events such as MVB formation (Figure 1.9). It is made up of the Bro1, V-shaped and proline-rich domains (Fujii et al., 2007). The YPXnL motif of Gag binds the V-shaped domain of ALIX (Lee et al., 2007; Munshi et al., 2007). To engage ESCRT-III, the Bro1 domain of ALIX recruits CHMP4. CHMP4 then recruits CHMP2 that binds VPS4. Mutations in the CHPM4-binding site on ALIX inhibit the ability of ALIX to support virus release (Fisher et al., 2007). In addition to binding Gag directly, ALIX is able to associate with Tsg101 (Strack et al., 2003) through its proline-rich domain. However, the Tsg101-ALIX interaction is not essential for virus budding, since the two proteins can be recruited independently to mediate membrane scission. Although HIV-1 has two late domain motifs, PTAP is the dominant motif because mutations in the PTAP motif severely reduce virus release in many cell systems, compared to mutations in the YPXnL motif (Demirov et al., 2002b; Fujii et al., 2009). The interaction between YPXnL and ALIX may be weaker than the PTAP and Tsg101 interaction (Pincetic and Leis, 2009). Furthermore, endogenous levels of ALIX are not able to rescue defects in Tsg101 recruitment (Fujii et al., 2009). However, expression of higher levels of ALIX may compensate for the weak interaction, as overexpression of ALIX can rescue viruses with mutations in the PTAP motif (Carlton et al., 2008; Chung et al., 2008).

1.5.6 Virus maturation

During or immediately after scission of immature virus particles from the producer cell, Gag and Gag-Pol polyproteins are cleaved by the viral PR. The PR, synthesised as part of the Gag-Pol polyprotein (see section 1.4.3), dimerises during HIV assembly to become active (Lee et al., 2012b). Autocatalysis of PR releases the PR from the Gag-Pol polyprotein. Through a positive feedback loop, the released PR is able to cleave more Gag-Pol, thereby liberating more PR together with RT and IN. The viral PR cleaves the Gag polyprotein into its sub-domains (Konnyu et al., 2013). Premature

activation of the PR can occur when Gag-Pol and Gag are highly expressed in cells (Carlson et al., 2010).

The proteolytic cleavage of Gag proceeds sequentially (Figure 1.10) (Pettit et al., 1994; Bell and Lever, 2013). First, the Gag polyprotein is cleaved to produce p41 (MA-CA-p2) and p15 (NC-p1-p6) processing intermediates. These are processed further to ultimately yield individual Gag subdomains as shown in Figure 1.10. Whereas the amino acid sequence is crucial for cleavage, context also plays an important role in determining the efficiency of this process. For instance, the binding of viral RNA to NC promotes Gag cleavage at the p1-p6 sites, but it does not affect the rate of cleavage at the p2-NC (Lee et al., 2012a). It is not clear how RNA binding promotes cleavage, however, it has been suggested that the RNA may serve as a cofactor for the PR, or promote some conformational change in the cleavage site in favour of the reaction (Lee et al., 2012a).

Proteolytic processing of HIV-1 Gag results in mature virions characterised by structural and morphological changes (Ganser-Pornillos et al., 2008; Briggs and Krausslich, 2011). The cleavage of different sites is not equally important for virus morphology and infectivity. For example, in tissue culture, separation of NC and p1 (SP2) is not essential for maturation and infectivity (de Marco et al., 2012). HIV-1 mutants lacking SP2 are infectious to the same extent as WT virus, suggesting that SP2 is dispensable in the replication cycle of HIV-1, at least in tissue culture. However, the failure to separate SP2 and p6 has detrimental effects to the virus, resulting in reduced infectivity and formation of a high proportion of irregular cores. Seemingly, the liberated p6 determines replicative capacity and morphogenesis of HIV-1 (de Marco et al., 2012). Once Gag has been cleaved, the CA reassembles to form the virus core seen in mature particles (Figure 1.3 and 1.10).

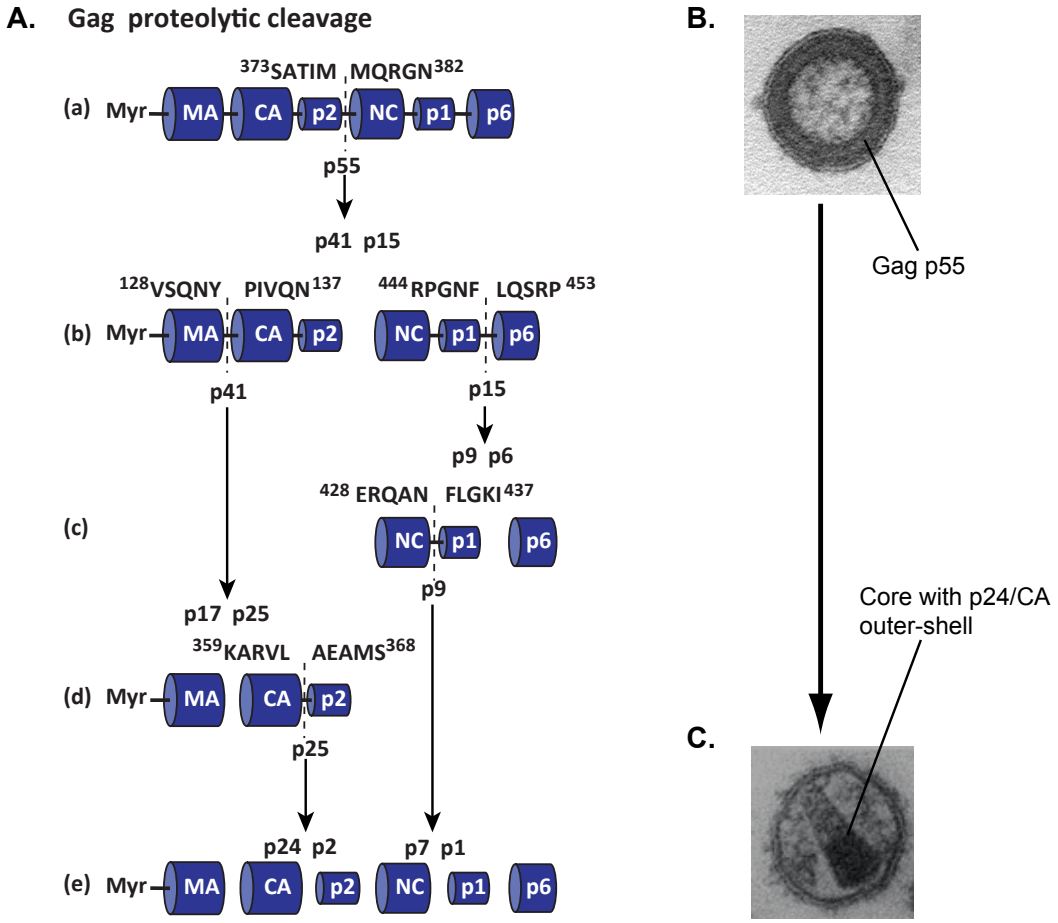

Figure 1.10: Maturation of HIV-1 by proteolysis.

(A) Sequential proteolytic processing of the Gag polyprotein (p55) shown in (a) to ultimately yield mature viral proteins shown in (e) **(B)** An immature virus particle with an electron dense Gag shell and translucent centre. **(C)** A mature virus particle with an electron dense core, produced from the proteolytic processing of Gag and the assembly of CA into a hexagonal lattice around the genomic RNA. Adapted from Bell and Lever (2013).

1.6 Target cells infected by HIV-1

HIV targets key immune system cells that typically express the CD4, CCR5 and/or CXCR4 molecules. These cells include a subset of T cells, macrophages, dendritic cells (DCs), and to a small extent monocytes. The physiological roles of these cells involve innate and adaptive immune responses (Hashimoto et al., 2011).

1.6.1 T cells

Early studies (in the 1980s) on the immunological parameters of HIV-infected individuals revealed that T cells were important in the pathogenesis of the infection. AIDS patients showed a decline in the population of Leu-3/OKT4 antigen-bearing T lymphocytes (CD4+ T cells), whilst the Leu-2/OKT8 antigen-bearing cells (CD8+ T cells) remained numerically normal so that their proportions relative to other T cells subpopulations were elevated (Schroff et al., 1983). Later, two laboratories independently identified CD4 molecules on T cells as essential for HIV entry into cells (Dalgleish et al., 1984; Klatzmann et al., 1984). However, CD4 molecules were not sufficient for entry as the virus could not infect non-human cells expressing the CD4 molecule, and some HIV strains could infect activated T cells but poorly infect macrophages. This led to the hypothesis that a co-factor may be involved in HIV entry. The search for the co-factor(s) resulted in the discovery of the co-receptors CXCR4/fusin, which when co-expressed with CD4 on non-human cells, permitted HIV entry and replication, and virus entry could be blocked by an antibody against CXCR4/fusin (Feng et al., 1996). In addition, CCR5 was discovered and its role as a co-factor for virus entry into macrophages was inhibited by its ligands, RANTES and MIP-1α/β (Deng et al., 1996). CCR5 molecules are also expressed on CD4 T cells (Moore et al., 1997). Genetic polymorphism in CCR5 has been reported, where a deletion of 32-bp in the second extracellular loop leads to the production of a truncated protein (CCR5Δ32) that fails to traffic to the plasma membrane (Samson et al., 1996). Individuals with homozygous CCR5Δ32 are resistant to HIV infection, and the frequency of this mutation increases amongst the Caucasians from the southern to northern parts of Europe (Galvani and Novembre, 2005; Sidoti et al., 2005; Faure and Royer-Carenzi, 2008).

HIV infection is highly permissive in activated CD4+ T cells, compared to resting CD4+ T cells. Recent data show that inhibition of HIV replication in resting CD4+ cells is partially attributed to restriction by SAMHD1 (sterile alpha motif and HD domain-containing protein-1) (Baldauf et al., 2012). SAMHD1 acts by depleting the available deoxynucleoside triphosphates (dNTPs), thereby starving the virus of a building block essential for reverse transcription (Lahouassa et al., 2012). Notably, resting CD4+ T cells express high levels of SAMHD1 (Baldauf et al., 2012).

Although CD4+ T cells are directly infected by free viruses, they can also be infected through cell-cell transmission of viruses from other T cells (Jolly and Sattentau, 2005), dendritic cells (DC) (Dong et al., 2007) or macrophages (Duncan et al., 2014; Giese and Marsh, 2014), through the so-called virological synapses (see Section 1.6.3).

1.6.2 Macrophages

Macrophages are terminally differentiated haematopoietic cells found in all tissues. They are related to dendritic cells in that they are derived from the same haematopoietic stem cells in the bone marrow (Figure 1.11) (Tsunetsugu-Yokota and Muhsen, 2013). Macrophages play key roles in both innate and acquired immunity (Geissmann et al., 2010; Hashimoto et al., 2011). Tissue macrophages have a wide range of pathogen-recognition receptors, which function in recognising, taking up and degrading microbes, foreign and damaged cells. Degraded peptides are presented on major histocompatibility (MHC) class II, important for antibody production. Macrophages also secrete cytokines to attract effector cells such as neutrophils.

Monocytes are morphologically heterogeneous, and can be divided into three subsets according to differential expression of CD14 (a lipopolysaccharide receptor) and CD16 (immunoglobulin gamma Fc region receptor III): classical CD14++CD16-, non-classical CD14+CD16+, and intermediate CD14++CD16+ cells. The intermediate subset expresses higher levels of CCR5, and are therefore preferentially infected by HIV (Gorry and Ancuta, 2011). CD16+ cells constitute a small proportion of circulating monocytes (about 5%) (Coleman and Wu, 2009), therefore few monocytes are infected by HIV. The infected monocytes can disseminate infection to tissues where they migrate and differentiate into macrophages.

In vivo, myeloid lineage cells can be infected with HIV-1 at two stages of differentiation: (1) as monocytes in the blood; and (2) as mature macrophages in tissues. HIV production in monocytes is inhibited at different stages of the replication cycle, including reverse transcription. For example, unlike macrophages, monocytes do not have a functional positive transcription elongation factor b (P-TEFb), required to complex with Tat on the 5'LTR of the integrated HIV provirus (Coleman and Wu, 2009). Furthermore, monocytes are more refractory than macrophages to productive

HIV infection, because they express higher levels of SAMHD1 (Laguette et al., 2011). Since monocytes migrate to different tissues or anatomic sites, including the brain, kidneys, lungs and the gut-associated lymphoid tissues (GALT) where they differentiate into macrophages, they can disseminate and establish HIV infection at these sites *in vivo*.

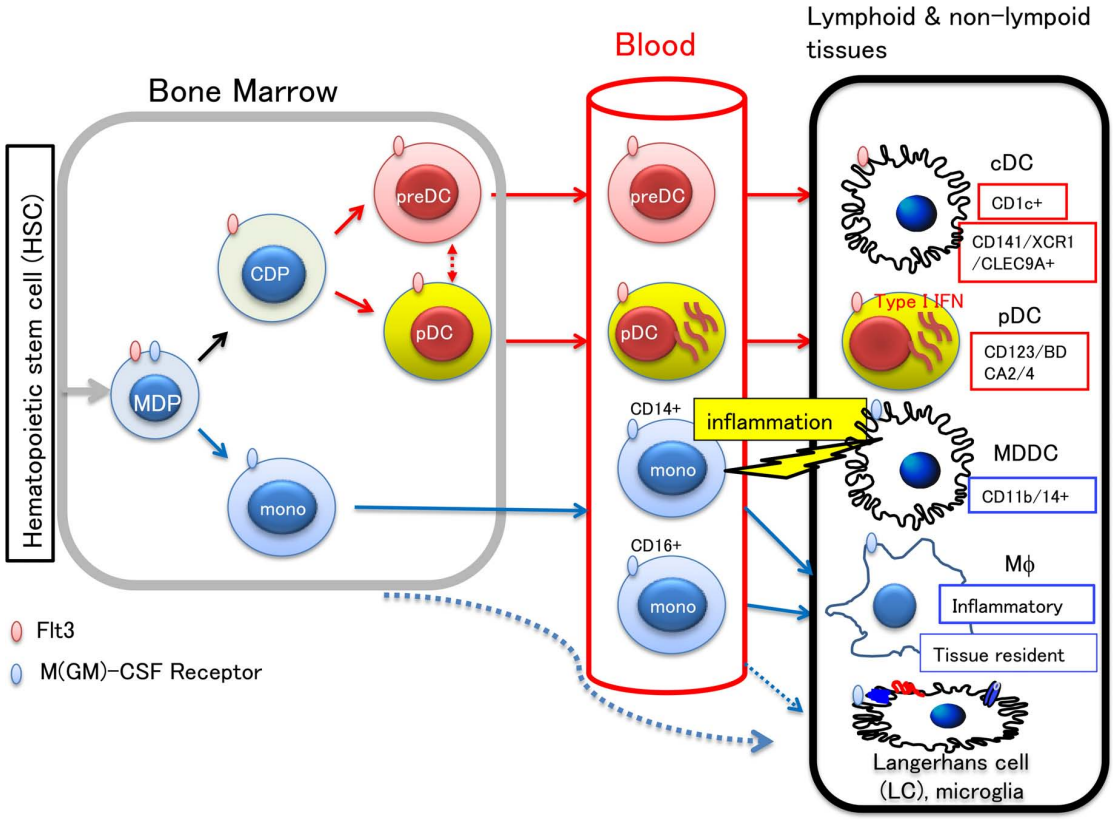

Figure 1.11: Development of monocytes, macrophages and dendritic cells.
Hematopoietic stem cells in the bone marrow differentiate into monocyte/macrophage and DC precursors (MDP), which can become monocytes (mono) or common DC precursors (CDP). The CDP differentiate to precursor DC (preDC) or plasmacytoid DC (pDC), which migrate to peripheral tissues through the blood. In both lymphoid and non-lymphoid tissues, preDC can become either of two types of conventional DC (cDC) with the indicated markers. Circulating monocytes are the source of macrophages (Mφ), Langerhans cells (LC) and microglia. LC precursors in the bone marrow can migrate to the skin. $CD14^+$ monocytes can migrate to inflamed tissue and differentiate into either migratory monocyte-derived DC (MDDC) or inflammatory Mφ. Cells committed to become DC express the Fms-like tyrosine kinase (Flt3), whereas those that commit to monocytes/macrophages express macrophage-colony stimulating factor (M-CSF) receptor. Therefore, Flt3 ligand and M-CSF are key molecules for the differentiation and proliferation of DC and monocytes/macrophages, respectively. Taken from Tsunetsugu-Yokota and Muhsen (2013).

1.6.2.1 The role of macrophages in HIV pathogenesis

Although monocytes/macrophages are target cells for HIV infection *in vivo*, their role in HIV pathogenesis remains unclear. Transmitted/founder viruses have been described as showing preference for T cells (Ochsenbauer et al., 2012), and the loss of T cells clearly plays a major role in the decline in immunological competence. However, compared to T cells, macrophages are resistant to the cytopathic effects of HIV, which makes them a viable reservoir for the virus.

Macrophages may play a critical role in HIV infection of the brain. About 50% of adults with HIV infections, and on ART, have varying degree of HIV-associated neurocognitive disorders (HAND), including dementia (Heaton et al., 2010). HIV-infected individuals on ART have increased chances of survival and this has been accompanied by an increased incidence of HAND (Gras and Kaul, 2010). Post-mortem analysis of brain tissues from patients who presented with dementia and died from AIDS showed HIV in macrophages (Koenig et al., 1986). Furthermore, the severity of dementia correlates with the amount of virus in perivascular macrophages and microglia (Glass et al., 1995). In SIV-infected rhesus macaques, transfused with fluorescein-labelled peripheral blood mononuclear cells (PBMCs), SIV positive and dye-labelled monocytes have been detected in the brain, indicative of monocyte infiltration into the central nervous system (CNS) (Clay et al., 2007). The secretion of chemokines by macrophages in the brain results in a chemotactic gradient across the blood-brain barrier, which promotes the recruitment of more infected/uninfected monocytes and T-cells. Furthermore, HIV in the CNS can evolve independently of circulating virus (Harrington et al., 2009), although it is unclear whether macrophages have a role to play in this evolution.

The main role of macrophages is phagocytosis and the destruction of unwanted particles such as cell debris and microorganisms. However, HIV infection can impair the phagocytic capacity of macrophages, such as alveolar macrophages obtained from HIV infected individuals (Jambo et al., 2014). One study suggests that Nef is responsible for inhibiting phagocytosis in primary macrophages (Mazzolini et al., 2010). In this study, Nef deleted HIV-1 or wild-type HIV-1 strains were used to infect MDM, and Nef-GFP or GFP expression vectors were electroporated into the macrophages. To assess

phagocytosis, IgG- or complement-opsonised sheep red blood cells, and complement receptor 3 and Fc receptor (FcR) were added to the cells. The efficiency of phagocytosis was reduced to approximately 50% in cells with WT virus or Nef expression vector. In support of these findings, inhibition of phagocytosis by Nef has also been reported in a macrophage cell line (Cui et al., 2012). Nef down-modulates the cell surface expression of CD4 and MHC-I and II molecules, which protects infected cells from secondary infection and cytotoxic T-lymphocyte-mediated killing (Mangasarian et al., 1999; Marsh and Pelchen-Matthews, 2000; Herbein et al., 2010). This modulation may apply to other surface molecules, such as FcR, thereby negatively regulating the immune system to the advantage of HIV.

1.6.2.2 Intracellular plasma membrane-connected compartments

In infected macrophages, HIV-1 accumulates in intracellular compartments (Gartner et al., 1986). These were initially thought to be part of the Golgi apparatus (Orenstein et al., 1988), but later work on HIV assembly in macrophages suggested that these virus-containing compartments could be of endosomal origin because they contain the tetraspanin CD63, a marker for late endosomes or MVBs (Raposo et al., 2002; Pelchen-Matthews et al., 2003). There is now substantial and compelling evidence that the intracellular compartments where HIV assembles in macrophages (Figure 1.12) are intracellular plasma membrane-connected compartments (IPMCs) (Deneka et al., 2007; Jouve et al., 2007; Welsch et al., 2007; Bennett et al., 2009; Marsh et al., 2009; Welsch et al., 2011; Chu et al., 2012a; Gaudin et al., 2012; Pelchen-Matthews et al., 2012; Berre et al., 2013; Gaudin et al., 2013a; Mlcochova et al., 2013; Giese and Marsh, 2014; Mariani et al., 2014).

1.6.2.3 Morphological and biochemical features of the IPMCs

It has been demonstrated that the IPMCs are connected to the cell surface by labelling intact primary macrophages with the PM impermeable dye ruthenium red (RR) and analysing the cells by EM (Deneka et al., 2007; Welsch et al., 2007). The dye labelled the cell surface, the virus containing compartment membranes, as well as virus particles in the compartments, but it did not stain membranes of the cells' internal organelles such as endosomes, the Golgi and mitochondria. There is also access of fluid-phase markers such as horseradish peroxidase and membrane dyes such as CellMask and FM

4-64 (Deneka et al., 2007; Mlcochova et al., 2013). Most importantly, conduits connecting the IPMCs to the cell surface were also revealed by EM studies (Deneka et al., 2007; Welsch et al., 2007; Bennett et al., 2009). Notably, the IPMCs have neutral pH, whilst late endosomes and lysosomes are acidic (Jouve et al., 2007), further indicating that the internal compartments are distinct from early and late endosome, as well as lysosomes.

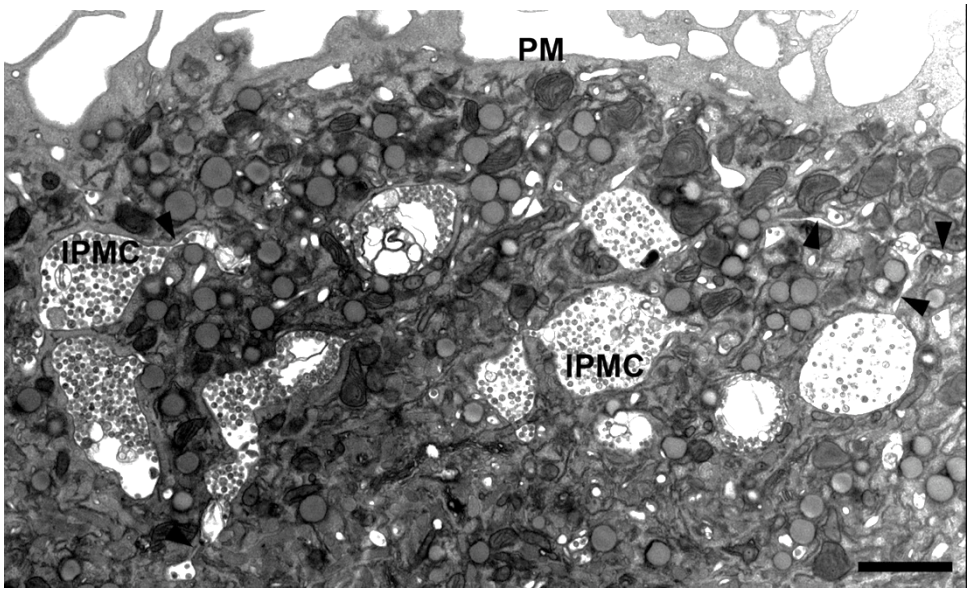

Figure 1.12: Epon EM of IPMC in an HIV-infected MDM.

MDM with a group of virus containing compartments. Arrowheads point to narrow tubes connecting some pockets of the IPMC. Notably, virus particles or budding figures were not seen at the cell surface. Bar, 2 µm. Taken from Deneka et al. (2007).

IPMCs are morphologically heterogeneous in shape and size. Several studies have shown that they are present in uninfected macrophages, and that the IPMCs expand in size upon accumulation of HIV-1 (Welsch et al., 2011; Pelchen-Matthews et al., 2012; Berre et al., 2013; Mlcochova et al., 2013; Giese and Marsh, 2014). Analysis of the IPMCs' architecture showed that they are morphologically complex, with vacuole-like elements, as well as swirls of tightly apposed membranes, and sponge-like arrays (Deneka et al., 2007; Welsch et al., 2007; Pelchen-Matthews et al., 2012). Although these structures may appear to exist as different units in two-dimensional EM images, three-dimensional EM imaging of RR-labelled cells indicates that they may in fact belong to the same network of continuous membrane (Welsch et al., 2011). Immature virus profiles have been identified in IPMCs, and budding virus structures have been

seen on the limiting membranes of IPMCs showing that the virus can assemble here (Figure 1.13) (Deneka et al., 2007; Welsch et al., 2007). Recently, live-cell imaging of MDM labelled with various fluorescent markers or probes have revealed that the IPMCs are stable but dynamic structures (Gaudin et al., 2013a; Mlcochova et al., 2013).

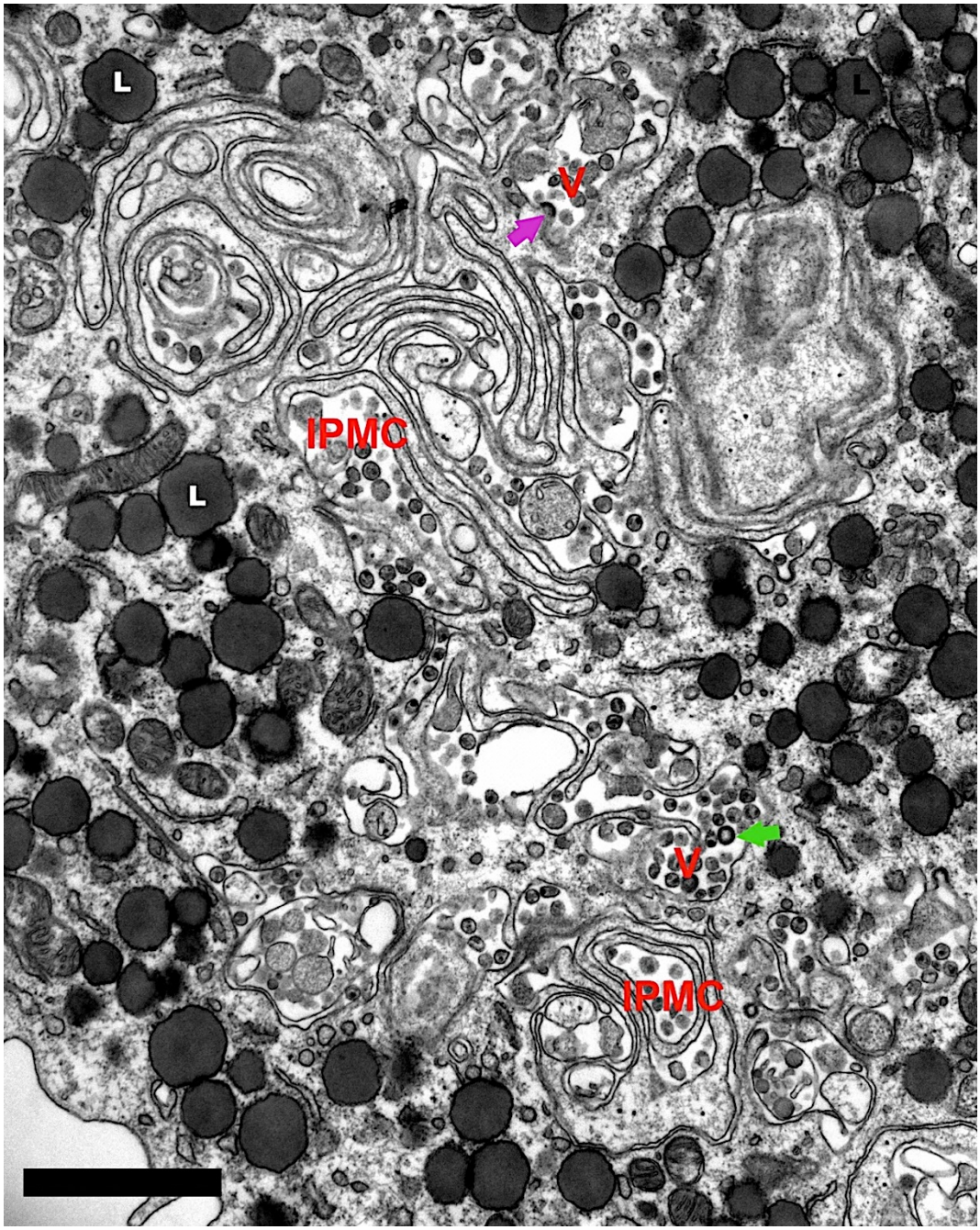

Figure 1.13: Virus assembly compartments in MDM.

The internal plasma membrane-connected compartments (IPMCs) where HIV assembles are morphologically complex, consisting of interconnected vacuole-like structures filled with viruses (V). HIV buds into the IPMC (magenta arrow). The green arrow points to an immature virus in the IPMC. L, lipid droplet. Scale bar, 1 µm. EM by A. Pelchen-Matthews.

Several markers that are found on the cell surface membranes of MDM have also been found on IPMCs. These include the tetraspanins CD9, CD81 and CD53 (Deneka et al., 2007). In addition, IPMCs also contain the PM marker CD44 (Welsch et al., 2007; Pelchen-Matthews et al., 2012), a hyaluronic acid receptor that is incorporated into budding virions (Lawn et al., 2000; Chertova et al., 2006). In uninfected macrophages, the tetraspanin CD63 is associated with endosomes labelled with the lysosomal-associated membrane protein 1 (LAMP-1) but is not detected in IPMCs. However, in HIV infected cells, CD63 accumulates in IPMCs and is incorporated into virions, suggesting that this marker cycles through the assembly compartments (Deneka et al., 2007; Ruiz-Mateos et al., 2008; Marsh et al., 2009). IPMCs do not contain or they poorly label with early endosome antigen 1 (EEA-1), an early endosome marker, or LAMP-1 (Deneka et al., 2007; Marsh et al., 2009; Giese and Marsh, 2014). Moreover, IPMCs fail to label with 2x FYVE-GFP (double FYVE[2] zinc finger domain fused to GFP) which binds phosphatidylinositol 3-phosphate that is predominantly on early endosomes and intralumenal vesicles of MVBs, further indicating that the compartments are not endosomal (Mlcochova et al., 2013). A recent study has shown that CD36, a multi-ligand scavenger receptor present on the surface of macrophages, is also present on the IPMCs of uninfected and infected cells (Berre et al., 2013).

A prominent feature of IPMCs seen in EM is the presence of extensive electron dense coats on the cytoplasmic aspects of the membrane (Pelchen-Matthews et al., 2012). These are morphologically distinct to clathrin coats and do not label with anti-clathrin antibodies. Detailed screening experiments showed these structures have features in common with focal adhesions, that is, they contain the integrin complex CD18/CD11b/c, as well as the focal adhesion proteins paxillin, talin and vinculin often in close association with filamentous actin. Several investigations have revealed that the cytoskeleton and the focal adhesion complex proteins are important in maintaining the integrity of the IPMCs (Gaudin et al., 2012; Pelchen-Matthews et al., 2012; Mlcochova et al., 2013). Depletion of CD18 results in the dispersal of the usually compact IPMCs and disappearance of the electron-dense coats. However, virus release was not significantly affected (Pelchen-Matthews et al., 2012). The dispersed IPMC

[2]Named after the four cysteine-rich in which it was initially identified: **F**ab 1, **Y**OTB, **V**ac 1 (vesicle transport protein), and **E**EA1 (early endosome antigen 1).

morphology has also been observed when latrunculin is used to depolymerise actin in MDM, and this is paralleled by increased virus release (Mlcochova et al., 2013). Furthermore, microtubule networks have been implicated in the maintenance of IPMCs, whereby kinesin KIF3A was reported to drive the transport of IPMCs towards the cell surface, thus facilitating virus release from macrophages (Gaudin et al., 2012).

It is currently controversial how IPMCs are formed (Chu et al., 2012a; Giese and Marsh, 2014). It has been suggested that the compartments form when HIV is tethered at the plasma membrane by tetherin/CD317/BST-2 (bone marrow stromal cell antigen 2) and subsequently phagocytosed by the macrophages (Chu et al., 2012a), in support of a previous study (Jouvenet et al., 2006). Tetherin is a glycoprotein made up of a short N-terminal transmembrane domain, an extracellular coiled-coil domain, and a C-terminal glycophosphatidylinositol lipid anchor (Malim and Bieniasz, 2012). It is interferon-α–inducible and can restrict several enveloped viruses by physically tethering newly assembled particles at the plasma membrane. However, HIV-1 has evolved to antagonise tetherin through its accessory protein, Vpu, which promotes proteasomal and/or lysosomal degradation of tetherin (Neil et al., 2008; Mangeat et al., 2009; Hotter et al., 2013; Venkatesh and Bieniasz, 2013). By using HIV-1 *vpu* mutants defective in counteracting tetherin, as well as depleting tetherin with siRNA, our group has demonstrated that tetherin is not required for the formation or maintenance of the IPMCs in primary human macrophages (Giese and Marsh, 2014). However, it is still not clear how IPMCs develop, nor the function of the compartment in infected cells.

1.6.3 Dendritic cells

Like macrophages, (DCs) are derived from haematopoietic progenitors and they reside in most lymphoid and non-lymphoid tissues (Section 1.6.2, Figure 1.11) (Geissmann et al., 2010; Hashimoto et al., 2011; Tsunetsugu-Yokota and Muhsen, 2013). DCs capture and present extracellular antigens to CD4+ T cells, and therefore initiate specific (adaptive) immune responses. For antigen presentation, DCs and CD4+ T cells form intimate supermolecular contacts called immunological synapses. (Dustin, 2014; Shimauchi and Piguet, 2014).

Although HIV infects DCs, these cells have low levels of CD4, CCR5 and CXCR4 molecules for HIV binding (Wu and KewalRamani, 2006). Dendritic cells exhibit two mechanisms of HIV transmission: *cis*-infection where the cells are productively infected; and *trans*-infection where DC-SIGN (dendritic cell-specific intercellular adhesion molecule-3- grabbing non-integrin) molecules on the surface of DCs capture the virus from the extracellular milieu, and transmit it to uninfected CD4+ T cells, without becoming infected themselves (Turville et al., 2004). EM studies of DCs have revealed deep invaginations of the plasma membrane, containing numerous virus particles (Garcia et al., 2005; Felts et al., 2010). This compartmentalised virus can be transferred through intimate contacts, the so-called virological synapses (VS), between donor and target cells. Some authors use distinct names for the cell contacts depending on whether the donor cell is infected or not, as in the case of DCs (Figure 1.14). Contacts made between uninfected donor and target cells have been dubbed infectious synapses, whilst those made between infected donor and target cells have been named VS (Tan and Sattentau, 2013).

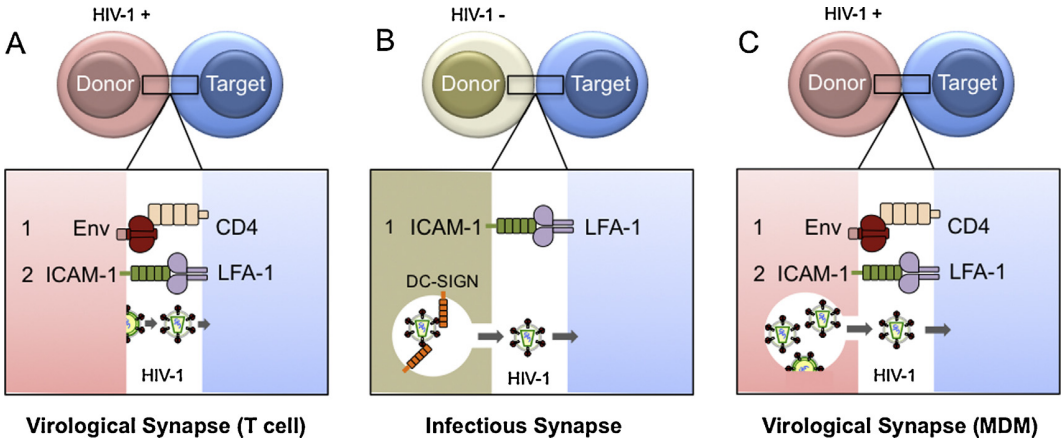

Figure 1.14: Cell contacts that facilitate HIV transmission.

(A) VS architecture (T cell). The primary signal for VS assembly is Env-CD4 binding. Subsequent stabilization is achieved by interactions between ICAM-1 and LFA-1. Virus buds at the interface and infects the target cell in a CD4-dependent manner. **(B)** Infectious synapse architecture (Dendritic cell). The synapse forms as cell adhesion molecules interact, resulting in release of mature HIV-1 virions from the surface-accessible virus-containing compartment into which mature HIV-1 particles were previously captured by various cell-surface molecules including DC-SIGN. **(C)** VS architecture (Monocyte-derived macrophage, MDM). DC-SIGN, dendritic cell-specific intercellular adhesion molecule-3- grabbing non-integrin; ICAM-1, intracellular adhesion molecule 1; LFA-1, lymphocyte function associated antigen 1. Taken from Schiffner et al. (2013)

1.7 HIV-1 pathogenesis

HIV-1 infections in humans has three distinct phases involving different pathogenic mechanisms: (1) acute/early infection; (2) chronic/asymptomatic infection; and (3) AIDS (Figure 1.15) (Simon and Ho, 2003; Maartens et al., 2014). The acute phase is observed in the first 2-3 weeks following infection. It is characterised by very high levels of viremia, and a transient but dramatic decline in the memory CD4+ T cells in the mucosal tissues. In both HIV and SIV early infections, the virus massively infects and depletes mucosal-associated lymphoid tissue (MALT) CD4+CCR5+ memory T cells (Derdeyn and Silvestri, 2005). The host then mounts a humoral immune response (sero-conversion), resulting in a decline in the viral load until it reaches a certain set point, and recovery in the CD4+ T cell count, which may differ between individuals and can be influenced by host factors and the virus genotype. A slow rate of lowering viremia and high viral set point are linked to higher level of proviral diversity in HIV-1C gp120, from zero to 200 days following sero-conversion (Novitsky et al., 2009), which may impact on disease progression in the absence of therapy.

The chronic infection phase that follows sero-conversion is characterised by a slow decline of CD4+ T cells in the peripheral blood. Chronic immune activation is believed to fuel the depletion of CD4+ T cells, thereby compromising host immunity. This depletion may be caused by (1) activated CD4+ T cells becoming new targets for HIV replication and cell death; and/or (2) disruption of cell cycle control, leading to activation-induced apoptosis. The chronic phase is variable, but generally long and asymptomatic. Chronic immune activation characterises progressive HIV infection, with circulating microbial products contributing to activation (Brenchley et al., 2006). The compromised immune system predisposes individuals to opportunistic infections, an aggregate of which may lead to death if untreated. It is the aggregate of these opportunistic infections and the decline in immunity that give rise to the clinical condition known as AIDS.

There is variation in the rate of disease progression in HIV infected people. Generally, AIDS manifests itself within 10 years in most HIV positive people, whilst about 1-5% do not develop AIDS until after about 15 years or more (Carrington et al., 2001). Many factors act in concert to determine progression rate. In addition to viral attributes, host

factors are important in disease progression (Carrington et al., 2001; Arenzana-Seisdedos and Parmentier, 2006). Though HIV is not a genetic disease, about 10% variation in disease progression in the United States, where HIV-1B is the predominant subtype, has been attributed to host genetics (O'Brien and Nelson, 2004). Therefore, both viral and host factors are important in the outcome of HIV-1 infections.

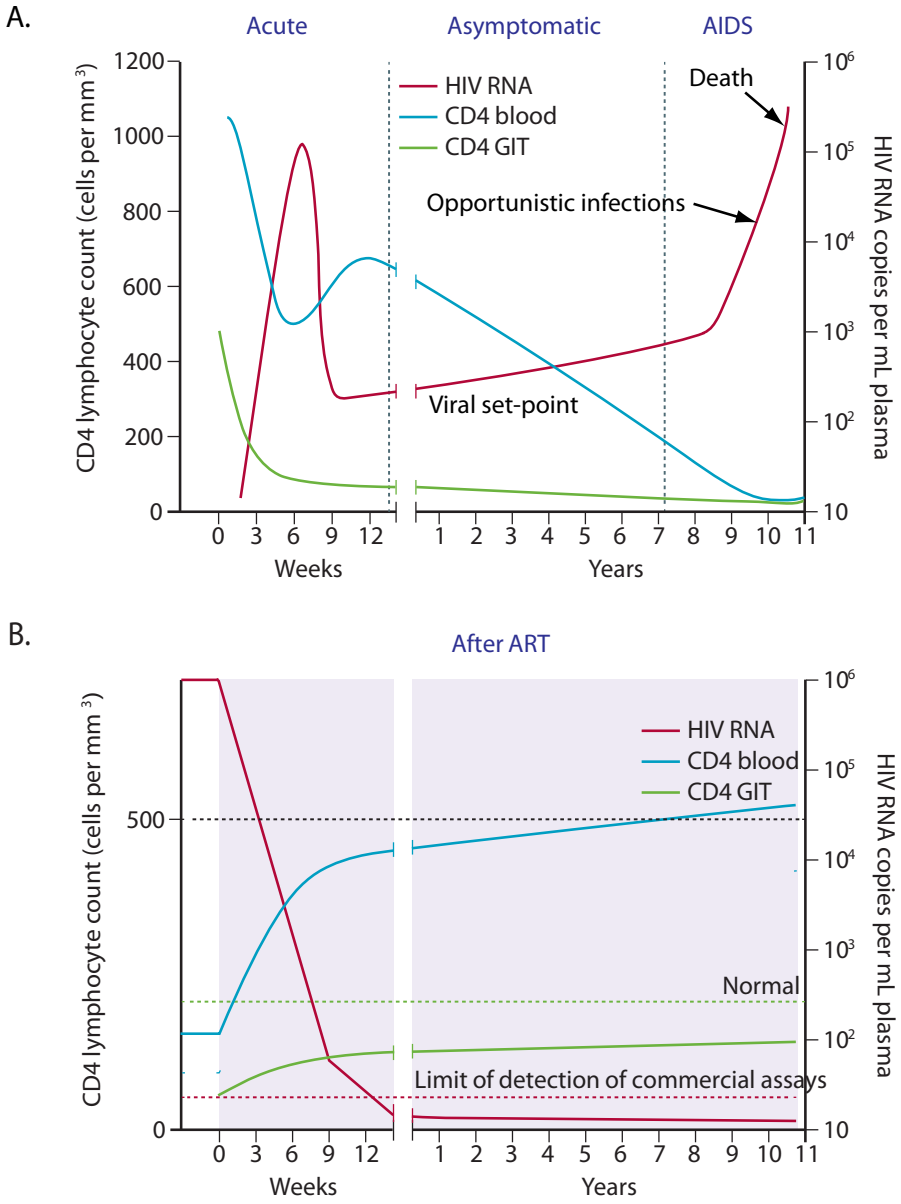

Figure 1.15: The natural course of untreated HIV-1 infection, and changes after anti-retroviral therapy (ART).

(A) In response to HIV infection, the body initially produces non-neutralising antibodies and HIV-specific CD4+ and CD8+ T cells, associated with a transient decline in HIV-1 RNA in the blood. **(B)** In the presence of ART, the viral load is reduced, with the subsequent recovery of the CD4+ T cells. GIT, gastrointestinal tract. Adapted from Maartens et al. (2014).

Currently, there is still no effective cure or vaccine for HIV infection. The most widely used treatment is a combination of three or more ART drugs that act on different viral targets, and that constitute what is known as highly active anti-retroviral therapy (HAART). The World Health Organisation recommends that individuals with CD4+ T cell count of ≤350 cells/mm^3 of blood should be initiated on HAART even if they are asymptomatic, whilst anyone else who has AIDS defining clinical conditions should be put on HAART irrespective of the CD4+ T cell count (WHO, 2013). Worldwide, about 12.9 million people received this treatment at the end of 2013, showing about 37% coverage of all the people who are living with HIV (UNAIDS, 2014). The aim of HAART is to reduce circulating virus (viral load) to undetectable levels, with the result that CD4+ T cell counts improve and disease progression is delayed. Despite the beneficial effects of the HAART, the emergence of drug-resistant HIV strains and drug toxicities are a great concern in the management of HIV infections (Doualla-Bell et al., 2006; Novitsky et al., 2007; Wester et al., 2009; MacLeod et al., 2010; Wester et al., 2010; Wester et al., 2012; Tourret et al., 2013). Thus, there is a continued need for new approaches to treat or prevent HIV replication. To this end, an increasing effort is being directed at understanding how HIV interacts with host cells, including macrophages, with the view that these might offer novel therapeutic targets.

1.8 Aims of this thesis

Several independent studies have shown that in macrophages HIV-1 buds into IPMCs. Currently it is not clear whether IPMCs are the only sites for HIV-1 assembly and budding in macrophages, or whether the cell surface is also used, as viruses that bud at the surface may dissociate (Figure 1.16) and be lost from the samples. Therefore, the main aim of this thesis was to examine in detail the sites where HIV assembles in primary human macrophages. This was achieved by modulating HIV-ESCRT interactions to arrest virus budding, thereby forming stable budding intermediates. The assembly sites for HIV-1 were then examined and quantitatively analysed to determine where HIV was enriched in macrophages.

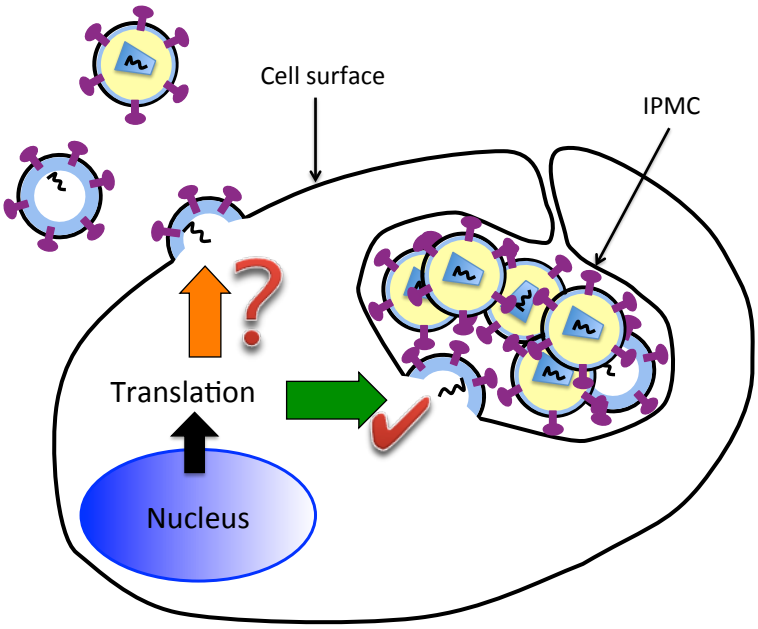

Figure 1.16: Schematic representation of HIV-1 budding in macrophages.
Several reports show that HIV-1 can be targeted (green arrow) to the IPMCs. Currently it is not clear whether and how much HIV is also targeted (orange arrow) to the cell surface in macrophages.

In Chapter 3, I investigated the requirement of the ESCRT machinery in HIV-1 budding in macrophages, as this has not been previously examined to any great extent in this cell type. Two approaches were used to achieve this: (1) using siRNA to deplete Tsg101 and ALIX in infected macrophages; (2) mutating the motifs that recruit Tsg101 and ALIX in HIV-1 Gag constructs or a full HIV-1 molecular clone. siRNA of the key ESCRT factors, Tsg101 and ALIX, had only limited effects on virus release. Therefore a second approach was developed, in which I disrupted the Gag-ESCRT interaction using HIV-1 mutants defective in ESCRT recruitment. Specifically, I generated full-length molecular clones of HIV-1 R3A where the Tsg101 and ALIX recruiting motifs were mutated to generate HIV-1 R3A PTAP^{-}, PTAP^{-}YP^{-} and Δp6. Inhibition of virus release was demonstrated biochemically in HEK 293T cells and in primary macrophages. This chapter therefore describes how I developed the tools that were later used to investigate HIV assembly in macrophages.

Chapter 4 describes the morphological characterisation of these HIV mutants (HIV-1 R3A PTAP^{-}, PTAP^{-}YP^{-} and Δp6) in HEK 293T cells. I used electron microscopy approaches to analyse the budding of these virus mutants. The mutants showed only arrested budding profiles, confirming that ESCRT recruitment is required to complete

HIV particle release. Furthermore, I developed approaches to rescue particle production for these mutants in order to produce infectious mutant virus stocks for the investigations in Chapter 5.

In Chapter 5, macrophages were infected with the virus mutants. Infected cells were immuno-labelled for HIV-1 Gag and imaged by confocal microscopy so that virus distribution could be determined quantitatively. On 77% of cells, I could only detect virus budding into IPMCs. To analyse the location of HIV assembly at higher resolution, viruses were also visualised by EM. Infected cells were identified using correlative on-grid immuno-labelling, and the distribution of the immature viruses was determined. I found that 97% of the viruses were in the IPMCs. Two-dimensional stereology was employed to estimate the area of plasma membrane associated with the IPMCs and with the cell surface. This revealed that HIV was highly enriched in the IPMCs. Together, the immunofluorescence and EM analyses demonstrate that in mature human MDMs, HIV-1 assembly is specifically targeted to IPMCs.

2. Materials and Methods

2.1 Antibodies and reagents

All chemicals were obtained from Sigma-Aldrich (Dorset, UK), media and supplements were obtained from Life Technologies (Paisley, UK), restriction enzymes and the DNA ladder were purchased from Promega (Southampton, UK), EM chemicals and supplies where procured from TAAB Laboratories (Reading, UK), unless otherwise specified. Tissue culture plasticware was obtained from Thermo Fisher Scientific (Cramlington, UK) or Techno Plastic Products AG (Trasadingen, Switzerland).

Table 2.1: List of antibodies used in this thesis

Antibody		Species and Isotype	Obtained from
HIV-1 proteins	Anti-p24 (Kal-1)	Mouse IgG1	Dako (Ely, UK)
	Anti-p24 (38:96K, ARP365)	Mouse IgG1	NIBSC Centre for AIDS Reagents (South Mimms, UK)
	Anti-p24 (EF7, ARP366)	Mouse IgG1	NIBSC Centre for AIDS Reagents (South Mimms, UK)
	Anti-p17 (4C9, ARP342)	Mouse IgG2a	NIBSC Centre for AIDS Reagents (South Mimms, UK)
	Anti-Nef (EH1)	Mouse IgG1	Jim Hoxie, University of Pennsylvania, PA, USA
	Anti-gp120 (2G12)	Human IgG1	NIBSC Centre for AIDS Reagents (South Mimms, UK)
Cell proteins	Anti-Adaptin-γ	Mouse	BD Biosciences (Oxford, UK)
	Anti-ALIX	Rabbit polyclonal	Wes Sundquist (University of Utah, Salt Lake City, USA)
	Anti-CD195	Mouse anti-human	BD Biosciences (Oxford, UK)
	Anti-CD14	Mouse anti-human	BD Biosciences (Oxford, UK)
	Anti-CD4	Mouse anti-human	BD Biosciences (Oxford, UK)
	Anti-CD3	Mouse anti-human	BD Biosciences (Oxford, UK)
	Anti-CD44 (MEM-85)	Mouse IgG2b	Abcam (Cambridge, UK)
	Anti-Tsg101 (M-19)	Goat IgG polyclonal	Santa Cruz Biotech. (Santa Cruz, USA)
	Anti-VDAC-1 (ab15895)	Rabbit IgG polyclonal	Abcam (Cambridge, UK)
Secondary Antibodies	Anti-Mouse IgG1 (A488)	Goat	Life Technologies (Paisley, UK)
	Anti-Mouse IgG2a (A568, A594, A647)	Goat	Life Technologies (Paisley, UK)
	Anti-Mouse IgG2b (A568, A594, A647)	Goat	Life Technologies (Paisley, UK)
	Anti-Mouse IgG (H+L)	Rabbit	Rockland, Gilbertsville (PA, USA)
	Anti-mouse IgG (H+L) A488	Rabbit	Life Technologies (Paisley, UK)
	Anti-Goat HRP	Donkey	Santa Cruz Biotech. (Santa Cruz, USA)
	Anti-Mouse HRP	Goat	Thermo Fisher Scientific (Cramlington, UK)
	Anti-Rabbit HRP	Goat	Thermo Fisher Scientific (Cramlington, UK)

2.2 Cells

2.2.1 Cell lines

HeLa cells were used to test small interfering RNA (siRNA) oligonucleotides before optimising the protein knockdown in primary human monocyte-derived macrophages (MDM). TZM-bl cells, a gift from J. Martin-Serrano (Kings College London, London, UK), were used to determine titres for virus stocks. The TZM-bl cells are a CXCR4-positive HeLa cell clone engineered to express β-Galactosidase, CD4 and CCR5 (Platt et al., 1998; Wei et al., 2002). HEK 293T (ATCC, Teddington, UK) cells were used for testing expression of molecular clone constructs.

To prepare new cultures, cells cryo-preserved in medium supplemented with 10% v/v dimethylsulfoxide (DMSO) and 20% v/v heat-inactivated foetal bovine serum (FBS) (PAA, Yeovil, UK) were retrieved from liquid nitrogen storage and thawed at 37°C. The cell suspension was added to 10 mL pre-warmed complete DMEM (that is, DMEM supplemented with 10% v/v FBS, 2 mM L-glutamine, 100 units/ml of penicillin and 100 μg/ml of streptomycin), centrifuged at 500 *g* for 8 min, and then resuspended in 10 mL medium. The suspension was plated in a 10-cm tissue culture dish and incubated at 37°C, 5% CO_2 until 70-80% confluency, before passage.

Adherent cells were normally trypsinised in 1 mL 0.05% v/v trypsin-EDTA. Cells were maintained in complete DMEM. As HEK 239T cells have poor adhesion to tissue culture surfaces, for experiments, they were plated on surfaces coated with 0.01% w/v sterile tissue culture grade poly-L-lysine. Poly-L-lysine is a polycation that enhances electrostatic interactions between negatively charged components of the cell membrane and the culture surface. The following tissue culture plate formats were used for both HEK 293T cells and HeLa cells: 6-well (4.2×10^5 cells/well in 3 mL medium), 12-well (0.75×10^5 cells/well in 500 μL) or 24-well (1.5×10^5 cells/well in 1mL).

2.2.2 Preparation of macrophages

Monocytes were isolated from peripheral blood mononuclear cells (PBMCs) by gelatine adherence and then differentiated to macrophages with macrophage-colony stimulating factor (M-CSF) and recombinant human interleukin-2 (IL-2), both purchased from R&D Systems (Abington, UK). PBMCs were isolated from buffy coats obtained from

healthy blood donors (National Blood Services, Essex, UK). The buffy coats (about 50 mL) were mixed with PBS (Life Technologies, Paisley, UK) at a ratio of 1:1. The diluted buffy coats were overlaid on 15 mL Lymphoprep (Alere, Stockport, UK) in 50-mL centrifuge tubes, and centrifuged at 930 *g* for 30 min at 20°C to separate components. The white PBMC layers were collected from the interface, washed in PBS and pelleted at 500 *g* for 8 minutes. The cells were resuspended in RPMI 1640 supplemented with 10% v/v human serum (HS) and plated on 15-cm tissue culture dishes coated with 2% w/v gelatine. For the monocytes to adhere to the gelatine coating, the plates were incubated for 2 hrs at 37°C, 5% CO_2. The plates were washed in RPMI 1640 to remove unattached monocytes. Fresh RPMI with 10% v/v HS was added, and the plates were left to incubate overnight.

The next day, cells from each donor were pooled into a 50-mL centrifuge tube, and 5 mM EDTA (ethylenediaminetetraacetic acid) in PBS was added to plates to detach the remaining cells. The cells were then washed once in PBS by centrifugation as described above. Cells were resuspended in RPMI 1640 and enumerated using the Scepter automated counter (Millipore, Watford, UK). A small aliquot of the cells was set aside for routine analysis of the monocytes for surface markers CD4, CD3, CD14 and CCR5 by flow cytometery (Figure 2.1). CD14 is a marker for monocytes, whilst CD3 is a maker for T cells. CD4 and CCR5 are the receptor and co-receptor, respectively, required for HIV binding and entry into cells.

Prior to immunostaining, non-specific binding of antibodies to Fc receptors on the cells needed to be blocked. To this end, cells were maintained in FACS block (PBS, 1% v/v FBS, 0.05% v/v Na Azide, 6 µg/mL Human IgG) at 4°C for 30 min. A mixture of antibodies (90 µL FACS block, 45 µL anti-CD3-PerCP, 45 µL anti-CD4-FITC, 45 µL anti-CD14-APC, 45 µL anti-CCR5-PE) was prepared and 100 µL of the mixture was added to washed cells. Washes were performed in 100 µL FACS buffer (PBS, 1% v/v FBS, 0.01% v/v Na Azide) by centrifugation at 500 *g*. The cells were incubated on a shaker at 4°C for at least 1 hr. Washed cell were resuspended in FACS buffer for analysis with the FACSCalibur flow cytometer (BD Biosciences, Oxford, UK) and the FlowJo software (TreeStar, Ashland, USA) (Figure 2.1).

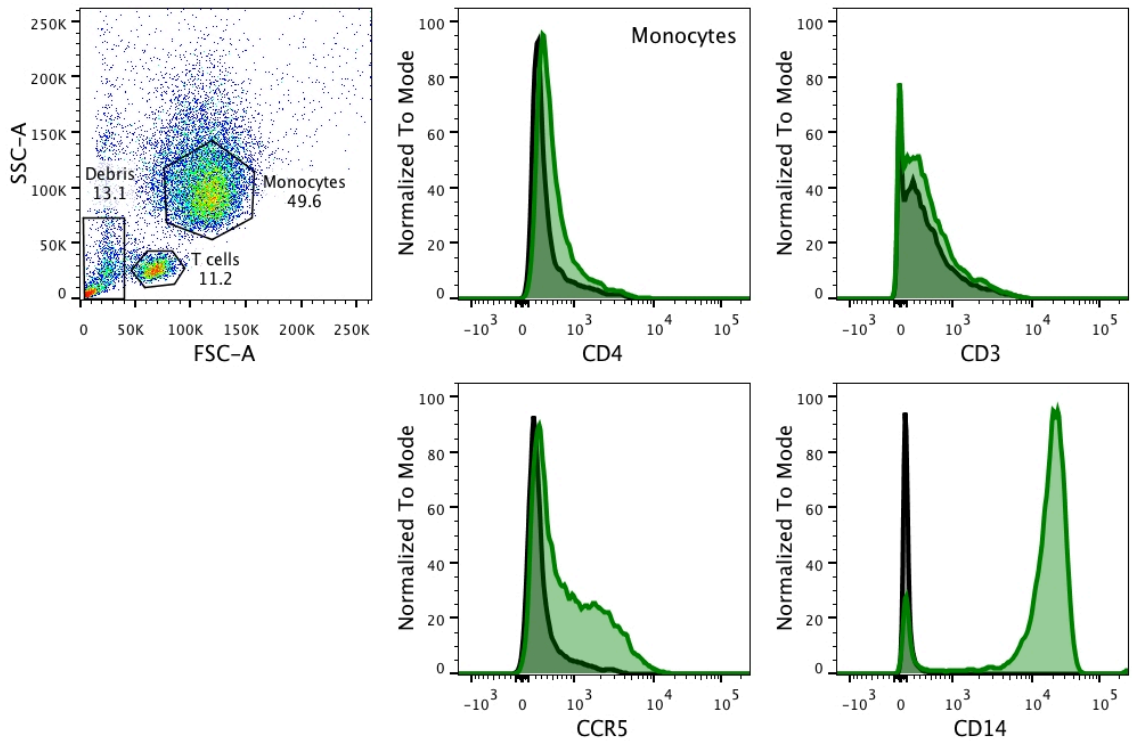

Figure 2.1: A typical analysis of monocytes for cell surface markers.

Monocytes were isolated from PBMCs and analysed for the expression of CD3, CD4, CCR5 and CD14. The dot plot on the left shows gating on populations of T cells and monocytes labelled with antibodies coupled to different fluorochromes against the makers indicated on the axis of the histograms. The proportions of cells in the cell suspension are also indicated, for example, 49.6% of the cells were monocytes. The green curves show expression levels of the markers, whilst the black curves show unlabelled control cells.

Different densities of cells were plated in tissue culture plates and dishes according to experimental requirements: $5x10^6$ cells per 25 cm^2 flasks; $2x10^6$ cells per 6-well (9 cm^2); $1x10^6$ cells per 12-well (3.8 cm^2) and $0.4x10^6$ cells per 24-well (1.9 cm^2). Where required, coverslips were placed in the wells before seeding. The cells were incubated for 2 hrs at 37°C, and medium was changed to add RPMI 10% HS containing 10 ng/mL M-CSF and 5 ng/mL IL-2. The cultures were incubated for 2 days at 37°C before replacing the M-CSF-containing medium with RPMI 10% HS, and adhered monocytes were allowed to differentiate into monocyte-derived macrophages (MDM) until used for experiments, 7-8 days after isolation.

2.3 Virus preparation

2.3.1 HIV-1 BaL WT

HIV-1 BaL is an R-5 tropic strain, originally isolated from lung tissue of an HIV infected patient in 1986 (Gartner et al., 1986). The initial stock of the virus used in this thesis was obtained from R. Shattock, St. George's Hospital, London, UK. To make virus stocks, PBMC-grown HIV-1 BaL was used to inoculate MDM in 25 cm^2 flasks. Culture supernatants were collected every 3 to 4 days, and cleared of cell debris by centrifugation at 500 *g* for 8 min. Virus aliquots were frozen and stored in liquid nitrogen until required.

2.3.2 Determination of virus titres

Infectious virus titres were measured on TZM-bl cells. The cells were seeded in 96-well plates at 2 x 10^4 cells/well in 100-µL complete DMEM, and grown overnight. The cells were infected by spinoculation (centrifugation at 1,300 *g* and 25°C for 2 hrs) with 100 µL of serially diluted virus. Spinoculation enhances CD4-dependent binding of HIV-1 to cells (O'Doherty et al., 2000). A virus stock of known titre (in focus forming units [FFU/mL]) was used as a standard. After 24 hrs of incubation of the infected cultures, the Galacto-Star Reporter Gene Assay System (Life Technologies, Paisley, UK) was used to quantify β-Galactosidase activity in cell lysates, according to the manufacturer's instructions (Figure 2.2). The luminescence (expressed as relative light units [RLU]) was read using the PHERAstar Plus microplate reader (BMG LABTECH, Aylesbury, UK).

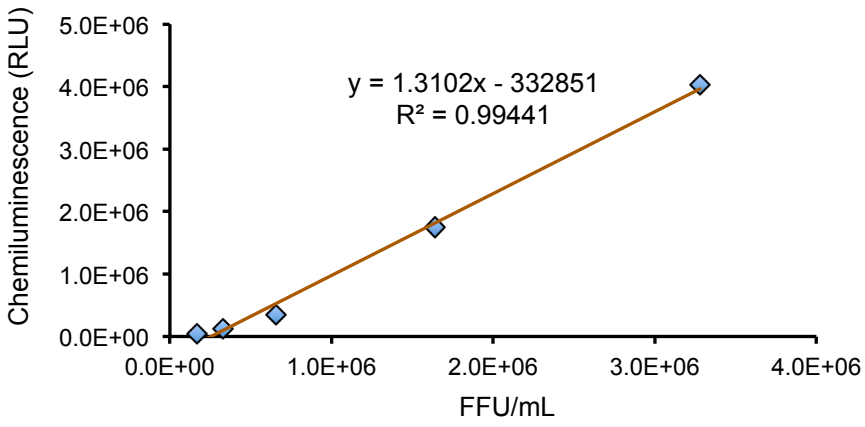

Figure 2.2: A typical standard curve for the reference virus (HIV-1 BaL).
The standard curve was used to calculate titres in newly prepared virus stocks.

2.4 Infection of MDM with HIV-1

MDM in tissue culture plates were infected with HIV-1 WT and mutant viruses at 3 and 6 focus forming units per cell (FFU/cell), respectively, by spinoculation and incubated for 24 hrs. The culture media were replaced with fresh media and incubated further, according to the experimental requirements, or transfected with siRNA oligonucleotides.

2.5 siRNA transfections

To deplete the ESCRT/ESCRT-associated proteins, Tsg101 and ALIX, HIV-1-infected MDM were transfected with the respective siRNA, using Lipofectamine™ RNAiMAX (Life Technologies, Paisley, UK) as the transfection reagent. To prepare the transfection complex, 60 nM of duplex siRNA oligonucleotides (Table 2.2) were mixed with 8 µL Lipofectamine™ RNAiMAX in Opti-MEM reduced serum medium to a total volume of 250 µL, for one well in a 12-well plate. Cultures were incubated at 37°C, 5% CO_2. The virus and cells were harvested 6 days after siRNA transfection. I had determined that the proteins were optimally depleted on day 6, by setting up two parallel cultures transfected with either 60 or 90 nM of Tsg101 siRNA oligonucleotides per experiment, and incubating one set-up for 3 days, and other for 6 days. Protein levels were analysed by western blotting and quantified as shown in Figure 2.3. The optimal conditions for the depletion of Tsg101 were also optimal for ALIX depletion in MDM.

Table 2.2: siRNA used to deplete Tsg101 and ALIX

	Sequences (5' to 3')	Supplier
Tsg101	GCAUGUACGUCUUCUGUCCCGUAAA UUUACGGGACAGAAGACGUACAUGC	Life Technologies (Paisley, UK)
ALIX	CCAGAGAACCUAGUGCUCCUUCAAU AUUGAAGGAGCACUAGGUUCUCUGG	

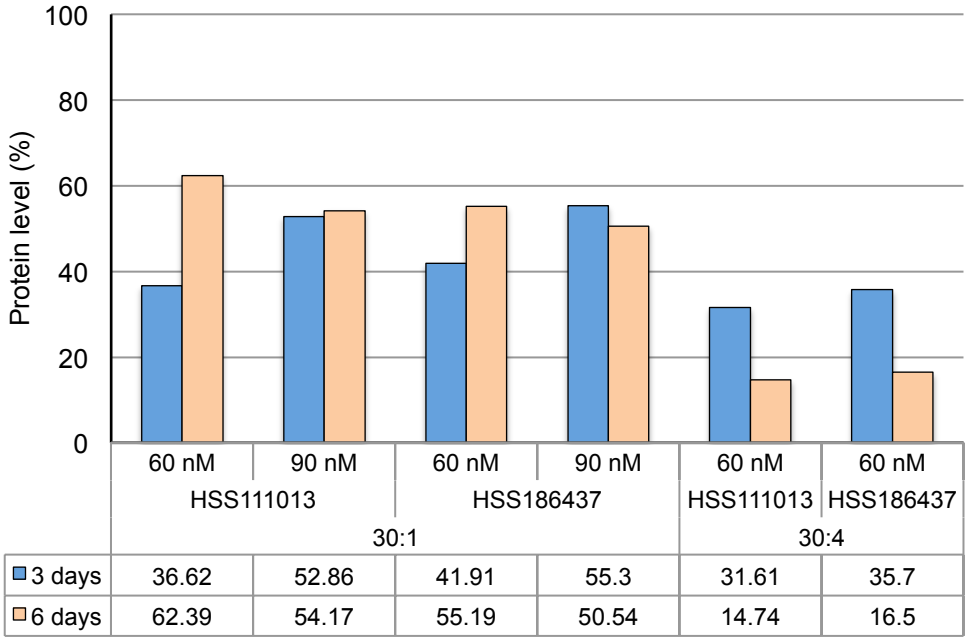

Figure 2.3: Optimisation of Tsg101 depletion in MDM.

Different Tsg101 siRNA oligonucleotides (sequence ID numbers: A = HSS111013; and B = HSS186437) were tested in MDM at 60 and 90 nM. Two parallel experiments were set-up and incubated for 3 and 6 days each. The protein level was depleted when the transfection siRNA and RNAiMAX were used at a ratio of 30:4, and incubated for 6 days. Notably, the residual protein levels are still high on day 3 post-transfection, and this may be sufficient to support virus release and accumulation in the IPMCs before day 6.

2.6 Plasmid DNA transfections

In this thesis, introducing plasmid DNA into cell lines using the reagent-based transfection method is simply referred to as transfection. This method was used to transfect HEK 239T or HeLa cells with the constructs shown in Table 2.3. Cells were seeded a day prior to transfection. Briefly, plasmid DNA and FuGENE HD transfection reagent (Roche, Welwyn Garden City, UK) were mixed at a ratio of 1:3 [µg DNA:µl FuGENE HD] in OptiMEM to form transfection complexes, and incubated for 15 min at room temperature, before adding to cell cultures. Transfected cultures were incubated for 24 to 48 hrs as required.

Table 2.3: List of plasmids used in this thesis

Name	Obtained from
pCMS28-mCh-Alix	J. Martin-Serrano (Kings College London, London, UK)
pCR3.1 HA-Alix	J. Martin-Serrano (Kings College London, London, UK)
pGag-EGFP WT and PTAP^{-}	Wesley Sundquist (University of Utah, Salt Lake City, USA)
pGFP-VPS4 WT and EQ	Adrian Isaacs (University College London, London, UK)
pNL4.3-R3A WT	Jim Hoxie (University of Pennsylvania, Philadelphia, USA)
pNL4.3-R3A PTAP^{-}, YP^{-}, PTAP^{-}YP^{-}, & Δp6	This thesis
pRK5Gag$_{BaL}$ WT	Marsh Lab, UCL
pRK5Gag$_{BaL}$ PTAP^{-}, YP^{-}, PTAP^{-}YP^{-}	This thesis

2.7 Nucleofection/Electroporation

Nucleofection or electroporation is an instrument-based transfection method. The procedure was used to introduce plasmids into macrophages because this cell type is difficult to transfect using reagent-based methods (Stacey et al., 1993). Using an empty pmaxGFP vector, I had determined that the transfection efficacy of primary macrophages varied between 15 and 35% for cells from different blood donors. Monocytes were differentiated into macrophages for 14 days so that IPMCs can develop before electroporation (Pelchen-Matthews et al., 2012; Mlcochova et al., 2013). The cells were washed in PBS, incubated on ice to detach, resuspended in PBS and counted. The suspended cells (10^6 cells) were pelleted and, mixed with plasmid DNA (10 μg HIV-1 plasmid; 5 μg other plasmid DNA), and electroporated using the Amaxa Human Macrophage Nucleofector Kit and Amaxa Nucleofector II device (Lonza, Kent, UK). Electroporated cells were replated and incubated for 24 hrs at 37°C, 5% CO_2.

2.8 Western blotting

Western blotting (or immunoblotting) was carried out to analyse cells for the expression of specific proteins. Cell cultures were washed in PBS and lysed in Laemmli sample buffer (Sigma-Aldrich, Dorset, UK). For viruses or virus-like particles (VLPs) released into culture supernatants, the medium was first centrifuged to pellet cell debris. To concentrate viruses or VLPs, the supernatant was overlaid on a 20% w/v sucrose cushion, and centrifuged at 100,000 *g* for 2 hrs at 4°C. The viruses or VLPs were lysed in Laemmli sample buffer. All lysates were heated at 95°C for 10 min, under β-mercarptoethanol reducing conditions.

Proteins in lysates were resolved using sodium dodecyl sulphate polyacrylamide gel electrophoresis (SDS-PAGE). Separated proteins were transferred to an Immobilon-P polyvinylidene diflouride membrane (PVDF) (Millipore, Watford, UK) using the Trans-Blot SD Semi-Dry Transfer Cell (Bio-Rad, Hemel Hempstead, UK). The blots were blocked with blocking buffer (PBS, 0.1% v/v Tween, 5% w/v milk powder [Premier Foods, St. Albans, UK]) for 1 hr at room temperature, and incubated overnight at 4°C with the appropriate primary antibodies. All antibodies were prepared in blocking buffer. The antibodies were washed off in 0.1% v/v Tween in PBS. The blots were incubated for 1 hr with Horseradish peroxidase (HRP)-conjugated secondary antibodies (Table 2.1) and washed off. Subsequently, membranes were incubated for 5 min in SuperSignal® West Dura Extended Duration Substrate (Thermo Scientific, Rockford, IL, USA), and chemiluminescence was detected using ImageQuant LAS400 mini (GE Healthcare UK Limited, Buckinghamshire, UK). Signal intensities were quantified using ImageJ software (Open Access).

To quantify band signals on western blots, the integrated density (sum of the values of the pixels in the image or selection) was divided by the area (area of selection in square pixels), using ImageJ. HIV release efficiency was calculated using equations 1 and 2 for MDM and HEK 293T cells, respectively. The release efficiency of VLPs from HEK 239T cells was calculated using equation 3.

Equation 1 (for MDM):

$$\text{Virus release efficiency (\%)} = \frac{\text{p24c} + \text{p24v} + \text{p55v}}{\text{p24c} + \text{p55c} + \text{p24v} + \text{p55v}} \text{ x } 100\%$$

Where: p24c is cell-associated p24
p55c is cell-associated p55
p24v is virion p24
p55v is virion p55

Because in macrophages HIV accumulates in IPMCs, viral p24 in cell lysates represents mature virus that is detached from the host membrane.

Equation 2 (for HEK 293T cells):

$$\text{Virus release efficiency (\%)} = \frac{\text{p24v} + \text{p55v}}{\text{p24c} + \text{p55c} + \text{p24v} + \text{p55v}} \text{ x } 100\%$$

For the HIV-1 Δp6 mutant that produces a truncated Gag polyprotein, the p55Δp6 band was used for the calculations.

Equation 3 (for HEK 293T cells):

$$\text{VLP release efficiency (\%)} = \frac{\text{p55vlp}}{\text{p55c}} \text{ x } 100\%$$

Where: p55vlp is VLP p55
p55c is cell-associated p55

2.9 Mutagenesis and subcloning

2.9.1 Site-directed mutagenesis

To generate mutants of Gag or an HIV-1 full molecular clone, site-directed mutagenesis was performed using the QuikChange® Site-Directed Mutagenesis Kit (Agilent Technologies, Wokingham, UK) following the manufacturer's instructions. Briefly, a 50-µL polymerase chain reaction (PCR) was set up containing 20 ng template plasmid, 100 ng/µL of each primer, high-fidelity *PfuTurbo* DNA polymerase, dNTPs, reaction buffer and nuclease-free sterile water. The PCR was performed in a Biometra T1 Thermocycler (Thistle Scientific, Glasgow, UK) with the following conditions: a 30-sec denaturation step at 95°C, followed by 18 cycles of 95°C for 30 sec, 50°C for 1 min, and 68°C (1 min per kb length of plasmid). The reaction products were cooled down and held at 4°C. The parental double-stranded DNA was digested at 37°C for 1 hr with DpnI endonuclease, which targets methylated and hemimethylated DNA. *E. coli* XL10 Gold Ultracompetent cells (Agilent Technologies, Wokingham, UK) were transformed with the mutated DNA plasmid.

2.9.2 Polymerase chain reaction

To amplify fragments of plasmids for subcloning, PCR was carried out using Phusion polymerase (New England Biolabs, Hitchin, UK). The PCR reaction mixture contained 10 pmol of each primer, dNTPs, Phusion HE buffer containing 1mM $MgCl_2$, and Phusion Hot Start DNA Polymerase. The following PCR conditions were used: a 30-sec denaturation step at 98°C, followed by 30 cycles at 98°C for 10 sec (denaturation), 60°C for 30 sec (annealing), 72°C for 30 sec per kb (extension), and a final extension for 10 min at 72°C. The reaction was held at 4°C. The products were purified using the QIAquick PCR Purification Kit (QIAGEN, Manchester, UK), according to the manufacturer's instructions.

2.9.3 Restriction enzyme digestion of DNA

To generate inserts and vectors for subcloning, PCR products or DNA plasmids were digested with the appropriate restriction enzymes. Digestions were performed in a 20-µL-reaction volume containing 1 µg DNA, 2 µL of 10X reaction buffer, 0.2 µL acetylated bovine serum albumin (10 µg/uL) supplied with the restriction enzyme, and nuclease free water. These were scaled up or down as required. The mixture was incubated at 37°C for 1-2 hrs.

Digestion products were separated on 0.8% w/v agarose gels (Life Technologies, Paisley, UK) with 0.5 µg/mL of ethidium bromide (Life Technologies, Paisley, UK) in Tris-acetate-EDTA buffer (National Diagnostics, Atlanta, USA). The insert and vector DNA bands were cut and extracted from the gel using the QIAquick gel extraction kit (QIAGEN, Manchester, UK), according to the manufacturer's instructions.

2.9.4 Ligation

To construct plasmids by subcloning, vectors and inserts made by restriction digestion were ligated at 1:3 molar ratio using the LigaFast™ Rapid DNA Ligation System (Promega, Southampton, UK). Ligation reactions consisted of 100 ng vector and 88 ng insert, mixed with 5 µL 2X Rapid ligation buffer and 3 units T4 DNA ligase. Reaction volumes were made up to 10 µL. The ligation products (2 µL) were used to transform XL10 Gold Ultracompetent cells.

2.9.5 Transformation of competent cells with DNA plasmids

2.9.5.1 XL10 Gold Ultracompetent cells

All plasmids, except the full molecular clone of HIV-1, were produced through the transformation of XL10 Gold Ultracompetent cells, according to the manufacturer's instructions. Briefly, competent cells (100 µL) were added to pre-chilled 14-ml BD Falcon polypropylene round-bottom tubes on ice. 10 ng of plasmid DNA or 2 µL of ligation reaction was added to the cells on ice. The cells were incubated for 30 min on ice, and heat-pulsed in a water bath at 42°C for 30 sec. To stimulate the cells, SOC (Super Optimal broth with Catabolite repression) medium was added to the cells and incubated at 37°C for 1 hr, with shaking at 225-250 rpm. The transformation mixture (≤ 200 µL) was plated on Luria-Bertani (LB) agar (Sigma-Aldrich, Dorset, UK) containing the appropriate selection antibiotic, and incubated at 37°C for 16 hrs. Colonies were picked to inoculate LB broth (Sigma-Aldrich, Dorset, UK) supplemented with an appropriate antibiotic. The cultures were incubated at 37°C for 16 to 24 hrs.

2.9.5.2 NEB 10-beta competent cells

To produce HIV-1 full molecular clone plasmids for transfections, NEB 10-beta cells (New England Biolabs, Hitchin, UK) were transformed with HIV-1 plasmids from ligation reactions, following the manufacturer's protocol. Briefly, DNA (2 µL) from HIV-1 R3A ligation reactions was added to 50 µL of cells in chilled 14-mL round-bottom polypropylene tubes. The mixture was incubated on ice for 30 min, and then heat shocked (42°C for 30 sec). The cells were stimulated in SOC medium (30°C for 90 min, shaking), plated on LB agar and incubated for 24 hrs at 30°C. Bacteria colonies were picked and grown in Terrific broth (Sigma-Aldrich, Dorset, UK).

2.9.6 Purification of DNA plasmids

DNA plasmids were purified from bacteria grown in broth on a small scale (5 mL) using the QIAprep MiniPrep kit, or on large scale (100 mL) using the Endofree Plasmid Maxi (QIAGEN, Manchester, UK). The plasmids were purified according to the manufacturer's instructions, and quantified with the NanoDrop spectrophotometer (Thermo Fisher Scientific, Cramlington, UK). The plasmids were verified by restriction enzyme digestion, and/or DNA sequencing carried out through Source Bioscience

(Cambridge, UK) with the following platform: Applied Biosystems 3730xl using Big Dye Terminator v3.

2.9.7 Generation of Gag mutants

2.9.7.1 Native Gag $_{BaL}$

The pRK5Gag$_{BaL}$ used in this study was derived from HIV-1 BaL by B. Kramer, a former PhD student in the Marsh Group. Primers (Table 2.4) PTAP_FWD and PTAP_REV were used to change the PTAP to LIRL, and YP_FWD and YP_REV were used to change the YP in the YPXnL motif to SR, using site-directed mutagenesis (Section 2.9.1), thereby generating single and double mutants: pRK5Gag$_{BaL}$ PTAP^{-}, YP^{-} and PTAP^{-}YP^{-}. XL10 Gold Ultracompetent cells were transformed with the plasmids that were purified with Qiagen kits (Section 2.9.6).

Table 2.4: Oligonucleotide sequences used for mutagenesis and regular PCR

	Sequences (5' to 3')	Supplier
Primers		
PTAP FWD	TCAGAGCAGACCAGAGCTAATACGCCTACCAGCCCCACCAGAGG	Sigma-Aldrich (Dorset, UK)
PTAP REV	CCTCTGGTGGGGCTGGTAGGCGTATTAGCTCTGGTCTGCTCTGA	
YP FWD	CTGATAGACAAGGAACTGTCTCGTTTAGCTTCCCTCAGATCA	
YP REV	TGATCTGAGGGAAGCTAAACGAGACAGTTCCTTGTCTATCAG	
YP_HXB2_FWD	CCGATAGACAAGGAACTGTCTCGTTTAACTTCCCTCAGATCA	
YP_HXB2_REV	TGATCTGAGGGAAGTTAAACGAGACAGTTCCTTGTCTATCGG	
R3A_PTAP FWD	TTTTCTTCAGAGCAGACCAGAGCTAATACGCCTACCAGAAGAGAGCTTCAGGTTTG	Eurofins, (Ebersberg, Germany)
R3A_PTAP REV	CAAACCTGAAGCTCTCTTCTGGTAGGCGTATTAGCTCTGGTCTGCTCTGAAGAAAA	
R3A_YP FWD	CGATAGACAAGGAACTGTCTCGTTTAGCTTCCCTCAGATC	
R3A _YP REV	GATCTGAGGGAAGCTAAACGAGACAGTTCCTTGTCTATCG	
R3A_p6Del FWD	CCCACAAGGGAAGGCCAGGGAATTTTTAACAGAGCAGACCAGA	
R3A_p6Del REV	TCTGGTCTGCTCTGTTAAAAATTCCCTGGCCTTCCCTTGTGGG	
GAG1 (Fwd)	CCGCCCCATTGACGCAAATGGGCGGTAGGCG	
GAG2 (Rev)	CCCCCGCGGCCGCCTATTGTGACGAGGGGTCGTTGCC	

2.9.7.2 Codon-optimised Gag

The codon-optimised GagGFP WT and PTAP^{-} were gifts from Wes Sundquist (University of Utah, Salt Lake City) (Garrus et al., 2001), but the GagGFP WT was originally provided by Marylin Resh (Hermida-Matsumoto and Resh, 2000). To

generate codon-optimised Gag without the GFP tag (Figure 2.4), a forward primer (GAG1) (Table 2.4) was designed upstream of Gag, whilst the reverse primer was designed downstream of Gag (GAG2) but upstream of the GFP tag (Table 2.4), with the inclusion of sequences that would introduce a stop codon and NotI restriction site at the end of Gag. The Gag fragment (WT or PTAP^{-}) in the pGagGFP plasmid was amplified by PCR to generate Gag without the GFP tag, PCR products were purified and digested with XhoI and NotI restriction enzymes. Similarly, the pGagGFP was digested with XhoI and NotI restriction enzymes to remove the GagGFP, thereby generating the pCMV vector backbone. The vector and inserts were ligated with LigaFast reagents (Section 2.9.4). The ligation reaction was used to transform XL10 Gold Ultracompetent cells, and the plasmids were purified (Section 2.9.6) and verified by restriction enzyme digestion (Figure 2.5).

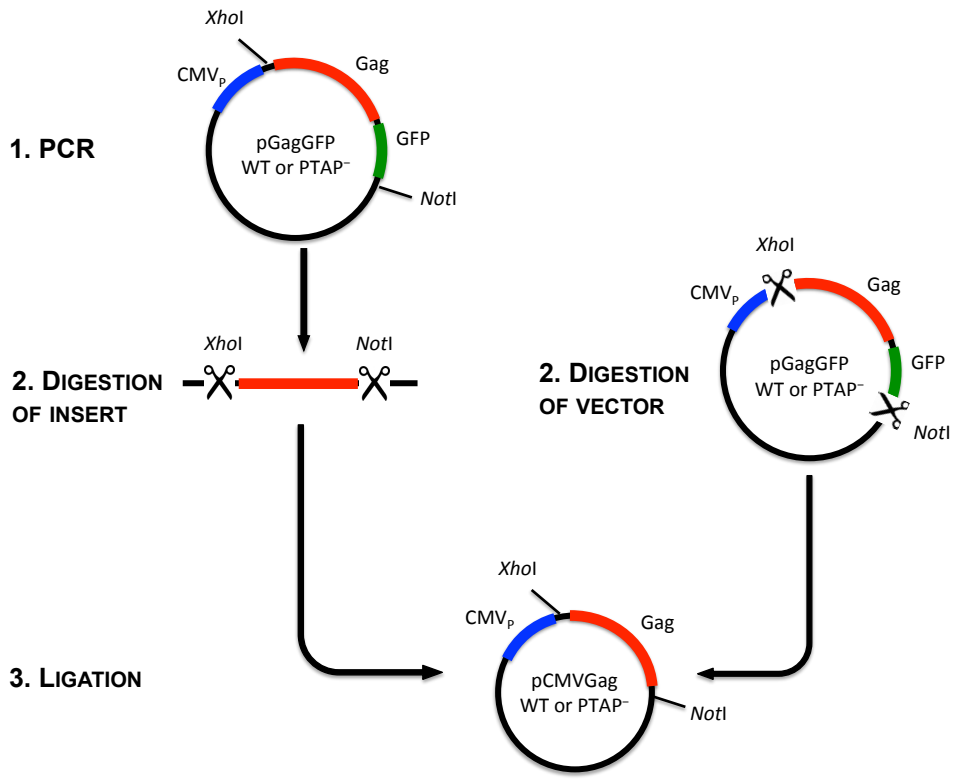

Figure 2.4: Schematic representation for the generation of pCMVGag constructs.
(1) A Gag fragment (WT or PTAP^{-}) in the pGagEGFP plasmid was amplified by PCR to generate Gag without GFP. (2) The purified Gag PCR product was digested with XhoI and NotI restriction enzymes to generate an insert. In parallel, pGagGFP was digested with the same enzymes to remove the GagGFP, thereby generating a vector that was named pCMV. (3) The Gag fragment was subcloned into the pCMV, generating a new plasmid, the pCMVGag (WT or PTAP^{-}). Site-directed mutagenesis was performed on the WT to generate YP^{-}, or PTAP^{-} to generate PTAP^{-}YP^{-}.

To generate other mutants, primers (YP_HXB2_FWD and YP_HXB2_REV) were designed and used to mutate the pCMVGag WT and PTAP^{-} to pCMVGag YP^{-} and PTAP^{-}YP, respectively, following the site-directed mutagenesis procedure described above. Plasmids were purified as above.

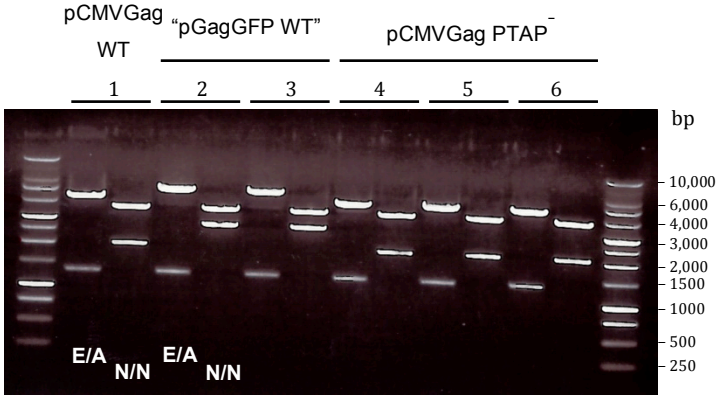

Figure 2.5: Restriction analysis of pCMVGag to verify plasmids.
Six plasmids were digested with either EcoRI and ApaI (E/A), or NdeI and NotI (N/N) pairs of restriction enzymes, and loaded in alternating lanes of an 0.8% agarose gel. Enzyme pairs, E/A or N/N, are shown at the bottom of lanes for the first two plasmids. Plasmids 1 and 4-6 have the expected digestion fragments for pCMVGag, whilst plasmids 2 and 3 have bands similar to digesting pGagGFP WT, which was originally used to generate the vector. 1 kbp DNA ladder was used (first and last lanes).

2.9.8 Generation of HIV-1 R3A mutants

HIV-1 R3A is a chimeric virus derived from the backbone of the NL4.3 molecular clone and *env* from the R3A strain (Meissner et al., 2004). Its plasmid, pNL4.3-R3A, was digested with EcoRI and ApaI restriction enzymes, to generate an insert with the entire p6 subdomain for subcloning. The digests were separated on agarose gel. The EcoRI/ApaI DNA fragment was extracted from the gel and quantified. Similarly, the cloning vector pEGFP-N1 was digested with EcoRI and ApaI restriction enzymes, run on an agarose gel, extracted, purified and the DNA quantified.

Ligation of the insert (EcoRI/ApaI fragment) and vector (pEGFP-N1) was carried out to generate a carrier plasmid (Figure 2.6). XL10 Gold Ultracompetent cells were transformed with the carrier plasmid. The plasmid was purified, and verified by restriction digestion. Mutagenesis was performed on the carrier plasmid, mutating the PTAP to LIRL (primers: R3A_PTAP FWD and R3A_PTAP REV), and YP to SR

(primer: R3A_YP FWD and R3A_YP REV). To truncate the p6 subdomain, R3A_p6Del FWD and R3A_p6Del REV primers were used to introduce a stop codon at the beginning of the p6 subdomain. XL10-Gold Ultra-competent cells were transformed with the mutagenesis products. DNA plasmids were purified and sequenced to confirm the mutations.

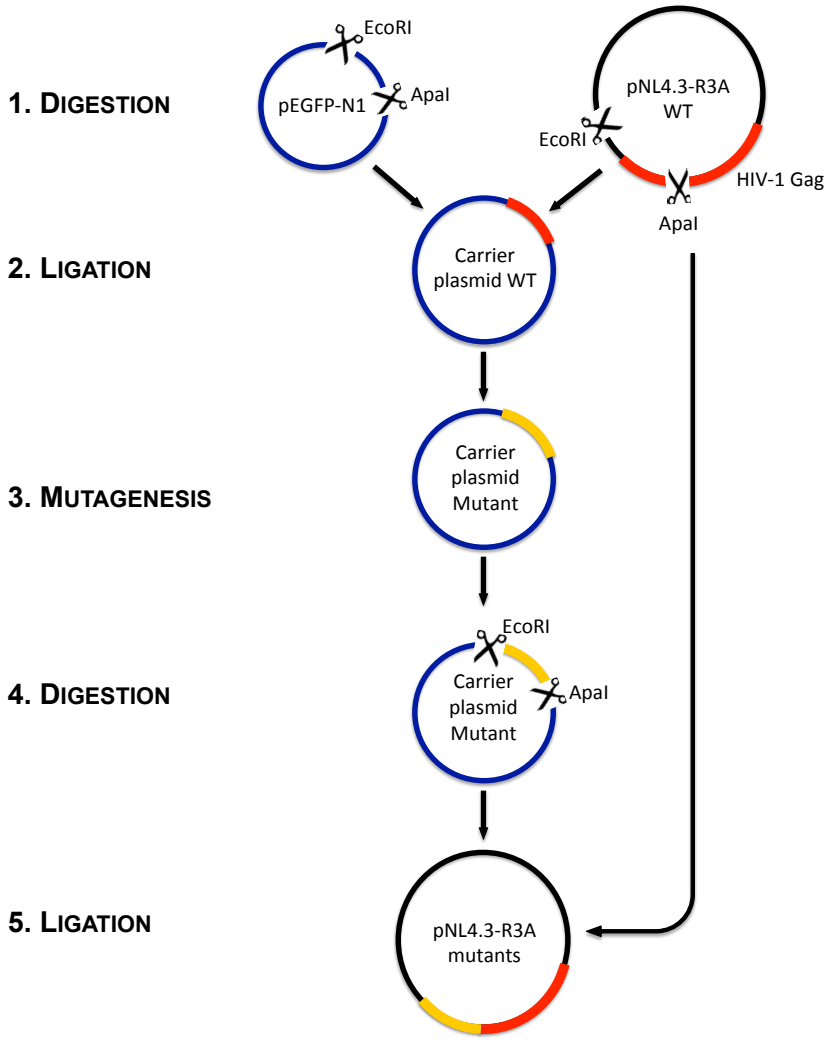

Figure 2.6: Schematic representation of how the HIV-1 R3A mutants were generated.
(1) Plasmids pEGFP-N1 and pNL4.3-R3A (WT Gag in red) were digested with EcoRI and ApaI restriction enzymes. The EcoRI/ApaI fragment from pNL4.3-R3A contained the entire p6 subdomain. (2) The fragment was subcloned into the EcoRI/ApaI digested site of pEGFP-N1. (3) The new plasmid, carrying the EcoRI/ApaI fragment from pNL4.3-R3A (hereafter, called "carrier plasmid") was mutagenised at the PTAP and YP residues. Alternatively, a stop codon was introduced at the beginning of p6. Mutants are represented in yellow. (4) The mutagenised carrier plasmids were digested to excise the EcoRI/ApaI fragments. (5) These fragments were used to substitute for the WT fragments in the pNL4.3-R3A.

To generate pNL4.3-R3A YP$^-$, PTAP$^-$, PTAP$^-$YP$^-$ and Δp6 mutants, the mutated carrier plasmids were digested with the EcoRI and ApaI restriction enzymes to generate inserts for substituting similar fragments in the pNL4.3-R3A WT. Here, ligation of the insert and vector was carried out using T4 DNA ligase reagents from NEB. Each ligation reaction contained 2 µL of 10X T4 DNA ligase buffer, 50 ng vector DNA, 17 ng insert DNA, 1 µL T4 DNA ligase. The reaction was made up to a final volume of 20 µL with nuclease free water, and then incubated at room temperature for 20 min before transformation of NEB 10-beta competent cells. Purified plasmids were confirmed by restriction enzyme digestion.

2.10 Production of HIV-1 R3A mutant viruses

To develop and optimise the production of infectious HIV-1 R3A viruses, two methods were explored: (1) co-transfection of HIV-1 R3A PTAP$^-$ with ALIX expression vectors; and (2) co-transfection of HIV-1 R3A PTAP$^-$ with codon-optimised Gag WT expression vectors. HEK 293T cells (4.2 x 10^5 cells/well) were seeded in a 6-well plate, incubated at 37°C and 5% CO_2 and transfected the following day. Transfection complexes were prepared in OptiMEM at a ratio of 1:3 [ng:µL] of DNA:FuGENE reagent. The pEGFP-N1 was used to normalise the plasmid concentration in the complexes. The complexes were added to the cultures, and incubated for 24 hrs. The virus and cells were harvested after 24 hrs, and analysed by western blotting. From these experiments, I determined the optimal conditions required for the production of infectious virus.

To make stocks of infectious HIV-1 R3A mutants (PTAP$^-$ or PTAP$^-$YP$^-$), HEK 293T cells were seeded in a T80 flask at 5 x 10^5 cells/ml in 20 mL of complete DMEM medium. Next day, the cells were transfected with pNL4.3-R3A PTAP$^-$ or PTAP$^-$YP$^-$ (30 µg), and pCMVGag WT (2.5 µg), complexed with FuGENE HD. After 48 hrs, the culture supernatants were pre-cleared by centrifugation and filtered through 0.2-µm-pore membrane. The viruses were concentrated by ultracentrifugation through a 20% w/v sucrose cushion, resuspended in RPMI 1640, and stored in liquid nitrogen. Virus titres were determined by titration on TZM-bl cells (Section 2.3.2).

2.11 Immunofluorescence (IF) microscopy

Whole cells (MDM or cell lines) on coverslips were fixed in 4% w/v paraformaldehyde (PFA), washed and free aldehyde groups were quenched in 50 mM NH_4Cl in PBS. The cells were permeabilised for 20 min with 0.1% v/v Triton X-100 in blocking buffer (6 mg/mL purified human IgG and 0.5% w/v BSA in PBS) for MDM or 0.1% v/v Triton-X100 in wash buffer (0.5% w/v BSA in PBS) for cell lines. As MDM express Fc receptors (Guilliams et al., 2014) that would non-specifically bind IgG antibodies, human IgG was used to block the Fc receptors. Cells were incubated in primary antibodies for an hour, washed and incubated in the respective secondary antibodies (Table 2.1) for 45 min to 1 hr in the dark. Nuclei were stained with 0.5 μg/mL Hoechst 33258 (Life Technologies, Paisley, UK) prepared in PBS, and the coverslips were mounted in Mowiol (2.4 g Mowiol 40-88, 6 g Glycerol, 12 ml Tris [0.2 M], 6 ml H_2O) on glass slides. Slides were kept at 4°C for at least 2 hrs before imaging on the confocal microscope. Confocal images were acquired with a Leica TCS SP3 confocal microscope, 63x oil objective and Leica LAS AF Software (Leica Microsystems, Milton Keynes, UK). Images were processed using ImageJ and assembled manually into montages using Adobe Illustrator CS4.

Semi-thin sections on glass slides (see Section 2.12, below) were quenched in 50 mM glycine/50 mM NH_4Cl in PBS, permeabilised for 6 minutes in 0.1% v/v TX-100 in PBS, and labelled with antibodies prepared in 1% w/v BSA in PBS. Nuclei were stained with 0.5 μg/mL Hoechst 33258, and the slides were mounted in Mowiol. Sections were examined with an Axioskop microscope (Carl Zeiss, Hertfordshire, UK). Images were recorded with charge-coupled device camera (Orca-ER; Hamamatsu), controlled by OPENLAB 5.0.2 software (Improvision, Perkin Elmer), and processed (adjusting brightness and contrast; assembling montages) using Adobe Photoshop CS4.

2.12 Preparation of cells for cryo-sectioning

For some of morphological studies by IF and EM, cells were prepared for cryo-sectioning by first adding an equal volume of pre-warmed double strength fixative (8% w/v PFA in 0.1 M sodium phosphate buffer, pH 7.4) into the culture medium. After 10 min at 37°C, the fixative was replaced with single-strength fixative (4% w/v PFA in 0.1 M sodium phosphate buffer, pH 7.4) for 2 hrs. Fixed cells were either stored in 0.2%

w/v PFA storage fixative for later processing or washed with 20 mM glycine in PBS, pelleted and embedded in 12% w/v gelatine. The samples were infiltrated with 2.3 M sucrose, a cryo-protectant, before freezing in liquid nitrogen. Sample processing and subsequent procedures were performed with help from Annegret Pelchen-Matthews who carried out all the cryo-sectioning. Semi-thin sections (500 nm) were cut and supported in 2.3 M sucrose on slides to be used for IF, whilst ultra-thin (50 nm) sections were cut and supported in 1:1 mixture of 2.3 M sucrose 2% and methyl cellulose, on formvar-coated regular or H6 finder grids (Agar Scientific, Essex, UK) for EM (Slot and Geuze, 2007). We worked together to immunolabel and image cryo-sections for IF and EM.

2.13 EM immunolabelling

The Tokuyasu EM method was used for immunolocalisation of viral antigens on cells (Deneka et al., 2007; Pelchen-Matthews and Marsh, 2007; Slot and Geuze, 2007). Cryo-sections (~50 nm) were incubated on melted 2% w/v gelatine at 37°C. They were subsequently quenched in 50 mM glycine/50 mM NH_4Cl for 15 min. Washed specimens were stained for 1 hr with primary antibodies prepared in 2% w/v BSA/0.2% BSA-c in PBS. BSA-c (Aurion, Wageningen, The Netherlands) is acetylated BSA that is linearised to increase the net negative charge of BSA, thereby further preventing non-specific binding of antibodies to the specimens. Where primary mouse IgG_1 monoclonal antibodies were used, sections were incubated with a rabbit anti-mouse bridging antibody (Rockland, Gilbertsville, PA, USA) before labelling with Protein A-gold (PAG) (The EM Lab, Utrecht University, The Netherlands). PAG does not recognise all classes of IgG such as those raised in mouse or goat (Bendayan and Garzon, 1988), therefore a bridging antibody is required. Where double labelling was performed, the first primary antibody and PAG labelling were followed by fixing in 1% w/v glutaraldehyde, and staining with the second antibody reagent and PAG of a different size (Pelchen-Matthews et al., 2012). Sections were stained in neutral uranyl acetate (filtered through a 0.2 µm filter) and embedded in uranyl acetate (filtered through a 0.2 µm filter) in 2% methylcellulose (1:9; v/v). Specimens were examined with a FEI T12 Tecnai Spirit transmission EM (FEI Tecnai, Eindhoven, The Netherlands). Images were taken with Morada 11 megapixel digital camera (Olympus Soft Imaging Solutions), and processed with Adobe Photoshop CS4.

For correlative light and electron microscopy (CLEM), cell sections on H6 finder grids were labelled with a primary antibody followed by a fluorescently tagged bridging antibody (rabbit anti-mouse A488), before labelling with PAG and fixing with 1% w/v glutaraldehyde. The sections were incubated with Hoechst 33258 to stain the nuclei, mounted in 50% v/v glycerol in H_2O for examination with an Axioskop microscope, and imaged, ensuring that the finder grid was also imaged to record coordinates of the labelled cells, so that they could be found at the electron microscope. After imaging, the grids were recovered and washed. As above, sections were stained with neutral uranyl acetate, examined by transmission EM, imaged, and the images were processed as above.

2.14 EM of Epon-embedded cells

HEK 293T cells were fixed for 30 min in a solution of 1.5% w/v glutaraldehyde and 4% w/v PFA prepared in 0.1 M sodium cacodylate buffer (pH 7.4), post-fixed in reduced osmium (1.5% w/v potassium ferricyanide, 1% w/v osmium tetroxide) at 4°C for 1 hr, and treated with 1% w/v tannic acid in 0.05 M sodium cacodylate for 45 min in the dark. The cells were further treated with 1% w/v sodium sulphate in 0.05 M sodium cacodylate (pH 7.4), and dehydrated sequentially in 70%, 90% and 100% ethanol. The cells were incubated in 50% v/v propylene oxide (PO) and 50% Epon 812 resin of medium hardness, before embedding in Epon 812 resin. J. Burden performed subsequent steps involving sectioning, staining and imaging of the specimens. The specimens were stained in uranyl acetate and examined using the transmission EM, imaged and processed as above (Section 2.13).

2.15 Analysis of budding morphologies

To determine the morphologies of budding particles quantitatively, EM images were analysed using the iTEM software (Olympus Soft Imaging Solutions). I estimated three parameters: the angle of Gag incorporation into the bud; the height of the bud from the cell surface; and the angle of bud closure (Figure 2.7A). The angle of Gag incorporation was measured by extrapolating a circle and measuring, from the centre of the circle, the angle enclosing the Gag layer. Bud height was measured from the base of a bud (including the virus stalk where present) – a base line was drawn to touch both side of

the plasma membrane at the bud opening into the cytosol (or the lower part of the stalk where present). To measure the angle of bud closure, an isosceles[3] triangle was extrapolated within the bud, with the base touching both sides of the plasma membrane at the bud opening. In practice, the three parameters followed closely (Figure 2.7B). In particular (i) and (ii) measure the same parameter, albeit in a different way, and therefore they mirrored each other. As (i) was easiest to analyse for large numbers of samples, this is the measure I used in Chapter 4.

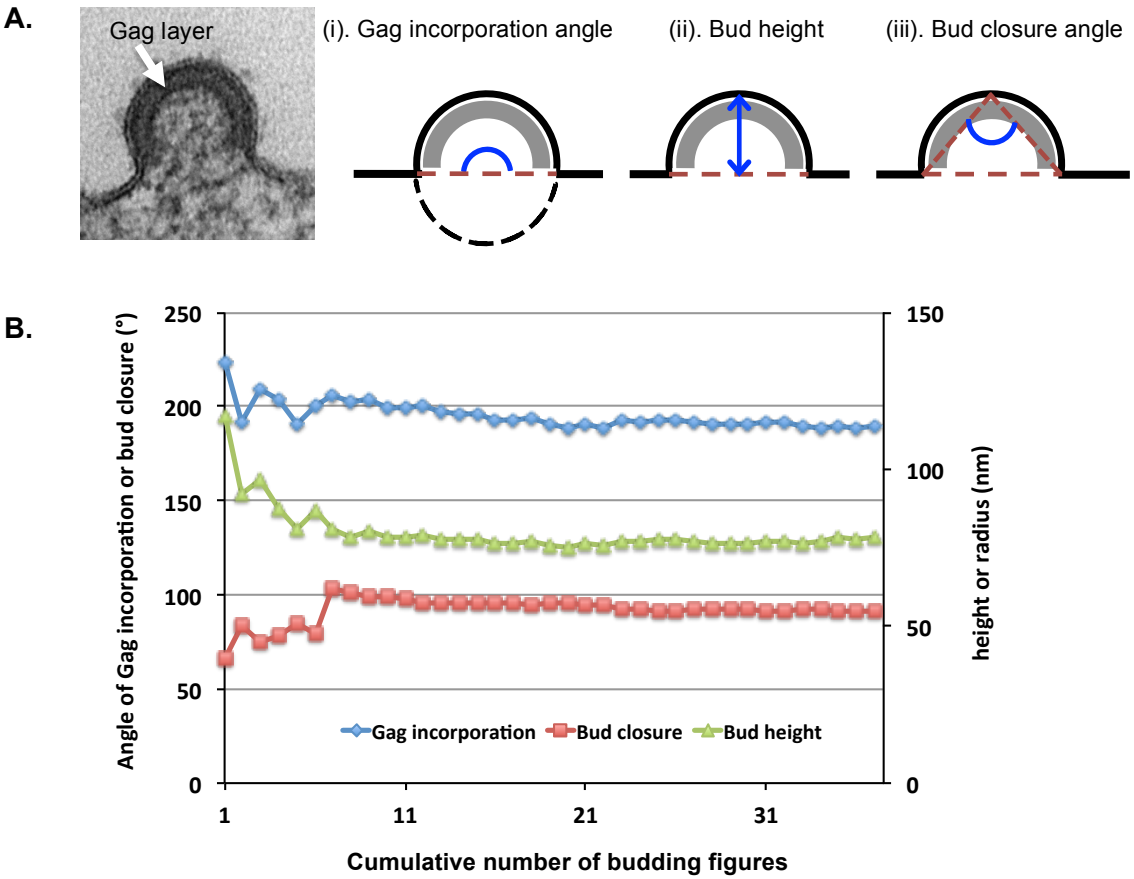

Figure 2.7: Quantitative analysis of morphology of virus budding profiles.
(A) The three measurements (explained in Section 2.15) taken on arrested virus profiles. **(B)** The measurements were compared graphically for one mutant (HIV-1 R3A PTAP^{-}). Angles of Gag incorporation data mirrored angles of bud closure.

[3] An isosceles triangle has two equal sides and two equal angles. For analysis, the equal angles were adjacent to the base.

2.16 Stereology of cell profiles

High-magnification (23,000x or 30,000x) EM images were processed and aligned using Adobe Photoshop. Virus profiles were counted on multiple aligned images using the counter tool in Photoshop. To segment the IPMCs and cell surfaces on cell profiles, different colours of the brush tool were used to trace the plasma membrane (PM) on the high-resolution images. Segmented cell profiles were printed on A3 paper, and equi-distant (1-cm apart) straight lines were drawn across the images. The intersections of the lines with the PM-segmenting lines were counted and used to estimate the area of PM (West, 2012) (see details in Chapter 5).

3. The ESCRT Machinery is Required for HIV-1 Release from Monocyte-derived Macrophages

3.1 Introduction

HIV-1 assembly is orchestrated by the Gag protein, the sequence and structure of which facilitate targeting, membrane binding multimerisation and the recruitment of factors required for membrane fission (see General introduction, Section 1.5.4). The virus has two late (L) domain motifs in the p6 subdomain of Gag, PTAP and YPXnL, which recruit ESCRT pathway proteins and mediate virus release (Huang et al., 1995; Garrus et al., 2001; Strack et al., 2003; Dussupt et al., 2009; Fujii et al., 2009; Im et al., 2010; Sundquist and Krausslich, 2012). The PTAP motif recruits Tsg101, a component of the ESCRT-I complex; and the YPXnL motif, located downstream of the PTAP amino acid residues, recruits ALIX, an ESCRT accessory protein. These two proteins can mediate virus release independently; therefore, the virus does not need to recruit both (Fujii et al., 2009). Gag-bound ALIX, and/or ESCRT-I, then engages the ESCRT-III components that are assembled sequentially, to constrict the plasma membrane and finally the VPS4-LIP5 complex is recruited to catalyse the disassembly and recycling of ESCRT components, resulting in membrane fission to release virions from the host cell (Jouvenet et al., 2011).

The role of Tsg101 and ALIX in HIV release has been studied extensively in T cells and model cell lines, but has not been investigated to a great extent in primary monocyte-derived macrophages (Demirov et al., 2002b; Fujii et al., 2009; Gaudin et al., 2012). Therefore, the work described in this chapter aimed to establish whether Tsg101/ESCRT-I and/or ALIX play a similar role to that described in model cell lines. To determine the respective roles of ESCRT proteins in HIV-1 assembly in MDM, siRNA was used to deplete Tsg101 and ALIX in infected cells. The effects of the knockdowns were investigated either individually or in combination. Overall, downregulating Tsg101 and ALIX had only minimal inhibitory effects on HIV release in MDM, although the effect of Tsg101 depletion was greater than that of ALIX depletion.

To further investigate the role of ESCRT complexes in HIV assembly in primary macrophages, Gag mutants defective in Tsg101 and ALIX recruitment were generated by site-directed mutagenesis. Although a native Gag could not be expressed in MDM, a codon-optimised Gag was expressed. However, the ESCRT-recruitment defective mutants in codon-optimised Gag were released to the same extent as the WT in MDM. VPS4 is required at the end of ESCRT pathways, and accordingly the dominant negative VPS4 EQ inhibited the release of codon-optimised Gag and a full molecular clone of HIV-1 (HIV-1 R3A WT) in MDM, indicating that the ESCRT machinery is indeed required for HIV release in MDM. Therefore, proviral HIV-clones were generated, in which the PTAP and/or YPXnL motifs were mutated, or the entire p6 subdomain was deleted. When these mutants were characterised in HEK 293T cells by western blotting (WB), their release was impaired. Most importantly, the release of the mutants was inhibited in MDM, and a greater effect was observed when the Tsg101 recruiting motif (PTAP) was absent, compared to the absence of the ALIX recruiting motif (YPXnL). Therefore, the data presented in this chapter show that the ESCRT machinery is required for HIV release from primary macrophages, and that Tsg101 is more important than ALIX in mediating virus release in primary macrophages.

3.2 Results

3.2.1 Characterisation of primary MDM cultures

To analyse HIV-1 assembly in macrophages, monocytes from blood packs were used to generate primary macrophages. This study aims to mimic the *in vivo* system as close as possible, and it has been reported that macrophage cell lines such at U937, Mono Mac or THP-1 do not reflect all the properties of primary MDM (Cassol et al., 2006). The monocytes were isolated from peripheral blood mononuclear cells (PBMCs), and differentiated into macrophages in the presence of M-CSF and IL-2 cytokines. Monocytes were characterised by analysing cell surface markers CD4, CD14 and CCR5 by flow cytometer (see Materials and Methods, Section 2.2.2). CD14 is widely used as a marker for monocytes/macrophages (Jersmann, 2005). It was also important to confirm the expression of CCR5 on cells that would be infected with HIV, to avoid the possibility of using cells from a homozygous CCR5Δ32 individual. The deletion of 32 bp in the second extracellular loop of CCR5 leads to the production of a truncated

protein that fails to traffic to the plasma membrane, thereby conferring resistance to HIV-1 infection (Samson et al., 1996).

3.2.2 Downregulation of Tsg101 expression in MDM

Depletion of endogenous Tsg101 by siRNA has been shown to significantly impair HIV-1 release in HEK 293T cells (Garrus et al., 2001), so I tested whether downregulating the expression of Tsg101 in MDM would similarly inhibit virus release. For these experiments, I followed the schema shown in Figure 3.1A. MDM were infected with HIV-1 BaL strain, an R5-tropic virus originally isolated from the lung tissue of a child with AIDS and characterised in 1986 (Gartner et al., 1986). The infected cells were treated with either control or Tsg101 siRNA 24 hrs later (see Materials and Methods, Section 2.5). The experiments were performed in duplicate for cells from multiple blood donors. Cell and virus lysates were analysed by SDS-PAGE and western blotting.

The levels of Tsg101 in MDM were depleted for six days, as I had determined that the lowest levels were achieved on day six post-siRNA treatments (Materials and Methods, Figure 2.3). Cell lysates were analysed for Tsg101 depletion, using voltage-dependent anion-selective channel protein 1 (VDAC-1) as a loading control (Figure 3.1B). Tsg101 was depleted very efficiently and reproducibly to about 15 ± 7% in MDM from eight blood donors. In four experiments where the effect of Tsg101 depletion on virus production and release was assessed, Tsg101 was reduced to 17 ± 6%. As macrophages are post-mitotic, there was no cytopathic effects associated with block to cytokinesis in Tsg101 knockdowns, as noted from the loading control, and this is consistent with a recent report (Gaudin et al., 2012). To look at the effects of Tsg101 depletion on virus production and release, cell lysates were analysed for the viral protein Gag, by assessing the unprocessed and processed forms of the protein, with adaptin-γ as the loading control for these samples. Accumulation of Gag processing intermediates (see Chapter 1, Figure 1.10), such as p41, was noted for the Tsg101-depleted cultures compared to the control siRNA. A delay in scission may lead to inefficient proteolysis in the unscissioned buds, and hence the accumulation of processing intermediates. The p55 protein is unprocessed Gag polyprotein, whilst the p24 (CA) protein found in mature virus is one of the end products of p55 proteolysis. The p24 is not normally seen in cell

lysates, but these are samples from macrophages, which contain mature virus in the IPMCs. The p24 levels were not conspicuously reduced in virions and cell lysates of the Tsg101-depleted cultures. Although, Tsg101 was efficiently reduced (17 ± 6%; n = 4), the virus release efficiency remained at 76 ± 7%, suggesting that the loss of Tsg101/ESCRT-I had only a modest effect on virus release (Figure 3.1C).

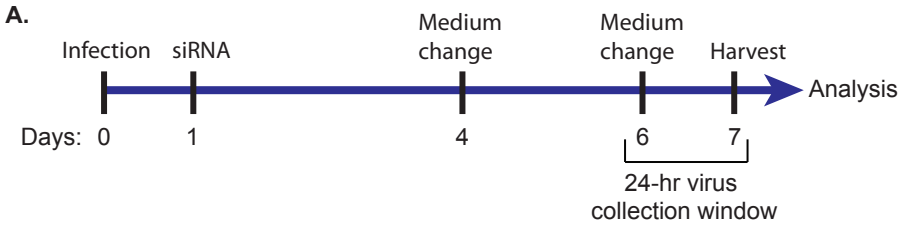

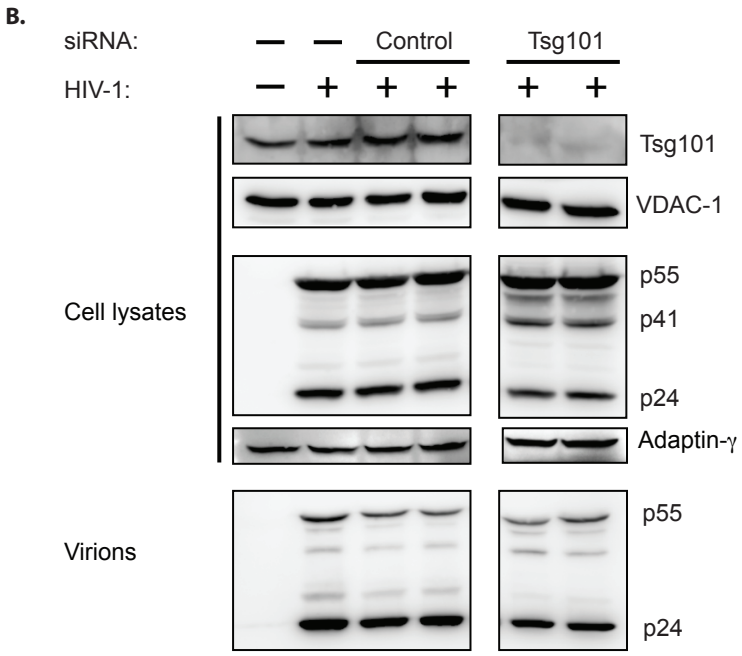

C.

Tsg101 level (%)	16.5 ± 6.4 (n = 4)
Virus release efficiency (%)	75.8 ± 6.8 (n = 4)

Figure 3.1: Depletion of Tsg101 has a modest effect on virus release in MDM.
(A) Experimental set-up of the siRNA knockdown in MDM. On day 0, which corresponds to the 7th or 8th day of cell culture post monocyte isolation, cells were infected with HIV-1 BaL (3 FFU). 24 hrs post-infection, duplicate culture wells per donor were transfected with siRNA. The virus released during the 24-hr window (days 6 to 7) was collected and concentrated by ultracentrifugation. The virus pellets and cells were lysed in Laemmli buffer, and analysed by western blotting. **(B)** Antibodies against Tsg101, VDAC-1, p24/55 and adaptin-γ were used to probe the WB. **(C)** A table summarising quantitative data from Tsg101 RNAi experiments. To analyse WB, unsaturated band signal intensities were quantified using ImageJ. Virus release efficiencies were calculated using equation No. 1 in Materials and Methods, Section 2.8. A representative blot is shown for cells from four different blood donors.

3.2.3 Downregulation of ALIX expression in MDM

The ESCRT accessory protein, ALIX, can be recruited independently to Gag by the p6 subdomain of HIV, to facilitate virus release. ALIX has several distinct domains, one of which is a proline-rich region that has a PSAP motif that can bind Tsg101. However, a functional PSAP motif is not essential for ALIX to mediate virus release (Fisher et al., 2007), which attests to the functional autonomy of Tsg101 and ALIX in HIV release. Overexpression of ALIX in HEK 293T cells can rescue virus mutants defective in recruiting Tsg101 (Usami et al., 2007; Carlton et al., 2008; Sette et al., 2010). Thus ALIX can facilitate ESCRT-III recruitment either directly or through ESCRT-I.

To assess the effect of ALIX on virus release in macrophages, ALIX siRNA oligonucleotides were transfected into HIV-1-infected macrophages, following the same protocol used for knockdown of Tsg101 (Figure 3.1A). Cells treated with ALIX siRNA were comparable to control siRNA-treated cells: that is, there was no obvious cytotoxicity or cell rounding and detachment due to reduced ALIX levels. As before, the virions and cells lysates were analysed for levels of ALIX and HIV-1 BaL proteins by WB. On the representative WB (Figure 3.2A), ALIX was efficiently depleted to almost undetectable levels. ALIX was reduced to 5 ± 5% in cells from ten blood donors. Depleting ALIX had only a small effect on the cell-associated p24, as well as on the virion-associated p55 and p24, suggesting only a small disruption of virus release. Four out of ten samples were further analysed for the corresponding effect on virus release as shown in Figure 3.2B. In these four samples, the average ALIX level was 7 ± 6%. Here, the average virus release was about 92 ± 5%, despite the very efficient depletion of ALIX. These data suggest that ALIX has only minimal effects on virus release in macrophages. Therefore, it appears Tsg101/ESCRT-I is probably the main ESCRT protein that is directly recruited by Gag to mediate membrane fission in MDM, as in other cells (Fujii et al., 2009). Collectively, these data show that the downregulation of Tsg101 or ALIX, individually, does not significantly impact on virus release in this system, albeit Tsg101 may have a stronger role.

A.

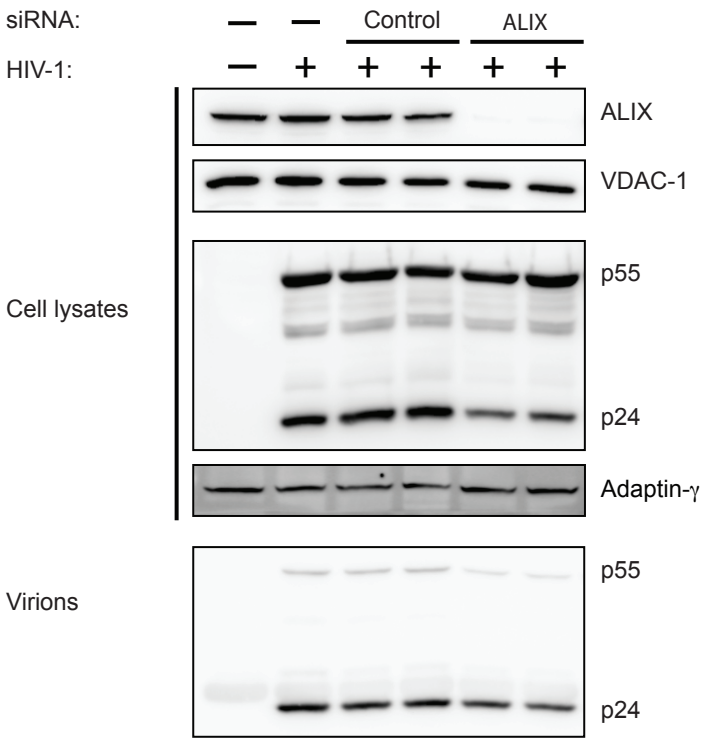

B.

ALIX level (%)	7.3 ± 6.3 (n = 4)
Virus release efficiency (%)	91.8 ± 5.3 (n = 4)

Figure 3.2: Knockdown of ALIX by RNAi had a minimal effect on virus release.
(A) WB for ALIX knockdown in MDM. HIV infection and ALIX depletion were carried out as described in Figure 3.1. Blots for cell lysates were probed with either anti-ALIX or HIV-1 Gag p24/55, using anti-VDAC-1 and anti-adaptin-γ, respectively, as loading controls. ALIX was depleted to almost undetectable levels. The reduced ALIX level had a small effect on virus release. **(B)** A summary of results from four experiments. ALIX was reproducibly reduced to near undetectable levels compared to control siRNA treatment. However, there was only a small effect on virus release.

3.2.4 Double knockdown of Tsg101 and ALIX in MDM

As shown above, depleting Tsg101 and ALIX, individually, produced only small effects on virus release, despite the efficient reduction in the levels of the proteins after siRNA treatments. Because the two proteins act independently in membrane scission events, it is possible that one may compensate for the absence of the other. Alternatively, the low levels of residual proteins may be sufficient to mediate scission of the membrane stalks connecting virions to host cells. Therefore, additional experiments were performed

where both proteins were downregulated together. This was conducted on cells from three blood donors. Following the experimental set-up in Figure 3.1, siRNA oligonucleotides for ALIX and Tsg101 were co-transfected into HIV-1 BaL-infected macrophages. This was followed by media changes on the fourth and sixth days post-infection. The media from day six were collected and released virus particles pelleted by ultracentrifugation. Virions and cells were lysed and analysed by WB to determine the effect of the double knockdown.

A.

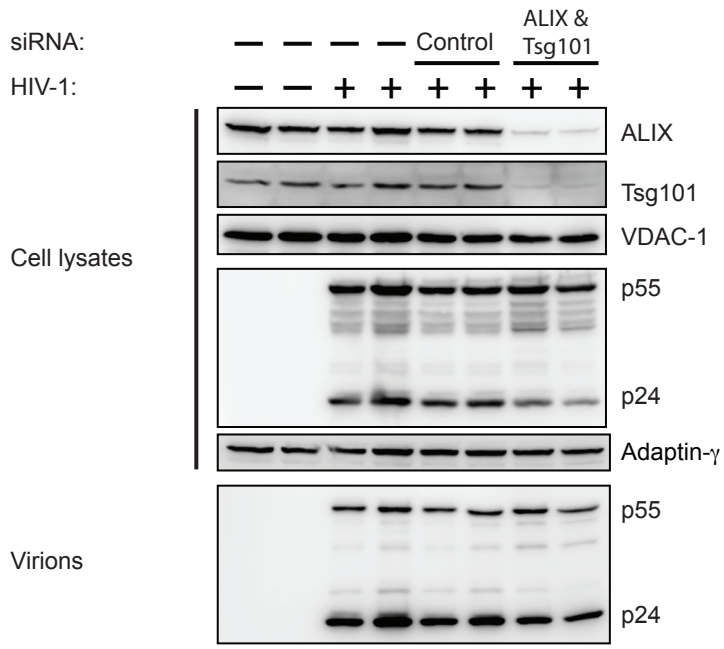

B.

%	ALIX	Tsg101
Protein level	14.0 ± 5.2 (n = 3)	24.0 ± 11.3 (n = 3)
Virus release efficiency	70.7 ± 8.5 (n = 3)	

Figure 3.3: Depletion Tsg101 and ALIX in MDM has an additive effect on virus release. **(A)** The experimental set up in Figure 3.1 was followed to perform the double knockdown. A representative WB for cells depleted of Tsg101 and ALIX. Antibodies against ALIX, Tsg101 and p24/55 were used to analyse blots for virions and cell-associated proteins. Both ALIX and Tsg101 were efficiently depleted, with minimal effect on HIV release. **(B)** A summary of the quantitation of the knockdown levels and release efficiencies for cells from three blood donors.

As with depleting Tsg101 and ALIX individually, depleting the two proteins simultaneously showed little effect on virus release (Figure 3.3). On average, ALIX was

reduced to approximately 14 ± 5%, whilst Tsg101 was reduced to about 24 ± 11% (Figure 3.3B). The depletion was not as efficient as in single knockdown (KD) experiments, where the proteins were depleted to about 16 and 7% for Tsg101 and ALIX, respectively (Figure 3.1 and Figure 3.2). The average virus release efficiency for the double KD was 71 ± 9 %, which was less than the 76 and 92% for the single KD of Tsg101 and ALIX, respectively. Although, depletion of each protein in the double KD was not as efficient as in the single KDs, virus release efficiency was slightly lower than in any of the single KDs (particularly, Tsg101), suggesting some possible synergistic effect in the double KD, but the difference between the means was not statistically significant for the Tsg101 and double KDs (Figure 3.4).

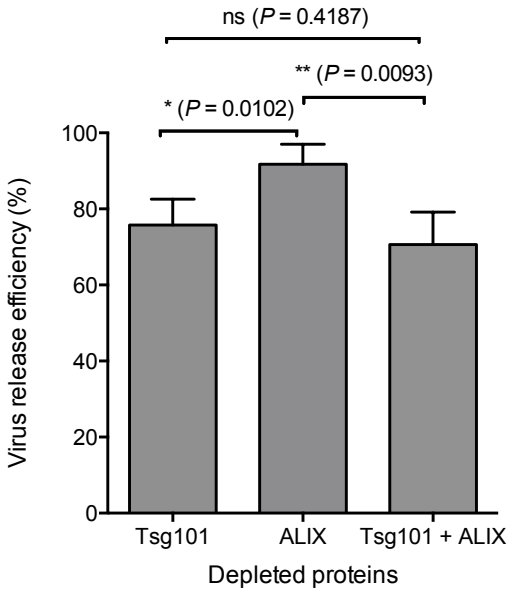

Figure 3.4: Comparison of virus release efficiencies for the single and double KDs of Tsg101 and ALIX.

The difference between the average virus release efficiencies for cells depleted of ALIX and Tsg101 were statistically significant. When the two proteins were depleted together and compared to depleting Tsg101 alone, the difference was not significant. The means were compared statistically using unpaired t-test ($P < 0.05$).

The small effect that the KDs have on virus release raises the question whether Tsg101 and ALIX are important for HIV release in macrophages, or whether indeed the ESCRT pathway is important. Secondly, if either of the two proteins is important, then the small effect could be attributed to the difficulties in transfecting siRNAs into a small number

of infected cells. In this scenario, this approach would not be sufficient to study virus formation in MDM, which is the ultimate goal of this thesis.

3.2.5 Mutagenesis of the ESCRT interacting motifs in the HIV-1 p6 domain

Although HIV release has been shown to depend on the ESCRT complexes (Garrus et al., 2001; Stuchell et al., 2004; Fujii et al., 2009), siRNA of the two ESCRT/ESCRT-associated proteins Tsg101 and ALIX, individually or together, did not have big effects on HIV-1 BaL release in MDM. As an alternative approach, the ESCRT interacting motifs within HIV-1 BaL Gag (Gag_{BaL}) were inactivated by site-directed mutagenesis. I took advantage of the fact that Gag, the main structural protein of HIV, can be expressed without other viral genes, and can orchestrate assembly and release of non-infectious VLPs that morphologically resemble immature virus particles (Bieniasz, 2009). The plasmid pRK5Gag_{BaL} (generated by Beatrice Kramer), carrying native Gag_{BaL}, was used to generate the mutants. The PTAP residues were changed to LIRL, whilst the YP residues in the YPXnL motif were changed to SR (Demirov et al., 2002b; Dussupt et al., 2009). Single ($PTAP^{-}$; YP^{-}) and double ($PTAP^{-}YP^{-}$) mutants were generated (Figure 3.5A).

To test whether the mutations inhibited Gag_{BaL} VLP release, I first transiently expressed the pRK5Gag_{BaL} constructs in HEK 293T cells, testing two molecular clones for each mutant. The proteins were analysed by WB (Figure 3.5B). The top panel of the WB shows that there were similar levels of Gag polyproteins in cells transfected with WT and the L domain mutants. Notably, there was variation in the mobility of mutants bearing the LIRL mutation, consistent with published data (Demirov et al., 2002b). The amount of VLPs released into medium of cells transfected with the mutants was almost undetectable for the Gag_{BaL} $PTAP^{-}$ and $PTAP^{-}YP^{-}$ mutants, 2.9 and 2.4%, respectively.The Gag_{BaL} YP^{-} mutants also had impaired particle release, 14.4%. These data are in agreement with published data (Fujii et al., 2009; Sette et al., 2010).

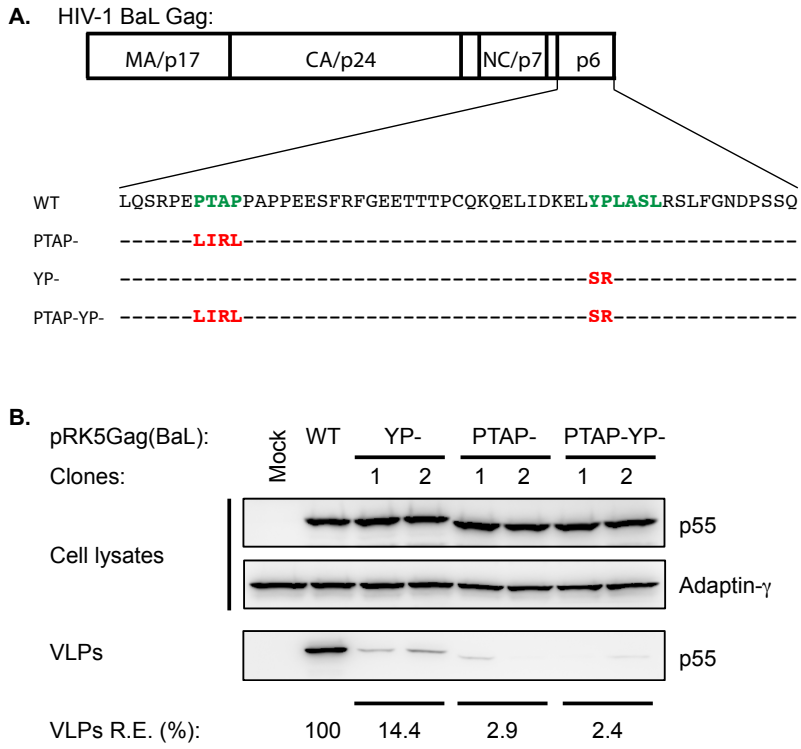

Figure 3.5: Mutagenesis of pRK5Gag$_{BaL}$ and expression of the mutants in HEK 293T cells.
(A) Organisation of the *gag* open-reading frame. The amino acid sequences for the p6 subdomain are shown below. In the WT, the Tsg101 and ALIX binding motif, the PTAP and YPXnL, respectively, are highlighted in green. Three mutants were generated by mutagenesis of the ESCRT binding motifs. For each named mutant, the corresponding amino acid changes are indicated in red. **(B)** Cells were transfected with 2 µg of the indicated construct, and two clones were tested for each mutant. Cultures were harvested after 48 hrs of incubation. Purified VLPs and cells were lysed and analysed by WB. As two clones were tested for each mutant, the average release efficiencies for the VLPs could be determined. All mutants were defective in release from cells, as shown by the weak Gag signal on the VLP blot. The PTAP and double mutants show more severe defects compared to the YP mutant. Release efficiencies (R.E.) are indicated below the blot.

3.2.6 Native Gag$_{BaL}$ is not expressed in MDM

Since the release of Gag$_{BaL}$ mutants was inhibited in HEK 293T cells, I introduced these mutants into MDM by electroporation. A vector expressing GFP only, pmaxGFP, was used as a positive control for the procedure. Electroporation is the application of short and intense electric pulses to trigger formation of transient hydrophilic pores in the plasma membrane and nucleus such that plasmid DNA can be delivered into the cell (Stacey et al., 1993; Pehlivanova et al., 2012). Electroporation was a method of choice to transfect macrophages because these cells are difficult to transfect using reagent-based transfection methods. Duplicate experiments were set up so that one could be incubated for 24 hrs, and a second for 48 hrs. Macrophages in the 24-hr set-up

experiment were fixed and analysed whilst those in the 48-hr set-up did not survive. Fixed cells were stained with antibodies against Gag and CD44, and examined by confocal microscopy. Although, GFP expressed efficiently from the pmaxGFP (24% positive cells), none of the cells transfected with pRK5Gag$_{BaL}$ WT or the mutants could be stained by anti-Gag antibodies, suggesting that they were not expressed. I also tested the role of different expression vectors and found that pRK5 is best (Appendix, Figure 8.1).

To investigate why Gag$_{BaL}$ was not expressed in MDM, several control experiments were performed. First, as a control for the Gag staining procedure, HeLa cells were transfected with either Gag$_{BaL}$ WT or PTAP^{-}. When expressed, Gag$_{BaL}$ does label with the antibodies used against p55 (Figure 3.6 A, B). The second and third controls involved electroporating MDM (see Materials and Methods, Section 2.7) with the following plasmids: pGagGFP WT containing codon-optimised Gag (Hermida-Matsumoto and Resh, 2000); or pcDNA3.1Nef that contained Nef, another HIV protein. These were performed in parallel with pRK5Gag$_{BaL}$ WT electroporation. The codon-optimised pGagGFP has previously been expressed in MDM by electroporation (Mlcochova et al., 2013). The discrepancy in expression between the native Gag$_{BaL}$ and codon-optimised GagGFP arises from the fact that the *gag* in the former has a high AU content, which makes its transcripts unstable. In an HIV-1 full molecular clone, the HIV accessory protein Rev is expressed and it binds to the RRE in the *gag* RNA to help stabilise it. Nef expression, on the other hand, is Rev-independent (Freed, 2001; Freed, 2002). In a codon-optimised Gag, site-directed mutagenesis has been used to inactivate sequences that hinder expression (Schwartz et al., 1992a; Schneider et al., 1997; Kotsopoulou et al., 2000). Analysis of the electroporated cells showed that although native Nef and codon-optimised GagGFP were expressed (Figure 3.6C, D), the native Gag$_{BaL}$ was not expressed in MDM. The proportion of cells expressing Nef was 14%, tested on cells from one donor only, whilst GagGFP expression was variable (6 and 38%) between MDM from two blood donors.

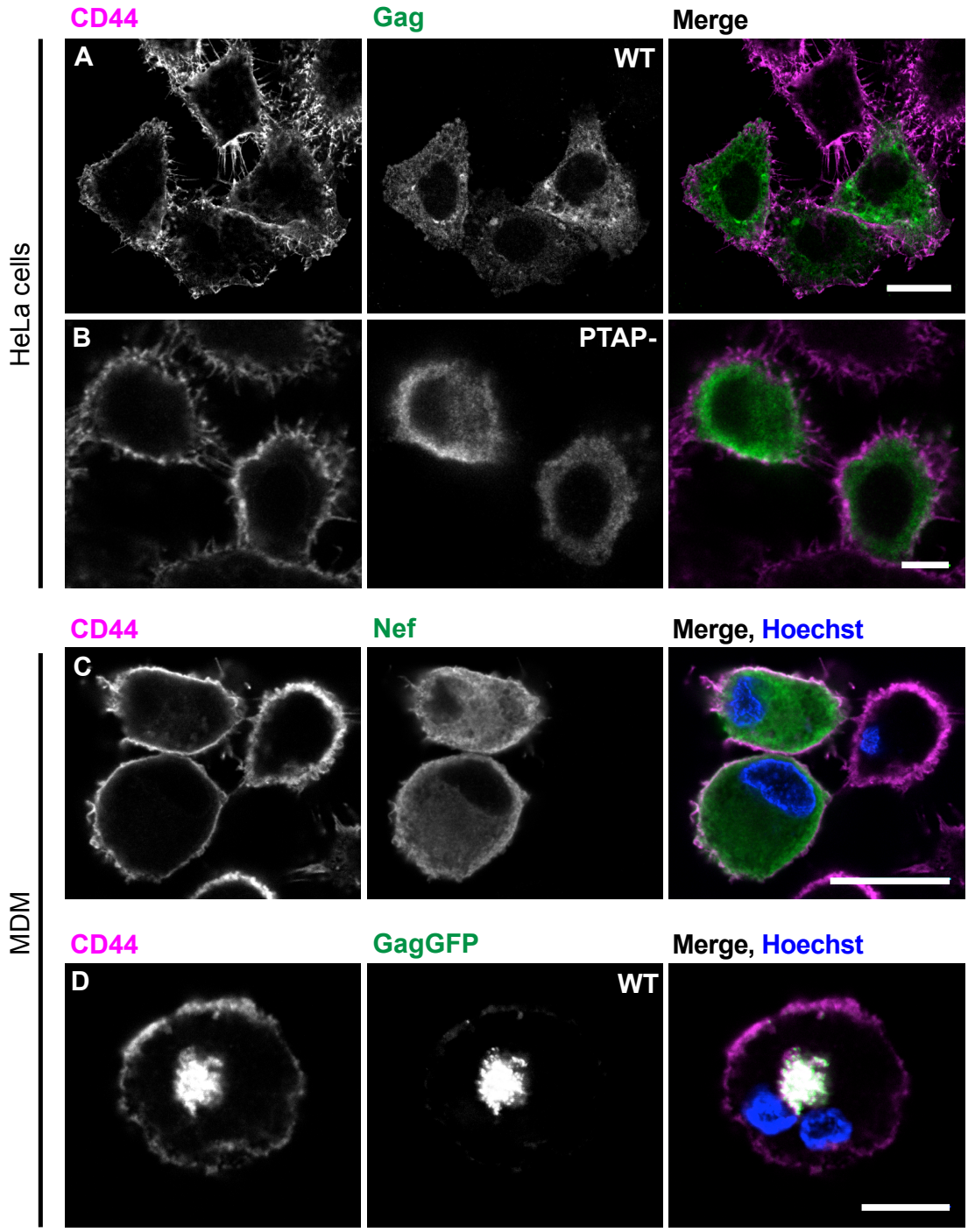

Figure 3.6: Immunofluorescence staining for the expression control experiments.
(A and **B)** Images of HeLa cells transfected with either pRK5Gag$_{BaL}$ WT or PTAP^{-}. Cells were incubated for 48 hrs post-transfection, fixed and immuno-stained for HIV Gag p24/55 and CD44. Single confocal sections were acquired. **(C** and **D)** MDM were electroporated with constructs expressing Nef or codon-optimised GagGFP. The cells were incubated for 24 hrs and then fixed. Cells electroporated with the Nef plasmid were immuno-stained for Nef and CD44 (C), whilst GagGFP-electroporated cells were immuno-stained for CD44 only (D). In D, the distribution of GagGFP is at the IPMC. Nuclei were visualised with Hoechst. Scale bars: 10 μm.

Collectively, these data demonstrate that Gag_{BaL} can be expressed in HeLa cells, but not in macrophages. This is likely because the high AU content make its transcripts unstable in macrophages. This could be overcome by codon-optimisation or co-expression of Rev.

3.2.7 Codon-optimised Gag can be expressed in MDM

I have shown that codon-optimised GagGFP could be expressed in macrophages by electroporation (Figure 3.6D). However, GagGFP produces aberrant particles or budding profiles, because GFP imposes steric interference on Gag packaging (Pornillos et al., 2003; Larson et al., 2005; Pelchen-Matthews and Marsh, 2007). To remove the GFP, I designed primers to amplify the codon-optimised Gag fragment of the pGagGFP, with the simultaneous introduction of a stop codon and a restriction site at the end of the p6 subdomain. The Gag fragment was re-cloned into the pCMV vector to generate pCMVGag (see Materials and Methods, Section 2.9.7). This procedure was repeated for the pGagGFP $PTAP^{-}$. The pCMVGag WT and $PTAP^{-}$ were further changed by site-directed mutagenesis, to generate Gag YP^{-} and $PTAP^{-}YP^{-}$ mutants.

The pCMVGag constructs were transfected into HEK 239T cells to test their expression. Cells and VLPs were harvested after 24 hrs, and analysed as before (Figure 3.7A). Good expression of the WT and mutants was observed. The quantitation in Figure 3.7B shows release efficiencies of about 62, 18 and 4% for YP^{-}, $PTAP^{-}$ and $PTAP^{-}YP^{-}$ mutants, respectively. This severe release defect observed when the PTAP residues were mutated is in agreement with Tsg101 having a stronger effect on HIV-1 release in many cell systems. Mutating the YP sequences to disrupt ALIX recruitment had a smaller effect compared to the PTAP mutations, while combining the mutations had an additive effect on VLP release in HEK 293T cells, consistent with data from a previous study (Fujii et al., 2009). Deleting the entire p6 subdomain, that has both the Tsg101 and ALIX binding sequences, has been shown to have a stronger effect than deleting the Tsg101-recruiting motif alone (Demirov et al., 2002b), suggesting an additive effect.

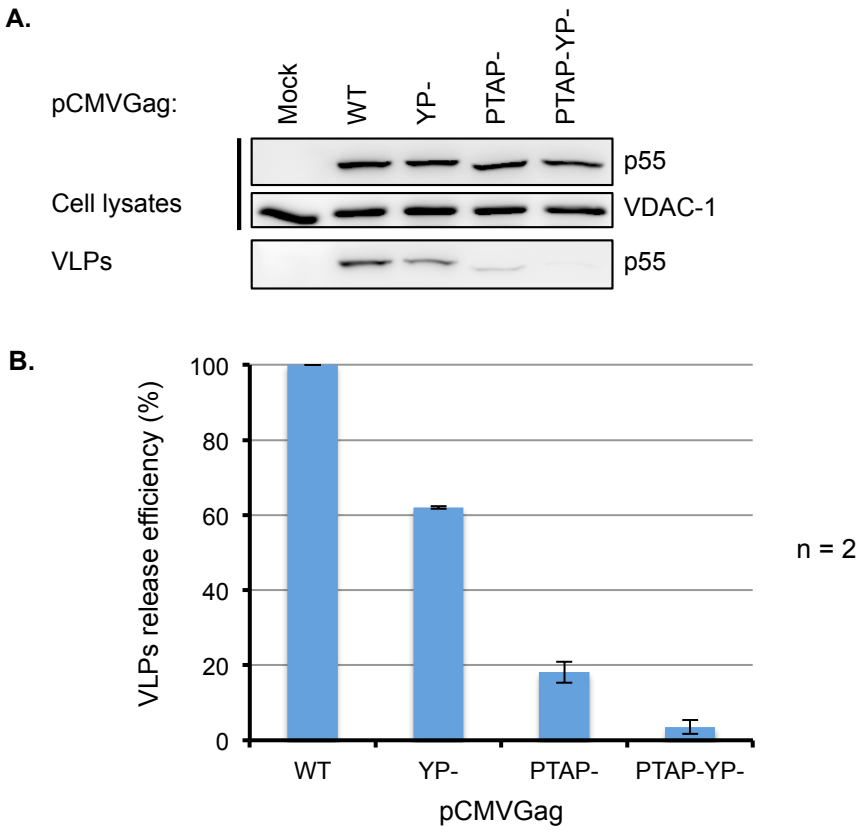

Figure 3.7: Biochemical characterisation of pCMVGag in HEK 293T cells.

(A) Cells were transfected with 2 µg of the indicated construct and incubated for 24 hrs. VLPs and cell lysates were analysed by WB. Mutants were less efficiently released compared to the WT, but severe effects were observed for the mutations on Tsg101 recruiting motif, PTAP, with almost undetectable p55 protein. **(B)** The p55 band signal intensities on WB were used to estimate the release efficiencies of VLPs, using equation No. 3 in Materials and Methods, Section 2.8.

As the pCMVGag constructs worked in HEK 293T cells, their expression was also tested in macrophages. MDMs were electroporated to deliver plasmid DNA into the cells, and then incubated for 24 hrs. Examination of cell lysates by WB revealed that the constructs were expressed, and that bands for the p55 were present in the cell lysates. The WB for VLPs showed that pCMVGag PTAP$^-$ and PTAP$^-$YP$^-$ mutants were released almost as efficiently as the WT (Figure 3.8A, B). Based on RNAi experiments in MDM (Figure 3.1 to 3.3), I had anticipated that the mutations would have a stronger inhibitory effect on the release of VLPs. Quantitative analysis showed release efficiencies of 95 ± 0.4% and 85 ± 17.1% for the PTAP$^-$ and PTAP$^-$YP$^-$ mutants, respectively. Therefore, this warranted further investigation to establish the requirement of the ESCRT pathway for HIV release in macrophages.

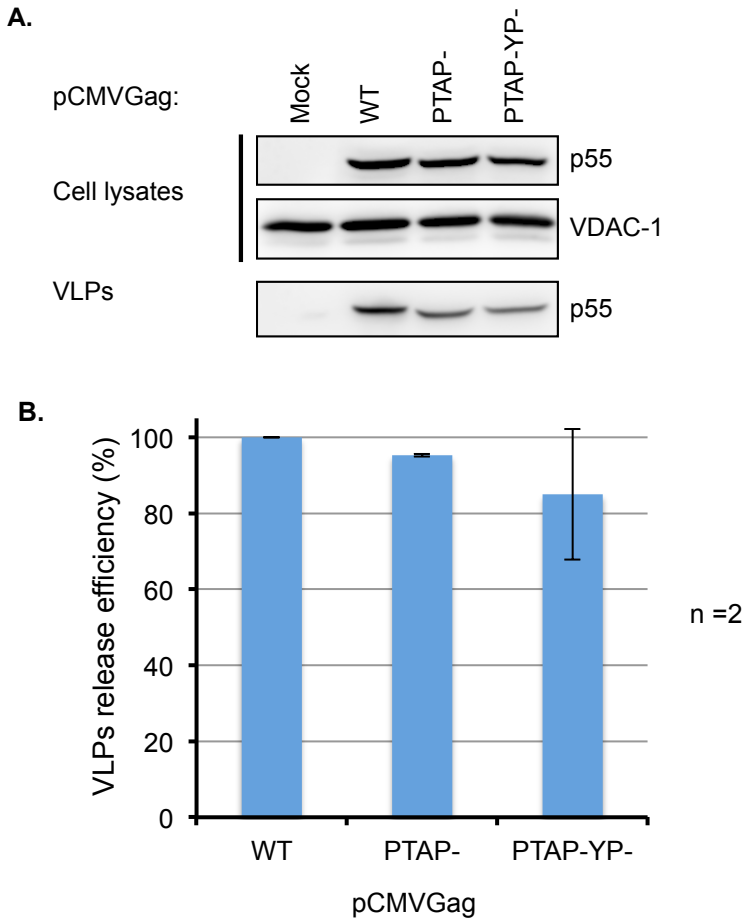

Figure 3.8: Biochemical characterisation of pCMVGag in MDM.

(A) The expression of pCMVGag constructs was examined by electroporation into MDM. After 24 hrs of incubation, VLPs and cells were harvested and lysed. Blots were probed with anti-p24/55 and -VDAC-1. Mutants were released almost to the same extent as the WT. **(B)** Results for cells from two donors were quantified and illustrated on the graph shown here.

3.2.8 Inhibition of HIV release with dominant negative GFP-VPS4

VPS4 is thought to be required at the end of the ESCRT pathway, recruited by the ESCRT-III complex to catalyse membrane fission (Votteler and Sundquist, 2013). It does this by converting the energy of ATP hydrolysis into mechanical work. Changing the VPS4 glutamic acid (E) at position 228 to glutamine (Q) blocks ATP hydrolysis, thereby abolishing the catalytic activity of substrate-bound VPS4 (Bishop and Woodman, 2000). Irrespective of the motif used to recruit the ESCRT proteins to budding sites, the VPS4 complex is ultimately recruited to the site of assembly and this recruitment is essential for ESCRT-dependent virus release. To further investigate the involvement of the ESCRT pathway in HIV release in macrophages, I exploited the capacity of the dominant negative VPS4 EQ to inhibit virus release.

In many cell lines, expression of VPS4 EQ results in the formation of endosomes with aberrant morphology characterised by enlarged vacuoles, reminiscent of the so-called class E aberrant endosomes (Bishop and Woodman, 2000). To verify this phenotype, GFP-VPS4 WT, or the dominant negative (GFP-VPS4 EQ), were transiently expressed in HEK 293T cells. As VPS4 EQ has been shown to affect endosome morphology, cells were stained for an endosome marker, the tetraspanin CD63 (Kobayashi et al., 2000). Cells expressing GFP-VPS4 WT had small CD63 puncta in the cytosol, whereas cells with the dominant negative GFP-VPS4 EQ, had swollen doughnut-shaped vacuoles with CD63 co-localising with GFP-VPS4 EQ on the perimeter (Figure 3.9A, B). CD63 is found on lumenal vesicles because that is where it is sorted from the perimeter membrane. These data suggested that the GFP-VPS4 EQ does inhibit disassembly and recycling of ESCRT components, and should therefore also disrupt HIV release (Garrus et al., 2001).

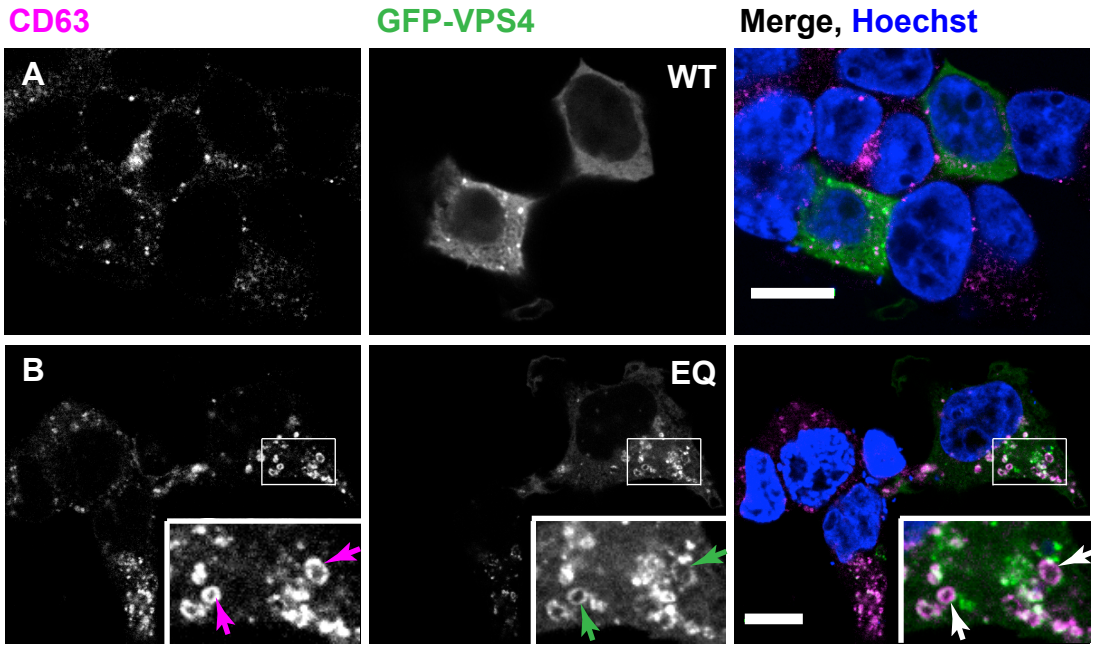

Figure 3.9: Expression of GFP-VPS4 in HEK 293T cells.

(A) GFP-VPS4 WT was transiently expressed in HEK 239T cells. The cells were fixed 24 hrs after incubation, and immuno-stained with anti-CD63, a late endosome marker. Hoechst was used to label the nuclei. Single optical section images of the cells were acquired by confocal microscopy. **(B)** As in A, but with cells expressing an ATP-hydrolysis defective mutant, GFP-VPS4 EQ. The insets are the enlarged snapshot of the boxed areas in the images, showing the swollen endosomes. Arrows show some examples of enlarged CD63-labelled vesicles that also contain the GFP-VPS4 EQ.

To determine whether the ESCRT pathway is involved in HIV assembly in MDM, cells were co-electroporated with pCMVGag WT and either pGFP-VPS4A WT or EQ. In parallel, MDM were also electroporated with the pCMVGag WT and PTAP^{-}YP^{-}. Cell cultures were harvested after 24 hrs and analysed by WB (Figure 3.10A). In cells co-electroporated with pCMVGag WT and pGFP-VPS4 EQ, there was a clear reduction in the amount of released virus compared to cells with pCMVGag WT and pGFP-VPS4, although there was less Gag synthesis in VPS4 EQ-treated cells. Similar to the data in Figure 3.7, the Gag PTAP^{-}YP^{-} mutant was released to the same extent as the Gag WT.

A.

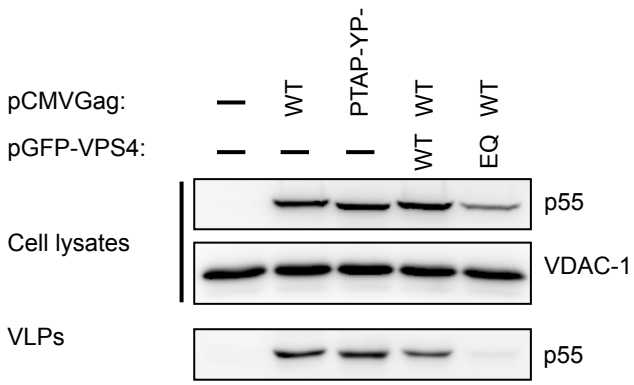

B.

Constructs	VLPs release efficiency (%) [n = 2]
pCMVGag WT	100.0 ± 0.0
pCMVGag PTAP-YP-	99.1 ± 4.7
pCMVGag WT + pGFP-VPS4 WT	100.0 ± 0.0
pCMVGag WT + pGFP-VPS4 EQ	41.9 ± 8.9

Figure 3.10: Co-expression of pCMVGag and pGFP-VPS4 in MDM.

(A) Cells were (co-)electroporated with 1 µg of the indicated vector(s). Total DNA was normalised to 2 µg with pEGFP-N1 empty vector in a 12-well plate. Cell cultures were incubated for 24 hrs, and then harvested. VLPs and cell lysates were analysed biochemically by WB. As before, anti-p24/55 and anti-VDAC-1 were used to probe membranes for proteins. Cells treated with GFP-VPS4 EQ had impaired VLP release, with a p55 signal that was barely above background. **(B)** Quantitation of the VLP release efficiency, where treatments are either compared to the Gag WT-transfected or cells transfected with pCMVGag WT and pGFP-VPS4 EQ.

To determine the extent of the inhibition by GFP-VPS4 EQ, the release efficiencies of VLPs for the treatments were quantified and compared to either the pCMVGag WT electroporation or pCMVGag WT + pGFP-VPS4 WT co-electroporation (Figure 3.10). The average virus release efficiency for the pGFP-VPS4 EQ-treated cells was 42 ± 9% relative to the pGFP-VPS4 WT treatment. The release of Gag PTAP^{-}YP^{-} compared to the Gag WT was 99 ± 5%, consistent with the unexpected data in Figure 3.10. However, the VPS4 EQ data indicate that the ESCRT machinery is required for HIV release in MDM.

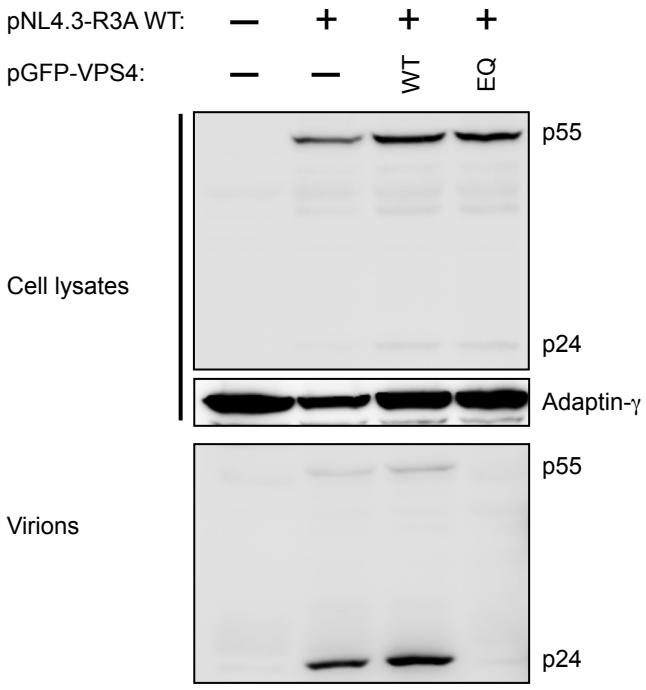

Figure 3.11: Co-expression of pNL4.3-R3A and pGFP-VPS4 in MDM.
Cells were co-electroporated with HIV-1 R3A provirus. Virus released into medium was harvested by ultracentrifugation through sucrose. Pelleted virus, and cells, were lysed in sample buffer and examined by WB. Anti-p24/55 was used to stain membranes for viral proteins, and adaptin-γ was used as a loading control.

When MDM were electroporated with codon-optimised Gag constructs with mutations that have been shown to inhibit ESCRT recruitment, unexpected results were observed (Figures 3.7 and 3.10). However, the dominant negative GFP-VPS4 EQ was able to inhibit VLP release, showing that the ESCRT system is required for HIV-1 release in macrophages. Therefore, the VPS4 was tested further in the context of an HIV-1

provirus (pNL4.3-R3A WT). The provirus was co-electroporated with either pGFP-VPS4 WT or EQ and analysed by WB (Figure 3.11). Relative to the loading control, Gag expression was the same in all lanes. Analysis of the virion-associated Gag showed that mature virus is produced in cells with the HIV-1 WT alone or with the HIV-1 WT and VPS4 WT. When cells were co-electroporated with pNL4.3-R3A WT and pGFP-VPS4 EQ, the Gag was almost undetectable in the virion fractions, consistent with the notion that VPS4 EQ inhibits HIV release (Garrus et al., 2001). Taken together, these data demonstrate that the ESCRT pathway is important for HIV release in macrophages, and suggests that a better approach to studying HIV-1 assembly in MDM would be to use a full molecular clone of HIV.

3.2.9 The generation of full-length release defective HIV-1

The plasmid construct pNL4.3-R3A WT (14.8 kb in size) was used to generate HIV provirus mutants defective in recruiting the ESCRT machinery. The pNL4.3-R3A, is derived from the backbone of NL4.3 strain and the envelope gene (*env*) from the R3A strain (Meissner et al., 2004).

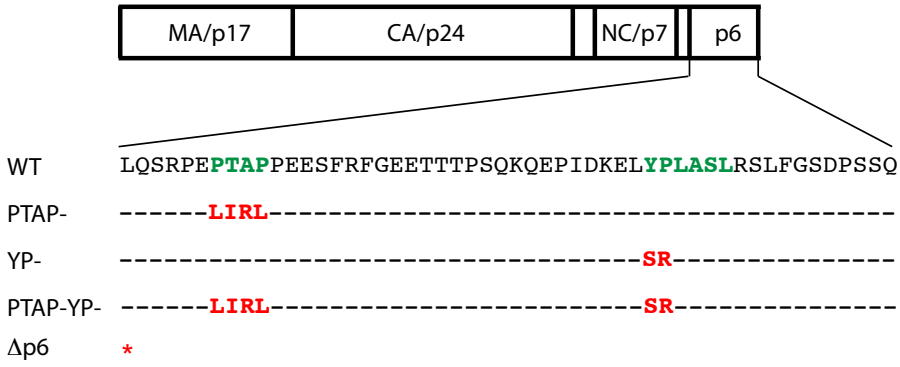

Figure 3.12: Schematic representation of the HIV-1 NL4.3-R3A Gag polyprotein.
The amino acid sequence of the p6 subdomain in the WT is shown with the Tsg101 and ALIX binding motifs, PTAP and YPLSTSL, respectively, highlighted in green. The dashes in the sequences for mutants ($PTAP^-$, YP^-, $PTAP^-YP^-$) denote amino acids identical to the WT. Changed sequences are shown in red. A red asterisk denotes the stop codon at the beginning Δp6.

It is difficult to carry out site-directed mutagenesis on plasmids larger than 10 kb. Therefore, I used an alternative approach to generate HIV-1 R3A mutants. WT provirus was digested with restriction enzymes to cut out a 3.7-kb fragment containing the entire

p6 subdomain of Gag (see Materials and Methods, Section 2.9.8). The fragment was subcloned into the pEGFP-N1 backbone, generating an 8.4-kb plasmid. Site-directed mutagenesis was then carried out on the p6 subdomain to change the PTAP sequence to LIRL, and YP to SR, individually or in combination: YP^{-}, $PTAP^{-}$ and $PTAP^{-}YP^{-}$. To delete the entire p6 subdomain, a stop codon was introduced at the beginning of the p6 subdomain. The mutagenised fragments were re-cloned into the pNL4.3-R3A, replacing the similar wild-type fragment, to generate HIV-1 R3A YP^{-}, $PTAP^{-}$, $PTAP^{-}YP^{-}$ and Δp6 mutants (Figure 3.12).

3.2.10 Characterisation of the HIV-1 R3A mutants in HEK 293T cells by WB

Mutating the PTAP to LIRL and YP to SR, respectively, or deleting the entire p6 in HIV-1 Gag, inhibited the release of VLPs in HEK 293T cells (Figure 3.5 and 3.7). To determine whether the full molecular clone HIV-1 R3A with the same mutations in Gag were defective in release, mutants were transfected into HEK 293T cells, and the cultures were harvested after 24 hrs of incubation. Virions released into the media and cell-associated virus proteins were resolved on SDS-PAGE gels and analysed by WB (Figure 3.13A). This revealed similar levels of the Gag polyprotein in the cell lysates, indicating that the mutations did not affect Gag synthesis. The characteristic mobility shift of the p55 band when PTAP is changed to LIRL was observed, similar to mutation in the Gag only construct (Figure 3.5). Notably, the 52 amino acid deletion to generate the Δp6 resulted in the lower molecular weight band Gag polyprotein (55Δp6), about 49 kb. A hallmark for mutagenesis of the p6 in HIV-1 is an increase in the levels of Gag processing intermediates, such as p41, in cell lysates (Huang et al., 1995; Demirov et al., 2002b). This was seen for the $PTAP^{-}$, $PTAP^{-}YP^{-}$ and Δp6 constructs.

Analysis of the released viruses is shown in the lower panel of Figure 3.13A. The p24 bands in the virion-associated Gag were hardly detectable for the $PTAP^{-}$, $PTAP^{-}YP^{-}$ and Δp6 mutants, which behave as expected. In addition, p55 and p55Δp6 bands were observed for the mutants, suggesting the presence of some unprocessed proteins, which could imply sheared immature particles, microvesicles or cell debris in the media. However, the fact that the band signals were stronger for the WT and YP^{-}, than they were for the $PTAP^{-}$, $PTAP^{-}YP^{-}$ and Δp6, is indicative of impaired release of these later mutants.

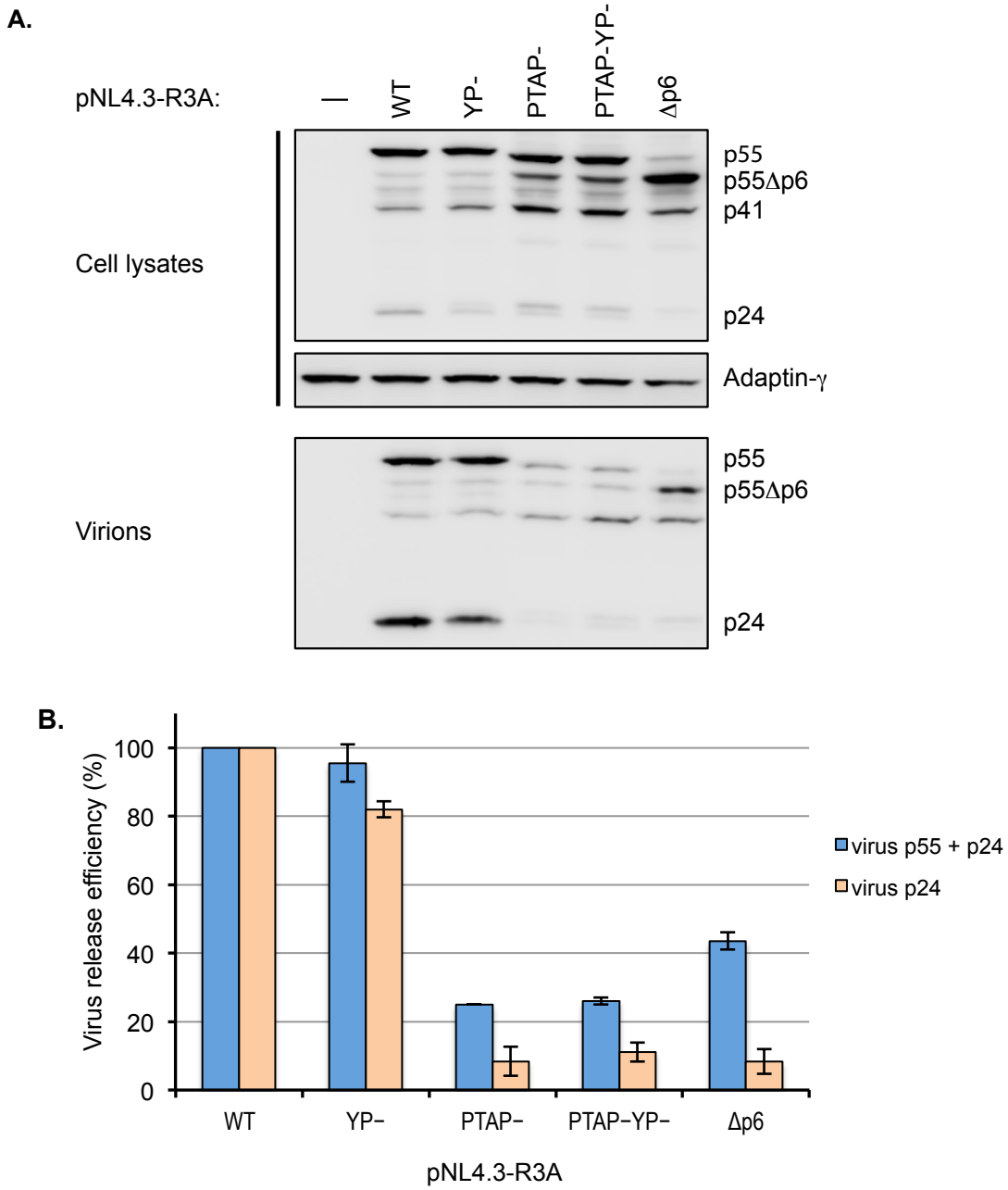

Figure 3.13: Immunoblotting of R3A mutants expressed in HEK 293T cells.

(A) Cells were transfected with the indicated pNL4.3-R3A constructs, and incubated for 24 hrs. Virions released into the media were purified by ultracentrifugation on 20% sucrose cushions. Virus pellets and cells were lysed in sample buffer under reducing conditions, loaded on 10% SDS-PAGE gels, and blotted onto PVDF membranes. The membranes were probed with antibodies against viral p24/55 or the loading control adaptin-γ. Bands were visualised using the ImageQuant imaging system. **(B)** Band signal intensities were quantified using ImageJ to determine virus release efficiency, first using either virus p55 (or p55Δp6) plus p24, and/or virus p24 only. Virus release efficiencies ± SD were determined for two experiments, using equation No. 2 given in Materials and Methods, Section 2.8.

To determine the virus release efficiencies, band intensities were measured for two independent experiments. The release efficiencies for the mutants were determined for virus p55 (or p55Δp6) plus p24 (Figure 3.13B, blue bars). As the p55 (or p55Δp6) bands may imply contamination, their inclusion in the quantitations may elevate virus release efficiencies for the mutants. The p24 represents released mature virus particles and was thus used as a more reliable measure of virus release efficiencies. Using the p24 levels in virions, the average release efficiency for the YP$^-$ mutant was 82.0 ± 2.4%, showing that this mutation had only a minimal effect on HIV release. The release efficiencies for the PTAP$^-$, PTAP$^-$YP$^-$ and Δp6 mutants were 8.3 ± 4.2, 11.1 ± 2.7 and 8.4 ± 3.7%, respectively. These data are consistent with the notion that the Tsg101-binding site (PTAP) is more important than the ALIX-binding site for HIV-1 release.

3.2.11 Characterisation of the HIV-1 R3A mutants in MDM by WB

To determine whether the release of the HIV-1 R3A mutants was also inhibited in MDM, cells were electroporated with the proviruses (see Materials and Methods, Section 2.7). The viruses and cells were harvested 24-hrs post-electroporation and analysed by WB (Figure 3.14A). The representative blot shows that it was not always easy to get equal amounts of expression for the proviruses. Electroporation stresses cells and they may not recover fully following the procedure, as most cultures showed reduced cell viability. Longer incubations of cultures (48 hrs) increased cell death. Nevertheless, examination of the WB shows that the p55 (or p55Δp6) bands for the R3A PTAP$^-$ and Δp6 mutants were stronger in the cell lysates, consistent with increased accumulation of unprocessed Gag when virus scission is hindered. There was reduced virion-associated p24 in the medium for the PTAP$^-$ and Δp6 mutants, suggesting virus release was inhibited.

Estimates of virus release are shown in Figure 3.14B. The PTAP$^-$ and Δp6 mutants were inhibited to similar levels, with release efficiencies of about 37.4 and 37.1%, respectively, compared to the YP$^-$ mutant that had 71.4% release efficiency. This is the same trend as in HEK 293T cells. Furthermore, these data again show that mutations in the Tsgl01 binding motif, have a profound inhibitory effect on virus release in MDM, compared to mutating the ALIX recruiting motif. Most importantly, the mutants work in

MDM, confirming the requirement of the ESCRT machinery in HIV release from MDM.

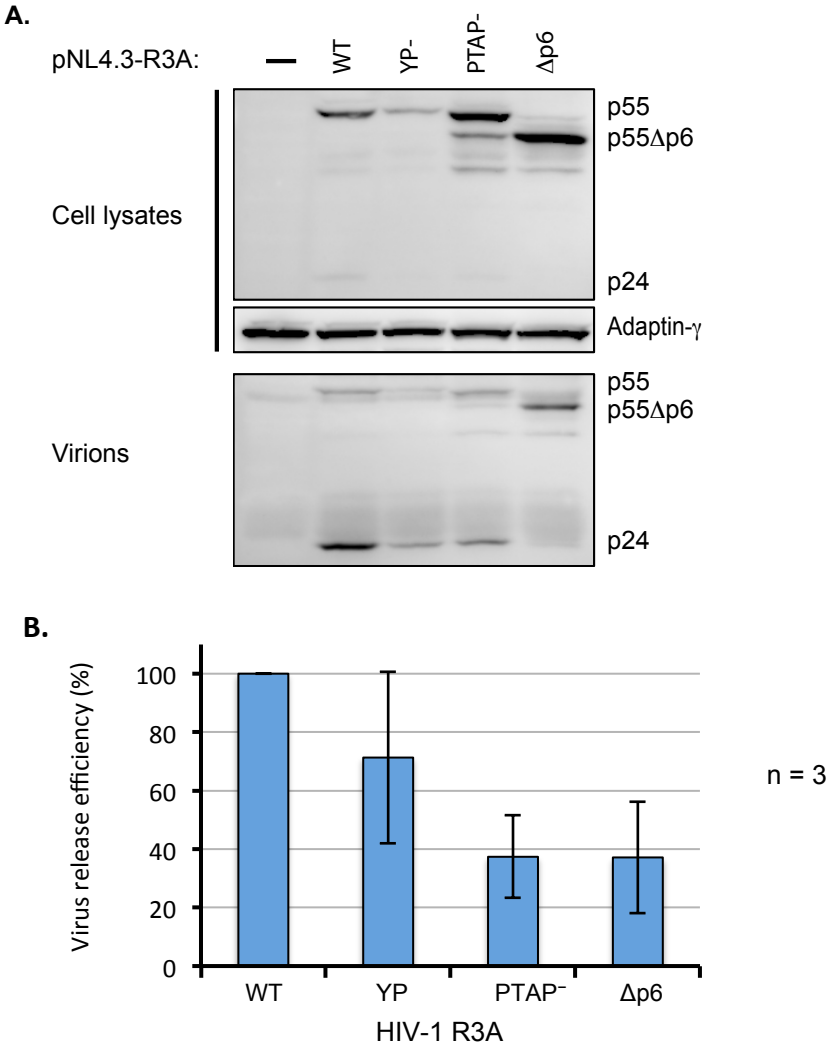

Figure 3.14: Biochemical analysis of virus release efficiency from MDM.

(A) Fourteen-day old MDM were electroporated with the respective constructs and incubated for 24 hrs. Virus was purified from the culture medium by ultracentrifugation on a 20% sucrose cushion. The virus pellet and cells were lysed in sample buffer. Lysates were analysed by SDS-PAGE separation and western blotting. The WB is a representative from three experiments. **(B)** Virus proteins were quantified on WB to determine the amount of virus released into the medium relative to total virus that was in the cell culture. The virus release efficiency ± SD is for three experiments.

3.3 Discussion

HIV-1 is targeted to the plasma membrane where it assembles. To complete the assembly process, the virus uses its late domain motifs in Gag, PTAP and YPXnL, to recruit ESCRT pathway proteins, Tsg101 and ALIX, which facilitate membrane fission

and virus release. Depleting ESCRT pathway proteins, using dominant negative forms of the proteins, or mutating the late domain motifs, all disrupt HIV release (Garrus et al., 2001; von Schwedler et al., 2003; Fujii et al., 2009; Sette et al., 2010). In the first approach, I used Tsg101 and ALIX siRNA to knockdown the proteins individually or together in HIV-infected MDM. Though the proteins were efficiently depleted, there was little effect on virus release. As an alternative approach to the RNAi, the late domain motifs, PTAP and YPXnL, were mutated in the native Gag_{BaL} expression plasmid, generating single and double mutants to disrupt recruitment of Tsg101 and ALIX, respectively. The release of the mutants was efficiently inhibited in HEK 293T cells. When introduced into MDM by electroporation, the native Gag_{BaL} WT and mutants were not expressed. However, when codon-optimised Gag mutants were expressed in MDM, they were unexpectedly released. To address this, the activity of VPS4 was inhibited using a dominant negative form, the VPS4 EQ. When the VPS4 EQ plasmid was co-transfected with either codon-optimised Gag or HIV-1 provirus plasmids, the release of VLPs or virions was inhibited, indicating the involvement of the ESCRT pathway in HIV-1 assembly in MDM. A dual tropic provirus, HIV-1 R3A provirus, was used to generate mutants ($PTAP^{-}$ $PTAP^{-}YP^{-}$ and Δp6) that are defective in recruiting the ESCRT machinery. The mutants were characterised by WB on HEK 293T cells, where their release was found to be impaired. The release of these mutants was also defective in MDM, as determined by WB analysis of electroporated cultures.

In order to disrupt ESCRT recruitment in infected MDM, the cells were transfected with siRNA to Tsg101 and ALIX. Individually, these proteins were depleted to very low levels, with ALIX being almost undetectable on average (Figures 3.1 and 3.2). Despite the efficient knockdown of Tsg101 or ALIX, the corresponding virus release was high, 76% and 92%, respectively. When the two proteins were depleted together, virus release was 71%, which still showed a small inhibitory effect, given the good levels of knockdowns. As both the single and double knockdowns had only small effects on blocking virus release, it was likely that the majority of the infected cells escaped siRNA transfection, or that residual levels of the proteins were enough to mediate virus release. During the course of this study, two reports showed that when Tsg101 is depleted in MDM with nearly 100% infection by VSV-G pseudotyped HIV-1, about 30-40% of p24 levels for the mature virions is detected in the culture supernatants (Gaudin

et al., 2012; Berre et al., 2013). That level of infection cannot be achieved using the physiological route of infecting macrophages with HIV-1. The best infection level I achieved in experiments with MDM was about 30%. It is possible that in my study infected MDM were difficult to transfect with siRNA, which probably did not matter in the two studies above if 100% of cells were infected. In the current study, protein depletions were optimal on the sixth day after siRNA transfections. It is possible that the virus that is detected was produced and stored in the IPMCs whilst Tsg101 and ALIX levels were progressively being depleted during the incubation period of the cultures. Therefore, the virus released may have come from the IPMC reservoir.

As an alternative to siRNA studies, I decided to mutate the ESCRT interaction motifs, PTAP and YPXnL, in a native Gag plasmid, pRK5Gag$_{BaL}$, to generate Gag defective in recruiting the ESCRT machinery. The mutants were all severely defective in the release of VLPs (Figure 3.5). However, the pRK5Gag$_{BaL}$ constructs were not expressed in MDM during a 24-hr incubation, while a 48-hr incubation of the macrophages severely reduced the number of adhered viable cells as assessed by culture observations and trypan blue staining. Electroporation can be toxic to cells and it has been reported that in cells that survive, some cellular functions may be altered (Stacey et al., 1993). Temporary re-arrangement of the actin cytoskeleton has been reported in electroporated cells (Pehlivanova et al., 2012), which may affect adherence of macrophages in tissue culture, resulting in the loss of cells during fixing and staining.

The high AU content of unspliced native *gag* transcripts makes them inherently unstable, especially in primary human cells. Rev binding to these unspliced transcripts is required to help stabilise and export them out of the nucleus (Schwartz et al., 1992a; Schwartz et al., 1992b; Nguyen et al., 2004). In the current study, the native Gag$_{BaL}$ was expressed without Rev, and therefore its transcripts may have been destroyed before translation in MDM. As an alternative to the native Gag, a codon-optimised GagGFP plasmid was electroporated into MDM, and in this case the Gag protein was expressed (Figure 3.6). However, several studies have demonstrated that GFP-tagged Gag forms aberrant particles or budding profiles that are larger and more heterogeneous in size, characterised by discontinuous Gag layers (Pornillos et al., 2003; Larson et al., 2005; Pelchen-Matthews and Marsh, 2007). Therefore, untagged codon-optimised Gag WT

and mutants were generated from the codon-optimised GagGFP constructs. In HEK 293T cells, the Gag PTAP^{-}YP^{-} showed the strongest inhibitory effect on the release of VLPs, followed by Gag PTAP^{-}, while Gag YP^{-} was weakly inhibited (Figure 3.7). These data agree with the notion that Tsg101 predominantly facilitates HIV-1 release in many cell systems (Demirov et al., 2002b; Fujii et al., 2009). However, when the codon-optimised Gag WT and mutants were tested in MDM, they were released almost to the same extent as the Gag WT (Figure 3.8). The expectation was that deleting the ESCRT-recruiting motifs in Gag would have a stronger inhibitory effect on the release of VLPs, compared to using RNAi to disrupt the recruitment. It is possible that electroporated cells released some microvesicles that pelleted during ultracentrifugation of culture medium to harvest VLPs.

I exploited the ability of a dominant negative VPS4 EQ to inhibit virus budding (Garrus et al., 2001; von Schwedler et al., 2003) by first co-electroporating MDM with VPS4 EQ and Gag WT plasmids. The dominant negative VPS4 inhibited the release of Gag (Figure 3.10), showing that the ESCRT pathway is important for the release of VLPs. Next, HIV-1 provirus pNL4.3-R3A was co-electroporated, with either the pGFP-VPS4 EQ or WT into MDM, to test ESCRT requirement with a full virus clone. When analysed by WB, the dominant negative markedly blocked HIV release to almost undetectable levels (Figure 3.11), indicating that the ESCRT pathway is required for HIV-1 release in MDM, in agreement with recent studies (Gaudin et al., 2012; Berre et al., 2013). As electroporated MDM did not survive incubations beyond 24 hrs, using infectious virus with mutations in the PTAP and YPXnL motifs to infect cell was required for studying assembly in MDM.

Mutagenesis was carried out on the HIV-1 R3A strain, changing the PTAP motif that recruits Tsg101 to LIRL, and the YP residues within the ALIX-recruiting motif to SR. In addition, a stop codon was introduced at the beginning of p6, thus deleting the entire p6 subdomain and removing the binding sites for both Tsg101 and ALIX. However, it has been reported that ALIX can also bind the NC, but to mediate virus release it cooperates with late domain motifs (Dussupt et al., 2009). The mutagenesis was designed such that the reading frame for *pol* was not affected, so that functional viral protease would be produced (Demirov et al., 2002b; Votteler et al., 2009; Watanabe et

al., 2013). In HEK 293T cells, the mutants were released less efficiently compared to the WT (Figure 3.13), as determined from the p24 in the virions. The p24 protein is only detectable in mature virions whose Gag polyprotein has undergone proteolytic cleavage. In addition, p55 (or p55Δp6) was present in virus lysates for the mutants, perhaps a result of shearing off of the immature particles (see Chapter 4 Discussion). Severe release defects were observed in mutants that did not have Tsg101 recruiting motif, consistent with previous reports showing that Tsgl01 is more important than ALIX for HIV release in many cell systems (Demirov et al., 2002b; Fujii et al., 2009).

The HIV-1 R3A mutants were tested in MDM, and analysis of their expression by WB showed that the release of $PTAP^{-}$ and Δp6 viruses was impaired (Figure 3.14). Unlike cell lines, primary cells such as MDM are difficult to transfect using reagent-based methods (Dokka et al., 2000). Therefore, proviruses were introduced into MDM by electroporation (also called nucleofection). Although this method works for MDM, it has some undesirable effects on the cells. Poor cell adherence, which varied from donor to donor, was noticeable, and this could be attributed to the disturbance of the cytoskeleton caused by electroporation (Pehlivanova et al., 2012). The plasmids used for electroporation were of high purity and endotoxin-free, although hypothetically, the large plasmid size (14.8 kb) may also be responsible for low transfection levels, compared to smaller plasmids (<10 kb). It is possible that transient pores generated in the membranes during electroporation were not large enough to accommodate big plasmids. Therefore, I developed a method to rescue infectious release-defective mutants in HEK 293T cells (see Chapter 4), in order to infect MDM with the mutants.

In this chapter, I have shown the efficient depletion of ESCRT/ESCRT associated proteins in MDM by RNAi, and that this resulted in about 30% inhibition of virus release at most, which would not be sufficient for the intended morphology studies in macrophages. However, it emerged in these studies that Tsg101 is more important than ALIX for HIV release in macrophages, as in many cell systems. In the second approach to disrupt ESCRT recruitment, mutants defective in binding the ESCRT proteins were generated in Gag constructs, native Gag or codon-optimised Gag. In HEK 293T cells the mutants behaved as expected, showing a bigger inhibition effect with mutations in the Tsg101 recruiting motif, than in the ALIX recruiting motif. An additive effect was

seen when the two mutations were combined. In MDM, the effect of the mutations was not seen as mutants were released to the same extent as the WT. However, using the dominant negative VPS4 EQ demonstrated that the ESCRT pathway is indeed required for HIV release in macrophages. Therefore, I used an HIV-1 full molecular clone with mutations that disrupted Tsg101 and ALIX recruitment, and the release of HIV-1 R3A PTAP^{-} and Δp6 viruses was inhibited in MDM, showing that indeed the ESCRT machinery is required for virus release in MDM. The morphologies of the mutants will be described in Chapter 4.

"... I have discovered the secret that, after climbing a great hill, one only finds that there are many more hills to climb."

Nelson Rolihlahla Mandela

4. Characterisation of HIV-1 Full Molecular Clones Defective in Recruiting ESCRT Components

4.1 Introduction

Late in the assembly of HIV-1, the late domain sequences of HIV Gag, PTAP and YPXnL, recruit the ESCRT pathway proteins, Tsg101 and ALIX, respectively (Carlton and Martin-Serrano, 2007; Martin-Serrano and Marsh, 2007; Carlton et al., 2008; Sundquist and Krausslich, 2012). The engaged Tsg101 or ALIX bind to the ESCRT-III complexes, which in turn recruit the VPS4 ATPase to catalyse the disassembly and recycling of the ESCRT proteins. This facilitates fission of the membrane stalk connecting nascent virions to host cells. Inhibiting the ESCRT pathway impairs HIV release (Demirov et al., 2002b; Pornillos et al., 2003; Fujii et al., 2009; Sundquist and Krausslich, 2012) (see General introduction, Section 1.5.5).

In chapter 3, I depleted the ESCRT machinery components Tsg101 and ALIX, to investigate their importance in the assembly of HIV-1 in primary macrophages, but there was modest inhibition of virus release despite the efficient depletion of the proteins. However, mutagenesis of Gag in a full-molecular clone of HIV-1, in which the PTAP and/or YPXnL motifs were mutated, or the entire p6 subdomain was deleted, significantly inhibited HIV-1 release in HEK 293T cells and primary macrophages. As my approach to verifying the site of HIV assembly in primary macrophages required the formation of stable, arrested, budding intermediates, I set out to initially verify the phenotype of the mutants in HEK 293T cells by immunofluorescence and electron microscopy methods. Semi-thin sections, of HEK 293T cells transfected with the HIV-1 R3A WT and mutants ($PTAP^{-}$, $PTAP^{-}YP^{-}$ and Δp6), were immuno-stained and examined by fluorescence microscopy, revealing that the mutants produced immature viruses at the cell surface. To visualise the viruses, ultra-thin sections were examined using EM. Cells transfected with proviruses containing the late domain mutations showed accumulations of immature particles or arrested buds with the "lollipop" configuration that have been described previously (Garrus et al., 2001; von Schwedler et al., 2003; Carlson et al., 2008). As biochemical studies show that viruses were not released to the media (Chapter 3, Figure 3.13), these viruses were assessed to be

budding arrested. I therefore developed protocols in order to rescue the release-defective viruses so that they could be used to infect primary macrophages for the analysis of the virus distributions at the IPMCs and cell surface, as will be described in Chapter 5.

4.2 Results

4.2.1 Morphological characterisation of HIV-1 R3A mutants in HEK 293T cells

4.2.1.1 Screening transfected cells by immunofluorescence

The analysis of the HIV-1 R3A mutants by immunoblotting showed that the release of PTAP^{-}, PTAP^{-}YP^{-} and Δp6 was significantly impaired (Chapter 3, Figure 3.13). Therefore, I wanted to check whether the mutants actually produced arrested HIV-1 budding profiles, which needs EM. HEK 293T cells were transfected with the HIV-1 R3A WT, YP^{-}, PTAP^{-} and Δp6 proviruses and incubated for 24 hrs. Fixed cells were processed for EM. Initially, semi-thin sections of the transfected HEK 293T cells were screened by IF to determine transfection levels and locate infected cells. The sections were immuno-stained with anti-p24/55 in combination with anti-p17. The anti-p24/55 antibodies recognise both the unprocessed Gag polyprotein (seen as diffuse cytoplasmic staining), as well as the processed CA protein p24 in virus, which gives a punctate labelling pattern at the cell surface. The anti-p17 antibody 4C9 binds to a short amino acid sequence at the extreme C-terminus of the MA portion of Gag at the PR cleavage site, and as a result only binds to the processed p17 MA of mature viruses. This monoclonal antibody can therefore be used to identify mature virus particles. The immuno-stained sections were examined by fluorescence microscopy (see Materials and Methods, Section 2.11).

The p24/55 labelling on cells transfected with HIV-1 R3A WT showed diffuse cytosolic staining, presumably of unassembled Gag polyprotein, as well as puncta at the cell surface (Figure 4.1A). Notably, these puncta also labelled with the p17 antibody, suggesting that they were mature particles that had recently budded from the cells. Examination of the HIV-1 R3A PTAP^{-} and Δp6 mutants in Figure 4.1B and C revealed that, on many cells, the cell surface was decorated with puncta that labelled with anti-p24/55 antibody, but not with anti-p17. Occasionally, cells with bright p24/55 cytosolic

staining also had a continuous layer of p17 labelling that bordered the PM. Examples of these cells are marked with an asterisk on Figure 4.1B and C. The presence of cleaved p17 at the plasma may be due to the viral protease (PR) being auto-activated as Gag-Pol accumulates at the PM. It has been reported that the viral PR can be activated before scission when Gag is overexpressed (Carlson et al., 2010). These results demonstrate that the PTAP^{-} and Δp6 mutants show a staining pattern characteristic of immature particles, which is consistent with the impaired release observed in the WB data presented in Chapter 3, Figure 3.13.

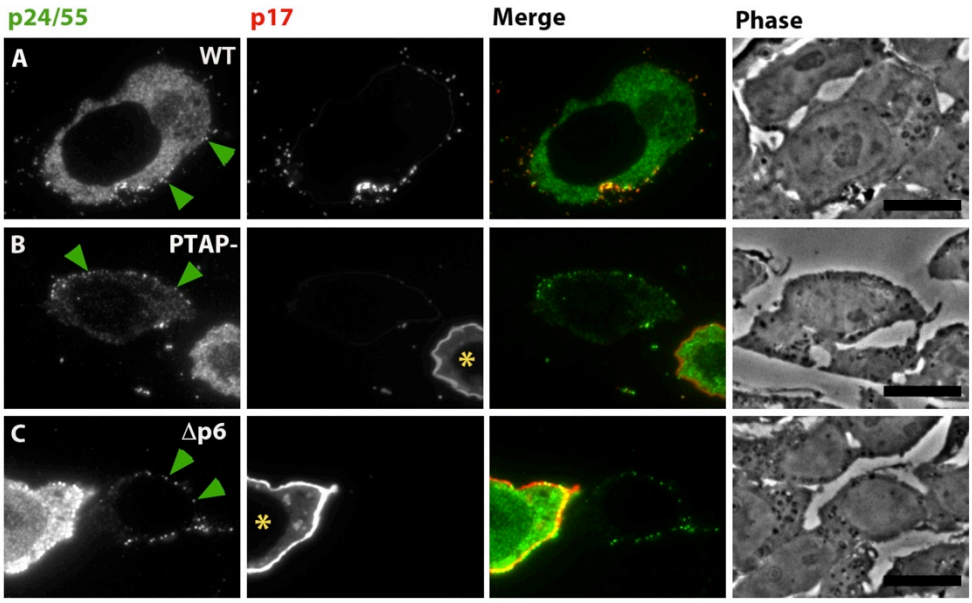

Figure 4.1: Analysis of the expression of HIV-1 R3A WT and mutants in HEK 293T cells by IF. The cells were transfected with the indicated proviruses, incubated for 24 hrs and then fixed. Semi-thin cryo-sections (0.5 µm) were double immuno-stained with anti-p24/55 (38:96K and EF7) and anti-p17 (4C9) (A to C). **(A)** Mature viruses co-stain with p24/p55 (green puncta; selected examples shown by arrowheads) and p17 (red puncta). **(B, C)** Immature viruses labelled with p24/p55 (green puncta) only. In cells with high expression of Gag, the viral protease is prematurely activated to cleave Gag, and the cells then label with anti-p17 (cell with yellow asterisk). Scale bars, 10 µm.

4.2.1.2 Ultra-structural analysis by EM

Immunofluorescence screening of transfected cells showed that the mutants did not produce virus puncta that labelled with the p17 antibody, suggesting that virus maturation might be impaired (Figure 4.1). To assess whether the mutants were arrested, the same samples were analysed by EM. Ultra-thin cryo-sections were labelled with either the anti-p24/55 or -p17 (4C9) antibodies, and protein A gold (PAG). Gold binds to the secondary antibody, which is in turn bound to the primary antibody. It

creates electron dense spots, allowing for identification of the structure labelled by the primary antibody. For HIV-1 R3A WT, it was difficult to find virus particles, presumably because they were released into the culture medium and, therefore, lost from the specimens. Viruses were so rare that they could only be located and identified because of the antibody label (Figure 4.2A, B). When they were found, the p24 staining was observed over the virus particles, sometimes near visible cores, while the p17 staining was on the periphery of the particles adjacent to the lipid membrane (explained in Figure 4.2 legend). The morphology of these viruses shows that they are indeed mature particles that have been detached from the cell membrane, in support of the IF data (Figure 4.1).

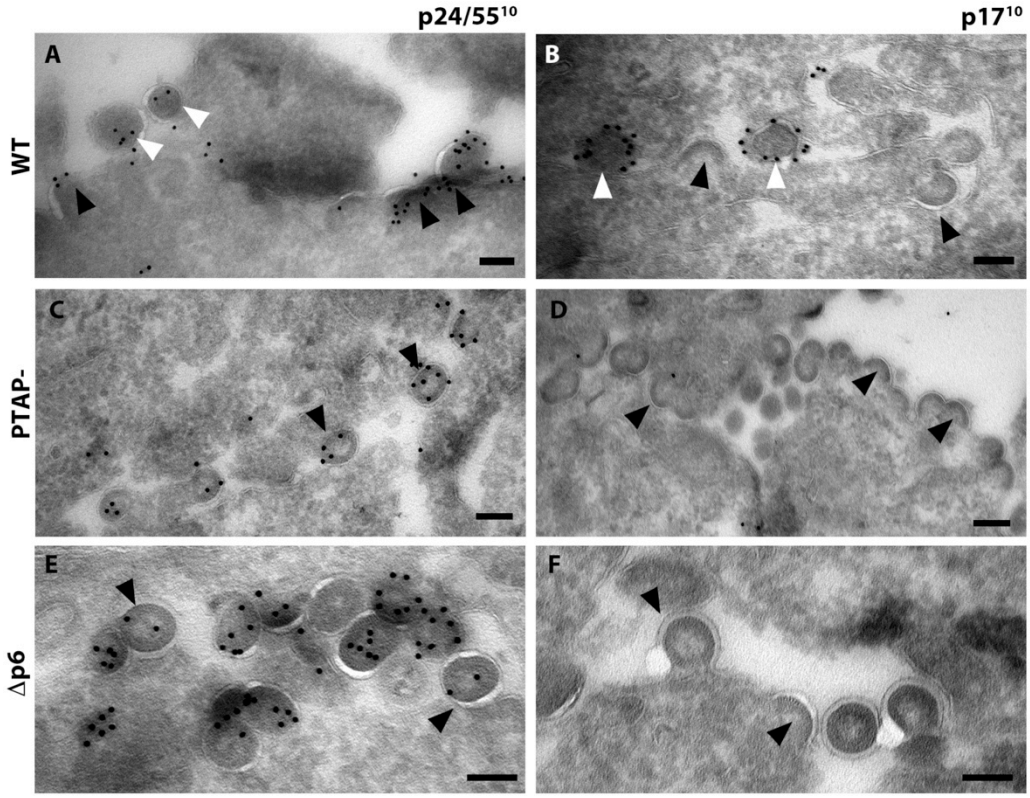

Figure 4.2: Ultra-structure of HIV-1 R3A WT and mutants in HEK 293T cells.
Immunolabelling of cryo-sections from HEK 293T cells transfected with the indicated HIV-1 R3A proviruses. Ultra-thin sections (50 nm) were immunolabelled with either p24/55/PAG10 (images on the left) or p17/PAG10 (on the right). **(A, B)** HIV-1 R3A WT mature viruses label with anti-p24/55 or p17. For p24, the gold labelling is over the centre of the virus particles, while p17 staining is near the outer membrane (within 20 nm of the outer membrane, consistent with two layers of antibodies i.e. p17 / rabbit anti-mouse / PAG10). Buds and mature virus particles are indicated with black, and white arrowheads, respectively. **(C to F)** HIV-1 R3A PTAP^{-} and Δp6 virus profiles are immature and arrested budding intermediates observed at the cell surface, and labelled with anti-p24/55, but not with anti-p17. Scale bars, 100 nm.

For the PTAP^{-} and Δp6 mutants, numerous arrested budding profiles were observed. These had electron-dense Gag layers under the bud membrane as described elsewhere (von Schwedler et al., 2003), and were predominantly labelled with anti-p24/55 antibodies. On many of the cells, there was no labelling with anti-p17 antibody (Figure 4.2D and F), in agreement with the IF data. These EM images confirm that both the PTAP^{-} and Δp6 mutants were arrested late in budding, as expected for ESCRT recruitment deficiency.

4.2.1.3 Ultra-structural analysis by Epon EM

Most of the previous studies that examined the ultra-structure of arrested budding HIV used plastic embedding EM (Garrus et al., 2001; von Schwedler et al., 2003; Dussupt et al., 2009). Therefore, classical Epon embedding EM was used to further characterise the mutants in HEK 239T cells. Compared to gelatine-embedded and cryo-sectioned specimens, Epon-embedded cells have clearer morphology, due the use of osmium tetroxide to enhance membrane contrast. However, the harsh fixation steps and dehydration used for Epon EM destroys many antigens on the specimens, making them generally unsuitable for immuno-labelling.

To analyse the morphology of viruses by Epon EM, HEK 293T cells were transfected with the proviruses HIV-1 R3A WT, PTAP^{-}, PTAP^{-}YP^{-} and Δp6. The cells were fixed and embedded in Epon (Materials and Methods, Section 2.14). As observed in immuno-EM, it was difficult to locate virus particles on the WT-transfected cells. Occasionally, a few virus particles were seen, trapped between adjacent cells. Where sectioned equatorially, they typically had electron dense cores, indicative of the mature HIV phenotype (Figure 4.3A and A'). These images show that most of the WT virus is released, in agreement with the WB results. Examination of cells transfected with HIV-1 R3A PTAP^{-}, PTAP^{-}YP^{-} and Δp6 showed arrested budding profiles decorating the surface of cells (Figure 4.3B and B'). The buds had a prominent Gag layer of immature non-cleaved Gag. A range of morphologies was observed, including shallow buds, the arrested "lollipops" that have been described previously, as well as some duplexes or rosettes (Figure 4.3B to D). These morphologies were only rarely observed on WT transfected cells presumably because they are transient intermediates of assembly.

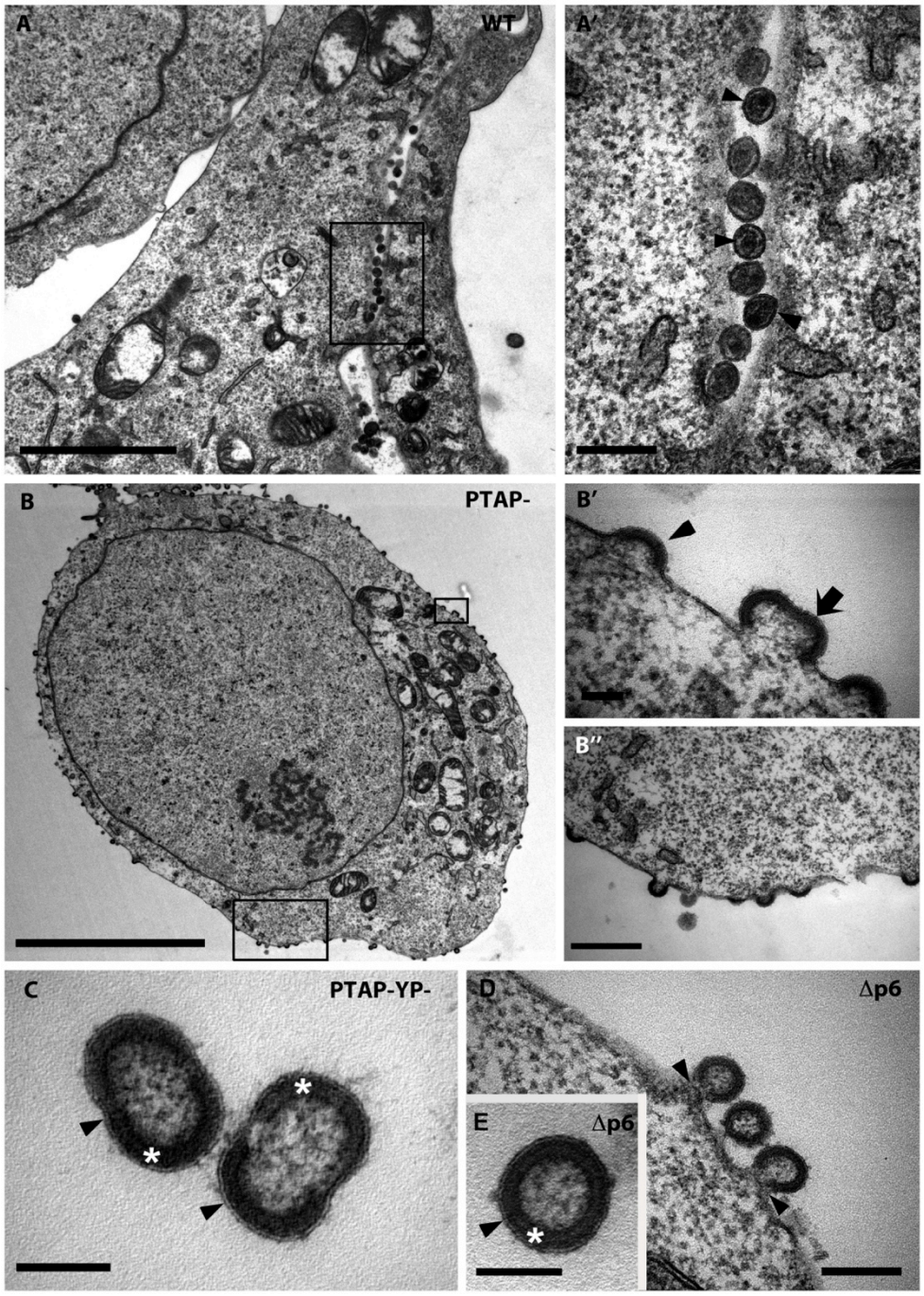

Figure 4.3: Epon-EM of HEK 293T cells transfected with HIV-1 R3A plasmids.

The cells were transfected with the indicated plasmids, incubated for 24 hrs, then fixed and Epon-embedded. Sections (70 nm) were examined by transmission EM. **(A)** Mature WT particles (selected examples indicated by arrowheads on A') are trapped between the PMs of adjacent cells. **(B-E)** PTAP^{-} (B), PTAP^{-}YP^{-} (C) and Δp6 (D, E) budding profiles decorate the cell surface. **(B)** Overview of a typical cell with buds. In (B'-E), budding structures are shown at higher magnification. **(B)** A single shallow bud is indicated with an arrowhead. Some duplex buds are shown with an arrow. **(C, E)** The budding profiles that did not have visible connections to the plasma membrane appear as released immature particles. Asterisks are on the electron dense layer formed by non-cleaved immature Gag layers, whilst arrowheads point to the bi-layer membrane derived from cells. **(D)** The arrowheads point to virus stalks. Scale bars: A, 2 μm; A', 250 nm; B, 5 μm; B', 100 nm; B", 500 nm; C, 100 nm; D, 200 nm; E, 100nm.

The examination of R3A PTAP$^-$ and PTAP$^-$YP$^-$ virus profiles revealed that many had fairly shallow bud morphology, while most Δp6 budding profiles appeared more spherical (compare Figure 4.3B' and D). Where there were no visible connections to the PM, virus profiles appeared as released immature and spherical or dumbbell-shaped particles, with a thick Gag layer (Figure 4.3C and E), and this was particularly common with the Δp6. The average width of the bud opening (at the base where they were connected to the PM), or membrane stalks where present, was about 140 nm for PTAP$^-$YP$^-$ or PTAP$^-$, and about 75 nm for Δp6. The narrow stalks on Δp6 meant that the membrane connections were not always captured within the section (typically 70 nm). These narrower stalks could be more susceptible to shearing off from the cell membrane, which may explain the higher levels of virion-associated Gag (p55Δp6) for the Δp6 mutant, compared to p55 for PTAP$^-$ or PTAP$^-$YP$^-$ in the WB experiments (see Chapter 3, Figure 3.13). Given that most WT particles are released and therefore lost from cells, the fact that the mutant particles were easily found in the specimens suggested that they remained attached to the host cells.

To follow up the differences, I counted virus profiles on EM images, and classified the profiles into mature and immature. The immature profiles were further subdivided into profiles connected to, and those without visible connections to, the PM. This was carried out for the HIV-1 R3AWT, and PTAP$^-$, PTAP$^-$YP$^-$ and Δp6 mutants. A total of 1,301 profiles were analysed (Figure 4.4). Although a small number of profiles were found for the WT, a high proportion of those (74%) were mature. For the PTAP$^-$ and PTAP$^-$YP$^-$ mutants, more that 80% of the profiles were connected to the PM, whilst only 40% of the Δp6 profiles had visible connections. The data are consistent with the notion that the width of the membrane stalks may influence what is observed as connected or not connected to the plasma membrane, and therefore, data on ultra-thin sections need to be interpreted with caution.

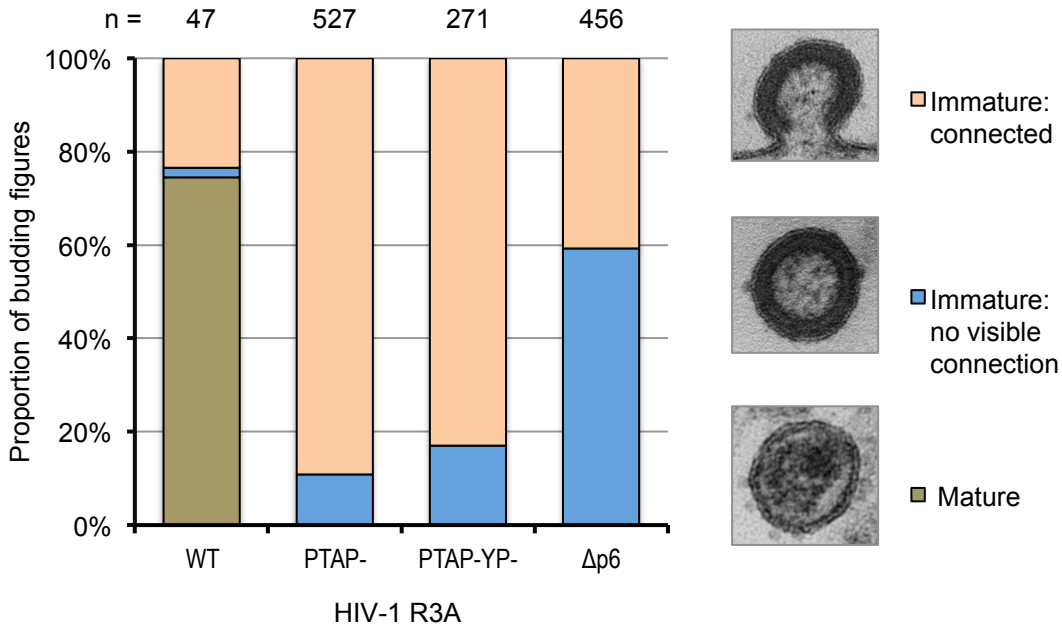

Figure 4.4: Estimating the proportions of virus profiles connected to host cells.
For each provirus used to transfect HEK 293T cells, virus figures were counted on EM images and scored as immature and mature. Immature figures were divided further into those connected to, and those without any visible connections to, the PM. The proportions for each category were determined per virus construct.

As noted above, the PTAP$^-$ and PTAP$^-$YP$^-$ arrested virus profiles appeared shallower than those for the Δp6. To quantitatively analyse the dimensions for the budding virions, a set of measurements were taken for each bud profile (illustrated and described in Materials and Methods, Section 2.15): (i) the angle of Gag incorporation, (ii) the bud height, and (iii) the angle of bud closure. For this analysis, only HIV bud structures showing membrane continuity with the producer cell were measured. To analyse the budding morphology for the PTAP$^-$, PTAP$^-$YP$^-$ and Δp6 mutants, the angle of Gag incorporation was measured on a total of 256 virus profiles. There was no significant difference between the averages for the angle of Gag incorporation for the PTAP$^-$ (180.3 ± 55.1°) and PTAP$^-$YP$^-$ (176.3 ± 57.1°). However, the average for the Δp6 (266.9 ± 54.4°) was significantly different to that of the PTAP$^-$ or PTAP$^-$YP$^-$ mutants (Figure 4.5B). Additionally, the radii of any buds ≥180° were measured for each mutant: PTAP$^-$ (71.6 ± 4.1); PTAP$^-$YP$^-$ (69.7 ± 4.3); and Δp6 (67.6 ± 4.1), and were found to be similar, indicating that the mutations did not affect the size of the virus particles which correspond to the size of HIV (130 nm diameter) (Briggs and Krausslich, 2011).

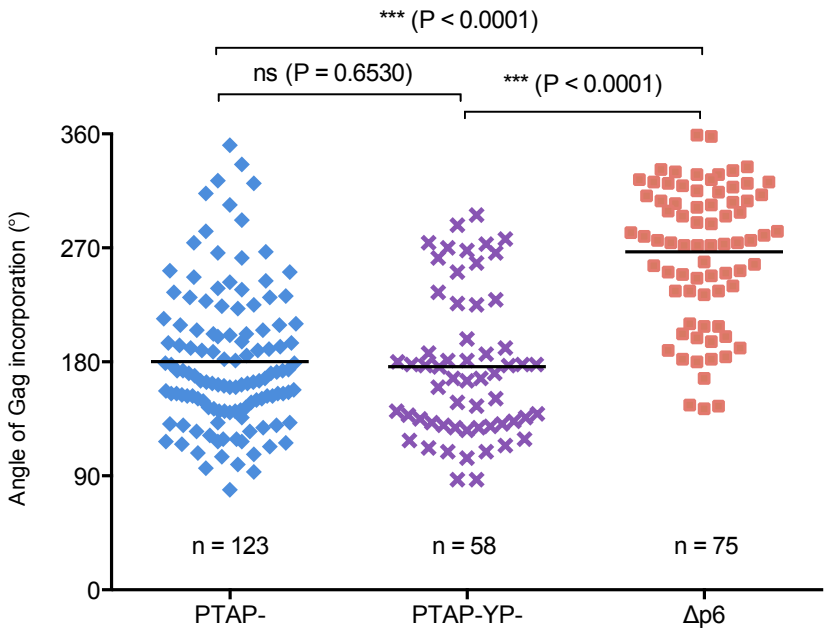

Figure 4.5: Quantitative analysis of the morphology of virus budding profiles.
The angle of Gag incorporation was measured by extrapolating a circle, and measuring from the centre of the circle, an angle enclosing the Gag layer (see Materials and Methods, Figure 2.7A). Statistical analyses were performed using the unpaired t-test at $p<0.05$.

Taken together, the EM observations together with biochemical analysis in Chapter 3, Figure 3.13, show directly that in HEK 293T cells, budding intermediates accumulate for PTAP^{-}, PTAP^{-}YP^{-} and Δp6, that is, they are arrested. The higher angle of Gag incorporation for HIV-1 R3A Δp6 suggests that the p6 subdomain may have additional role(s) in HIV biogenesis, including regulation of the HIV assembly process, possibly through other biochemical modifications.

4.2.2 Preparation of infectious mutant viruses

In Chapter 3, Figure 3.13, I showed that when HIV-1 R3A PTAP^{-}and Δp6 proviruses were introduced into primary macrophages by electroporation and analysed by WB, virus release was inhibited, suggesting that the mutants could produce arrested budding intermediates for the study of HIV assembly in macrophages. However, about half of the cells did not survive electroporation. Initial morphological studies, where MDM from three different blood donors were electroporated with the mutants and examined by IF to assess the distribution of mutant viruses were, extremely challenging to do, with <1% of cells expressing the virus (see Chapter 5). To overcome these difficulties, I decided to avoid electroporation and develop a virus to infect macrophages. However,

the mutants are budding arrested and therefore cannot produce mature infectious particles. Therefore, I tested different strategies to rescue the arrested virus in producer cells by co-expressing the mutants with either ALIX or wild-type Gag plasmids.

4.2.2.1 ALIX-mediated rescue of HIV-1 PTAP$^-$

As a first approach to produce infectious provirus mutants, I tested reports that when ALIX is overexpressed it can support efficient release of an HIV-1 PTAP$^-$ mutant (Fisher et al., 2007; Usami et al., 2007; Carlton et al., 2008). The PTAP$^-$YP$^-$ and Δp6 mutants cannot be rescued by co-expression with ALIX, because the ALIX recruiting motif of PTAP$^-$YP$^-$ is inactivated by mutagenesis whilst the Δp6 mutant does not express the two motifs that wild-type HIV uses to recruit the ESCRT machinery. HEK 293T cells were co-transfected with HIV-1 R3A PTAP$^-$, and either haemagglutinin-tagged ALIX (HA-ALIX), or ALIX tagged with monomeric Cherry (mCh-ALIX) (Carlton and Martin-Serrano, 2007; Carlton et al., 2008). Different amounts of ALIX plasmid DNA (0.25 or 0.75 μg) were used with 3 μg of HIV-1 R3A plasmid. The transfected cells were incubated for 24 hrs before harvesting virus from the medium. Biochemical analysis of cell lysates showed that equal amounts of p55 were expressed for all transfections, except where 0.75 μg of mCh-ALIX plasmid was used (Figure 4.6A). Using 0.25 μg of either HA-ALIX or mCh-ALIX plasmids did not increase the amount of released virus, compared to transfections with HIV-1 R3A PTAP$^-$ only. A 3-fold increase in the concentration of HA-ALIX plasmid resulted in modest increase in virus release; therefore, I proceeded with this plasmid. A similar increase in the amount of mCh-ALIX appeared inhibitory to Gag synthesis or toxic to the cells, as noted from the low expression level of cell-associated Gag and the loading control.

To determine whether increasing HA-ALIX input in the rescue experiments would result in a further increase in the amount of rescued virus, 0.75 and 2.25 μg of the plasmid was used. However, increasing the input of HA-ALIX by 3x did not increase the amount of rescued virus, suggesting that the system was probably saturated (Figure 4.6B). Overall, these results show that rescue with ALIX is not efficient. Moreover, ALIX would not rescue the PTAP$^-$YP$^-$ double mutants. Therefore an alternative approach for rescuing the virus was required.

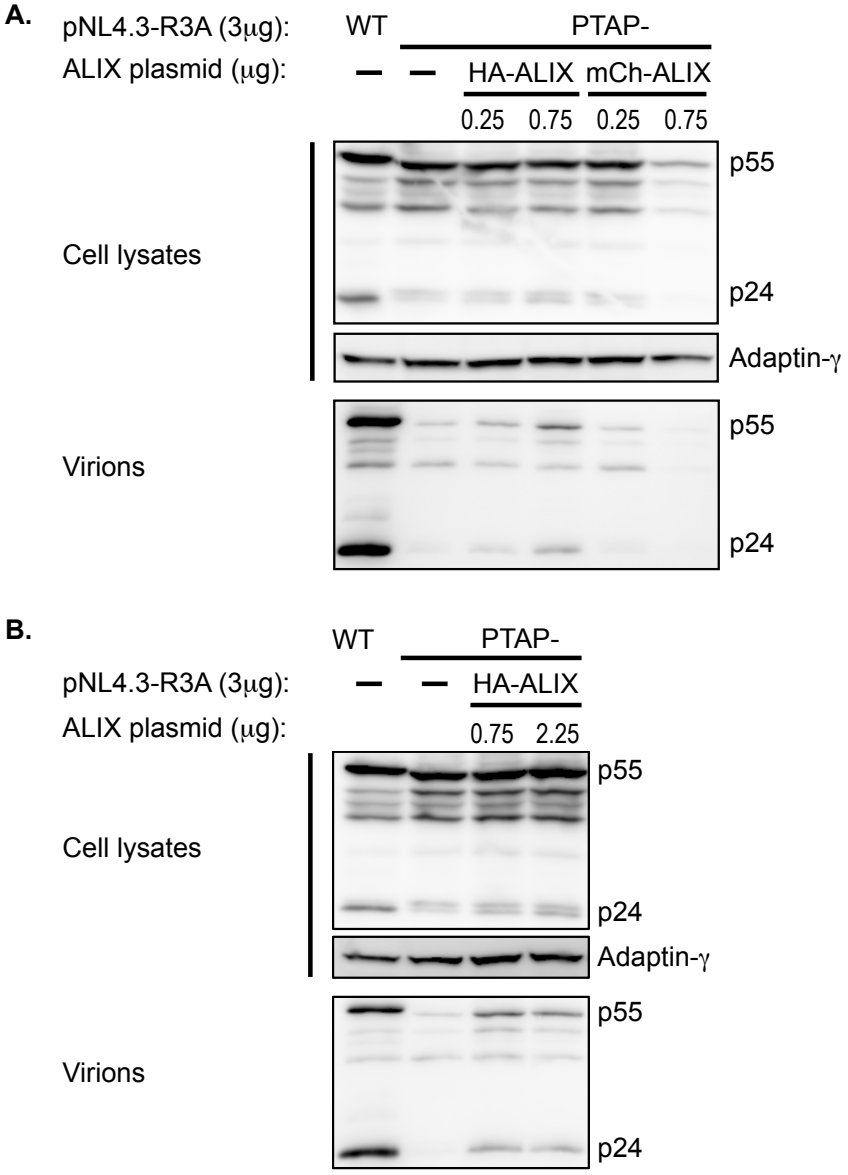

Figure 4.6: Rescue of Tsg101-binding site mutant virus by overexpressing ALIX.
(A) HEK 293T cells (1.4 x 10^5 cells/mL in 3 mL medium, on 6-well plate) were transfected with WT, or PTAP$^-$ plus one of the indicated ALIX plasmids at two concentrations. Total DNA was normalised to 3.75 µg with an empty pEGFP vector. Cells were incubated for 24 hrs. Pelleted virus and cells were lysed in sample buffer. Cell- and virion-associated Gag were analysed by WB. **(B)** HEK 293T cells were transfected with the indicated plasmids. Total DNA was normalised to 5.25 µg with empty pEGFP plasmid. Cultures were treated as in A.

4.2.2.2 Gag WT rescues the release defective PTAP$^-$ and PTAP$^-$YP$^-$ mutants

As an alternative approach, I exploited the codon-optimised Gag WT that is released efficiently from HEK 293T cells (Chapter 3, Figure 3.7), to rescue the HIV-1 R3A PTAP$^-$ and PTAP$^-$YP$^-$ mutants. HEK 293T cells were co-transfected with pNL4.3-R3A PTAP$^-$ and pCMVGag WT. Whilst keeping the pNL4.3-R3A PTAP$^-$ constant (3 µg),

increasing concentrations pCMVGag WT were used to determine the amount required to achieve optimal rescue of the HIV-1 R3A PTAP^{-} virions. Cell lysates and virions were harvested and analysed by WB (Figure 4.7A). The blot for virion-associated Gag shows that p24 levels decreased with increasing Gag WT input, suggesting that a small amount of the Gag WT plasmid was sufficient to recruit the ESCRT machinery and allow the release and subsequent maturation of virions.

To quantify the amount of released mature virus from the co-transfected cells, p24 levels were measured. These were compared to the amount of p24 (100%) from cultures that were transfected with HIV-1 R3A WT. Although the p24 level in cells co-transfected with 0.25 µg Gag WT plasmid was 84.5 ± 27.6% (Figure 4.7B), higher concentrations of the Gag WT plasmid in the co-transfections reduced the levels of p24 released. At 0.75 and 2.25 µg Gag WT plasmid, the p24 levels were 52.5 ± 13.4 and 21.5 ± 6.4%, respectively. These data show that Gag WT can efficiently rescue the HIV-1 R3A PTAP^{-} viruses, and low concentrations of Gag WT were required to optimally achieve this. The optimal plasmid ratio of Gag WT : HIV-1 R3A PTAP^{-} plasmid was 1:12 for efficient rescue.

To produce stocks of the HIV-1 R3A PTAP^{-} or PTAP^{-}YP^{-} viruses, the 1:12 ratio for GagWT : provirus plasmids was used to scale up virus production (see Materials and Methods, Section 2.10). Virus titres were determined by infecting TZM-bl cells (see Materials and Methods, Section 2.3.2), which shows that infectivity is also rescued (Figure 4.7C).

Taken together, these data show that viruses defective in ESCRT recruitment, and thus release, can be rescued by co-expression with Gag WT, and that these viruses were infectious as determined on TZM-bl cells. Therefore, the HIV-1 R3A mutant viruses can be used to infect macrophages where virus budding intermediates will be arrested at all sites assembly sites, allowing for quantitative analysis of HIV assembly in macrophages.

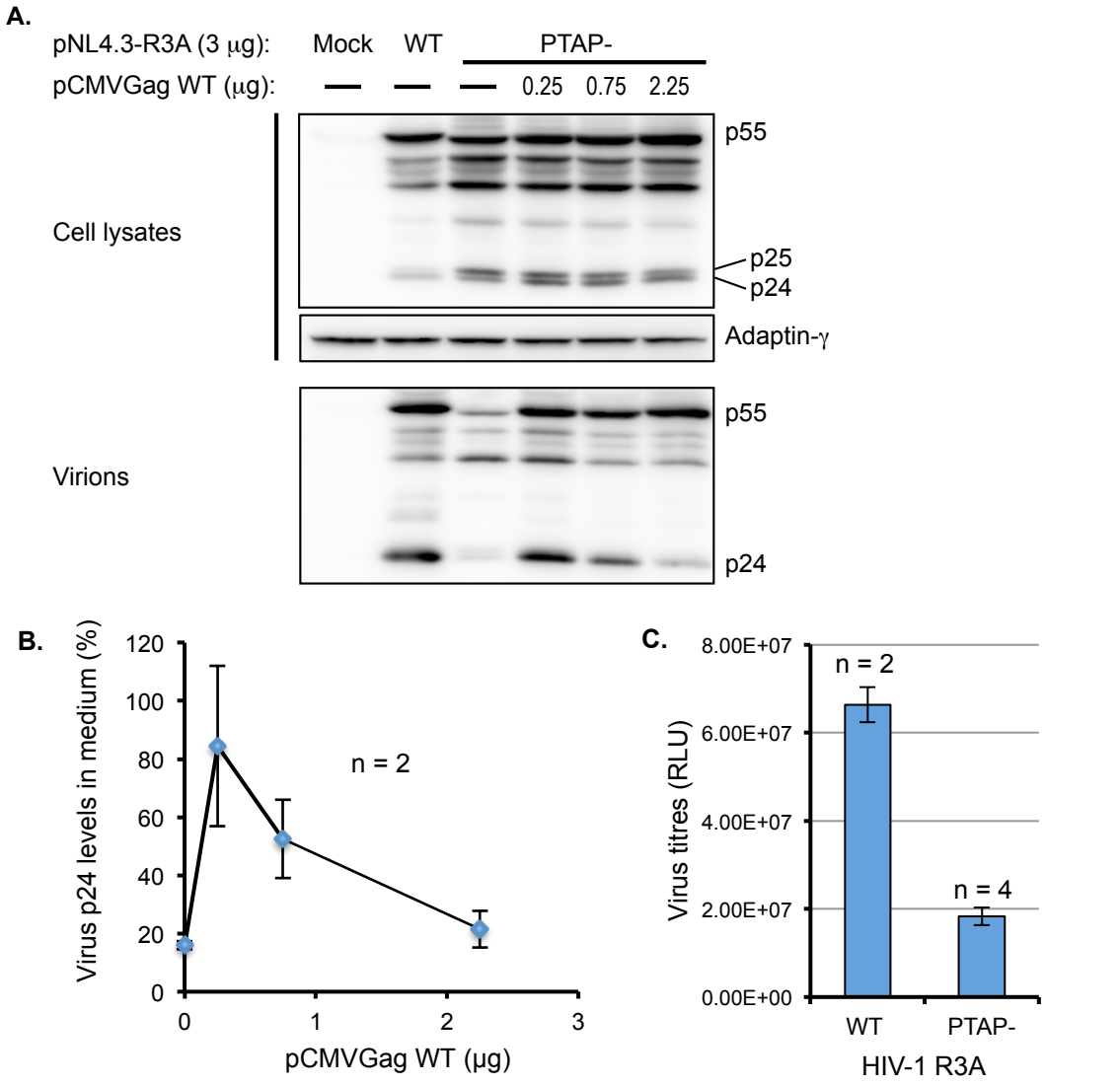

Figure 4.7: Gag WT-mediated rescue of release defective HIV-1 mutants.

(A) HEK 293T cells were transfected with pNL4.3-R3A WT, PTAP$^-$ alone, or PTAP$^-$ plus increasing concentrations of the vector expressing pCMV Gag WT. Cells were incubated for 24 hrs. Virus production and Gag expression levels were compared by WB with anti-p24/55 antibodies. **(B)** Quantitative analysis of p24 levels ± SD for the rescued HIV-1 R3A PTAP$^-$ virions in two independent experiments. **(C)** A typical graph showing virus titres for the HIV-1 R3A WT and mutants (e.g. PTAP$^-$) as determined on TZM-bl cells.

4.3 Discussion

The ESCRT pathway is essential for the release of HIV-1 from infected cells (Sundquist and Krausslich, 2012). ESCRT proteins are recruited by Gag to the plasma membrane, where HIV-1 assembles in different cell types, including primary macrophages. In macrophages the virus mainly uses the internally sequestered plasma membrane domains for assembly (Marsh et al., 2009; Pelchen-Matthews et al., 2012), but it is not

clear whether assembly also occurs at the cell surface. In order to study HIV assembly in MDM, I needed to generate and characterise mutants that would be defective in release. To this end, provirus mutants (HIV-1 R3A PTAP^{-}, PTAP^{-}YP^{-} and Δp6) were generated from the dual tropic provirus HIV-1 R3A and characterised by WB in Chapter 3. In this chapter, the mutants were further characterised by morphological methods. Analysis of these mutants by IF revealed virus unable to undergo PR-mediated proteolysis at the plasma membrane of HEK 293T cells. Furthermore, ultra-structural analysis by EM showed the accumulation of immature viruses and buds at the cell surface, thereby confirming that these mutants are indeed budding arrested. Introducing the mutants into MDM by electroporation revealed that the procedure was toxic to the cells. Therefore, infectious stocks of mutant viruses were produced by rescuing production in HEK 293T cells, so that MDM could subsequently be infected with the release-defective mutants.

Immunofluorescence was used to examine the morphology of the viruses in HEK 293T cells transfected with the HIV-1 R3A PTAP^{-} and Δp6 mutants. Puncta of p24/55 staining, presumably assembling virus particles, were seen at the cell surface. Notably, these puncta were not labelled with 4C9 anti-p17, suggesting lack of processing of MA, and consistent with an immature virus phenotype (Figure 4.1). In agreement, some punta co-staining with p24/55 and p17 were seen at the surface of WT expressing cells. Occasional cells that had very high expression of the mutants, indicated by stronger p24/55 labelling, tended to also have a continuous layer of p17 labelling the plasma membrane, suggesting premature protease activation (Carlson et al., 2010). To directly verify the structure of HIV particles at the surface of HEK 293T cells, I used EM, the only technique that has the resolution to show the fine structure of the particles. Both immuno-EM and Epon EM techniques were used. For immuno-EM, ultrathin cryo-sections of HEK 293T cells, transfected with plasmids for HIV-1 R3A WT and the mutants (PTAP^{-}, Δp6), were labelled with either anti-p24/55 or -p17 and protein A gold (Figure 4.2). Gold labelling helps in locating rare structures and aids in the identification of structures even if not oriented optimally in the section. Mature particles produced by R3A WT were labelled with anti-p24/55 and -p17, consistent with labelling for mature HIV-1 (Deneka et al., 2007; Pelchen-Matthews et al., 2012). As these were the same antibodies used for IF, similar specificities of the antibodies were

observed, that is, anti-p24/55 labelled both the mature and immature viruses, whilst anti-p17 only labelled the mature particles.

When Epon-EM was used to further characterise the morphology of the HIV-1 R3A PTAP^{-}, PTAP^{-}YP^{-} and Δp6 mutants, budding arrested HIV-1 profiles were seen decorating the surfaces of HEK 293T cells (Figure 4.3 B, D). This was consistent with previous studies, where the ultra-structural analysis of budding arrested HIV-1 was mainly conducted on plastic embedded specimens (Garrus et al., 2001; Pornillos et al., 2003; von Schwedler et al., 2003). The clearer morphology of the HIV-1 buds made it easy to recognise some subtle differences in phenotypes produced by HIV-1 R3A PTAP^{-} or PTAP^{-}YP^{-} and Δp6. For the PTAP^{-} and PTAP^{-}YP^{-} mutants, a large number of more shallow buds, mostly half complete Gag shells (~180° Gag incorporation), were observed. The virus shells for the Δp6 were more complete (on average three-quarters, ~270° Gag incorporation) (Figure 4.7). The Δp6 virus profiles, in agreement, had narrow membrane stalks (~75 nm). It is possible that the thinner stalks might be sheared off more easily, perhaps explaining the release of some p55 virion-associated Gag into the medium as seen in the WB (Chapter 3, Figure 3.13).

It is not clear what causes these differences in bud completeness of the HIV-1 R3A PTAP^{-}YP^{-} or PTAP^{-} and Δp6, though it is tempting to speculate that the p6 portion of Gag may regulate HIV-1 assembly. Both HIV-1 R3A PTAP^{-}YP^{-} and Δp6 do not recruit ESCRT, including VPS4. On the other hand HIV-1 R3A PTAP^{-} can recruit ALIX, although endogenous levels of ALIX do not overcome the PTAP^{-} defect to mediate virus release in HEK 293T cells. Two recent studies has suggested that VPS4 may be involved early in HIV particle biogenesis and the formation of intralumenal vesicles in MVBs, in addition to acting late to depolymerise and recycle the ESCRT components (Adell et al., 2014; Cashikar et al., 2014). However, as both the HIV-1 R3A PTAP^{-}YP^{-} and Δp6 cannot recruit the ESCRT-III, and ultimately VPS4 complexes, the average differences in bud morphology may not be explained in terms of VPS4. Furthermore, in preliminary studies with J. Burden, we have observed cells co-transfected with dominant negative VPS4 and R3A WT had virus budding profiles that were even shallower, with on average 149.5° of Gag incorporation (Apendix, Figure 7.2).

Therefore, the function(s) of VPS4 in membrane fission events require more investigations to clarify how it interacts with other ESCRT components.

As the mutants were producing arrested budding structures in HEK 293T cells, the potential to rescue infectious viruses was investigated. To this end, two approaches were tested in HEK 293T cells, which involved co-expressing the mutants with either ALIX or Gag WT. Previous studies have demonstrated that when ALIX is overexpressed, it can rescue HIV-1 PTAP^{-} viruses (Fisher et al., 2007; Usami et al., 2007; Carlton et al., 2008). However, when I used ALIX to rescue the PTAP^{-} mutant, there was only a minimal effect on virus release (Figure 4.6). In parallel, I tested rescue with Gag WT as an alternative, with promising results. Using Gag WT also offered the advantage of rescuing the R3A PTAP^{-}YP^{-} that lacks the ALIX binding motif. The concentrations of Gag WT and R3A PTAP^{-} plasmids required for optimal rescue were obtained by performing titrations (Figure 4.7). Surprisingly, higher concentrations of Gag WT plasmid sometimes reduced the levels of mature virus. These higher concentrations of the Gag WT plasmid in the co-transfections may have favoured the production of VLPs over infectious virions. A full molecular clone of HIV-1 produces one GagPol molecule for every 20 Gag molecules (Jacks et al., 1988; Pettit et al., 2005; Bell and Lever, 2013). Therefore, a higher input of the Gag WT plasmid might upset this 20:1 ratio of Gag:GagPol in the cell. This could result in the competitive exclusion of some GagPol during virus assembly, which may affect auto-activation of the viral protease. Therefore, the resulting released particles would not mature and would not be infectious. The optimal plasmid concentrations were then scaled up to produce infectious virus stocks.

In conclusion, to investigate HIV assembly in macrophages, I need to infect rather than electroporate MDM, as electroporation damages the cells. Therefore, a full molecular virus clone, HIV-1 R3A, was used to generate proviruses lacking ESCRT interaction motifs. The mutants were characterised on HEK 293T cells by WB and a range of light and electron microscopy techniques, and then rescued to generate infectious virus stocks. The infectious mutants have been used to infect MDM and study HIV assembly, as described in Chapter 5.

5. Morphological Analysis of HIV-1 in Primary Monocyte-derived Macrophages

5.1 Introduction

HIV-1 targets key cells in the immune system, such as CD4+ T cells and macrophages. In T cells, HIV-1 assembly occurs at the cell surface, whilst in macrophages the virus accumulates in intracellular compartments, and budding structures have been seen on the limiting membrane of these compartments, which suggests that HIV assembles at these sites (Gartner et al., 1986; Deneka et al., 2007; Welsch et al., 2007; Pelchen-Matthews et al., 2012). Following the initial observation that HIV-1 assembly in macrophages may be different to T cells, understanding the nature of these compartments has been growing. The current view is that these are intracellular plasma membrane-connected compartments (IPMCs) (see General introduction, Section 1.6.2).

The IPMCs where HIV assembles in macrophages are morphologically heterogeneous. They can have complicated structures, with various interconnected internal membranes (Deneka et al., 2007; Bennett et al., 2009; Welsch et al., 2011; Pelchen-Matthews et al., 2012). The cytoplasmic face of the IPMCs can have thick flat coats that contain integrin adhesion complex proteins (Pelchen-Matthews et al., 2012). This complex, as well as the actin cytoskeleton, maintains the integrity of the IPMCs (Gaudin et al., 2012; Pelchen-Matthews et al., 2012; Mlcochova et al., 2013). Although HIV accumulates at the IPMCs and budding structures have been seen on the limiting membranes of the IPMCs, it is not clear whether the IPMCs are sites where the virus assembles, as viruses budding from the cell surface would be lost.

The aim of this chapter was to address whether the IPMC is the main site selectively targeted by the virus for assembly in MDM, compared to the exposed cell surface. To achieve this, primary human MDM were infected with HIV-1 mutants defective in release, thereby capturing budding intermediates at all sites where HIV-1 assembles. The infected cells were then examined by IF and EM. For the IF studies, the plasma membrane marker CD44 was used to identify cell surfaces and IPMCs, whilst Gag staining was used to visualise the virus. This allowed for (i) an estimation of virus

distribution, and (ii) the quantitation of Gag fluorescence at the two plasma membrane domains, the IPMC and cell surface. EM allowed direct counting of the numbers of virus buds or particles at the different sites, while two-dimensional (2D) stereology was used to estimate the relative areas of plasma membrane at the cell surface and in the IPMCs. These studies showed that HIV-1 predominantly (>90%) assembled at the IPMCs in primary human macrophages.

5.2 Results

5.2.1 Morphology of MDM infected with R3A WT and rescued late domain mutants

Analysis of the HIV-1 R3A late domain mutants, PTAP^{-} and Δp6 showed that their release from MDM was inhibited, suggesting that they were arrested, as observed in HEK 293T cells (Chapter 4, Figure 4.2 and 4.3). To verify how the rescued HIV-1 R3A PTAP^{-}YP^{-} mutant virus behaves in MDM, cells were infected with HIV-1 R3A PTAP^{-}YP^{-}, or HIV-1 R3A WT for comparison. Cells were incubated for 7 days, fixed and then immuno-labelled with antibodies against the PM marker CD44 and viral proteins p24/55 and p17. The p24/55 antibody recognises immature and mature forms of HIV-1 Gag, whilst monoclonal anti-p17 (4C9) binds the proteolytically cleaved p17 subdomain of Gag and can therefore discriminate between the two virus forms by labelling mature virions only (see Chapter 4, Section 4.2.1.1). The fluorescence was examined by confocal microscopy.

In MDM infected with HIV-1 R3A WT, clumps of strong p24/p55 labelling were associated with the intracellular CD44 staining for the IPMCs (Figure 5.1 A to C). For the PTAP^{-}YP^{-} mutant, the p24/55 labelling was weaker and exhibited scattered punctate staining on the IPMCs (Figure 5.1D, E). This suggested low expression of the PTAP^{-}YP^{-} compared to the WT.

The p17 staining was examined in the HIV-1 R3A WT- and mutant-infected MDM. Cells infected with the WT had strong p17 labelling that co-localised with the p24/55 stain at the IPMCs. Conversely, very weak p17 staining was observed on the PTAP^{-}YP^{-}, where the majority of p24/55 puncta did not label with p17. Therefore, HIV-1 R3A PTAP^{-}YP^{-} shows little processing of Gag polyprotein by the viral protease,

suggesting an immature arrested phenotype, similar to that observed when the mutant was characterised in HEK 293T cells (Chapter 4, Figure 4.1).

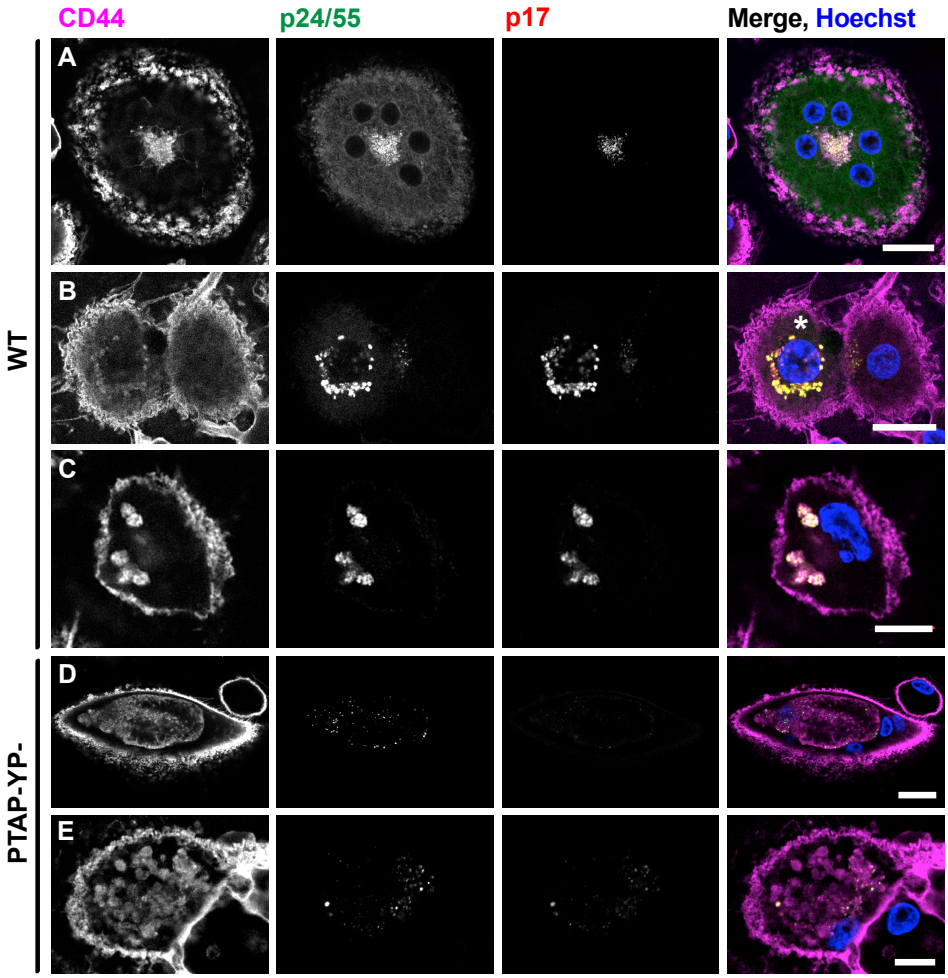

Figure 5.1: Morphology of infected MDM.

Seven-day old MDM were infected with HIV-1 R3A WT (A to C) or the rescued release-defective virus, HIV-1 R3A PTAP^{-}YP^{-} (D, E). Cultures were incubated for 7 more days, fixed and immuno-labelled with antibodies against p24/55 (Kal-1), p17 (4C9) and CD44 (MEM-85), and examined by confocal microscopy. Representative images of cells shown here are single confocal sections. See the enclosed CD with movies showing 3D image of cells shown in B and E (Appendix, Section 8.3). Mature and immature viruses were found at IPMCs with diverse morphologies. Scale bars = 10 μm.

The detailed morphologies of the IPMCs on the infected cells were examined. Labelling with CD44 showed that the IPMCs had a wide range of morphologies: a few examples are shown (Figure 5.1). In Figure 5.1A, the virus-containing compartment is at the centre of the syncytium and surrounded by nuclei. The reverse of this arrangement can be seen in Figure 5.1B (cell with asterisk), where the IPMC encircles the nucleus. Clumps of seemingly compact IPMC were also observed in some cells (Figure 5.1C). In

Figure 5.1D, an ovoid cell has a mass of similarly ovoid IPMCs. The macrophage in Figure 5.1E, shows a complex IPMC occupying most of the cytosolic space (with morphology akin to raw cotton). Markedly, some cells were multinucleated, referred to as syncytia. A syncytium forms when viral Env proteins in infected cells bind CD4 and co-receptors of neighbouring cells(s), culminating in fusion and the generation of giant cells with several nuclei. Cells with more that 100 nuclei have been reported for macrophages infected with HIV-1 (Gartner et al., 1986). The IPMCs were very diverse in size and morphology, in agreement with previous reports (Gaudin et al., 2013a; Mlcochova et al., 2013).

Notably, for MDM infected with either HIV-1 R3A WT or mutants, the virus staining was on the CD44-labelled IPMCs. Moreover, the fact that immature virus was found at the IPMCs implies that HIV-1 assembles at this plasma membrane domain.

5.2.2 Analysis of the distribution of HIV-1 in MDM by IF

To evaluate the distribution of HIV-1 R3A in MDM, cells from eight blood donors were electroporated or infected with either the single mutant PTAP^{-}, or the double mutant PTAP^{-}YP^{-}. Electroporation experiments were performed initially, prior to the development of the rescued mutants in HEK 293T cells, which could be used to infect MDM. The cells were immuno-stained with antibodies against CD44 and viral proteins p24/55 as well as a monoclonal antibody against p17. The cells were then analysed by confocal microscopy to assess the distribution of viral proteins. Qualitative analysis of the p24/55 staining pattern on CD44-labelled membranes revealed a diverse set of morphologies that were scored into one of three categories. There were cells where virus was at the IPMC only, or cells with virus at the cell surface. Notably these latter cells lacked the IPMCs. In a few cells, virus was seen at both the IPMC and the cell surface. To document infected cells, random fields were imaged using the same settings, on z-stack mode with the confocal microscope to capture 3D images of the cells. The images were acquired in four channels comprising the nucleus, CD44, p24/55 and p17. Representative images of cells infected with the HIV-1 R3A WT and PTAP^{-}YP^{-} mutant are shown in Figures 5.2A to D, illustrating cells within the three categories described above. Movies for the 3D images are on CD (Appendix, Section 8.3).

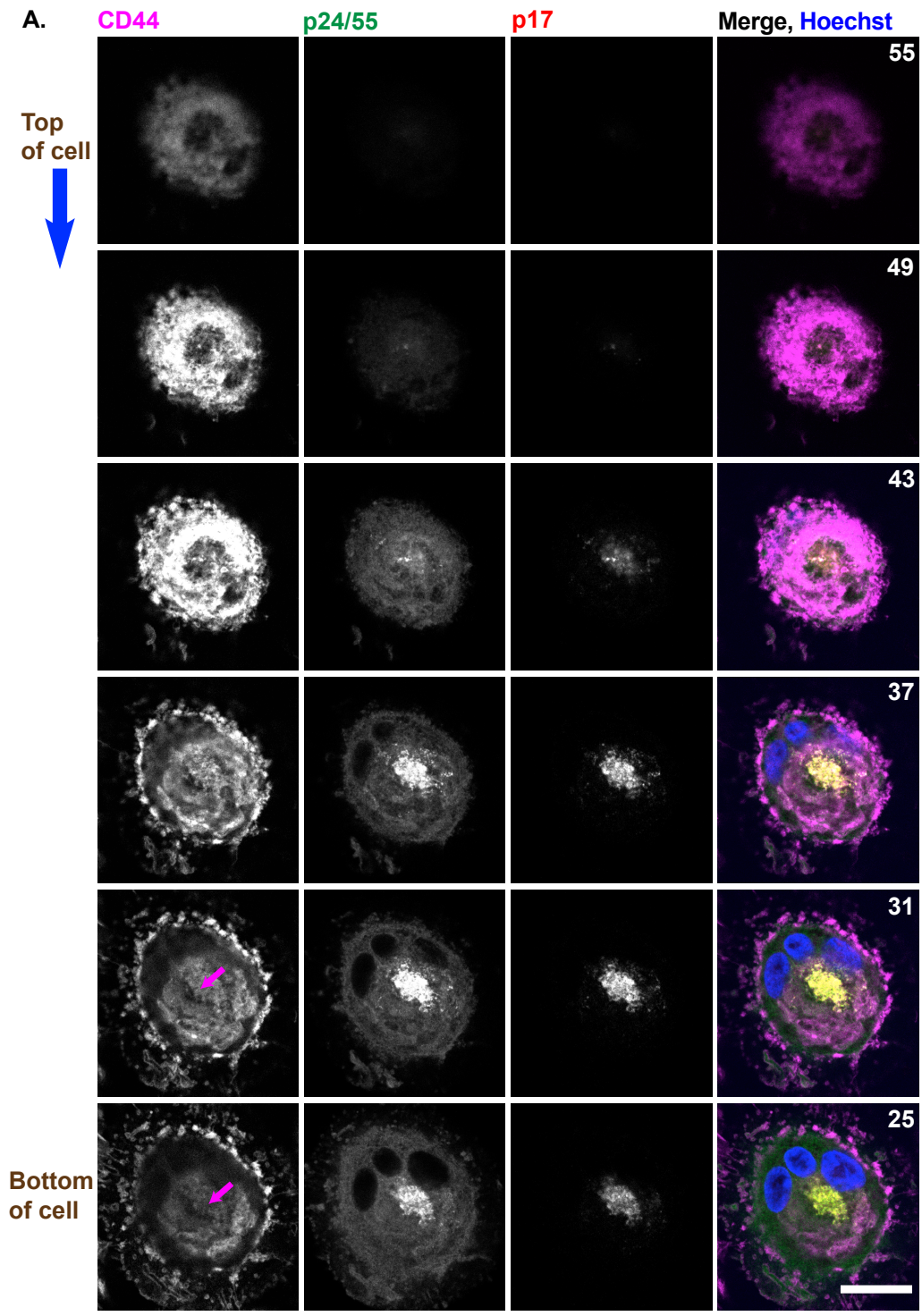

Figure 5.2: The distribution of HIV-1 R3A WT and PTAP^{-}YP^{-} in MDM.

MDM were immuno-stained with antibodies against p24/55 (Kal-1), p17 (4C9), and CD44. Images were acquired with the z-stack mode of the confocal microscope. The numbers on the merged image panels indicate the position of the sections in the z-stack, shown from the top to the bottom of the cell (See movies on CD, Appendix, Section 8.3). Arrows (magenta) on CD44 images (far left) point to the IPMC on the selected cell sections. **(A)** HIV-1 R3A WT virus only in IPMCs. The cell is multinucleated with a compact IPMC near the nuclei. Scale bar, 20 µm.

The figure continues on the next pages.

Figure 5.2 continues

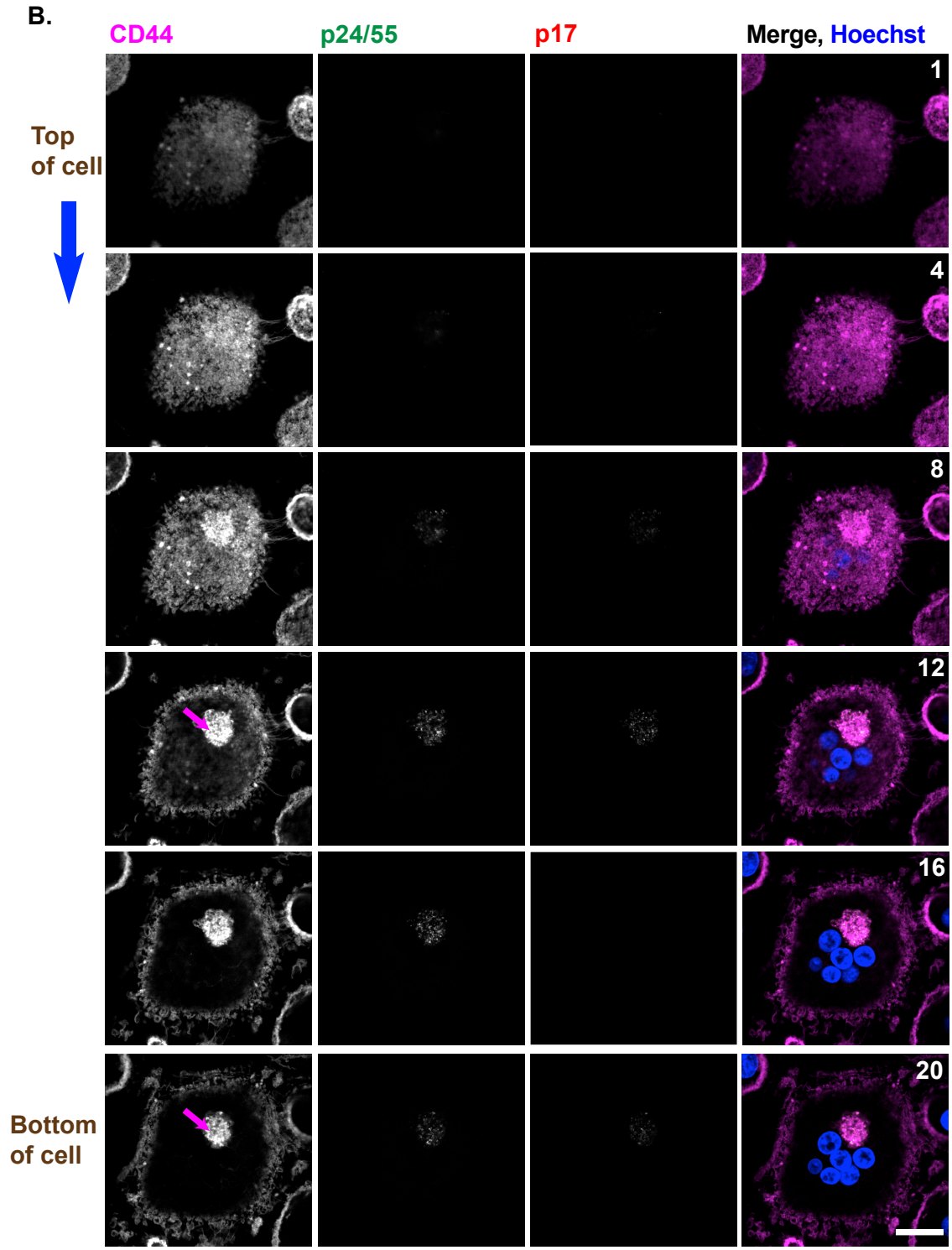

(B) Multinucleated cell with HIV-1 R3A PTAP^{-}YP^{-} in IPMCs only. Scale bar, 20 μm.

Figure 5.2 continues

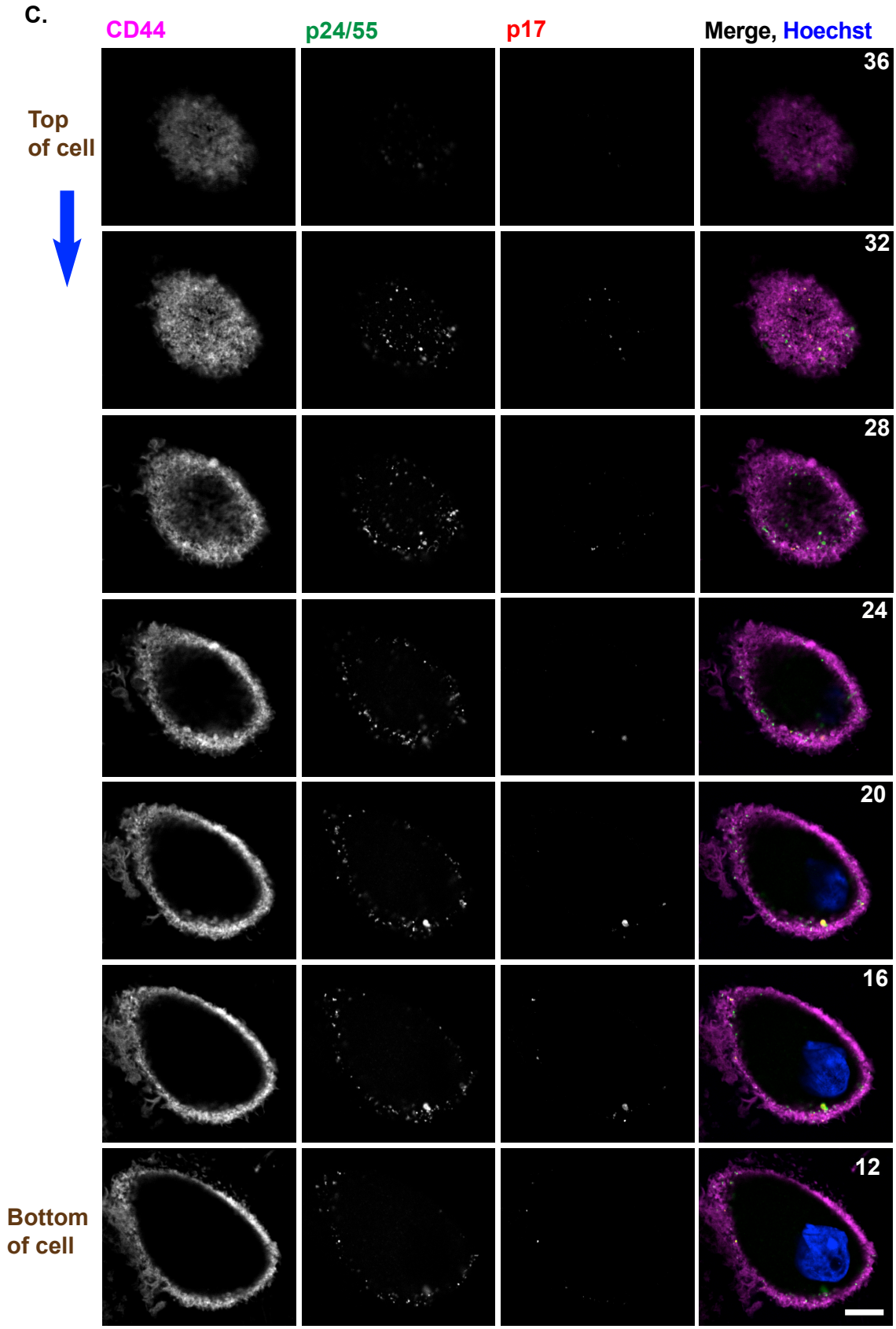

(C) HIV-1 R3A PTAP^{-}YP^{-} assembly at the cell surface only. Note that CD44 shows this cell lacks an IPMC. Scale bar, 10 μm

Figure 5.2 Continued

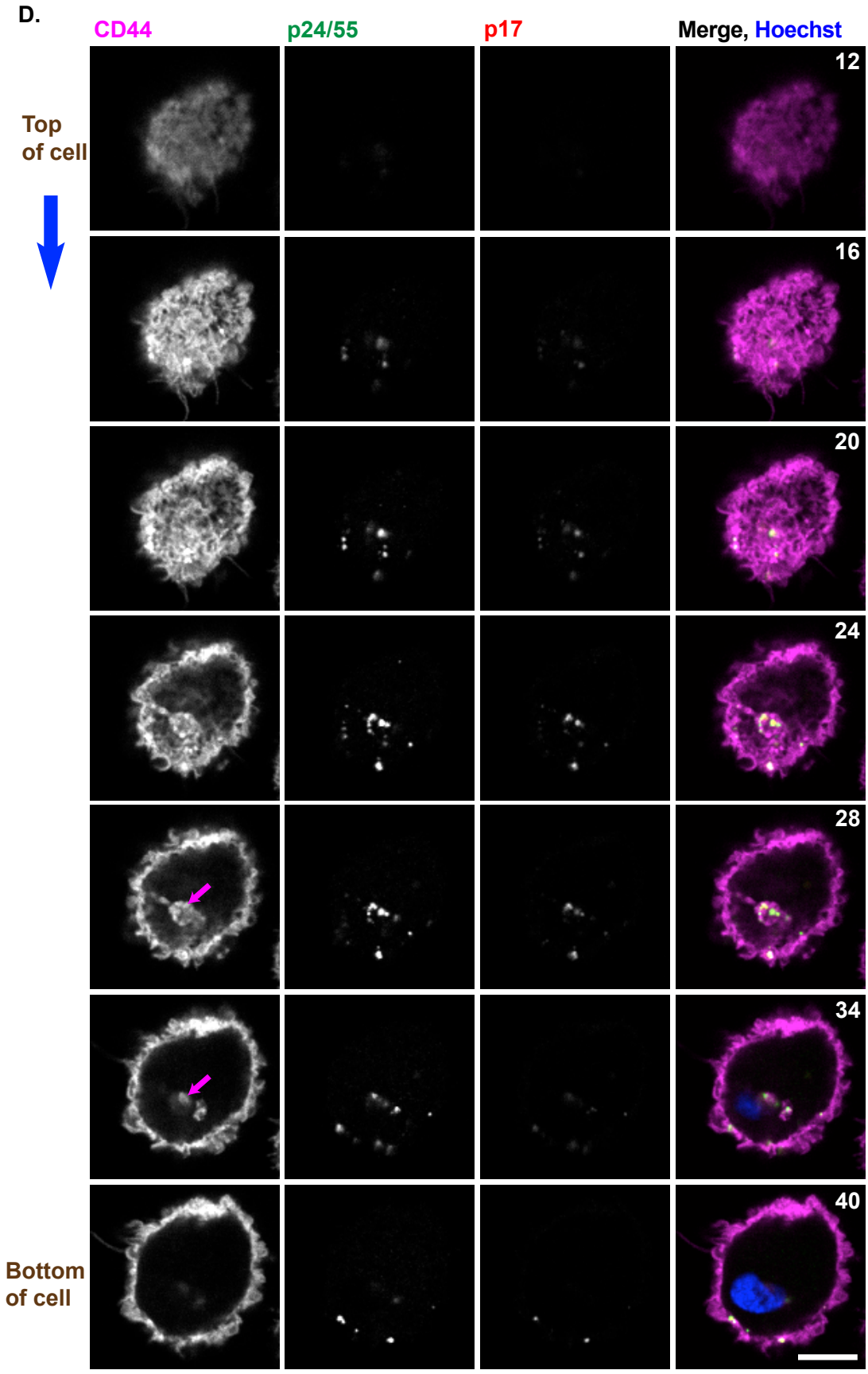

(D) HIV-1 R3A PTAP^{-}YP^{-} distributed to the IPMC and cell surface. Scale bar, 10 μm

To quantitatively analyse the virus distributions in MDMs, coverslips were scanned in a rasterised manner, and the cells were carefully observed and scored into the three categories described above. A total of 1,120 random cells (448 for R3A WT, and 662 for R3A PTAP$^-$ and PTAP$^-$YP$^-$) were analysed (Figure 5.3). For all viruses, there were a high proportion of cells with virus staining at the IPMCs only (brown bars), although this was variable from donor to donor, ranging from 43 to 100% (Figure 5.3A). Since electroporated cells had low transfection efficiencies (<1%), all cells expressing Gag were included in the analysis. The lowest numbers of transfected cells were for D383, and here the entire Gag staining for the WT and mutant was at the IPMCs. Although electroporation with provirus resulted in few virus-expressing cells, the data was comparable to that obtained for cells inoculated with infectious virus (Figure 5.3B). On average, 66 and 77% of cells expressing the WT and mutants, respectively, showed virus at the IPMCs only (Figure 5.3C). In a small proportion of cells, virus staining was found at both the IPMC and cell surface: 10% and 5% for the WT and mutants, respectively. Furthermore, virus staining was observed at the surface of cells that lacked IPMCs, representing 24% of cells with WT infection, and 18% of cells with the mutants. Taken together, these results suggest that HIV-1 is primarily distributed to the IPMCs in MDM expressing HIV-1 R3A WT and PTAP$^-$ or PTAP$^-$YP$^-$ mutant viruses.

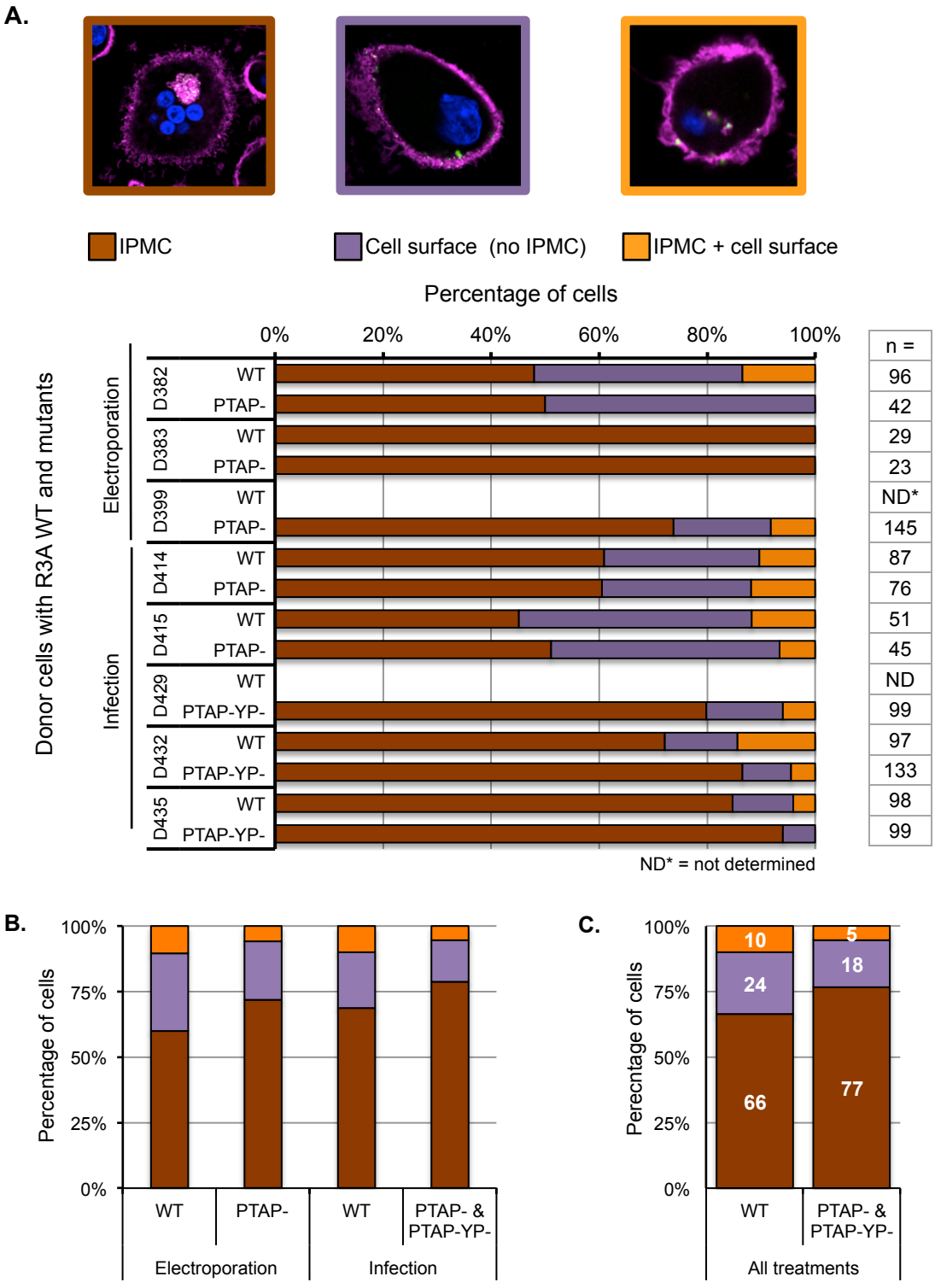

Figure 5.3: HIV-1 mainly distributes to the IPMC in MDM.

(A) Cells from eight blood donors were either electroporated or infected with the indicated viruses. Immunolabelled cells were examined by confocal microscopy and scored into three categories, as illustrated above the graph (see z-stacks images in Figures 5.2). For each donor, the proportions of cells in each category were determined. **(B)** Averages are shown according to the method used to express the virus in MDM. **(C)** A summary, comparing the WT and mutants for all the treatments, shows that the virus was predominantly located in IPMCs. (All treatments = electroporation and infection methods).

5.2.3 Quantitation of virus fluorescence intensities in infected cells

During the analysis of virus distribution in MDM, it was evident that most cells had virus in the IPMCs only, and a small percentage of cells (5%, PTAP$^-$ and PTAP$^-$YP$^-$; 10%, WT) had virus at both the cell surface and IPMCs. Also, the p17 staining on the mutants was generally weaker than on the WT. To determine how much virus staining there was at the IPMCs and the cell surfaces, Gag (p24/55 and p17) fluorescence intensities were quantified on randomly imaged MDM from two blood donors: 88 and 39 MDM from D435, expressing HIV-1 R3A WT and PTAP$^-$YP$^-$, respectively; and 55 MDM from D429, expressing PTAP$^-$YP$^-$. Using CD44 as a maker for the cell surface and IPMC, detailed examination of z-stack images was performed, employing "3-D Viewer" and "Orthogonal Views" features of ImageJ software (Figure 5.4A, B) to dissect the locations of the Gag p24/55 and p17 fluorescence. The "3D Object Counter" plugin (Bolte and Cordelieres, 2006; Cordelieres, 2009) was used to quantify Gag fluorescence associated with each site, as illustrated in Figure 5.4C and D for a macrophage from D429 infected with the PTAP$^-$YP$^-$ mutant.

Initially, the total fluorescence intensities for p24/55 and p17 were determined on the imaged cells. The average fluorescence intensities of p24/55 on WT virus in the D435 MDM was 2.6 x 10^6 arbitrary units (A.U.), compared to 1.1 x 10^6 A.U. of p24/55 on the PTAP$^-$YP$^-$-expressing MDM from the same donor (Figure 5.5A). This shows a 2-fold difference that is consistent with the lower expression levels of the mutant, although not statistically significant (*P* value = 0.1638). Additionally, fluorescence intensities for p17 were estimated on the same D435 cells. On average, the fluorescence intensities of p17 for the WT and PTAP$^-$YP$^-$ were 3.6 x 10^6 and 0.49 x 10^6 A.U., respectively (Figure 5.5B), representing a 7-fold difference, which is statistically significant (*P* value = 0.0017). To account for the lower expression of the PTAP$^-$YP$^-$ mutant, ratios of the p24/55 to p17 were calculated for the D435 cells infected with the WT and mutant viruses, and they were 1.38 and 0.45 respectively, showing 3-fold decrease in the p17 fluorescence. Furthermore, a comparison was made between the average fluorescence intensities of either p24/55 or p17 for the PTAP$^-$YP$^-$ expressing MDM from D435 and D429. The differences between the averages were not statistically significant (p24/55 averages, *P* value = 0.1230; p17 averages, *P* value = 0.4484). Collectively, these data support the notion that the PTAP$^-$YP$^-$ virus is scission-impaired.

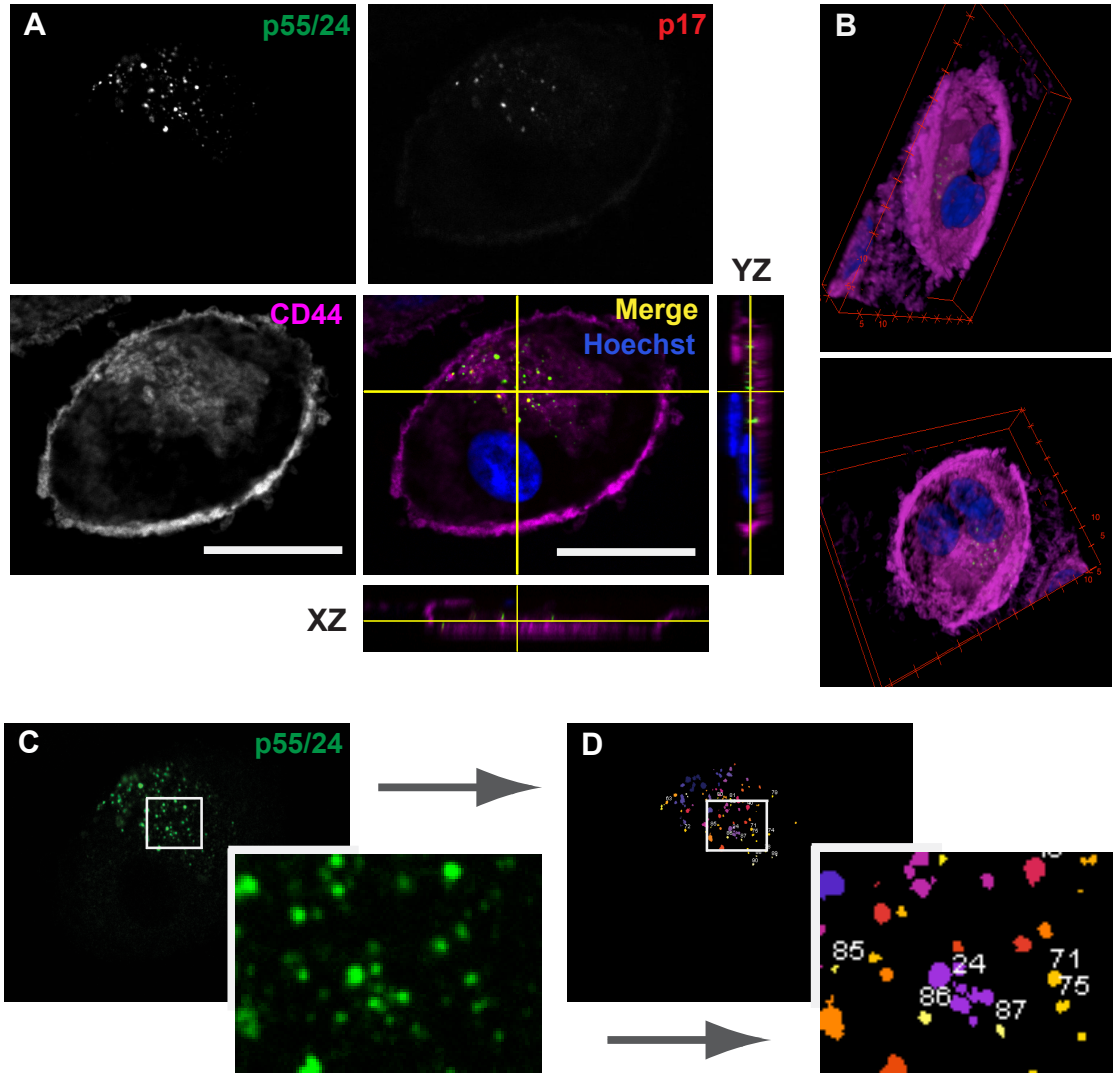

Figure 5.4: Quantitation of fluorescence intensity for Gag p24/55 and p17.

(A) Orthogonal views and, **(B)** 3D views of the cell, to identify plasma membrane domains and Gag at these domains. **(C)** The p24/55 staining channel (so-called image object) for estimating fluorescence intensity using the 3D Object counter plugin in ImageJ software. First, a threshold was set on the image, resulting in a binarised image. The software then runs a 2-pass analysis on this binarised image. The first pass involves scanning the image objects (for instance, HIV-1 p24 fluorescence staining in C) from the top left corner to the lower right corner. **(D)** During this pass, tags (numbers) are assigned to the object's pixels. To resolve any ambiguities, the software performs a second pass. For example, a U-shaped image object that has been scanned and assigned separate tags at the beginning of the z-stack (i.e. the top part of the U-shape) would be resolved by replacing the higher tags with the lowest tags on the whole image. (Note that all tags are not shown on the zoom, as these would have been shown on previous z-stack slices). Fluorescence intensity was calculated as an integrated density (in arbitrary units), which is the sum of all the intensities of the object's voxels. A voxel is a volume element that represents pixels in a 3-D space. Scale bar = 20 µm. (See also videos on the enclosed CD, Appendix, Section 8.3)

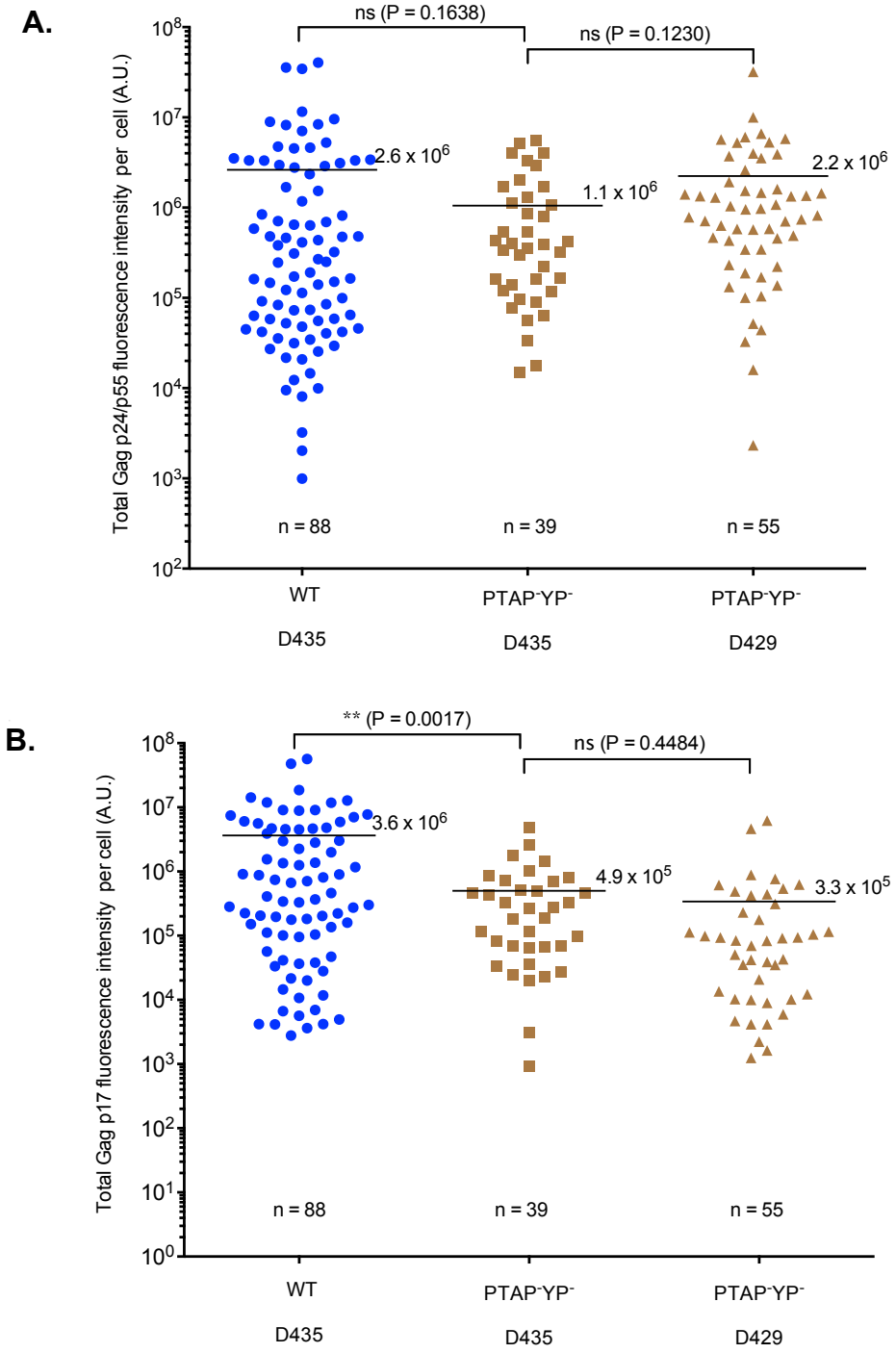

Figure 5.5: Quantitative analysis of Gag fluorescence intensity on MDM.

MDM from blood donors, D435 and D429, were infected with HIV-1 R3A WT or PTAP$^-$YP$^-$, and double stained with antibodies against p24/55 and p17, and CD44 to identify IPMCs. Using confocal microscopy, random whole-cell images were acquired in z-stack mode. **(A, B)** Quantitation of fluorescence intensity for p24/55 and p17 staining was analysed on 3-D images using ImageJ software as in Figure 5.4. Graphs show p24/55 (A) and p17 (B) fluorescence intensities per cell. For statistical analysis, an unpaired t-test was performed to compare the average fluorescence intensities.

Next, I sought to determine the proportion of Gag p24/55 found at the IPMC and the cell surface in those cells that had viruses at the cell surface and IPMCs. Whole cell images of infected MDM from D435 and D429 were sorted into the three categories described in Figure 5.3, and the results are shown in Table 5.1. In agreement with the data obtained by scanning slides of cells and then scoring them at the microscope, there were more cells with virus at the IPMCs only: 85.2% WT and 89.7% PTAP^{-}YP^{-} for D435; and 74.5% PTAP^{-}YP^{-} for D429. A small percentage of cells showed virus at both PM domains: 11.4% WT and 7.7% PTAP^{-}YP^{-} for D435; and 18.2% PTAP^{-}YP^{-} for D429 (Table 5.1).

Table 5.1: Categorising cell images from D435 and D429, according to virus distribution.

Cells categories according to site for p24/55 fluorescence	Number of cells (%)					
	D435				D429	
	R3A WT		R3A PTAP^{-}YP^{-}		R3A PTAP^{-}YP^{-}	
1. Cell surface (no IPMC)	3	(3.4)	1	(2.6)	4	(7.3)
2. IPMC	75	(85.2)	35	(89.7)	41	(74.5)
3. IPMC and cell surface	10	(11.4)	3	(7.7)	10	(18.2)
(a) analysed	6		3		9	
(b) not analysed	4		n/a		1	
TOTAL	88	(100)	39	(100)	55	(100)

As shown in Table 5.1, 4/10 cells expressing the WT (for D435) and 1/13 expressing the PTAP^{-}YP^{-} (for D435 and D429) could not be analysed because it was difficult to accurately resolve the IPMCs and cell surface. This could be attributed to the IPMCs being in close proximity to the cell surface. To estimate the proportion of virus at the IPMCs, p24/55 fluorescence at the IPMC was divided by the total p24/55 fluorescence in the cell (Figure 5.6A). On average, the PTAP^{-}YP^{-} mutant showed 96.1% and 92.1% of virus in the IPMCs, for D435 and D429, respectively. The WT-expressing cells had 81.3% of the virus in the IPMCs. However, the averages between the WT and the mutants were not statistically different (*P* value = 0.3096). These data show that even in cells that have virus at the IPMCs and cell surface, the IPMC is the main PM domain where the virus is found.

A. $$Proportion\ (\%) = \frac{\text{IPMC p24\&55}}{\text{Cell Total p24\&55}}\ \text{x}\ 100$$

B.

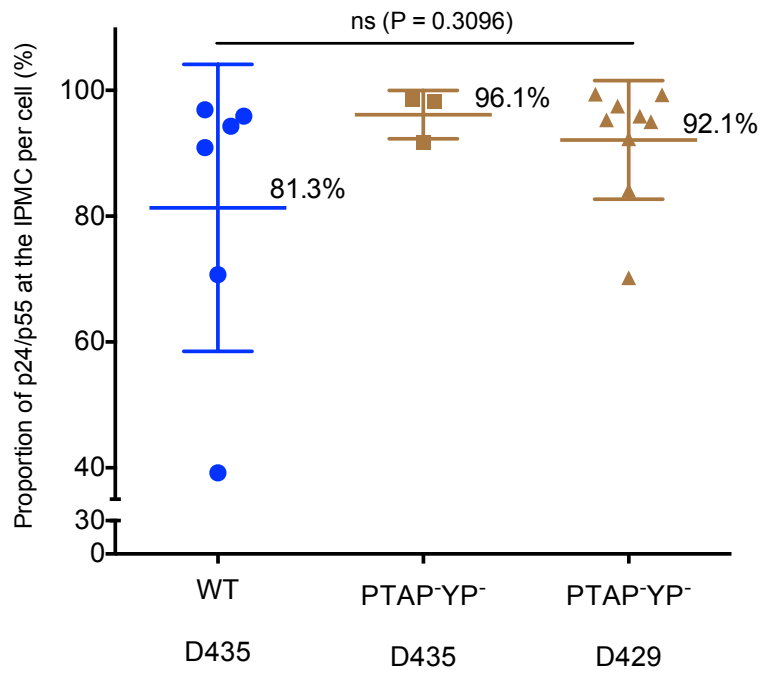

Figure 5.6: Gag fluorescence is predominantely at the IPMC in MDM.
(A) For cells with Gag p24/55 at both the IPMC and cell surface, the proportion of p24/p55 at the IPMC was estimated using the equation. **(B)** Estimates for MDM from the two donors were graphed as shown, including the arithmetic mean for each group of cells.

Together, these immunofluorescence data on the distribution of virus in MDM showed more than 90% of the virus located in the IPMC of cells infected with the HIV-1 R3A PTAP^{-}YP^{-} mutant, and more than 80% in the WT-infected cells. The WT was slightly lower, possibly due to stronger infection, resulting in the virus redirecting to the cell surface when the IPMC is full, or some virus being released from the IPMC and remaining bound to PM. These data strongly suggest that HIV-1 predominantly assembles in IPMCs in primary human macrophages.

5.2.4 EM analysis of IPMC ultra-structure and HIV budding

Immunofluorescence studies of macrophages infected with HIV-1 R3A WT and PTAP^{-} or PTAP^{-}YP^{-} showed that the virus distributes mainly to the IPMCs. To follow up on these IF observations, the ultrastructure of infected macrophages was investigated using EM, and the data was analysed qualitatively and quantitatively.

5.2.4.1 IF screening of semi-thin sections of infected MDM

The analysis of whole MDM revealed that cells expressing the HIV-1 R3A mutants were rare and virus expression levels in the cells were also weak. In addition, infection was variable from donor-to-donor. Therefore, in order to assess infection levels prior to EM, semi-thin sections of MDM infected with R3A WT or PTAP^{-}YP^{-} were immuno-labelled with antibodies against p24/55 and p17. For each specimen, three or four random images of stained sections were acquired at low power magnification (40x) by fluorescence microscopy (Figure 5.7A, B). Individual cells were imaged at higher magnification. Figure 5.7C and D shows examples of MDM infected with the WT and PTAP^{-}YP^{-} viruses. Cells infected with the WT had high expression level of p24/55, which was frequently seen as large aggregates, compared to the punctate staining of the PTAP^{-}YP^{-} mutant. Similar to the observations made on whole cells, the p17 staining was weaker on the PTAP^{-}YP^{-} compared to WT. This systematic screening of semi-thin sections, allowed for the identification of MDM with relatively high PTAP^{-}YP^{-} infection levels, to stain specimens for EM.

The number of cell profiles labelled with p24/55 were counted on each field (at 40x) and averaged to estimate infection levels. The data in Figure 5.8 show a ranking of infection levels for MDM expressing the HIV-1 R3A WT or the PTAP^{-}YP^{-} mutant. Cells infected with HIV-1 R3A WT had higher infection levels compared to the mutant-infected cells. Based on data in Figure 5.8, cells from donors D429, D428, D435 and D432 were chosen for the EM studies. Also included in these studies were MDM from D415, infected with the PTAP^{-} single mutant.

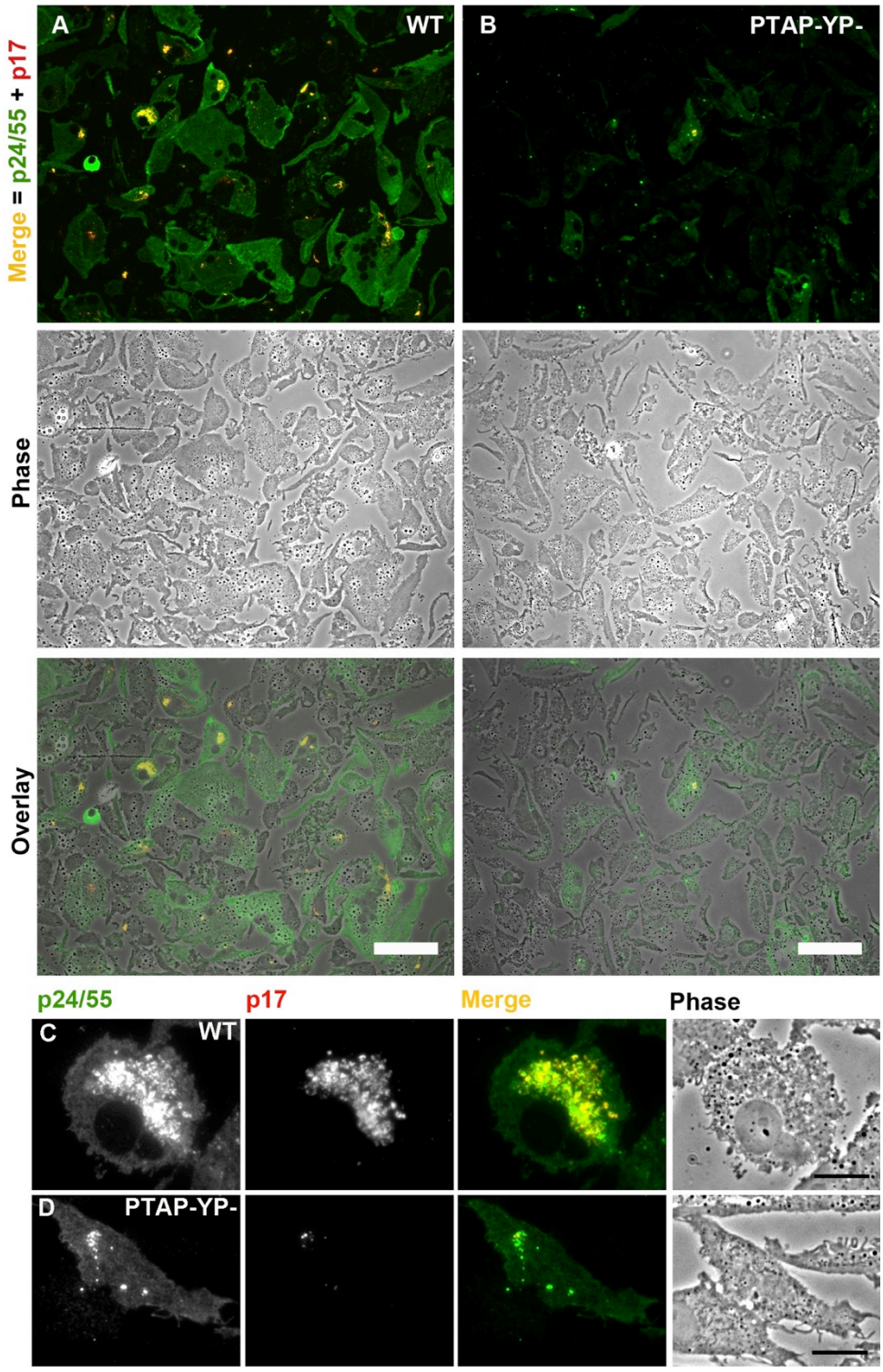

Figure 5.7: Determination of infection levels by IF analysis of MDM.

Semi-thin cryo-sections of MDM infected with the indicated viruses were double stained with antibodies against p24/55 (38:96K and EF7) and p17 (4C9). **(A, B)** An overview of a stained section. Infection levels were 43% and 28%, for the WT and PTAP^{-}YP^{-}, respectively. The top panels show merged images of the p24/55 (green) and p17 (red) channels. The p24/55 (green) labels WT- and PTAP^{-}YP^{-}-infected cells. Phase images are shown in the middle panels. Fluorescence and phase images have been overlaid in the lower panel. **(C, D)** Higher power magnification of stained cell sections. Scale bars: A and B, 50 µm, C and D, 10 µm.

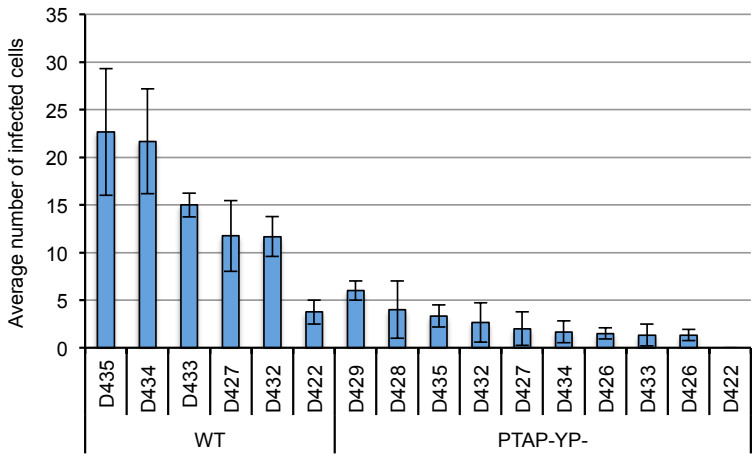

Figure 5.8: Estimation of the number of infected MDM.

Semi-thin sections stained with anti-p24 were analysed by IF to assess infection. Stained cell profiled were counted to estimate the number of infected cells per 40x field of view.

5.2.4.2 Correlative light and electron microscopy (CLEM) to identify infected cells

Given that fewer infected cells were observed for MDM infected with HIV-1 R3A PTAP^{-}YP^{-} it was apparent that surveying specimens to find cells infected with mutants at the EM would be a challenge. To address this problem, a different approach that combines IF and EM was used, termed correlative light and electron microscopy (CLEM). This procedure takes advantage of the fact that IF can be used to screen large areas of a sample at relatively low resolution, to identify areas of interest that can then be found again at the electron microscope to obtain ultra-structural details.

H6 finder grids with letters (Figure 5.9A) were used to support specimens that would be analysed using CLEM. An example of CLEM data output is shown in Figure 5.9B to G. In this example, MDM infected with R3A PTAP^{-}YP^{-} were immuno-stained with anti-p24/55 and PAG on a finder grid. The nuclei were visualised by labelling with Hoechst. Specimens were examined by IF to identify infected cells labelled with the anti-p24/55 (Figure 5.9B). A cluster of p24/55 puncta near a nucleus, suggestive of an IPMC, was observed (Figure 5.9C). Grid bars and letters, as well as the cells' nuclei were visualised during imaging in order to locate structures at the electron microscope. Thus, the fluorescence in Figure 5.9C coincided with the ultra-structural features on the overview micrograph in Figure 5.9D. When the area with p24/55 fluorescence was examined using EM at higher magnification (Figure 5.9E), virus profiles with immature morphology were observed in the IPMC (Figure 5.9F, G).

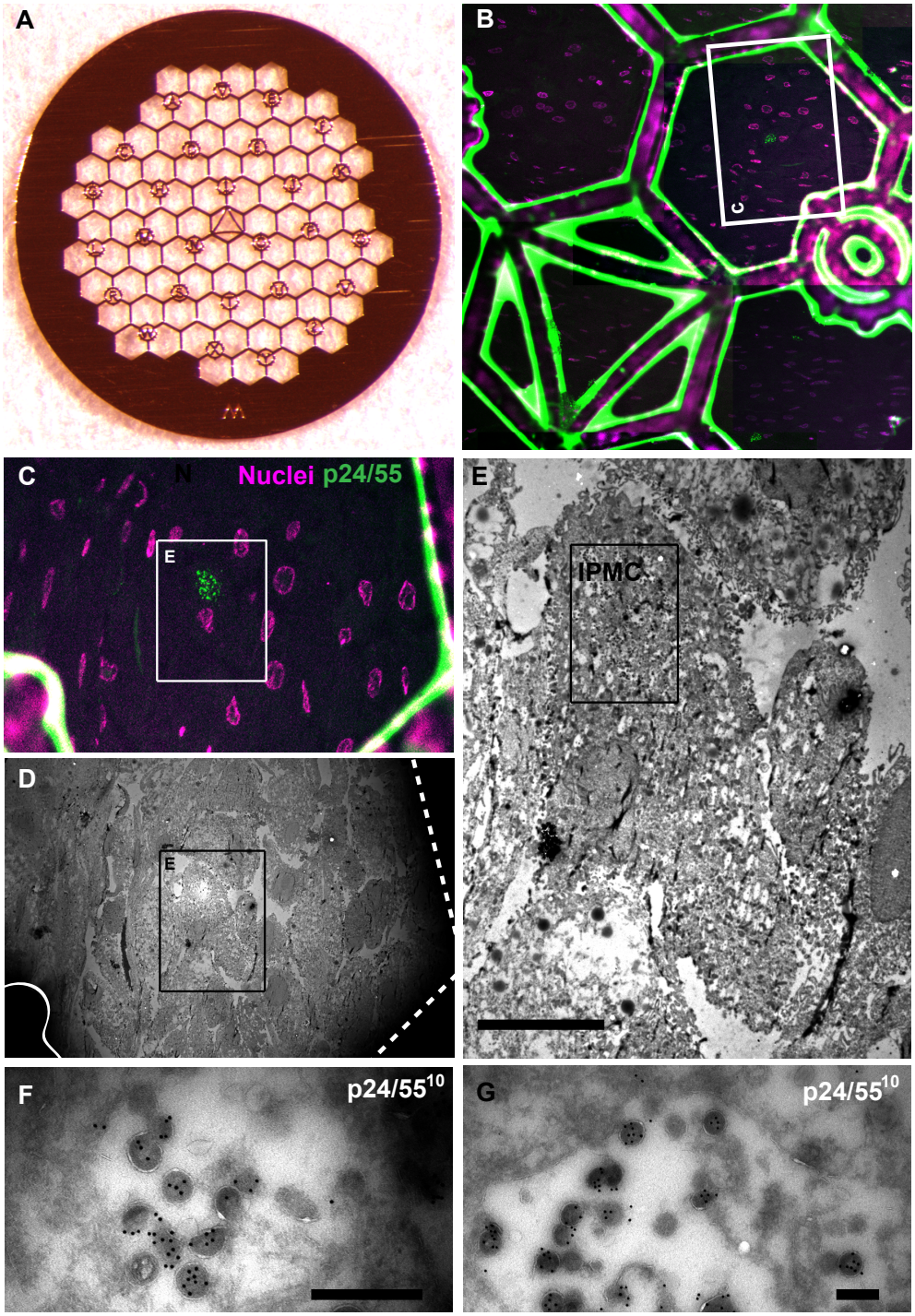

Figure 5.9: Using CLEM to localize and image infected cells.

(A) Image of an H6 finder grid used to support specimens. **(B)** IF overview showing part of the finder grid mesh: ultra-thin sections of MDM infected with HIV R3A PTAP^{-}YP^{-} for 7 days were labelled with anti-p24/55, rabitt anti-mouse Alexa-488 antibody and 10-nm PAG. Hoechst was used to visualise the nuclei (pink). Fluorescence micrographs were stitched together or aligned to display part of the finder grid (containing the letter O). [Note the Hexagon O1 (bump)]. Overviews like this were used to locate infected cells during EM imaging. **(C)** The fluorescence corresponds with electron dense features in the EM overview shown in **(D). (E)** Higher-magnification EM image of the boxed area shown in D, revealing the ultra-structure of the MDM. **(F, G)** Immature virus profiles were labelled with 10-nm PAG for the p24/55 on the budding profiles. Scale bars: E, 10 µm; F, 500 nm; G, 200 nm.

The results show that the procedure can be used reliably to identify infected cells when infection levels are low. Furthermore, the data demonstrate directly that the R3A PTAP^{-}YP^{-} produces an arrested virus phenotype in the IPMC.

5.2.4.3 The ultra-structure of HIV assembly in the IPMC

To study the morphology of assembling HIV in the IPMCs, MDM infected with HIV-1 R3A WT were examined. Cryo-sections of infected cells were either labelled with antibodies against CD44 or p24/55 and Protein A-gold (PAG). Initially, CD44 was used as a marker for the IPMCs. Various intracellular PM domains were labelled, even on cell profiles that did not contain virus particles (Figure 5.10). These IPMCs had varying morphologies, ranging from the large loose vacuoles seen in Figure 5.10A, to others with convoluted tightly apposed membranes (Figure 5.10 C, D). On infected MDM, the IPMCs were densely packed with mature virus particles (Figure 5.11A). At higher power, the electron-dense cores of the viral capsid could be identified (Figure 5.11B-D; black arrows). In addition, immature particles characterised by electron dense shells, were sporadically found in the IPMCs (Figure 5.13B and E-G; white arrows). Both the mature virus particles and the immature profiles labelled strongly for p24/p55 (Figure 5.11 E, F). Moreover, other features noted on the IPMCs included clathrin-coated pits and thick flat coats on cytoplasmic face of the PM (Figure 5.11G, H), as previously reported (Welsch et al., 2007; Pelchen-Matthews et al., 2012).

To study the ultra-structure of MDM infected with HIV-1 R3A PTAP^{-} or PTAP^{-}YP^{-} mutants, infected MDMs had to be located using CLEM. In the first study, ultra-thin sections of MDM infected with the PTAP^{-} mutant were labelled with antibodies against p24/55 and PAG, located by CLEM and examined at the EM. A virus-containing compartment with immature virus profiles is shown in Figure 5.12A. This IPMC appeared loosely filled with particles with similar electron-dense shells noted for immature HIV-1 R3A WT (Figure 5.11). At high magnification, these profiles were labelled specifically with anti-p24/55 visualised with immunogold (Figure 5.12B, C). Other features of the IPMCs, such as tightly apposed membranes that appear to connect separate pockets of the compartments were also observed (Figure 5.12C). Examination of the surface of this cell profile did not reveal any budding virus profiles at this location. These observations show that, as in HEK 293T cells, the HIV-1 R3A PTAP^{-}

virions have the immature morphology, and in this case all budding particles were in IPMC.

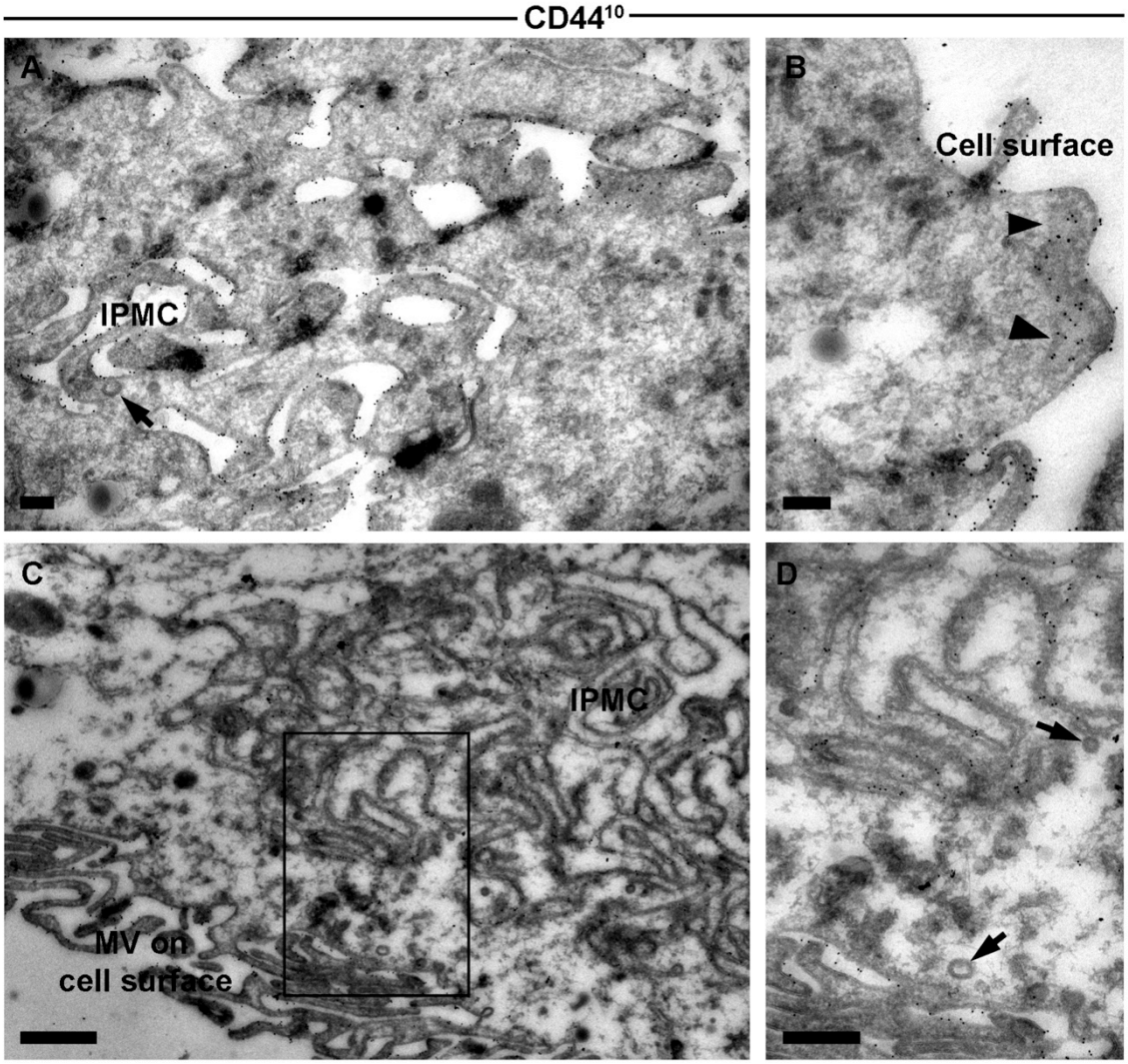

Figure 5.10: Morphology of IPMC on cell profiles without virus.

Ultra-thin cryo-sections were labelled with CD44 and 10-nm PAG. **(A)** CD44 labelling showed vacuole-like IPMC structures that were dispersed in the cytoplasm. The arrow points to a clathrin coated pit on the IPMC. **(B)** CD44 labelling at the cell surface. **(C)** A complex IPMC with convoluted interconnected tightly apposed membranes. The cell surface has numerous microvilli (MV) that are also labelled for CD44. **(D)** Higher power view of the area marked in C. Clathrin-coated vesicles/pits are indicated by black arrows. Scale bars: A and B, 200 nm; C, 1 μm; D, 500 nm.

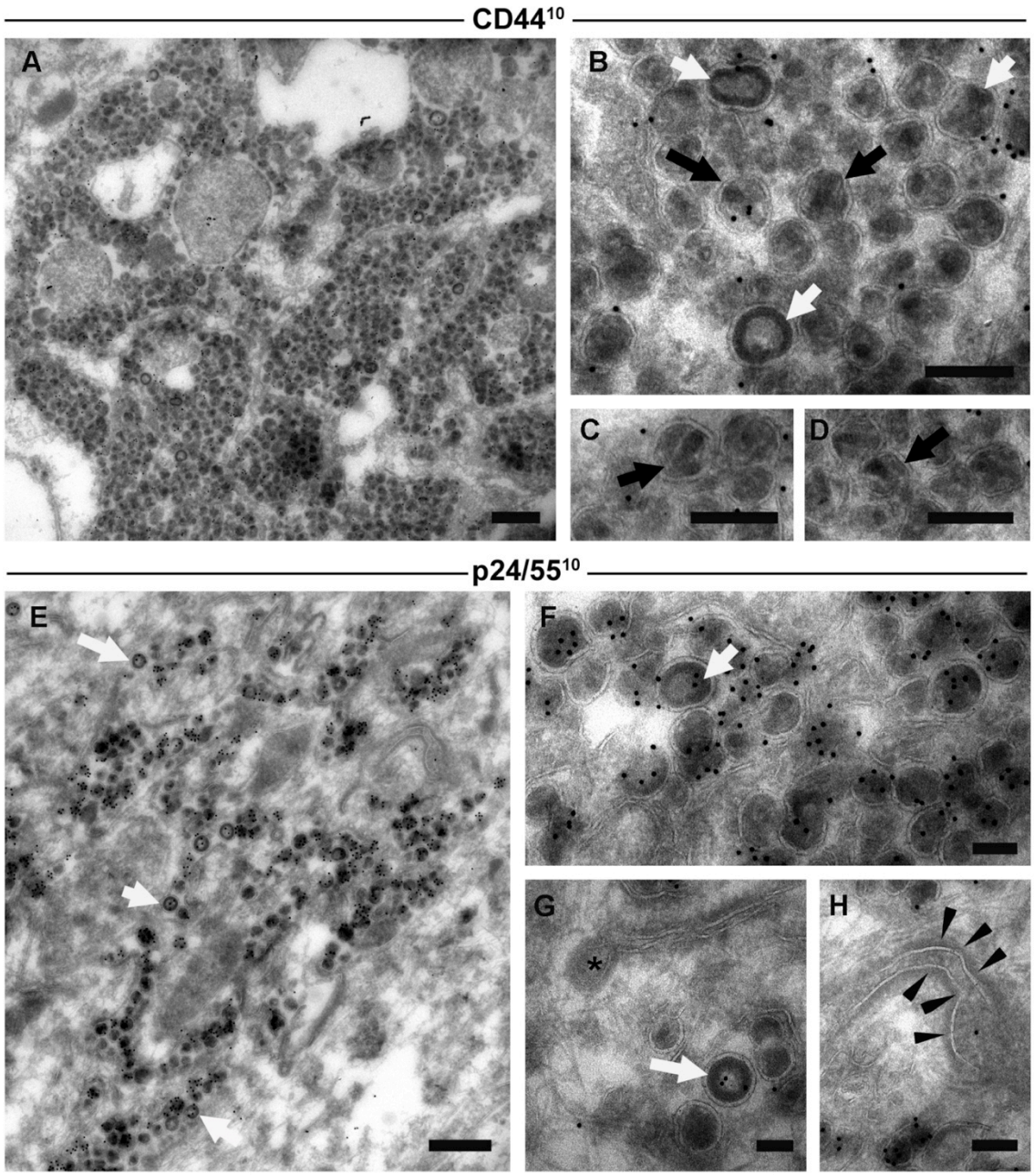

Figure 5.11: Ultra-structure of HIV-1 R3A WT virions in the IPMCs.

MDM infected with the HIV-1 R3A WT were immunolabelled with anti-CD44 (MEM-85) in A to D, or anti-p24 in E to H. **(A)** Overview of a large IPMC, densely packed with mature virus particles. **(B-D)** Enlarged views showing mature particles (black arrows) and immature figures (white arrows). **(E)** Overview of an IPMC containing mature and immature virus profiles. White arrows point to immature virus profiles. **(G)** Part of the IPMC, showing a clathrin coated pit (black asteriks), and an immature virus figure (white arrow). **(H)** Arrowheads point to electron dense flat coats that sometimes decorate parts of IPMCs. Scale bars: A, 500 nm; B-D, 200 nm; E, 500 nm; F-G, 100 nm.

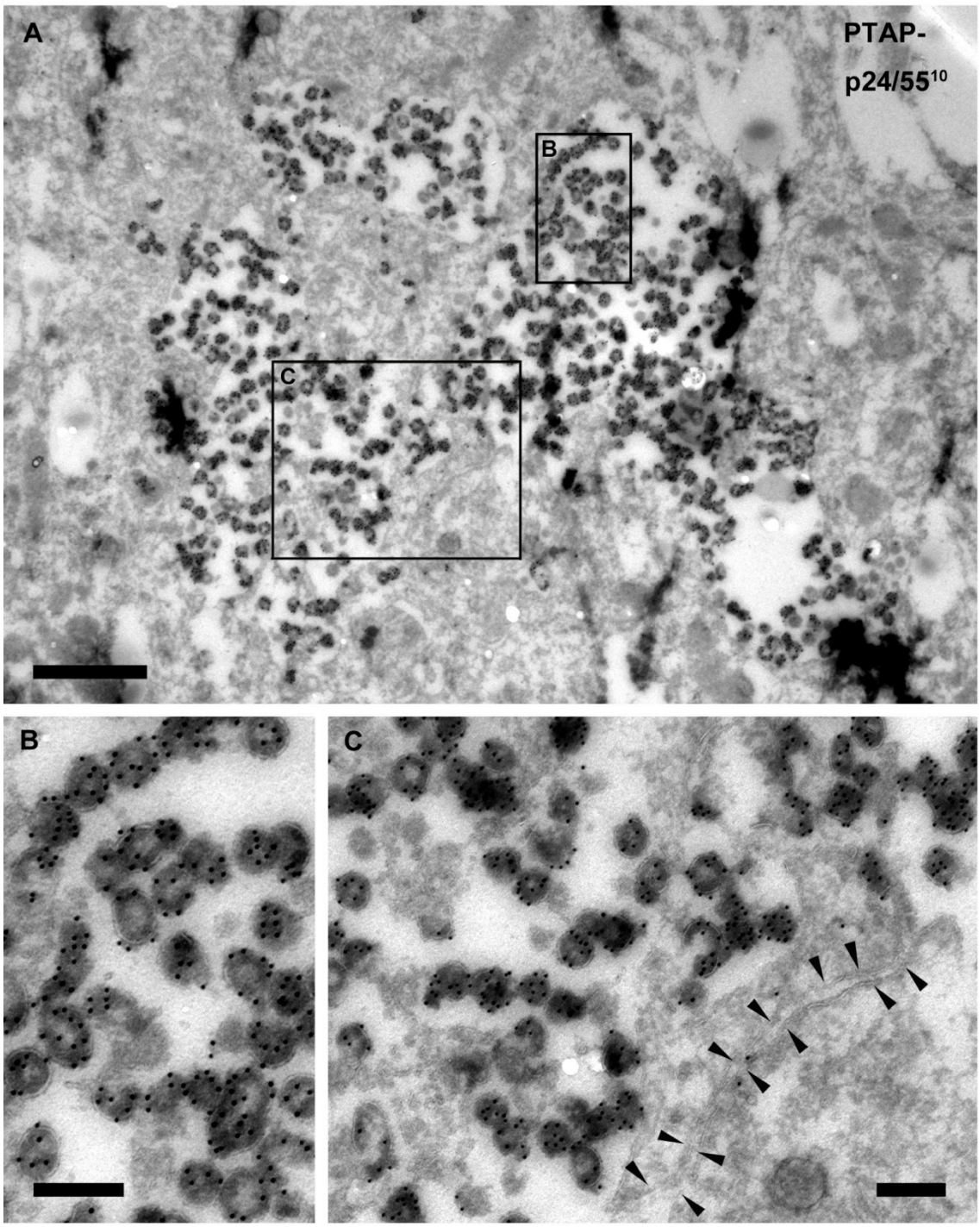

Figure 5.12: Ultra-structure of HIV-1 R3A PTAP^{-} virions in an IPMC.

Primary human MDM were infected with HIV-1 R3A PTAP^{-} for 7 days. Ultra-thin sections of the cells were immunolabelled with anti-p24/55 and 10-nm PAG. **(A)** An overview of an IPMC (located by CLEM) with immature virus profiles, characterised by electron dense shells. **(B, C)** Higher-magnification views of virus profiles shows that they label with 10-nm gold particles, that is, contain the HIV-1 Gag protein. In C, arrowheads point to closely apposed membranes connecting pockets of the IPMC. Scale bars: A, 1 µm; B & C, 200 nm.

5.2.4.4 Analysis of PTAP⁻YP⁻-infected MDM by CLEM

The ultra-structure of the IPMCs was also analysed in the context of the R3A PTAP⁻ YP⁻ mutants. A large number of cell profiles with associated virus buds were located using CLEM. As described below, the infected cell profiles showed a variety of IPMC morphologies, ranging from loose IPMCs close to the cell surface (Figure 5.13) and structures with sponge-like interconnected membranes (Figure 5.14) to apparent vacuoles filled with immature particles (Figure 5.15). Cell profiles were analysed in detail, photographed, and the locations of the virus buds recorded.

In Figure 5.13, a loose IPMC (on cell A) was observed near the cell surface. The IPMC opened up to the extra-cellular space in close proximity to another cell (cell B). Tunnels of closely apposed membranes connected some parts of the IPMC (Figure 5.13C), and were lined with thick flat coats of integrins CD18/CD11b,c (Pelchen-Matthews et al., 2012). This structure suggests that Cell A may be in the process of transferring virus to Cell B, as has been described (Gousset et al., 2008). On this cell, 94 virus profiles were seen in the IPMC, whilst only three were at the cell surface. Some virus buds had visible connections to the IPMC (Figure 5.13E, F). Notably, all observed virus profiles had immature morphology.

Some IPMCs containing viruses were sponge-like in appearance (Figure 5.14). Different sizes of the sponge-like IPMC have been observed. The cell in Figure 5.14 A, B had a small sponge-like IPMC with few virus profiles in a labyrinth of membranes that appeared to form individual pockets of IPMC. On 2D images, these may appear isolated (Deneka et al., 2007), but it is known from 3D image reconstructions that these are likely to be connected (Welsch et al., 2011). There were 12 immature virus profiles in the IPMC, and none on the cell surface. A much larger sponge-like IPMC with an extensive maze of membranes containing budding profiles of R3A PTAP⁻ YP⁻ is shown in Figure 5.14 C to G. Some of the membranes formed vacuole-like enclosures containing budding viruses. In addition, several narrow tunnels and rings of membranes were also found in the IPMC network (Figure 5.14G). Furthermore, there were arrested virus particles that double labelled with anti-p24/55 (5-nm gold) and anti-Env (10-nm gold) (Figure 5.14E, F). The labelling with anti-Env indicates that these were likely to

be infectious viruses. Virus profiles were enumerated; 255 were seen in the IPMC and none were found at the cell surface.

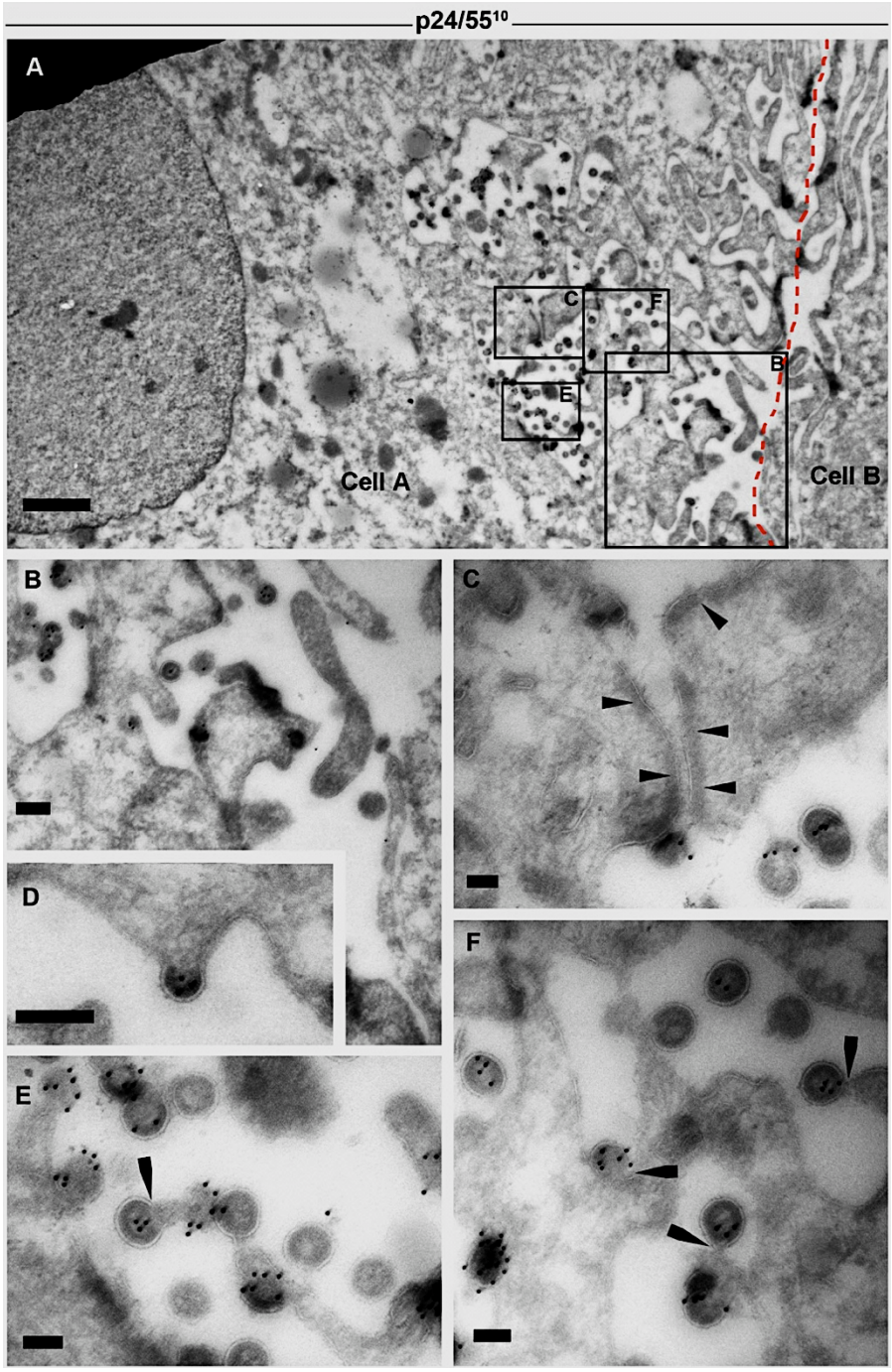

Figure 5.13: Loose IPMC near cell surface.

Ultra-thin cryo-sections from MDM infected with HIV R3A PTAP^{-}YP^{-} for 7 days were stained with p24/55 (10-nm PAG). **(A)** The approximate boundaries for two adjecent cells is indicated by a red dashed line. B-F show a higher magnification from cell B **(C)** Arrowheads identify the thick integrin coat that lines parts of the IPMC. **(D)** One of the three virus buds found at the cell surface among microvilli. **(E, F)** Immature virus profiles in the IPMC. Membrane stalks linking virions to the IPMC were visible, as indicated by black arrows. Scale bars: A, 1 µm; B, 200 nm; C-D, 100 nm.

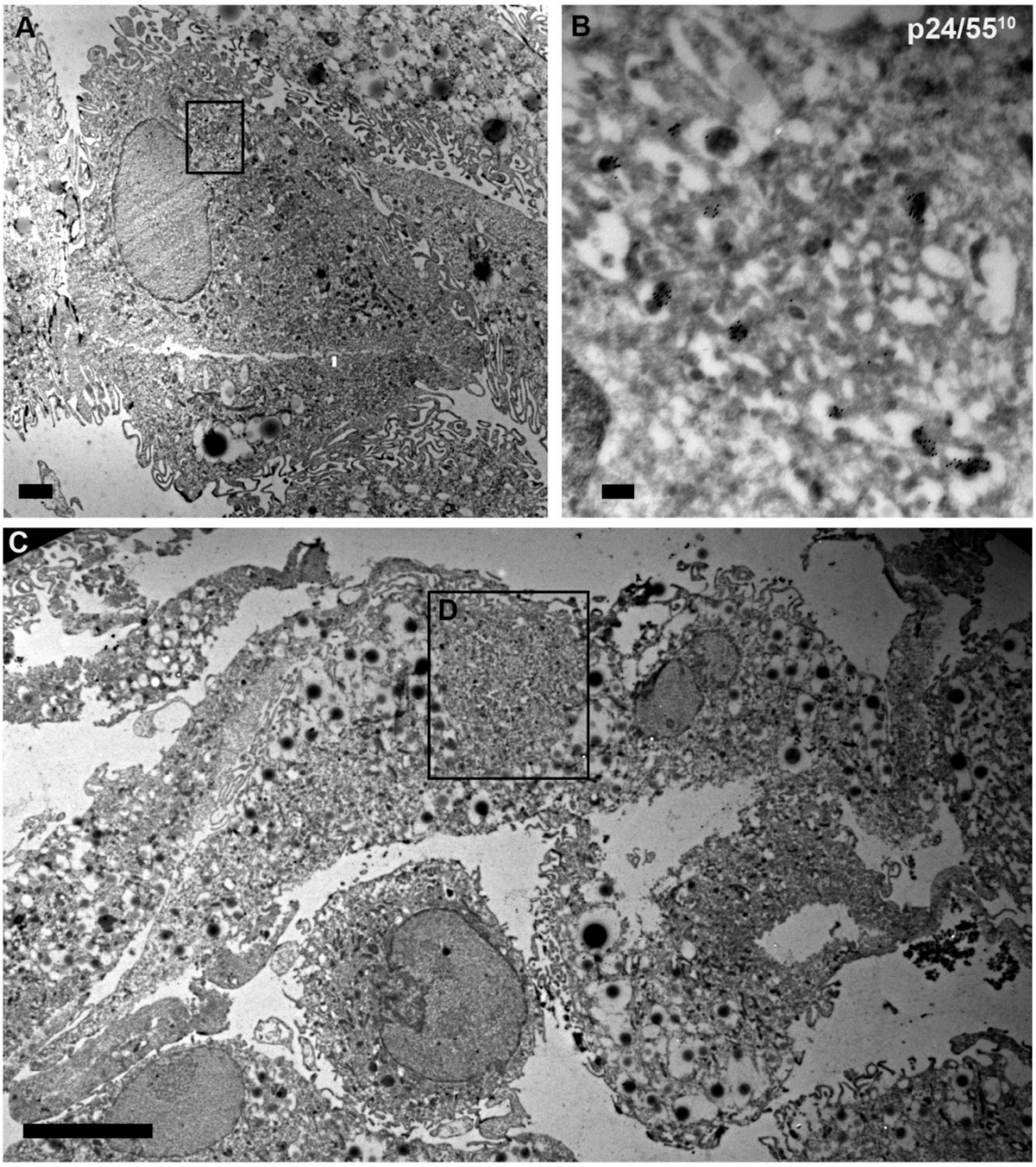

Figure 5.14. Sponge-like IPMCs in MDM.

MDM infected with HIV-1 R3A PTAP^{-}YP^{-} were labelled with indicated antibodies and PAG. **(A)** An overview of a cell with a small IPMC (boxed). **(B)** MDM specimens were single labelled with p24/55 and detected with 10-nm PAG. **(C)** An overview of MDM with a large IPMC (boxed). Scale bars: A, 2 μm; B, 200 nm; C. **The figure and legend continue on the next page.**

Figure is continued from the previous page.

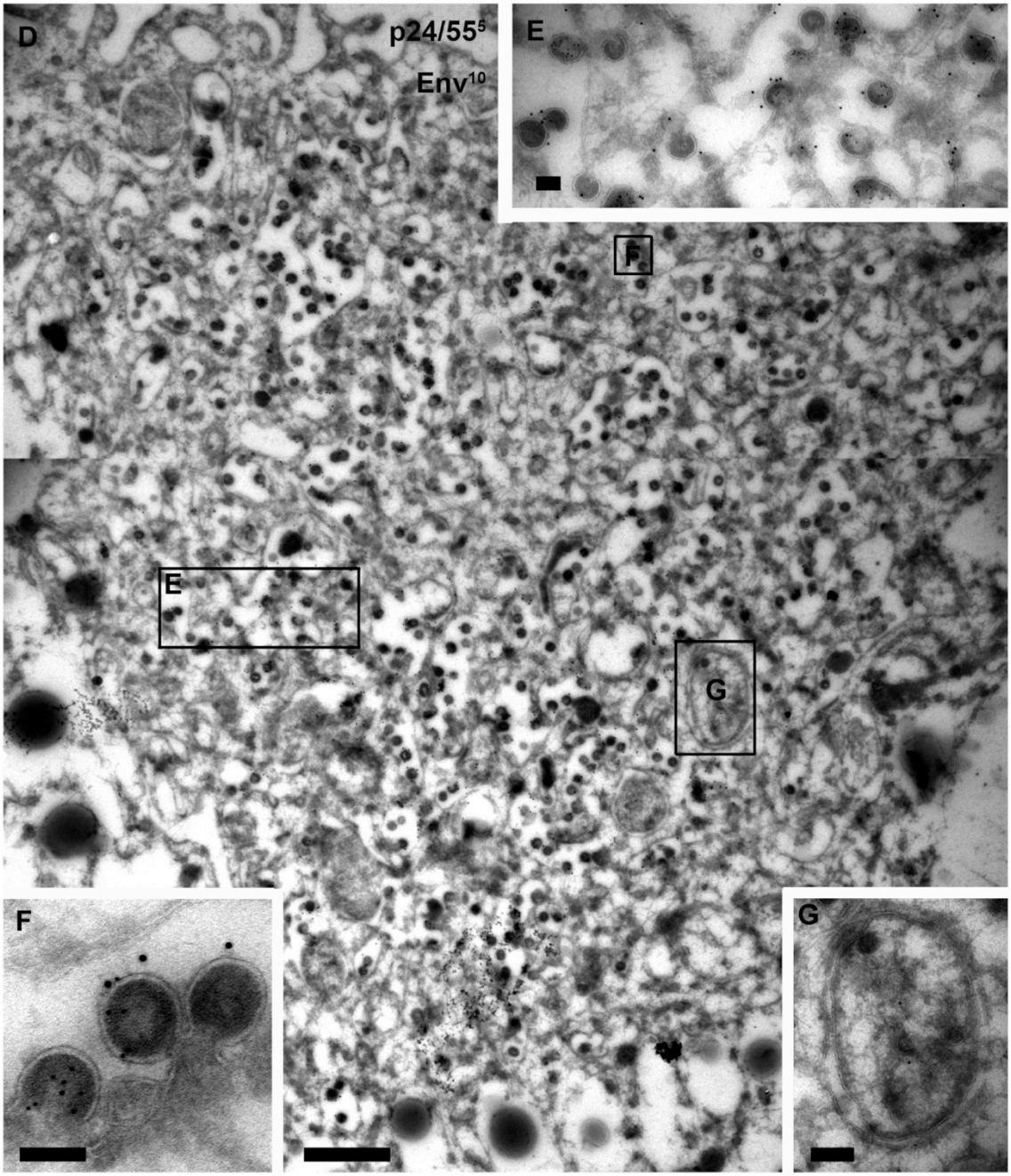

Figure 5.14: Sponge-like IPMCs in MDM.

(D) An alignment of IPMC images at high magnification. **(E, F)** Arrested $PTAP^{-}YP^{-}$ budding intermediates at the IPMC, double labelled with p24/55 (5-nm PAG) and Env (10-nm PAG). Black arrows point at membrane necks connecting virus profiles to the PM. **(G)** A ring of closely apposing membranes found in an IPMC. Scale bars: 10 μm; D, 1 μm; E and F, 100 nm; G, 200 nm.

The third type of IPMC observed was a loose vacuole-like compartment. Here, budding profiles appeared enclosed in a continuous limiting membrane that may have connection to the cell surface in another plane (Figure 5.15A, B). The IPMC was deep within the cell and contained immature virus figures that were labelled with antibodies against p24/55 and Env viral proteins. In total, 69 virus profiles were found in two pockets of the IPMC in this cell, while there were no virus profiles on the cell surface. Together, these data show immature viruses in IPMCs with diverse morphologies. Notably, only few virus profiles were observed on the cell surface.

To quantitatively assess the distribution of virus on EM micrographs in addition to the cells described above, virus profiles were counted on 29 cell profiles expressing either HIV-1 R3A PTAP^{-} or PTAP^{-}YP^{-} (Table 5.2). For these cell profiles, 19/29 (66%) and 9/19 (31%) had HIV-1 at the IPMC, and IPMC plus cell surface, respectively. Notably, only 1/29 (3%) of the cells examined had all virions only at the cell surface, though it is not clear whether this cell would have an IPMC in a different plane, or whether it is one of the MDMs lacking the IPMC (see also Section 5.2.2). Collectively, 3003/3089 (97%) virus profiles were observed associated with IPMCs, and 86/3089 (3%) were at the cell surface (Table 5.3). These results support the IF data and indicate that most virus and virus assembly is associated with IPMCs.

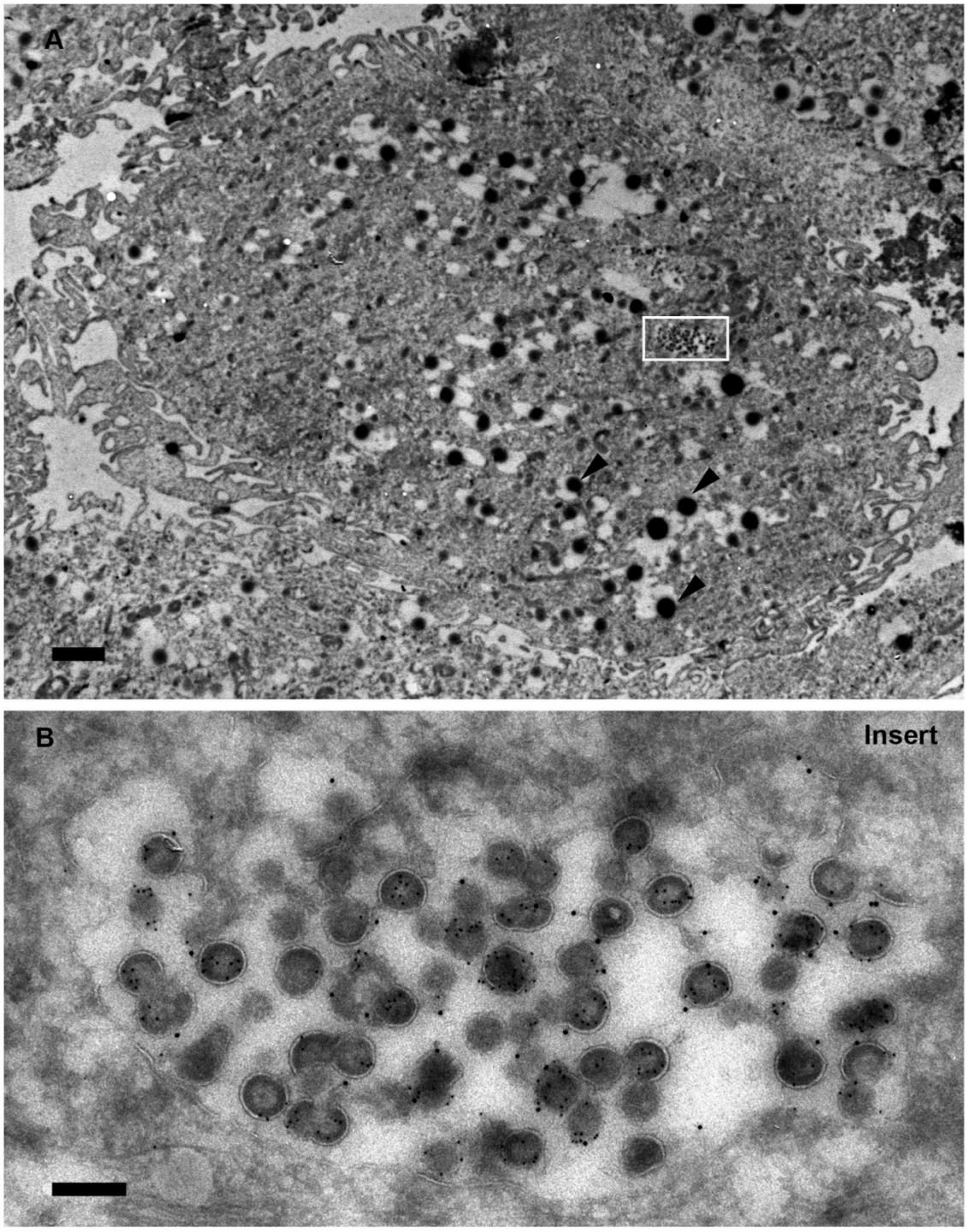

Figure 5.15: Tight vacuole-like IPMC in MDM

(A) Ultra-thin cryo-section of MDM infected with HIV-1 R3A PTAP^{-}YP^{-}. The dark spots (arrowheads) in A represent lipid droplets. **(B)** Immature virus profiles in a vacuole-like compartment double labelled with antibodies against p24/55 (5-nm PAG) and Env (10-nm PAG). Scale bars: 2 µm; 200 nm.

Table 5.2: Direct bud counts: numbers of virus profiles associated with IPMCs and the cell surface of MDM infected with HIV-1 R3A PTAP$^-$ or PTAP$^-$YP$^-$.

Cells profiles where buds were seen at both IPMCs and the cell surface are in bold font, whilst the cell with virus at the cell surface only is in italics. The data in regular font refers to cell profiles where virus was found in IPMCs only.

Donor (Mutant)	Cell profile	Numbers of virus per cell profile	
		IPMC	Cell surface
		Virus profiles	Virus profiles
D415 (PTAP$^-$)	1	265	0
	2	312	0
	3	**45**	**15**
	4	139	0
	5	72	0
	6	80	0
D428 (PTAP$^-$YP$^-$)	7	193	0
	8	20	0
	9	165	0
	10	10	0
	11	47	0
	12	27	0
	13	**175**	**2**
	14	47	0
	15	35	0
D429 (PTAP$^-$YP$^-$)	**16**	**281**	**3**
	17	-	*24*
	18	129	0
	19	**62**	**1**
	20	69	0
	21	255	0
D432 (PTAP$^-$YP$^-$)	**22**	**58**	**20**
	23	118	0
	24	38	0
	25	**118**	**4**
	26	12	0
	27	**18**	**2**
	28	**119**	**12**
	29	**94**	**3**
Total (or sum)		3003	86
Proportion (%)		97.2	2.8

5.2.4.5 Morphometric analysis of MDM infected with HIV R3A PTAP$^-$YP$^-$

The analysis of number of virus profiles on EM cell profile images revealed that 97% of the budding-arrested virions were found at the IPMC. Because a lot of membrane is folded up in the IPMCs, virus may simply be budding at the most abundant membrane surface. Therefore, I wanted to estimate the area of membrane at the cell surface or in the IPMCs on cells with budding arrested particles. Relative membranes areas were measured on EM images using standard stereological methods (West, 2012).

Segmentation of the plasma membrane at the IPMC and cell surface was performed on highly magnified EM images (23,000x or 30,000x), by manually tracing the relevant compartments (Figure 5.19-5.21). Straight lines, 1-cm apart, were then superimposed on the images. Points were counted where the lines intercepted the segmentation lines (Figures 5.19). Using the number of intercepts, the surface areas covered by the membranes were estimated using the mathematical relationship below (Figure 5.18).

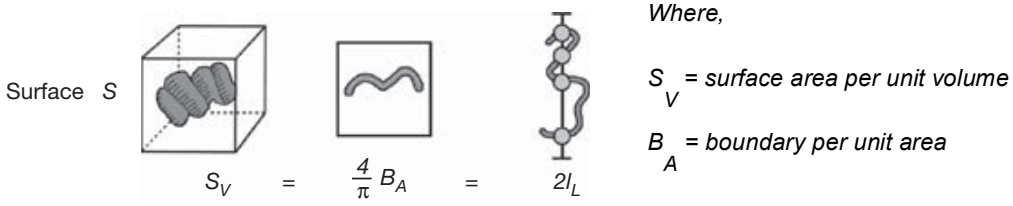

Figure 5.16: Morphometric analysis of biological samples or objects.
Diagram showing the mathematical relationships between 3D structural features of objects (left) and the interaction of the line probe/interceptor with features of the object apparent in section.

For these estimates, the cells with complete membranes covering both the cell surface and IPMC were chosen. These profiles were analysed using the above stereology procedure, to estimate membrane surface areas, at the IPMC and cell surface in arbitrary units (A.U.) (Table 5.3). The data shows that Cell 16 had similar amounts of membrane area at the IPMC and cell surface. The cell surface area of Cell 19 was about 28-fold more than that of the IPMC, whilst cell 21 had about twice the amount of membrane at the cell surface than at the IPMC. The ratios of virus profiles to membranes were calculated and are presented in Table 5.3. The results indicate that targeting of the virus to any particular site did not depend on the amount of membrane present at either the IPMC or cell surface, as all the virus was predominantly at the IPMC for the three profiles analysed.

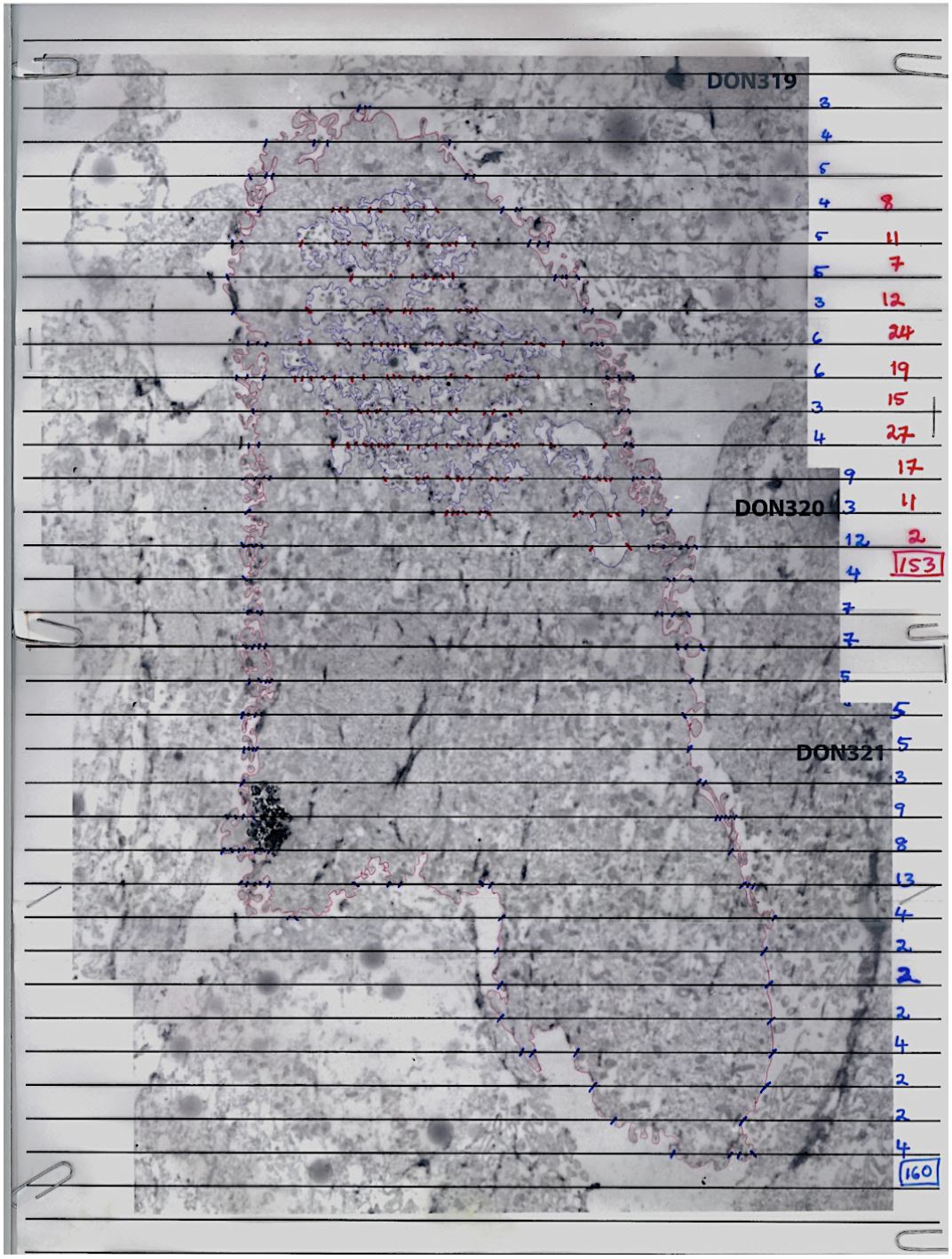

Figure 5.17: 2D Stereology for cell No. 16 in Table 5.2.

High-magnification images (DON319-DON321) of the cell were aligned to assemble the entire cell profile. The montage was printed on A3 paper and segmented manually using pens with different colours for the IPMC and cell surface. Points of interception of the straight line probes and segmentation lines (red and blue) were counted and scored as shown on the right side of the image. (Note that this is the same cell shown in Figure 5.12)

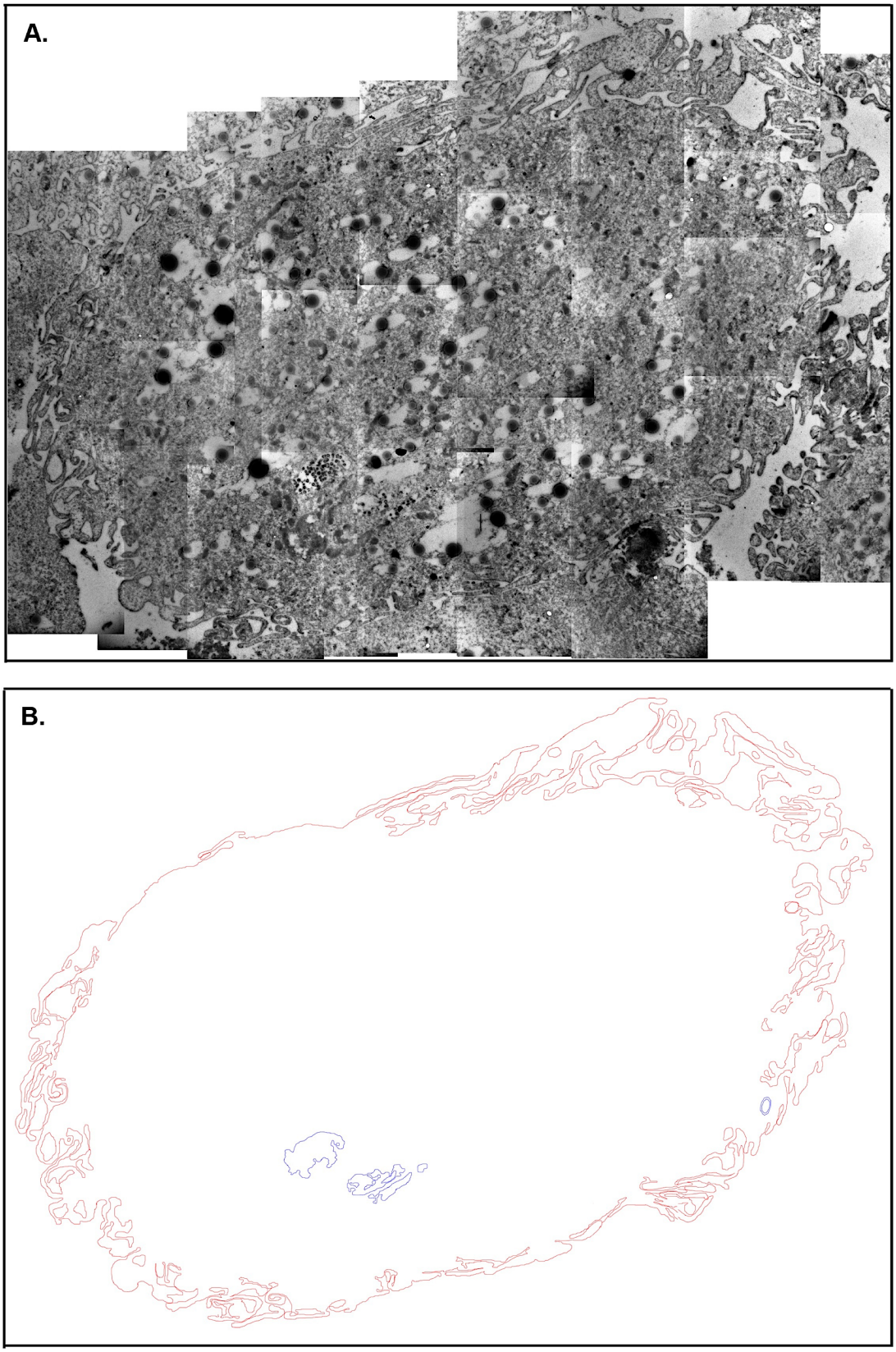

Figure 5.18: Segmentation of cell No. 19 in Table 5.2.

(A) An alignment of multiple high-magnification images, to assemble the cell profile. (B) The segmentation of plasma membrane (red) and IPMC (blue), here done by adding brush lines in Photoshop CS.

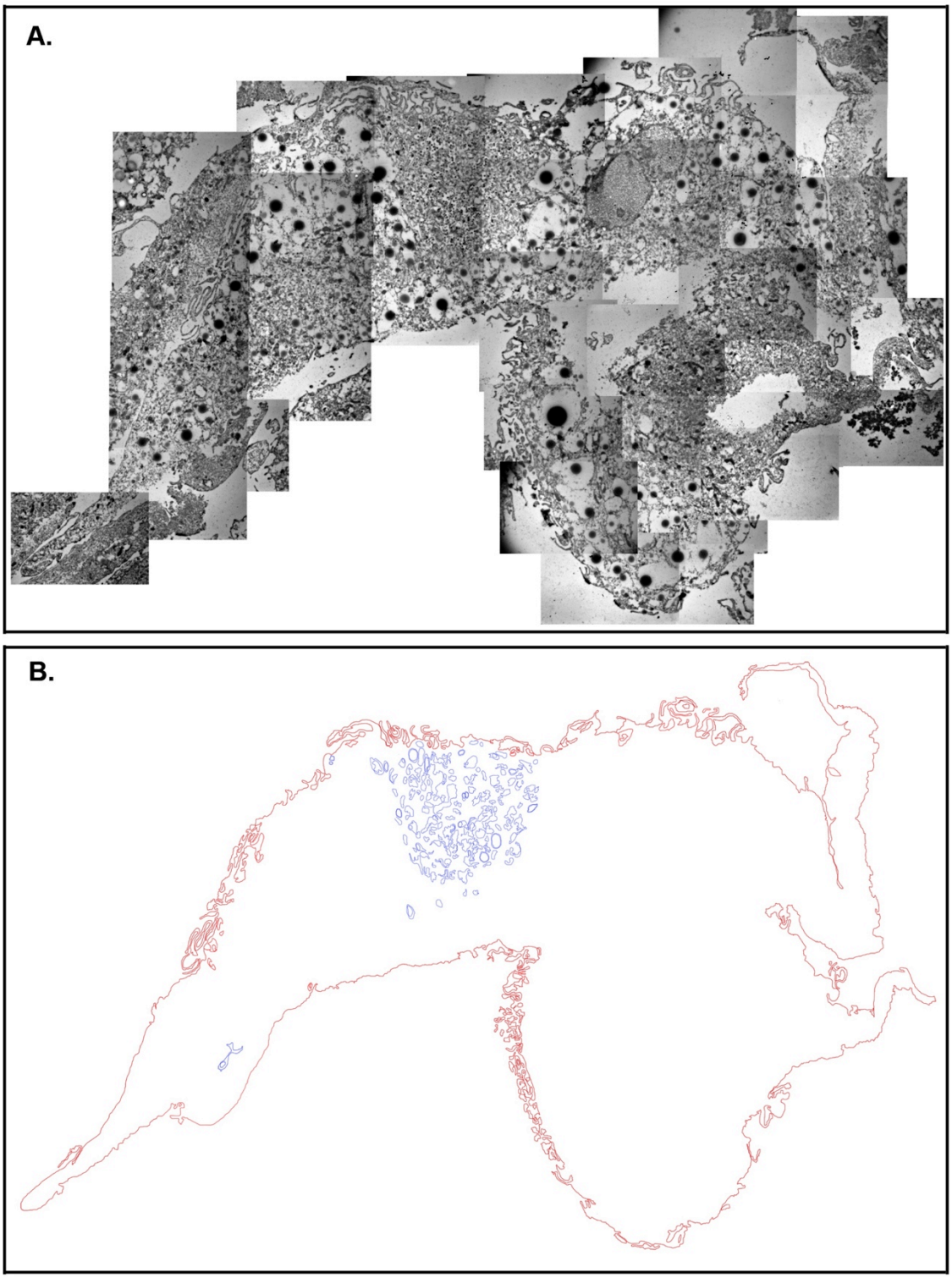

Figure 5.19: Segmentation of cell No. 21 in Table 5.2.

(A) An alignment of multiple high-magnification images, to assemble the cell profile. (B) The segmentation of plasma membrane (red) and IPMC (blue).

Table 5.3: Estimations of virus relative to membranes at the IPMC and cell surface.
Cell profiles used for this analysis were all from D429 (MDM infected with HIV-1 R3A PTAP^{-}YP^{-}).

Membrane	Estimates	Cell profiles		
		No. 16	No. 19	No. 21
IPMC	S_V (A.U.)	306	30	404
	Virus profiles	281	62	255
	Profiles/S_V	**0.918**	**2.067**	**0.631**
Cell surface	S_V (A.U.)	320	828	754
	Virus profiles	3	1	0
	Profiles/S_V	**0.009**	**0.001**	**0.000**

In conclusion, my analysis of IF data for the HIV-1 R3A mutant revealed that more than 90% of Gag labelling was found at the IPMCs. Then when individual viruses were identified and counted at higher resolution using EM, 97% of the viruses were in the IPMCs. If the virus was budding at the cell surface and later phagocytosed, as suggested by some reports (Jouvenet et al., 2006; Bennett et al., 2009; Chu et al., 2012a), then I would not have found barely 3% of arrested viruses at the cell surface. Estimations of the amount of membrane at the IPMC and cell surface in infected cells showed that the virus was enriched in IPMCs, suggesting specific targeting. Taken together, these data provide the first conclusive evidence that the IPMC is the principal site for HIV-1 assembly in primary human macrophages.

5.3 Discussion

Since it was discovered that in primary human macrophages HIV-1 accumulates in intracellular compartments (Gartner et al., 1986), understanding the nature of these structures has been growing over the years, with the current view being that they are internally sequestered plasma membrane domains. Different names all referring to the same structures have been used in the literature: for example, the internal plasma membrane-connected compartments (IPMCs) (Pelchen-Matthews et al., 2012; Mlcochova et al., 2013; Giese and Marsh, 2014) and virus containing compartments (VCC) (Chu et al., 2012b; Gaudin et al., 2013a; Duncan et al., 2014; Mariani et al., 2014). As the former name suggests, connections of these compartments to the cell surfaces have been observed (Deneka et al., 2007; Bennett et al., 2009; Welsch et al.,

2011; Pelchen-Matthews et al., 2012). These compartments have also been seen in uninfected macrophages, and clearly are not formed/induced as a consequence of infection (Welsch et al., 2011; Pelchen-Matthews et al., 2012; Berre et al., 2013; Giese and Marsh, 2014). Therefore, we have opted to call them IPMCs. Although HIV-1 accumulates in IPMCs and budding viruses have been found on the limiting membranes of IPMCs, it is still controversial whether IPMCs are the main site for HIV-1 assembly in primary human macrophages (Jouvenet et al., 2006; Chu et al., 2012a). Since HIV-1 recruits the ESCRT machinery to mediate scission of the membrane stalk that links new virions to their producer cell, HIV-1 mutants defective in ESCRT recruitment were generated to inhibit membrane fission. Rescued mutants were used to infect MDM, and analysed by IF and EM. Quantitation of IF data showed that, on average more than 90% of the viral antigens were located in the IPMCs of infected cells. Furthermore, EM was used to directly identify and analyse the distribution of individual virus particles, and estimate the amount of membrane at each cell surface and IPMC. The data revealed the enrichment of virus in the IPMCs.

The IPMCs where HIV-1 assembles in macrophages vary in size and morphology. For IF analysis, immuno-staining of MDM with the plasma membrane marker CD44 was used to identify the cell surface and IPMC. The CD44-containing membrane structures were variable from cell-to-cell, ranging from simple to very complex (Figures 5.1 and 5.3), consistent with recent reports (Berre et al., 2013; Mlcochova et al., 2013). Although in some cases the compartments would appear as individual structures in a single confocal section, in the majority of cases these were inter-connected when whole cells imaged in z-series were reconstructed into 3D images. This agrees with similar reconstructions of 3D EM image series (Bennett et al., 2009; Welsch et al., 2011). By immunofluorescence staining for the HIV-1 structural proteins, Gag p24/55 and p17, the virus was found mostly in these diverse and complex IPMCs. Notably, for MDMs infected with HIV-1 WT or the $PTAP^{-}$ or $PTAP^{-}YP^{-}$ mutants, virus staining was observed mainly in the IPMCs.

Analysis of infection levels by IF showed there were fewer macrophages infected with the mutants, and Gag was poorly expressed in the infected cells, compared to the WT (Figures 5.1 and 5.8). There was some donor-to-donor variation in infection levels, as

reported before (Bol et al., 2009). For the HIV-1 R3A WT, infectious particles are released from the infected MDM, allowing a spreading infection in the cultures, while the budding-arrested mutants are not able to establish a spreading infection. This probably explains why infection levels were low for the mutants, even though higher titres were used to infect the MDM. Moreover, earlier reports had suggested that mutations in the L domain of HIV-1 reduces the replication kinetics of VSV-G pseudotyped viruses used to infect different cell lines and primary cells including MDM (Demirov et al., 2002b; Fujii et al., 2009). In these studies, the kinetics of the L domain mutants were determined by monitoring reverse transcriptase (RT) activity. In most cases, the RT activity of the mutants began to rise above baseline on the sixth day post infection. Therefore, these published observations may explain the low expression levels of mutants in the current study. Because the L domain mutations do not overlap with the open reading frame of RT, it is not clear how they would influence RT activity. Quantitation of the IF data revealed that HIV-1 was mainly found at the IPMC (Figure 5.3). Overall, in 66% and 77% of cells expressing HIV-1 R3A WT or the mutants, respectively, HIV staining was seen at the IPMC only. For cells with virus at both the IPMC and cell surface, more that 90% of virus fluorescence was associated with IPMCs. However, one limitation with quantifying virus fluorescence is the low resolution of confocal microscopy, which made it difficult or even impossible in some cases to separate the IPMC from the cell surface when the two membrane domains were in close proximity.

There is currently no specific marker for the IPMC. Therefore, fluorescence studies of the IPMC have relied on markers that recognise both IPMCs and the cell surface, such as CD9, CD81 and CD44 (Deneka et al., 2007; Welsch et al., 2007). Furthermore, using CD44 as a surrogate marker for the IPMC and cell surface PM in quantitative IF is not always reliable as the staining for this molecule at IPMCs can be reduced in cells containing a large amount of virus, presumably due to its incorporation into virions (Lawn and Butera, 2000; Lawn et al., 2000; Chertova et al., 2006). EM was used in order to identify individual viruses and quantify membranes. Immature viruses were observed primarily at the IPMC of infected macrophages expressing HIV-1 PTAP^{-} and PTAP^{-}YP^{-} mutants (Figure 5.12 and 5.15; Table 5.2). The appearance of these buds was very similar to that of the few immature buds in MDM infected with HIV-1 WT

(Figure 5.11). They typically contained an electron-dense layer of Gag beneath the membrane and an electron-lucent centre, consistent with the reported morphologies of the budding arrested HIV particles (Garrus et al., 2001; von Schwedler et al., 2003). More than 95% of viruses counted were in the IPMCs with diverse morphologies and sizes. The type of morphologies observed included IPMCs that were loose or compact, some more vacuole-like and others sponge-like, as described before (Deneka et al., 2007; Welsch et al., 2011; Pelchen-Matthews et al., 2012). The predominance of buds in the IPMCs may simply be due to the large amount of membrane in these structures. Therefore, 2D stereology was used to determine the number of buds per unit membrane for particles at the IPMC or at the cell surface. This showed that the amount of membrane in the IPMCs is not very much greater than that at the cell surface (Table 5.3). For example, for cell profile 16 there was a similar amount of membrane at both the IPMC and cell surface, giving an enrichment of virus buds in the IPMC of over 100x, while virus targeting to the IPMCs was even greater for the other two cells analysed. This clearly defines this site as the target for HIV assembly in macrophages, in support of earlier reports (Deneka et al., 2007; Welsch et al., 2007). Furthermore, a recent study using live-cell imaging has shown HIV-1 Gag fluorescence accumulation in the IPMCs of infected macrophages (Berre et al., 2013), suggesting assembly is initially targeted to the IPMCs. Collectively, the live-cell imaging study and the current study, provide convincing evidence that IPMCs are indeed directly targeted for HIV assembly in macrophages.

In this chapter, I have shown systematically, using various morphological techniques and quantitative analysis, that the IPMC is indeed the main plasma membrane domain for HIV-1 assembly in macrophages. This suggests that Gag is specifically targeted to IPMCs in macrophages. The mechanism of this targeting is not clear. A study from our group showed that the pleckstrin homology domain of phospholipase Cδ fused to GFP, which specifically binds $PI(4,5)P_2$, was targeted to both the IPMC and cell surface plasma membranes (Mlcochova et al., 2013). This suggested that $PI(4,5)P_2$, which is important for targeting myristoylated Gag to the plasma membrane (Ono et al., 2004; Saad et al., 2006a), may be equally abundant at both the IPMC and cell surface membranes. Therefore, there are possibly other aspects of the membrane composition that influence HIV assembly at the IPMCs in macrophages. *In vitro* model studies using

liposomes have shown that increase in cholesterol content increases binding efficiency of Gag (Dick et al., 2012). Similarly, increasing the concentration of phosphatidylserine (PS) increases the binding of Gag to the liposome. In addition, HIV-1 MA could also bind, directly to liposomes made up of phosphatidylcholine (PC) and phosphatidylethanolamine (PE) with varying lengths of acyl chains, independently of myristoylation (Vlach and Saad, 2013). These are interesting studies that should be extended to intact cells to try and understand if there are differences in the composition of the membrane domains of macrophages where HIV-1 assembles.

In conclusion, I have taken advantage of the cellular ESCRT machinery that HIV recruits to bud from cells, and disrupted its engagement with the virus. This allowed for the infection of MDMs and generation of stable HIV-1 budding intermediates. By analysing the distribution of these arrested assembly intermediates, the IPMC was identified as the principal site for HIV assembly in macrophages. Because macrophages are found in all body tissues, and they are long-lived, they represent an important viral reservoir that may impact on HIV-1 pathogenesis. The virus in the IPMC is concealed from immune surveillance, and can be transferred to uninfected cells through cell-to-cell contacts (Giese and Marsh, 2014). With a better understanding of HIV-1 assembly in the IPMCs of macrophages, efforts can be made to therapeutically target this viral niche, to further reduce the HIV/AIDS disease burden.

"...if it wasn't for those first few failures, the future successes would never have happened."

Richard Branson, Founder of Virgin Group.

6. General Discussion

Macrophages are amongst the key immune cells that HIV infects *in vivo* and *in vitro*. Numerous studies have demonstrated that HIV assembles and accumulates in internal compartments of primary human monocyte-derived macrophages cultured *in vitro*. Initially, the nature of this compartment was unclear, but now there is compelling evidence from different research groups that these structures are internal plasma membrane-connected compartments (IPMCs), and that they are not induced by HIV infection (see Introduction, Section 1.6.3)

Although the majority of HIV seen in infected macrophages is associated with IPMCs, there has been concern that some virus particles may assemble at the cell surface. To address this question, I set out to establish an experimental system to determine whether HIV does assemble at the surface of infected cells and, if so, what proportion. As the ESCRT machinery is required for HIV budding in many cell systems, I disrupted the recruitment of this machinery, and first investigated its requirement for virus release in macrophages, since this has not been studied to any great extent in these cells. Using siRNA, ALIX and Tsg101 were depleted efficiently. Although the effects on virus release were minimal, Tsg101 had a greater effect than ALIX for HIV release in MDM. In the second approach I generated mutants (HIV-1 PTAP^{-}, YP^{-}, PTAP^{-}YP^{-}, Δp6) defective in recruiting the ESCRT machinery by mutating the sequences that bind Tsg101 and ALIX. The mutants were characterised in HEK 293T cells, and the release of PTAP^{-}, PTAP^{-}YP^{-} and Δp6 was inhibited. EM analysis showed that the mutants produced arrested budding profiles. As the mutants are defective in release, I developed a method to rescue HIV-1 PTAP^{-} and PTAP^{-}YP^{-} viruses for infecting MDM. I infected MDM with the rescued mutants and used IF and EM to analyse the specimens. In the vast majority of cells (77%), the virus was found at the IPMCs. Analysis by EM showed immature viruses predominantly (97%) in the IPMCs. Using morphometric analysis to estimate the area of PM at the cell surface and IPMC, I discovered that HIV was enriched in the IPMCs, suggesting specific targeting of viral components to the IPMC membrane. This thesis therefore provides the first conclusive quantitative evidence that the IPMCs are the main sites for HIV assembly in primary MDM. The implications of these findings for HIV pathogenesis and future directions are discussed below.

6.1 The ESCRT machinery is required for HIV assembly in primary macrophages

The ESCRT machinery mediates topologically equivalent membrane fission processes, such as HIV release, abscission and MVB intralumenal vesicles formation (see General introduction, Section 1.5.5). I investigated the requirement of the ESCRT machinery for HIV assembly in macrophages. Specifically, Tsgl01 and ALIX were efficiently depleted in infected MDM using siRNA. However, I observed limited effects on virus release (Figure 3.1 to 3.3). Two recent studies reported efficient inhibition of virus release in macrophages depleted of Tsg101 (Gaudin et al., 2012; Berre et al., 2013). In these studies, VSV G-pseudotyped HIV was used to infect macrophages to achieve almost 100% infection, whilst I used a replication-competent macrophage-tropic virus strain, HIV-1 BaL, to infect MDM. The level of infection achieved in the two studies cited above is difficult to achieve when emulating physiological conditions, which involve HIV-1 gp120 binding to CD4 and CCR5/CXCR4 on target cells (see General introduction, Section 1.4.1), and certainly CD4 levels are lower on MDMs. It is possible that cells that were infected in this thesis escaped siRNA transfection. Macrophages are more restrictive to productive HIV replication than T cells, and the restriction can occur at different stages of replication. Recently identified restriction factors in macrophages include SAMHD1, which depletes the dNTP pool required for reverse transcription (Laguette et al., 2011); and interferon-inducible protein 16 (IFI16) that senses and binds pathogen DNA, to stimulate innate immunity through the stimulator of interferon genes (STING) pathway (Jakobsen et al., 2013; Bhat and Fitzgerald, 2014). Therefore, I speculate that when macrophages are infected with VSV G-pseudotyped HIV, more virus particles will be taken up and the virus DNA generated may overwhelm the DNA sensing machinery, and therefore escape innate immunity. This may partially explain why Berre et al. (2013) and Gaudin et al. (2012) observed efficient virus inhibition when I did not. However, I chose not to use VSV-G pseudotyped viruses to avoid possible artefacts generated by infection through non-gp120/41 mediated entry.

Whilst optimising knockdown protocols, I found that Tsgl01 was depleted to lower levels on day 6 compared to day 3 after siRNA transfections (see Materials and Methods, Section 2.5). Therefore, I infected MDM and transfected them with siRNA oligonucleotides 24 hrs later. Cultures were incubated for 6 days after the siRNA

transfections (that is 7 days post-infection [dpi]), and then harvested for biochemical analysis. By contrast, Berre et al. (2013) and Gaudin et al. (2012) transfected MDM with siRNA oligonucleotides 8 hrs after infection. Their cultures were incubated 4 dpi, and then harvested for biochemical analysis (Gaudin et al., 2012). It is possible that Gaudin and colleagues (2012) used macrophages with less developed IPMCs. However, for their morphological experiments, where visualising the IPMCs was important, they harvested their cultures 7 dpi. IPMCs become more prominent as macrophages mature in tissue culture, as determined by following CD18 and CD44 expression (Pelchen-Matthews et al., 2012). Therefore, it is possible that in my experiments, the virus was able to accumulate in the developed IPMCs before the level of Tsg101 and ALIX were sufficiently low to inhibit budding. Although RNAi experiments had a limited effect on virus release, overall, Tsg101 had a greater effect than ALIX for virus release in macrophages, as in other cell types reported elsewhere (Garrus et al., 2001; Pornillos et al., 2003; Fujii et al., 2009).

To avoid the problems of balancing siRNA knockdown with infection, I generated HIV-1 R3A mutants defective in recruiting Tsg101 and ALIX, which were expressed in MDM and analysed by western blotting (Figure 3.13). The inhibition of virus release from MDM expressing HIV-1 R3A PTAP^{-} and Δp6 was greater than that of YP^{-}, further demonstrating that Tsg101 is more important than ALIX for virus release in MDM.

I also looked in detail at the morphologies of the PTAP^{-}, PTAP^{-}YP^{-} and Δp6 mutants in HEK 293T cells using EM. On average PTAP^{-} and PTAP^{-}YP^{-} exhibited half complete budding profiles (representing an early stage during assembly), whilst the Δp6 profiles were typically three-quarters complete (late stage during assembly) (Figure 4.5). The commonalities between these viruses are that (1) PTAP^{-}YP^{-} and PTAP^{-} have a full-length Gag polyprotein, and (2) PTAP^{-}YP^{-} and Δp6 cannot recruit the ESCRT machinery. These data suggest that the p6 subdomain may be involved in regulating HIV assembly. Furthermore, I co-transfected HEK 293T cells with dominant negative (DN) GFP-VPS4 EQ and HIV-1 R3A WT, and used correlative light and electron microscopy (CLEM) to examine the cells. The virus profiles were on average shallower than those for the PTAP^{-} and PTAP^{-}YP^{-} (Appendix, Figure 8.2), suggesting arrest at a

much earlier stage during assembly. This is in contrast to a previous report showing that DN VPS4 arrested viruses on HEK 293T cells at a later stage during assembly (von Schwedler et al., 2003).

Recently, two independent studies have suggested that VPS4 may be involved early in membrane fission processes, such as HIV assembly and MVB biogenesis (Adell et al., 2014; Cashikar et al., 2014). Cashikar and co-workers used siRNA to deplete VPS4 in HeLa cells, and the cells were unroofed to analyse the cytoplasmic surface of the plasma membrane using EM (Cashikar et al., 2014). Conical spirals that labelled with ESCRT-III antibodies were observed. These studies were extended to study HIV VLP assembly in HEK 293T cells by knocking down VPS4 in Gag transfected cells, and the researchers observed shallow Gag shells with fewer ESCRT-III filaments, compared to the deep exvaginations of Gag shell with tight spirals of ESCRT-III filaments in control cells. These data suggest similarity to my observations of shallow HIV-1 budding profiles when DN VPS4 was expressed. What makes these two independent observations interesting is the fact that Cashikar et al. (2014) depleted VPS4, whilst I overexpressed a dominant negative form of VPS4, but we have similar observations, suggesting an earlier involvement of ESCT-III and VPS4 in membrane remodelling. Other reports have shown that that VPS4 is recruited late and transiently during HIV assembly (Jouvenet et al., 2011; Bleck et al., 2014). It is possible that VPS4 has dual roles in HIV budding, similar to the dual role of dynamin in the formation of clathrin-coated vesicles (Mettlen et al., 2009; Grove et al., 2014). Furthermore, when Cashikar and co-workers used a GagΔp6 in their studies, they did not observe ESCRT-III filaments. However, they have not commented on the extent of exvagination for the Gag assemblies. The study also lacks quantitative characterisation of the observed structures, such as estimating the diameters of the VLP structures, which would have been more informative for comparisons.

Reconciling these two VPS4 studies [Cashikar et al. (2014) and my observations] with the data on mutants is not easy because neither the $PTAP^{-}YP^{-}$ nor the Δp6 recruit ESCRT components, but they have different degrees of bud completeness, suggesting that the p6 subdomain itself may modulate HIV assembly. The p6 subdomain might recruit additional cellular factors that influence assembly, thus giving different

phenotypes for full length Gag and GagΔp6. Maybe VPS4 is needed to remove these components for ESCRT binding, hence flatter profiles were seen with DN VPS4 or siRNA VPS4.

The ESCRT machinery is involved in vital membrane fission processes such as cytokinesis, plasma membrane repair, receptor recycling to modulate signalling, and microvesicle release into immunological synapses (see General introduction, Section 1.5.5). Enveloped viruses such as HIV have evolved to hijack this key cellular machinery whose components cannot be therapeutically targeted directly as that would be detrimental to cells. It seems that ESCRT machinery components are not viable drug targets, leaving the viral components as attractive targets. This has been tried before, where a cyclic peptide targeting Gag-Tsg101 inhibited VLP release without adverse effects on the cells (Tavassoli et al., 2008), although the mechanism is not clear. I obtained the cyclic-peptide and was unable to reproduce the data, and to the best of my knowledge there is no publication that repeated the work published in 2008.

6.2 HIV is targeted to IPMCs in primary macrophages

Several reports have shown that in macrophages, HIV-1 predominantly assembles in IPMCs. To investigate HIV assembly in macrophages, I infected MDM from eight blood donors with rescued release-defective HIV ($PTAP^{-}$ and $PTAP^{-}YP^{-}$ mutants) and analysed the distribution of the mutants by IF (Figure 5.2 and 5.3). In the majority of cells (77%), Gag staining was found in the IPMCs only. In situations where the virus was found at the IPMCs and cell surface, more than 90% of the staining was at the IPMCs, which is highly significant. Furthermore, 29 cell profiles were examined using EM, to directly identify and count individual budding profiles, and a very significant number of immature viruses (97%) were found in the IPMC. These data strongly suggest that IPMCs are the main sites for HIV assembly, consistent with published work from our group and others (see General introduction, Section 1.6.2). However, as the notion of virus assembly in internal compartments was evolving, there was a proposal that HIV initially assembles at the cell surface and some of it is internalised by endocytosis or phagocytosis (Jouvenet et al., 2006). In their study, Jouvenet and colleagues transfected 7-day old cultures post monocyte isolation with GagGFP, and analysed expression after 24 hrs. Since IPMCs develop as macrophages mature in tissue

culture (Pelchen-Matthews et al., 2012), it is not surprising that GagGFP was found at the cell surface of these young macrophages. In this thesis, I have found that when HIV-expressing macrophages do not have IPMCs, the virus assembles at the cell surface. Furthermore, where I performed transfections (electroporation) of macrophages with HIV, but on 14- not 7-day old cultures (post monocyte isolation), the distributions of the virus in transfected cells was very similar to that in infected cells (Figure 5.2), showing that the IPMCs are indeed the main site for HIV assembly in macrophages.

It is currently not clear how IPMCs are formed. However, a recent study has suggested that in macrophages the viral restriction factor, tetherin, is involved in the formation of IPMCs (Chu et al., 2012a). In their investigations, Chu and colleagues (2012a) found tetherin localised to the IPMCs and trans-Golgi network, but not at the cell surface. However, our group found tetherin at the cell surface, trans-Golgi network, as well as IPMCs, without any apparent enrichment (Giese and Marsh, 2014). Giese and Marsh state that tetherin antibodies have reduced binding to aldehyde-fixed cells, thus they labelled live cells on ice before fixation. Chu et al. labelled fixed cells, and this might explain the different staining patterns observed in the two studies, and therefore the data interpretation. The study by Giese and Marsh is consistent with the previous reports that HIV does not induce IPMC formation (Welsch et al., 2011; Pelchen-Matthews et al., 2012; Berre et al., 2013; Mlcochova et al., 2013), and my data affirm earlier findings that the IPMCs are the principal target sites for HIV assembly.

In this study, I have also shown enrichment of virus at the IPMCs by estimating the area of plasma membrane at the IPMCs and cell surface. The assembly of HIV at the IPMCs was independent of the amount of membrane at this site, suggesting specific targeting and enrichment of the virus to the IPMCs. It is not clear what viral or host factors determine this enrichment. It is possible that the lipid content of the membranes plays a role. As discussed in Chapter 5, studies with *in vitro* liposome models suggest that different compositions of lipids, other than $PI(4,5)P_2$, may influence Gag targeting.

6.3 Functions of the IPMCs

IPMCs are heterogeneous and dynamic structures that can have one or several connections to the cell surface (Mlcochova et al., 2013). IPMCs can be very complex

with an array of membranes that are sponge-like or that form swirls (Figures 5.10 to 5.15), consistent with previous reports (Deneka et al., 2007; Welsch et al., 2007; Welsch et al., 2011; Pelchen-Matthews et al., 2012). Morphologically similar compartments have been implicated in artherosclerosis, where macrophages take up aggregated low density lipoproteins (agLDL) into surface connected compartments (SCCs), and release lysosomal enzymes to digest the agLDL (Kruth et al., 1995; Zhang et al., 1997; Haka et al., 2009; Haka et al., 2013). To determine the connection of these compartments that sequester agLDL to the cell surface, ruthenium red was used to stain the cell. Interestingly, SCCs can be induced by the agLDL particles in culture medium (Kruth et al., 1995; Tan and Sattentau, 2013), but IPMCs are an intrinsic feature of mature primary MDM. Therefore, the relationship between these morphologically similar compartments is unclear.

HIV-containing compartments, similar to the MDM's IPMCs, have been seen in mature and immature DCs (Garcia et al., 2005; Garcia et al., 2008). Immature DCs are more efficiently infected by HIV than mature DCs (Shimauchi and Piguet, 2014). The virus-containing compartments (VCCs) in DCs are connected to the cell surface, and enriched in tetraspanins the CD81, CD82 and CD9 (Garcia et al., 2005; Garcia et al., 2008), similar to the compartments in MDM. Whilst the infected immature DCs can transfer the viruses they produce, both the mature and immature DCs use the C-type lectin DC-SIGN molecules on their cell surface to capture viruses and concentrate them in VCCs, from where they can be transferred through cell-to-cell contacts to target T cells in a process termed *trans*-infection (Shimauchi and Piguet, 2014). The VCCs of DCs that have captured virions from the extracellular milieu (*trans*-infection) are devoid of the tetraspanin CD63, whilst DCs that are productively infected (*cis*-infection) have moderate levels of CD63 (Garcia et al., 2008). In MDM, CD63 accumulates in the IPMCs during virus assembly (Deneka et al., 2007), probably as it is incorporated into virus particles during assembly.

Although IPMCs, and sequestered intracellular virus, have been observed in MDM maintained in tissue culture, it has remained unclear whether similar structures are present in macrophages *in vivo*. Intracellular HIV has been found in cells on lymph nodes and brain biopsies (Meyenhofer et al., 1987; Orenstein et al., 1988; Orenstein,

2007), suggesting that IPMCs may be present *in vivo*. Nevertheless, the nature of the cells and the compartment has not been unequivocally established. The existence of IPMCs *in vivo* has also been suggested by a recent study, where HIV was introduced into mice engrafted with human immune cells to investigate infection in the gut-associated lymphoid tissue (Ladinsky et al., 2014). The study shows sporadic pictures of macrophages with pools of intracellular viruses identified and interpreted as IPMCs, similar to what has been observed in tissue cultures of primary human macrophages. Although the study did not use any cell markers to definitively characterise the identified cells and compartments, the findings are very important because they show similar compartments to what has been described in this thesis and elsewhere.

The enrichment of HIV in the IPMCs as shown in this thesis (Figure 5.3) may offer the virus some reproductive advantages over cell surface assembly observed in T cells, such as efficient transfer through cell-to-cell contacts; concealing the virus from direct immune attack by neutralising antibodies, as the intricate structures of the IPMCs (Figures 5.10 to 5.15) can make it difficult for neutralising antibodies to access the IPMCs (Chu et al., 2012b; Koppensteiner et al., 2012a); limiting the exposure of viral structures on the macrophage surface, thereby protecting against virus-specific immune responses including CD8+ cytotoxic T-lymphocyte, and antibody-dependent cellular cytotoxicity (ADCC).

In the current study, immature HIV profiles were found predominantly in IPMCs of infected macrophages, with a very small proportion (3%) at the cell surface. Concentrating HIV in the IPMCs may have effects on virus transfer to other cells *in vivo*. Virus transfer between cells occurs by two modes: cell-free virus or cell-to-cell transfer (Waki and Freed, 2010; Schiffner et al., 2013). Cell-to-cell transfer occurs through intimate contacts between donor and target cells, the so-called virological synapses (VS), where HIV appropriates some of the molecules (ICAM-1 and LAF-1) used by the antigen presentation machinery (see General introduction, Section 1.6.3). Infected macrophages can directly transfer HIV to CD4+ T cells in clusters (Giese and Marsh, 2014), and the transfer is inhibited by antibodies against gp120, ICAM-1 and LAF-1, the structural components of VS (Duncan et al., 2014). Using live-cell imaging, Duncan and colleagues provided direct evidence for transfer of GFP-tagged HIV-1 from

IPMCs of infected macrophages to T cells in co-cultures, and demonstrated that the macrophage-T cell contacts were transient, lasting 30-40 min. The transfer of HIV from macrophages to T cells is estimated to be 20- to 250-fold more efficient than cell-free transfer (Duncan et al., 2014). These *in vitro* studies show that IPMCs in macrophages may provide an efficient system of infecting other cells *in vivo*. It is also possible that the release of virions in the IPMCs is regulated, such that release of multiple particles coincides with the activation of T cells upon interaction with infected macrophages.

It is not clear what stimulates the release of the HIV from IPMCs. Nonetheless, recent studies that examined how IPMCs are maintained provide some clues (Gaudin et al., 2012; Pelchen-Matthews et al., 2012; Mlcochova et al., 2013). The three studies identified different components of the cytoskeleton that maintain the IPMCs. A study by our group suggested that focal adhesion complexes, often seen on closely apposed membranes adjacent to the plasma membrane, may regulate HIV release, as knocking down the β2 integrin CD18 disrupted IPMCs, making them smaller and more dispersed (Pelchen-Matthews et al., 2012). Another study showed that the kinesin KIF3A drives the transport of IPMCs on microtubules towards the cell surface, as depleting KIF3A reduced virus release from the MDM (Gaudin et al., 2012). The most recent investigation, also by our group, showed that disrupting the actin cytoskeleton causes dispersal of IPMCs, resulting in increased virus release (Mlcochova et al., 2013). It is likely that intra- and extra-cellular signals impacting on the cytoskeleton in macrophages may regulate virus release.

6.4 Future directions

It has emerged from my analysis of HIV budding profiles that, on average, the Δp6 mutant buds were two-thirds complete, whilst the PTAP^{-} and PTAP^{-}YP^{-} mutants were half complete virus shells. In addition to recruiting the ESCRT machinery for HIV assembly, it seems the p6 subdomain of Gag may also regulate HIV assembly in other ways, possibly by interacting with other host molecules(s), or even viral protein(s) such as Vpr that interact with the p6 subdomain. The role of p6 could be investigated by generating HIV-1 Δp6 mutant with a fluorescent tag, expressing it in cells, and then performing live-cell super-resolution microscopy to assess assembly dynamics of the

mutant, compared to HIV-1 WT. This may shed light on other potential role(s) for the p6 in HIV biogenesis.

Studies demonstrating the existence of IPMCs *in vivo* are still lacking. *In vivo*, myeloid lineage cells are infected with HIV-1 at two stages of differentiation: (1) as monocytes in the blood; and (2) as mature macrophages in tissues. Only a small proportion of circulating monocytes (5%) is susceptible to HIV infection and can harbour the virus without productive replication. Since monocytes migrate to different tissues or anatomic sites including the brain, kidneys, lungs and the gut-associated lymphoid tissues (GALT), where they differentiate into macrophages, they can disseminate and establish HIV infection in different tissues. Monocytes can cross the blood-brain barrier, which explains how the brain is infected with HIV. Therefore, studies using animal models will be important in identifying infected macrophages *in vivo*, and identifying the presence or not of IPMCs. This would give medical merit to conceiving new therapeutic strategies targeting virus in IPMCs, such as the use of nanoparticles to deliver drugs to the IPMCs. Furthermore, antibodies against the scavenger receptor CD36, can block virus release by tethering viruses within IPMCs, and this has been proposed as a possible therapeutic strategy that could prevent virus release from IPMCs (Berre et al., 2013).

HIV-infected macrophages may play a role in kidney nephropathies such as focal segmental glomerulosclerosis (FSGS). FSGS involves injury to podocytes and scarring of the glomeruli, and these may have several causes including HIV infection (Kopp and Winkler, 2003). Macrophages are the main inflammatory cells in the kidneys (Duffield, 2010), which may afford them the opportunity to promote nephropathies if infected with HIV. The pathology of HIV may alter the physiological functions of macrophages in many tissues including kidneys. There are reports suggesting that HIV-infected macrophages have impaired phagocytic function (Mazzolini et al., 2010; Jambo et al., 2014). It is reasonable to speculate that the role of HIV infected macrophages in kidney diseases may be underestimated due to limited studies on this subject. Therefore, more studies are required in the context of macrophage involvement in FSGS.

The data presented in this study show enrichment of HIV at the IPMCs. It is not clear what host factors could be mediating this specific targeting to this plasma membrane compartment. One possibility is that the lipid composition of the membranes that can influence targeting (see Section 5.3 Discussion). Currently, marker(s) specific for the IPMC have not been identified. So more investigations need to be conducted into the properties of the IPMCs that influence targeting of HIV to this site. Laurdan, a fluorescent dye that detects changes in membrane phase properties, has been used to study the properties of host cell-derived membranes on HIV particles (Lorizate et al., 2009), and the effect of HIV Nef on the properties of mouse macrophage cell lines (N7 and RAW 264.7) (Cui et al., 2012). If used to label macrophages, this dye may yield some interesting data about the difference(s) between the IPMC and cell surface plasma membrane of MDM.

Estimates from UNAIDS show a decline in the mortalities attributed to HIV/AIDS, and an increase in HIV prevalence (UNAIDS, November 2013). Currently, guidelines for HIV treatment indicate that individuals with CD4+ T cell count of ≤350 copies/mm^3 or with AIDS defining illnesses should be put on therapy. However, treating individuals with established infection, when the virus has already spread to anatomic sites that cannot be reached/penetrated by ART, such as the brain, means it will be difficult to eradicate the virus in these areas. Furthermore, HIV-associated neurological disorders (HAND) will increase, as there is already some evidence that about half of adults living with HIV have varying degrees of HAND. This could become a new public health problem as more people now live with chronic HIV infection. This may call for a revision of UNAIDS/WHO guidelines on when to initiate therapy. Currently, there have been debates to adopt the "test-and-treat" strategy for mitigating HIV infections in high-risk populations (Novitsky et al., 2010a; Kretzschmar et al., 2013). This would require regular testing of the high-risk populations, and putting them on ART if HIV infected, regardless of their CD4+ T cell status or clinical conditions. Macrophages and their potential impact on the epidemic are overlooked in rationalising this strategy. Starting treatment early may reduce the establishment of viral sanctuaries that are difficult to purge, such as in the brain, or at least delay the onset of HAND. Therefore, the "test-and-treat" strategy may be appealing in the context of curbing HIV infections, especially of the brain. Although, expensive for most developing countries in Africa,

which unfortunately are the hardest hit by the HIV pandemic, this may seem like an alternative approach to evade conditions such as HAND and HIV-associated nephropathies, and could be done in parallel with searching for new and less toxic ARV drugs. The cost-effectiveness of all these approaches will have to be carefully evaluated to come up with comprehensive strategies/policies.

In HIV infection and pathology, the role of macrophages has been largely overshadowed by the role played by T cells. Whilst T cells are highly permissive to HIV, they have a short lifespan compared to macrophages, due to their susceptibility to cytopathic effects of HIV. Although T cells may provide quantity hosts/substrates in term of reproductive rate, macrophages are quality hosts/substrates. Macrophages may compensate for their low virus reproductive rate by outliving T cells, archiving the virus in IPMCs, and making numerous contacts with uninfected T cells to inoculate them with virions released from IPMCs, hence fuelling infection in the host.

Despite numerous reports supporting the notion of HIV on intracellular membranes in macrophages, there has been on-going debate as to whether IPMCs are the only, or even the main, site of HIV assembly (Chu et al., 2012a; Tan and Sattentau, 2013; Giese and Marsh, 2014). My thesis has provided the first conclusive data that the IPMCs are unequivocally the main site for HIV assembly in macrophages. Probably what is limiting the work on tissue macrophages is the invasive nature of acquiring samples (biopsies) from patients. Nevertheless, more investigations are required at the molecular level to better understand macrophages in tissues. Tissue macrophages such as alveolar macrophages can be obtained from HIV patients, and could well be included in clinical parameters used to monitor HAART. Currently, individuals on HAART have scheduled tests to evaluate blood viral load, CD4+ T cell counts to evaluate immune recovery, and blood chemistry to monitor drug toxicities. Although, blood viral load is routinely used to monitor HAART, it does not reflect the viral load (and virus diversity if sequenced) of different anatomical sites, where macrophages may have a major role to play in HIV pathogenesis. Therefore, it is important to also identify surrogate marker(s) for HIV pathology in macrophages, so that the effect of HAART can be assessed more closely. Efforts to eradicate HIV-1 would be fruitless without increased research quality and funding devoted to investigations on HIV-macrophage interactions.

"...at the forefront of research there are so many difficulties that depression and low motivation are a constant danger. ...since the pursuit of good science was so difficult, it was essential that the problem being studied was an important one to justify the effort expended."

Sir Paul Nurse, Nobel Laureate 2001

7. BIBLIOGRAPHY

Adell, M.A., and D. Teis. 2011. Assembly and disassembly of the ESCRT-III membrane scission complex. *FEBS Lett*. 585:3191-3196.

Adell, M.A., G.F. Vogel, M. Pakdel, M. Muller, H. Lindner, M.W. Hess, and D. Teis. 2014. Coordinated binding of Vps4 to ESCRT-III drives membrane neck constriction during MVB vesicle formation. *J Cell Biol*. 205:33-49.

Affranchino, J.L., and S.A. Gonzalez. 2014. Understanding the process of envelope glycoprotein incorporation into virions in simian and feline immunodeficiency viruses. *Viruses*. 6:264-283.

Agromayor, M., N. Soler, A. Caballe, T. Kueck, S.M. Freund, M.D. Allen, M. Bycroft, O. Perisic, Y. Ye, B. McDonald, H. Scheel, K. Hofmann, S.J. Neil, J. Martin-Serrano, and R.L. Williams. 2012. The UBAP1 subunit of ESCRT-I interacts with ubiquitin via a SOUBA domain. *Structure*. 20:414-428.

Alkhatib, G. 2009. The biology of CCR5 and CXCR4. *Curr Opin HIV AIDS*. 4:96-103.

Alkhatib, G., C. Combadiere, C.C. Broder, Y. Feng, P.E. Kennedy, P.M. Murphy, and E.A. Berger. 1996. CC CKR5: a RANTES, MIP-1alpha, MIP-1beta receptor as a fusion cofactor for macrophage-tropic HIV-1. *Science*. 272:1955-1958.

Allan, J.S., J.E. Coligan, F. Barin, M.F. McLane, J.G. Sodroski, C.A. Rosen, W.A. Haseltine, T.H. Lee, and M. Essex. 1985. Major glycoprotein antigens that induce antibodies in AIDS patients are encoded by HTLV-III. *Science*. 228:1091-1094.

Ambrose, Z., and C. Aiken. 2014. HIV-1 uncoating: connection to nuclear entry and regulation by host proteins. *Virology*. 454-455:371-379.

Arenzana-Seisdedos, F., and M. Parmentier. 2006. Genetics of resistance to HIV infection: Role of co-receptors and co-receptor ligands. *Semin Immunol*. 18:387-403.

Arhel, N. 2010. Revisiting HIV-1 uncoating. *Retrovirology*. 7:96.

Babst, M., B. Wendland, E.J. Estepa, and S.D. Emr. 1998. The Vps4p AAA ATPase regulates membrane association of a Vps protein complex required for normal endosome function. *EMBO J*. 17:2982-2993.

Balasubramaniam, M., and E.O. Freed. 2011. New insights into HIV assembly and trafficking. *Physiology (Bethesda)*. 26:236-251.

Baldauf, H.M., X. Pan, E. Erikson, S. Schmidt, W. Daddacha, M. Burggraf, K. Schenkova, I. Ambiel, G. Wabnitz, T. Gramberg, S. Panitz, E. Flory, N.R. Landau, S. Sertel, F. Rutsch, F. Lasitschka, B. Kim, R. Konig, O.T. Fackler, and O.T. Keppler. 2012. SAMHD1 restricts HIV-1 infection in resting CD4(+) T cells. *Nat Med*. 18:1682-1687.

Bell, N.M., and A.M. Lever. 2013. HIV Gag polyprotein: processing and early viral particle assembly. *Trends Microbiol*. 21:136-144.

Bendayan, M., and S. Garzon. 1988. Protein G-gold complex: comparative evaluation with protein A-gold for high-resolution immunocytochemistry. *J Histochem Cytochem*. 36:597-607.

Bennett, A.E., K. Narayan, D. Shi, L.M. Hartnell, K. Gousset, H. He, B.C. Lowekamp, T.S. Yoo, D. Bliss, E.O. Freed, and S. Subramaniam. 2009. Ion-abrasion scanning electron microscopy reveals surface-connected tubular conduits in HIV-infected macrophages. *PLoS Pathog*. 5:e1000591.

Berlioz-Torrent, C., B.L. Shacklett, L. Erdtmann, L. Delamarre, I. Bouchaert, P. Sonigo, M.C. Dokhelar, and R. Benarous. 1999. Interactions of the cytoplasmic domains of human and simian retroviral transmembrane proteins with components of the clathrin adaptor complexes modulate intracellular and cell surface expression of envelope glycoproteins. *J Virol*. 73:1350-1361.

Berre, S., R. Gaudin, B. Cunha de Alencar, M. Desdouits, M. Chabaud, N. Naffakh, M. Rabaza-Gairi, F.X. Gobert, M. Jouve, and P. Benaroch. 2013. CD36-specific antibodies block release of HIV-1 from infected primary macrophages and its transmission to T cells. *J Exp Med*. 210:2523-2538.

Bhat, N., and K.A. Fitzgerald. 2014. Recognition of cytosolic DNA by cGAS and other STING-dependent sensors. *Eur J Immunol*. 44:634-640.

Bieniasz, P.D. 2009. The cell biology of HIV-1 virion genesis. *Cell Host Microbe*. 5:550-558.

Bishop, N., and P. Woodman. 2000. ATPase-defective mammalian VPS4 localizes to aberrant endosomes and impairs cholesterol trafficking. *Mol Biol Cell*. 11:227-239.

Bleck, M., M.S. Itano, D.S. Johnson, V.K. Thomas, A.J. North, P.D. Bieniasz, and S.M. Simon. 2014. Temporal and spatial organization of ESCRT protein recruitment during HIV-1 budding. *Proc Natl Acad Sci U S A*.

Bol, S.M., Y. van Remmerden, J.G. Sietzema, N.A. Kootstra, H. Schuitemaker, and A.B. van't Wout. 2009. Donor variation in in vitro HIV-1 susceptibility of monocyte-derived macrophages. *Virology*. 390:205-211.

Bolte, S., and F.P. Cordelieres. 2006. A guided tour into subcellular colocalization analysis in light microscopy. *J Microsc*. 224:213-232.

Bowers, K., A. Pelchen-Matthews, S. Honing, P.J. Vance, L. Creary, B.S. Haggarty, J. Romano, W. Ballensiefen, J.A. Hoxie, and M. Marsh. 2000. The simian immunodeficiency virus envelope glycoprotein contains multiple signals that regulate its cell surface expression and endocytosis. *Traffic*. 1:661-674.

Breed, M.W., A.P. Jordan, P.P. Aye, C.F. Lichtveld, C.C. Midkiff, F.R. Schiro, B.S. Haggarty, C. Sugimoto, X. Alvarez, N.G. Sandler, D.C. Douek, M.J. Kuroda, B. Pahar, M. Piatak, Jr., J.D. Lifson, B.F. Keele, J.A. Hoxie, and A.A. Lackner. 2013. Loss of a tyrosine-dependent trafficking motif in the simian immunodeficiency virus envelope cytoplasmic tail spares mucosal CD4 cells but does not prevent disease progression. *J Virol*. 87:1528-1543.

Brenchley, J.M., D.A. Price, T.W. Schacker, T.E. Asher, G. Silvestri, S. Rao, Z. Kazzaz, E. Bornstein, O. Lambotte, D. Altmann, B.R. Blazar, B. Rodriguez, L. Teixeira-Johnson, A. Landay, J.N. Martin, F.M. Hecht, L.J. Picker, M.M. Lederman, S.G. Deeks, and D.C. Douek. 2006. Microbial translocation is a cause of systemic immune activation in chronic HIV infection. *Nat Med*. 12:1365-1371.

Bres, V., S.M. Yoh, and K.A. Jones. 2008. The multi-tasking P-TEFb complex. *Curr Opin Cell Biol*. 20:334-340.

Briggs, J.A., and H.G. Krausslich. 2011. The molecular architecture of HIV. *J Mol Biol*. 410:491-500.

Briggs, J.A., M.N. Simon, I. Gross, H.G. Krausslich, S.D. Fuller, V.M. Vogt, and M.C. Johnson. 2004. The stoichiometry of Gag protein in HIV-1. *Nat Struct Mol Biol*. 11:672-675.

Brighouse, A., J.B. Dacks, and M.C. Field. 2010. Rab protein evolution and the history of the eukaryotic endomembrane system. *Cell Mol Life Sci*. 67:3449-3465.

Buchkovich, N.J., W.M. Henne, S. Tang, and S.D. Emr. 2013. Essential N-terminal insertion motif anchors the ESCRT-III filament during MVB vesicle formation. *Dev Cell*. 27:201-214.

Byland, R., P.J. Vance, J.A. Hoxie, and M. Marsh. 2007. A conserved dileucine motif mediates clathrin and AP-2-dependent endocytosis of the HIV-1 envelope protein. *Mol Biol Cell*. 18:414-425.

Caillet, M., K. Janvier, A. Pelchen-Matthews, D. Delcroix-Genete, G. Camus, M. Marsh, and C. Berlioz-Torrent. 2011. Rab7A is required for efficient production of infectious HIV-1. *PLoS Pathog*. 7:e1002347.

Carlson, L.A., J.A. Briggs, B. Glass, J.D. Riches, M.N. Simon, M.C. Johnson, B. Muller, K. Grunewald, and H.G. Krausslich. 2008. Three-dimensional analysis of budding sites and released virus suggests a revised model for HIV-1 morphogenesis. *Cell Host Microbe*. 4:592-599.

Carlson, L.A., A. de Marco, H. Oberwinkler, A. Habermann, J.A. Briggs, H.G. Krausslich, and K. Grunewald. 2010. Cryo electron tomography of native HIV-1 budding sites. *PLoS Pathog*. 6:e1001173.

Carlson, L.A., and J.H. Hurley. 2012. In vitro reconstitution of the ordered assembly of the endosomal sorting complex required for transport at membrane-bound HIV-1 Gag clusters. *Proc Natl Acad Sci U S A*. 109:16928-16933.

Carlton, J.G., M. Agromayor, and J. Martin-Serrano. 2008. Differential requirements for Alix and ESCRT-III in cytokinesis and HIV-1 release. *Proc Natl Acad Sci U S A*. 105:10541-10546.

Carlton, J.G., and J. Martin-Serrano. 2007. Parallels between cytokinesis and retroviral budding: a role for the ESCRT machinery. *Science*. 316:1908-1912.

Carrington, M., G. Nelson, and S.J. O'Brien. 2001. Considering genetic profiles in functional studies of immune responsiveness to HIV-1. *Immunol Lett*. 79:131-140.

Cashikar, A.G., S. Shim, R. Roth, M.R. Maldazys, J.E. Heuser, and P.I. Hanson. 2014. Structure of cellular ESCRT-III spirals and their relationship to HIV budding. *Elife*:e02184.

Cassol, E., M. Alfano, P. Biswas, and G. Poli. 2006. Monocyte-derived macrophages and myeloid cell lines as targets of HIV-1 replication and persistence. *J Leukoc Biol*. 80:1018-1030.

Checkley, M.A., B.G. Luttge, and E.O. Freed. 2011. HIV-1 envelope glycoprotein biosynthesis, trafficking, and incorporation. *J Mol Biol*. 410:582-608.

Chertova, E., O. Chertov, L.V. Coren, J.D. Roser, C.M. Trubey, J.W. Bess, Jr., R.C. Sowder, 2nd, E. Barsov, B.L. Hood, R.J. Fisher, K. Nagashima, T.P. Conrads, T.D. Veenstra, J.D. Lifson, and D.E. Ott. 2006. Proteomic and biochemical analysis of purified human immunodeficiency virus type 1 produced from infected monocyte-derived macrophages. *J Virol*. 80:9039-9052.

Chojnacki, J., T. Staudt, B. Glass, P. Bingen, J. Engelhardt, M. Anders, J. Schneider, B. Muller, S.W. Hell, and H.G. Krausslich. 2012. Maturation-dependent HIV-1 surface protein redistribution revealed by fluorescence nanoscopy. *Science*. 338:524-528.

Choudhuri, K., J. Llodra, E.W. Roth, J. Tsai, S. Gordo, K.W. Wucherpfennig, L.C. Kam, D.L. Stokes, and M.L. Dustin. 2014. Polarized release of T-cell-receptor-enriched microvesicles at the immunological synapse. *Nature*. 507:118-123.

Chu, H., J.J. Wang, M. Qi, J.J. Yoon, X. Chen, X. Wen, J. Hammonds, L. Ding, and P. Spearman. 2012a. Tetherin/BST-2 is essential for the formation of the intracellular virus-containing compartment in HIV-infected macrophages. *Cell Host Microbe*. 12:360-372.

Chu, H., J.J. Wang, M. Qi, J.J. Yoon, X. Wen, X. Chen, L. Ding, and P. Spearman. 2012b. The intracellular virus-containing compartments in primary human macrophages are largely inaccessible to antibodies and small molecules. *PLoS One*. 7:e35297.

Chukkapalli, V., J. Inlora, G.C. Todd, and A. Ono. 2013. Evidence in Support of RNA-Mediated Inhibition of Phosphatidylserine-Dependent HIV-1 Gag Membrane Binding in Cells. *J Virol*. 87:7155-7159.

Chukkapalli, V., S.J. Oh, and A. Ono. 2010. Opposing mechanisms involving RNA and lipids regulate HIV-1 Gag membrane binding through the highly basic region of the matrix domain. *Proc Natl Acad Sci U S A*. 107:1600-1605.

Chung, H.Y., E. Morita, U. von Schwedler, B. Muller, H.G. Krausslich, and W.I. Sundquist. 2008. NEDD4L overexpression rescues the release and infectivity of human immunodeficiency virus type 1 constructs lacking PTAP and YPXL late domains. *J Virol*. 82:4884-4897.

Clay, C.C., D.S. Rodrigues, Y.S. Ho, B.A. Fallert, K. Janatpour, T.A. Reinhart, and U. Esser. 2007. Neuroinvasion of fluorescein-positive monocytes in acute simian immunodeficiency virus infection. *J Virol*. 81:12040-12048.

Coleman, C.M., and L. Wu. 2009. HIV interactions with monocytes and dendritic cells: viral latency and reservoirs. *Retrovirology*. 6:51.

Cordelieres, F.P. 2009. The 3D object counter plugin Manual. Vol. v2.0. http://imagejdocu.tudor.lu/doku.php?id=plugin:analysis:3d_object_counter:start.

Cosson, P. 1996. Direct interaction between the envelope and matrix proteins of HIV-1. *EMBO J*. 15:5783-5788.

Cui, H.L., A. Grant, N. Mukhamedova, T. Pushkarsky, L. Jennelle, L. Dubrovsky, K. Gaus, M.L. Fitzgerald, D. Sviridov, and M. Bukrinsky. 2012. HIV-1 Nef mobilizes lipid rafts in macrophages through a pathway that competes with ABCA1-dependent cholesterol efflux. *J Lipid Res*. 53:696-708.

Dalgleish, A.G., P.C. Beverley, P.R. Clapham, D.H. Crawford, M.F. Greaves, and R.A. Weiss. 1984. The CD4 (T4) antigen is an essential component of the receptor for the AIDS retrovirus. *Nature*. 312:763-767.

de Marco, A., A.M. Heuser, B. Glass, H.G. Krausslich, B. Muller, and J.A. Briggs. 2012. Role of the SP2 domain and its proteolytic cleavage in HIV-1 structural maturation and infectivity. *J Virol*. 86:13708-13716.

Demirov, D.G., A. Ono, J.M. Orenstein, and E.O. Freed. 2002a. Overexpression of the N-terminal domain of TSG101 inhibits HIV-1 budding by blocking late domain function. *Proc Natl Acad Sci U S A*. 99:955-960.

Demirov, D.G., J.M. Orenstein, and E.O. Freed. 2002b. The late domain of human immunodeficiency virus type 1 p6 promotes virus release in a cell type-dependent manner. *J Virol*. 76:105-117.

Deneka, M., A. Pelchen-Matthews, R. Byland, E. Ruiz-Mateos, and M. Marsh. 2007. In macrophages, HIV-1 assembles into an intracellular plasma membrane domain containing the tetraspanins CD81, CD9, and CD53. *J Cell Biol*. 177:329-341.

Deng, H., R. Liu, W. Ellmeier, S. Choe, D. Unutmaz, M. Burkhart, P. Di Marzio, S. Marmon, R.E. Sutton, C.M. Hill, C.B. Davis, S.C. Peiper, T.J. Schall, D.R. Littman, and N.R. Landau. 1996. Identification of a major co-receptor for primary isolates of HIV-1. *Nature*. 381:661-666.

Derdeyn, C.A., and G. Silvestri. 2005. Viral and host factors in the pathogenesis of HIV infection. *Curr Opin Immunol*. 17:366-373.

Dick, R.A., S.L. Goh, G.W. Feigenson, and V.M. Vogt. 2012. HIV-1 Gag protein can sense the cholesterol and acyl chain environment in model membranes. *Proc Natl Acad Sci U S A*. 109:18761-18766.

Dokka, S., D. Toledo, X. Shi, J. Ye, and Y. Rojanasakul. 2000. High-efficiency gene transfection of macrophages by lipoplexes. *Int J Pharm*. 206:97-104.

Dong, C., A.M. Janas, J.H. Wang, W.J. Olson, and L. Wu. 2007. Characterization of human immunodeficiency virus type 1 replication in immature and mature dendritic cells reveals dissociable cis- and trans-infection. *J Virol*. 81:11352-11362.

Doualla-Bell, F., A. Avalos, B. Brenner, T. Gaolathe, M. Mine, S. Gaseitsiwe, M. Oliveira, D. Moisi, N. Ndwapi, H. Moffat, M. Essex, and M.A. Wainberg. 2006. High prevalence of the K65R mutation in human immunodeficiency virus type 1 subtype C isolates from infected patients in Botswana treated with didanosine-based regimens. *Antimicrob Agents Chemother*. 50:4182-4185.

Du, X., A.S. Kazim, A.J. Brown, and H. Yang. 2012. An essential role of Hrs/Vps27 in endosomal cholesterol trafficking. *Cell Rep*. 1:29-35.

Duffield, J.S. 2010. Macrophages and immunologic inflammation of the kidney. *Semin Nephrol*. 30:234-254.

Duncan, C.J., J.P. Williams, T. Schiffner, K. Gartner, C. Ochsenbauer, J. Kappes, R.A. Russell, J. Frater, and Q.J. Sattentau. 2014. High-multiplicity HIV-1 infection and neutralizing antibody evasion mediated by the macrophage-T cell virological synapse. *J Virol*. 88:2025-2034.

Dussupt, V., M.P. Javid, G. Abou-Jaoude, J.A. Jadwin, J. de La Cruz, K. Nagashima, and F. Bouamr. 2009. The nucleocapsid region of HIV-1 Gag cooperates with the PTAP and LYPXnL late domains to recruit the cellular machinery necessary for viral budding. *PLoS Pathog*. 5:e1000339.

Dustin, M.L. 2014. What counts in the immunological synapse? *Mol Cell*. 54:255-262.

Fassati, A. 2012. Multiple roles of the capsid protein in the early steps of HIV-1 infection. *Virus Res*. 170:15-24.

Faure, E., and M. Royer-Carenzi. 2008. Is the European spatial distribution of the HIV-1-resistant CCR5-Delta32 allele formed by a breakdown of the pathocenosis due to the historical Roman expansion? *Infect Genet Evol*. 8:864-874.

Felts, R.L., K. Narayan, J.D. Estes, D. Shi, C.M. Trubey, J. Fu, L.M. Hartnell, G.T. Ruthel, D.K. Schneider, K. Nagashima, J.W. Bess, Jr., S. Bavari, B.C. Lowekamp, D. Bliss, J.D. Lifson, and S. Subramaniam. 2010. 3D visualization of HIV transfer at the virological synapse between dendritic cells and T cells. *Proc Natl Acad Sci U S A*. 107:13336-13341.

Feng, Y., C.C. Broder, P.E. Kennedy, and E.A. Berger. 1996. HIV-1 entry cofactor: functional cDNA cloning of a seven-transmembrane, G protein-coupled receptor. *Science*. 272:872-877.

Fisher, R.D., H.Y. Chung, Q. Zhai, H. Robinson, W.I. Sundquist, and C.P. Hill. 2007. Structural and biochemical studies of ALIX/AIP1 and its role in retrovirus budding. *Cell*. 128:841-852.

Freed, E.O. 2001. HIV-1 replication. *Somat Cell Mol Genet*. 26:13-33.

Freed, E.O. 2002. Viral late domains. *J Virol*. 76:4679-4687.

Fujii, K., J.H. Hurley, and E.O. Freed. 2007. Beyond Tsg101: the role of Alix in 'ESCRTing' HIV-1. *Nat Rev Microbiol*. 5:912-916.

Fujii, K., U.M. Munshi, S.D. Ablan, D.G. Demirov, F. Soheilian, K. Nagashima, A.G. Stephen, R.J. Fisher, and E.O. Freed. 2009. Functional role of Alix in HIV-1 replication. *Virology*. 391:284-292.

Fultz, P.N., P.J. Vance, M.J. Endres, B. Tao, J.D. Dvorin, I.C. Davis, J.D. Lifson, D.C. Montefiori, M. Marsh, M.H. Malim, and J.A. Hoxie. 2001. In vivo attenuation of simian immunodeficiency virus by disruption of a tyrosine-dependent sorting signal in the envelope glycoprotein cytoplasmic tail. *J Virol*. 75:278-291.

Gallo, S.A., C.M. Finnegan, M. Viard, Y. Raviv, A. Dimitrov, S.S. Rawat, A. Puri, S. Durell, and R. Blumenthal. 2003. The HIV Env-mediated fusion reaction. *Biochim Biophys Acta*. 1614:36-50.

Galvani, A.P., and J. Novembre. 2005. The evolutionary history of the CCR5-Delta32 HIV-resistance mutation. *Microbes Infect*. 7:302-309.

Ganser-Pornillos, B.K., M. Yeager, and W.I. Sundquist. 2008. The structural biology of HIV assembly. *Curr Opin Struct Biol*. 18:203-217.

Garcia, E., D.S. Nikolic, and V. Piguet. 2008. HIV-1 replication in dendritic cells occurs through a tetraspanin-containing compartment enriched in AP-3. *Traffic*. 9:200-214.

Garcia, E., M. Pion, A. Pelchen-Matthews, L. Collinson, J.F. Arrighi, G. Blot, F. Leuba, J.M. Escola, N. Demaurex, M. Marsh, and V. Piguet. 2005. HIV-1 trafficking to the dendritic cell-T-cell infectious synapse uses a pathway of tetraspanin sorting to the immunological synapse. *Traffic*. 6:488-501.

Garrus, J.E., U.K. von Schwedler, O.W. Pornillos, S.G. Morham, K.H. Zavitz, H.E. Wang, D.A. Wettstein, K.M. Stray, M. Cote, R.L. Rich, D.G. Myszka, and W.I. Sundquist. 2001. Tsg101 and the vacuolar protein sorting pathway are essential for HIV-1 budding. *Cell*. 107:55-65.

Gartner, S., P. Markovits, D.M. Markovitz, M.H. Kaplan, R.C. Gallo, and M. Popovic. 1986. The role of mononuclear phagocytes in HTLV-III/LAV infection. *Science*. 233:215-219.

Gaudin, R., S. Berre, B. Cunha de Alencar, J. Decalf, M. Schindler, F.X. Gobert, M. Jouve, and P. Benaroch. 2013a. Dynamics of HIV-containing compartments in macrophages reveal sequestration of virions and transient surface connections. *PLoS One*. 8:e69450.

Gaudin, R., B.C. de Alencar, N. Arhel, and P. Benaroch. 2013b. HIV trafficking in host cells: motors wanted! *Trends Cell Biol*. 23:652-662.

Gaudin, R., B.C. de Alencar, M. Jouve, S. Berre, E. Le Bouder, M. Schindler, A. Varthaman, F.X. Gobert, and P. Benaroch. 2012. Critical role for the kinesin KIF3A in the HIV life cycle in primary human macrophages. *J Cell Biol*. 199:467-479.

Geissmann, F., M.G. Manz, S. Jung, M.H. Sieweke, M. Merad, and K. Ley. 2010. Development of monocytes, macrophages, and dendritic cells. *Science*. 327:656-661.

Ghanem, I., M.E. Riveiro, V. Paradis, S. Faivre, P.M. de Parga, and E. Raymond. 2014. Insights on the CXCL12-CXCR4 axis in hepatocellular carcinoma carcinogenesis. *Am J Transl Res*. 6:340-352.

Giese, S., and M. Marsh. 2014. Tetherin Can Restrict Cell-Free and Cell-Cell Transmission of HIV from Primary Macrophages to T Cells. *PLoS Pathog*. 10:e1004189.

Gilbert, P.B., I.W. McKeague, G. Eisen, C. Mullins, N.A. Gueye, S. Mboup, and P.J. Kanki. 2003. Comparison of HIV-1 and HIV-2 infectivity from a prospective cohort study in Senegal. *Stat Med*. 22:573-593.

Glass, J.D., H. Fedor, S.L. Wesselingh, and J.C. McArthur. 1995. Immunocytochemical quantitation of human immunodeficiency virus in the brain: correlations with dementia. *Ann Neurol*. 38:755-762.

Gorry, P.R., and P. Ancuta. 2011. Coreceptors and HIV-1 pathogenesis. *Curr HIV/AIDS Rep*. 8:45-53.

Gousset, K., S.D. Ablan, L.V. Coren, A. Ono, F. Soheilian, K. Nagashima, D.E. Ott, and E.O. Freed. 2008. Real-time visualization of HIV-1 GAG trafficking in infected macrophages. *PLoS Pathog*. 4:e1000015.

Gras, G., and M. Kaul. 2010. Molecular mechanisms of neuroinvasion by monocytes-macrophages in HIV-1 infection. *Retrovirology*. 7:30.

Grove, J., D.J. Metcalf, A.E. Knight, S.T. Wavre-Shapton, T. Sun, E. Protonotarios, L.D. Griffin, J. Lippincott-Schwartz, and M. Marsh. 2014. Flat Clathrin Lattices: stable features of the plasma membrane. *Mol Biol Cell*:mbc.E14-06-1154. [Epub ahead of print].

Guilliams, M., P. Bruhns, Y. Saeys, H. Hammad, and B.N. Lambrecht. 2014. The function of Fcgamma receptors in dendritic cells and macrophages. *Nat Rev Immunol*. 14:94-108.

Haka, A.S., I. Grosheva, E. Chiang, A.R. Buxbaum, B.A. Baird, L.M. Pierini, and F.R. Maxfield. 2009. Macrophages create an acidic extracellular hydrolytic compartment to digest aggregated lipoproteins. *Mol Biol Cell*. 20:4932-4940.

Haka, A.S., I. Grosheva, R.K. Singh, and F.R. Maxfield. 2013. Plasmin promotes foam cell formation by increasing macrophage catabolism of aggregated low-density lipoprotein. *Arterioscler Thromb Vasc Biol*. 33:1768-1778.

Hallenberger, S., V. Bosch, H. Angliker, E. Shaw, H.D. Klenk, and W. Garten. 1992. Inhibition of furin-mediated cleavage activation of HIV-1 glycoprotein gp160. *Nature*. 360:358-361.

Hanson, P.I., R. Roth, Y. Lin, and J.E. Heuser. 2008. Plasma membrane deformation by circular arrays of ESCRT-III protein filaments. *J Cell Biol*. 180:389-402.

Harrington, P.R., G. Schnell, S.L. Letendre, K. Ritola, K. Robertson, C. Hall, C.L. Burch, C.B. Jabara, D.T. Moore, R.J. Ellis, R.W. Price, and R. Swanstrom. 2009. Cross-sectional characterization of HIV-1 env compartmentalization in cerebrospinal fluid over the full disease course. *AIDS*. 23:907-915.

Hashimoto, D., J. Miller, and M. Merad. 2011. Dendritic cell and macrophage heterogeneity in vivo. *Immunity*. 35:323-335.

Heaton, R.K., D.B. Clifford, D.R. Franklin, Jr., S.P. Woods, C. Ake, F. Vaida, R.J. Ellis, S.L. Letendre, T.D. Marcotte, J.H. Atkinson, M. Rivera-Mindt, O.R. Vigil, M.J. Taylor, A.C. Collier, C.M. Marra, B.B. Gelman, J.C. McArthur, S. Morgello, D.M. Simpson, J.A. McCutchan, I. Abramson, A. Gamst, C. Fennema-Notestine, T.L. Jernigan, J. Wong, I. Grant, and C. Group. 2010. HIV-associated neurocognitive disorders persist in the era of potent antiretroviral therapy: CHARTER Study. *Neurology*. 75:2087-2096.

Heeney, J.L., A.G. Dalgleish, and R.A. Weiss. 2006. Origins of HIV and the evolution of resistance to AIDS. *Science*. 313:462-466.

Hemelaar, J., E. Gouws, P.D. Ghys, and S. Osmanov. 2011. Global trends in molecular epidemiology of HIV-1 during 2000-2007. *AIDS*. 25:679-689.

Henne, W.M., H. Stenmark, and S.D. Emr. 2013. Molecular mechanisms of the membrane sculpting ESCRT pathway. *Cold Spring Harb Perspect Biol*. 5:a016766.

Herbein, G., G. Gras, K.A. Khan, and W. Abbas. 2010. Macrophage signaling in HIV-1 infection. *Retrovirology*. 7:34.

Hermida-Matsumoto, L., and M.D. Resh. 2000. Localization of human immunodeficiency virus type 1 Gag and Env at the plasma membrane by confocal imaging. *J Virol*. 74:8670-8679.

Hotter, D., D. Sauter, and F. Kirchhoff. 2013. Emerging role of the host restriction factor tetherin in viral immune sensing. *J Mol Biol*. 425:4956-4964.

Huang, M., J.M. Orenstein, M.A. Martin, and E.O. Freed. 1995. p6Gag is required for particle production from full-length human immunodeficiency virus type 1 molecular clones expressing protease. *J Virol*. 69:6810-6818.

Hurley, J.H., and P.I. Hanson. 2010. Membrane budding and scission by the ESCRT machinery: it's all in the neck. *Nat Rev Mol Cell Biol*. 11:556-566.

Im, Y.J., L. Kuo, X. Ren, P.V. Burgos, X.Z. Zhao, F. Liu, T.R. Burke, Jr., J.S. Bonifacino, E.O. Freed, and J.H. Hurley. 2010. Crystallographic and functional analysis of the ESCRT-I /HIV-1 Gag PTAP interaction. *Structure*. 18:1536-1547.

Ivanchenko, S., W.J. Godinez, M. Lampe, H.G. Krausslich, R. Eils, K. Rohr, C. Brauchle, B. Muller, and D.C. Lamb. 2009. Dynamics of HIV-1 assembly and release. *PLoS Pathog*. 5:e1000652.

Jacks, T., M.D. Power, F.R. Masiarz, P.A. Luciw, P.J. Barr, and H.E. Varmus. 1988. Characterization of ribosomal frameshifting in HIV-1 gag-pol expression. *Nature*. 331:280-283.

Jakobsen, M.R., R.O. Bak, A. Andersen, R.K. Berg, S.B. Jensen, J. Tengchuan, A. Laustsen, K. Hansen, L. Ostergaard, K.A. Fitzgerald, T.S. Xiao, J.G. Mikkelsen, T.H. Mogensen, and S.R. Paludan. 2013. IFI16 senses DNA forms of the lentiviral replication cycle and controls HIV-1 replication. *Proc Natl Acad Sci U S A*. 110:E4571-4580.

Jalalirad, M., J. Saadatmand, and M. Laughrea. 2012. Dominant role of the 5' TAR bulge in dimerization of HIV-1 genomic RNA, but no evidence of TAR-TAR kissing during in vivo virus assembly. *Biochemistry*. 51:3744-3758.

Jambo, K.C., D.H. Banda, A.M. Kankwatira, N. Sukumar, T.J. Allain, R.S. Heyderman, D.G. Russell, and H.C. Mwandumba. 2014. Small alveolar macrophages are infected preferentially by HIV and exhibit impaired phagocytic function. *Mucosal Immunol*. 7:1116-1126.

Jersmann, H.P. 2005. Time to abandon dogma: CD14 is expressed by non-myeloid lineage cells. *Immunol Cell Biol*. 83:462-467.

Jimenez, A.J., P. Maiuri, J. Lafaurie-Janvore, S. Divoux, M. Piel, and F. Perez. 2014. ESCRT machinery is required for plasma membrane repair. *Science*. 343:1247136.

Jolly, C., and Q.J. Sattentau. 2005. Human immunodeficiency virus type 1 virological synapse formation in T cells requires lipid raft integrity. *J Virol*. 79:12088-12094.

Jouve, M., N. Sol-Foulon, S. Watson, O. Schwartz, and P. Benaroch. 2007. HIV-1 buds and accumulates in "nonacidic" endosomes of macrophages. *Cell Host Microbe*. 2:85-95.

Jouvenet, N., S.J. Neil, C. Bess, M.C. Johnson, C.A. Virgen, S.M. Simon, and P.D. Bieniasz. 2006. Plasma membrane is the site of productive HIV-1 particle assembly. *PLoS Biol*. 4:e435.

Jouvenet, N., S.M. Simon, and P.D. Bieniasz. 2009. Imaging the interaction of HIV-1 genomes and Gag during assembly of individual viral particles. *Proc Natl Acad Sci U S A*. 106:19114-19119.

Jouvenet, N., S.M. Simon, and P.D. Bieniasz. 2011. Visualizing HIV-1 assembly. *J Mol Biol*. 410:501-511.

Kamura, T., D. Burian, H. Khalili, S.L. Schmidt, S. Sato, W.J. Liu, M.N. Conrad, R.C. Conaway, J.W. Conaway, and A. Shilatifard. 2001. Cloning and characterization of ELL-associated proteins EAP45 and EAP20. a role for yeast EAP-like proteins in regulation of gene expression by glucose. *J Biol Chem*. 276:16528-16533.

Karn, J., and C.M. Stoltzfus. 2012. Transcriptional and posttranscriptional regulation of HIV-1 gene expression. *Cold Spring Harb Perspect Med*. 2:a006916.

Kerviel, A., A. Thomas, L. Chaloin, C. Favard, and D. Muriaux. 2013. Virus assembly and plasma membrane domains: which came first? *Virus Res*. 171:332-340.

Klatzmann, D., E. Champagne, S. Chamaret, J. Gruest, D. Guetard, T. Hercend, J.C. Gluckman, and L. Montagnier. 1984. T-lymphocyte T4 molecule behaves as the receptor for human retrovirus LAV. *Nature*. 312:767-768.

Klein, K.C., J.C. Reed, and J.R. Lingappa. 2007. Intracellular destinies: degradation, targeting, assembly, and endocytosis of HIV Gag. *AIDS Rev*. 9:150-161.

Kobayashi, T., U.M. Vischer, C. Rosnoblet, C. Lebrand, M. Lindsay, R.G. Parton, E.K. Kruithof, and J. Gruenberg. 2000. The tetraspanin CD63/lamp3 cycles between endocytic and secretory compartments in human endothelial cells. *Mol Biol Cell*. 11:1829-1843.

Koenig, S., H.E. Gendelman, J.M. Orenstein, M.C. Dal Canto, G.H. Pezeshkpour, M. Yungbluth, F. Janotta, A. Aksamit, M.A. Martin, and A.S. Fauci. 1986. Detection of AIDS virus in macrophages in brain tissue from AIDS patients with encephalopathy. *Science*. 233:1089-1093.

Konig, R., Y. Zhou, D. Elleder, T.L. Diamond, G.M. Bonamy, J.T. Irelan, C.Y. Chiang, B.P. Tu, P.D. De Jesus, C.E. Lilley, S. Seidel, A.M. Opaluch, J.S. Caldwell, M.D. Weitzman, K.L. Kuhen, S. Bandyopadhyay, T. Ideker, A.P. Orth, L.J. Miraglia, F.D. Bushman, J.A. Young, and S.K. Chanda. 2008. Global analysis of host-pathogen interactions that regulate early-stage HIV-1 replication. *Cell*. 135:49-60.

Konnyu, B., S.K. Sadiq, T. Turanyi, R. Hirmondo, B. Muller, H.G. Krausslich, P.V. Coveney, and V. Muller. 2013. Gag-Pol processing during HIV-1 virion maturation: a systems biology approach. *PLoS Comput Biol*. 9:e1003103.

Kopp, J.B., and C. Winkler. 2003. HIV-associated nephropathy in African Americans. *Kidney Int Suppl*:S43-49.

Koppensteiner, H., C. Banning, C. Schneider, H. Hohenberg, and M. Schindler. 2012a. Macrophage internal HIV-1 is protected from neutralizing antibodies. *J Virol*. 86:2826-2836.

Koppensteiner, H., R. Brack-Werner, and M. Schindler. 2012b. Macrophages and their relevance in Human Immunodeficiency Virus Type I infection. *Retrovirology*. 9:82.

Kotsopoulou, E., V.N. Kim, A.J. Kingsman, S.M. Kingsman, and K.A. Mitrophanous. 2000. A Rev-independent human immunodeficiency virus type 1 (HIV-1)-based vector that exploits a codon-optimized HIV-1 gag-pol gene. *J Virol*. 74:4839-4852.

Kretzschmar, M.E., M.F. Schim van der Loeff, P.J. Birrell, D. De Angelis, and R.A. Coutinho. 2013. Prospects of elimination of HIV with test-and-treat strategy. *Proc Natl Acad Sci U S A*. 110:15538-15543.

Kruth, H.S., S.I. Skarlatos, K. Lilly, J. Chang, and I. Ifrim. 1995. Sequestration of acetylated LDL and cholesterol crystals by human monocyte-derived macrophages. *J Cell Biol*. 129:133-145.

Ladinsky, M.S., C. Kieffer, G. Olson, M. Deruaz, V. Vrbanac, A.M. Tager, D.S. Kwon, and P.J. Bjorkman. 2014. Electron tomography of HIV-1 infection in gut-associated lymphoid tissue. *PLoS Pathog*. 10:e1003899.

Laguette, N., B. Sobhian, N. Casartelli, M. Ringeard, C. Chable-Bessia, E. Segeral, A. Yatim, S. Emiliani, O. Schwartz, and M. Benkirane. 2011. SAMHD1 is the dendritic- and myeloid-cell-specific HIV-1 restriction factor counteracted by Vpx. *Nature*. 474:654-657.

Lahouassa, H., W. Daddacha, H. Hofmann, D. Ayinde, E.C. Logue, L. Dragin, N. Bloch, C. Maudet, M. Bertrand, T. Gramberg, G. Pancino, S. Priet, B. Canard, N. Laguette, M. Benkirane, C. Transy, N.R. Landau, B. Kim, and F. Margottin-Goguet. 2012. SAMHD1 restricts the replication of human immunodeficiency

virus type 1 by depleting the intracellular pool of deoxynucleoside triphosphates. *Nat Immunol*. 13:223-228.

Larson, D.R., M.C. Johnson, W.W. Webb, and V.M. Vogt. 2005. Visualization of retrovirus budding with correlated light and electron microscopy. *Proc Natl Acad Sci U S A*. 102:15453-15458.

Lau, K.A., and J.J. Wong. 2013. Current Trends of HIV Recombination Worldwide. *Infect Dis Rep*. 5:e4.

Laughrea, M., and L. Jette. 1994. A 19-nucleotide sequence upstream of the 5' major splice donor is part of the dimerization domain of human immunodeficiency virus 1 genomic RNA. *Biochemistry*. 33:13464-13474.

Lawn, S.D., and S.T. Butera. 2000. Incorporation of HLA-DR into the envelope of human immunodeficiency virus type 1 in vivo: correlation with stage of disease and presence of opportunistic infection. *J Virol*. 74:10256-10259.

Lawn, S.D., B.D. Roberts, G.E. Griffin, T.M. Folks, and S.T. Butera. 2000. Cellular compartments of human immunodeficiency virus type 1 replication in vivo: determination by presence of virion-associated host proteins and impact of opportunistic infection. *J Virol*. 74:139-145.

Lee, S., A. Joshi, K. Nagashima, E.O. Freed, and J.H. Hurley. 2007. Structural basis for viral late-domain binding to Alix. *Nat Struct Mol Biol*. 14:194-199.

Lee, S.K., M. Potempa, M. Kolli, A. Ozen, C.A. Schiffer, and R. Swanstrom. 2012a. Context surrounding processing sites is crucial in determining cleavage rate of a subset of processing sites in HIV-1 Gag and Gag-Pro-Pol polyprotein precursors by viral protease. *J Biol Chem*. 287:13279-13290.

Lee, S.K., M. Potempa, and R. Swanstrom. 2012b. The choreography of HIV-1 proteolytic processing and virion assembly. *J Biol Chem*. 287:40867-40874.

Lin, N.H., L.M. Smeaton, F. Giguel, V. Novitsky, S. Moyo, R.M. Mitchell, J. Makhema, M. Essex, S. Lockman, and D.R. Kuritzkes. 2011. Prevalence and clinical associations of CXCR4-using HIV-1 among treatment-naive subtype C-infected women in Botswana. *J Acquir Immune Defic Syndr*. 57:46-50.

Lin, Y.S., Y.J. Chen, S.N. Cohen, and T.H. Cheng. 2013. Identification of TSG101 Functional Domains and p21 Loci Required for TSG101-Mediated p21 Gene Regulation. *PLoS One*. 8:e79674.

Lorizate, M., B. Brugger, H. Akiyama, B. Glass, B. Muller, G. Anderluh, F.T. Wieland, and H.G. Krausslich. 2009. Probing HIV-1 membrane liquid order by Laurdan staining reveals producer cell-dependent differences. *J Biol Chem*. 284:22238-22247.

Lu, K., X. Heng, and M.F. Summers. 2011. Structural determinants and mechanism of HIV-1 genome packaging. *J Mol Biol*. 410:609-633.

Maartens, G., C. Celum, and S.R. Lewin. 2014. HIV infection: epidemiology, pathogenesis, treatment, and prevention. *Lancet*. 384:258-271.

MacLeod, I.J., C.F. Rowley, I. Thior, C. Wester, J. Makhema, M. Essex, and S. Lockman. 2010. Minor resistant variants in nevirapine-exposed infants may predict virologic failure on nevirapine-containing ART. *J Clin Virol*. 48:162-167.

Maldonado, J.O., J.L. Martin, J.D. Mueller, W. Zhang, and L.M. Mansky. 2014. New insights into retroviral Gag-Gag and Gag-membrane interactions. *Front Microbiol*. 5:302.

Malim, M.H., and P.D. Bieniasz. 2012. HIV Restriction Factors and Mechanisms of Evasion. *Cold Spring Harb Perspect Med*. 2:a006940.

Mangasarian, A., V. Piguet, J.K. Wang, Y.L. Chen, and D. Trono. 1999. Nef-induced CD4 and major histocompatibility complex class I (MHC-I) down-regulation are governed by distinct determinants: N-terminal alpha helix and proline repeat of Nef selectively regulate MHC-I trafficking. *J Virol*. 73:1964-1973.

Mangeat, B., G. Gers-Huber, M. Lehmann, M. Zufferey, J. Luban, and V. Piguet. 2009. HIV-1 Vpu neutralizes the antiviral factor Tetherin/BST-2 by binding it and directing its beta-TrCP2-dependent degradation. *PLoS Pathog*. 5:e1000574.

Mariani, C., M. Desdouits, C. Favard, P. Benaroch, and D.M. Muriaux. 2014. Role of Gag and lipids during HIV-1 assembly in CD4(+) T cells and macrophages. *Front Microbiol*. 5:312.

Marsh, M., and A. Pelchen-Matthews. 2000. Endocytosis in viral replication. *Traffic*. 1:525-532.

Marsh, M., K. Theusner, and A. Pelchen-Matthews. 2009. HIV assembly and budding in macrophages. *Biochem Soc Trans*. 37:185-189.

Martin-Serrano, J. 2007. The role of ubiquitin in retroviral egress. *Traffic*. 8:1297-1303.

Martin-Serrano, J., and M. Marsh. 2007. ALIX catches HIV. *Cell Host Microbe*. 1:5-7.

Martin-Serrano, J., T. Zang, and P.D. Bieniasz. 2003. Role of ESCRT-I in retroviral budding. *J Virol*. 77:4794-4804.

Mazzolini, J., F. Herit, J. Bouchet, A. Benmerah, S. Benichou, and F. Niedergang. 2010. Inhibition of phagocytosis in HIV-1-infected macrophages relies on Nef-dependent alteration of focal delivery of recycling compartments. *Blood*. 115:4226-4236.

Meissner, E.G., K.M. Duus, F. Gao, X.F. Yu, and L. Su. 2004. Characterization of a thymus-tropic HIV-1 isolate from a rapid progressor: role of the envelope. *Virology*. 328:74-88.

Melikyan, G.B. 2008. Common principles and intermediates of viral protein-mediated fusion: the HIV-1 paradigm. *Retrovirology*. 5:111.

Mettlen, M., T. Pucadyil, R. Ramachandran, and S.L. Schmid. 2009. Dissecting dynamin's role in clathrin-mediated endocytosis. *Biochem Soc Trans*. 37:1022-1026.

Meyenhofer, M.F., L.G. Epstein, E.S. Cho, and L.R. Sharer. 1987. Ultrastructural morphology and intracellular production of human immunodeficiency virus (HIV) in brain. *J Neuropathol Exp Neurol*. 46:474-484.

Mlcochova, P., A. Pelchen-Matthews, and M. Marsh. 2013. Organization and regulation of intracellular plasma membrane-connected HIV-1 assembly compartments in macrophages. *BMC Biol*. 11:89.

Moore, J.P., A. Trkola, and T. Dragic. 1997. Co-receptors for HIV-1 entry. *Curr Opin Immunol*. 9:551-562.

Morita, E., V. Sandrin, J. McCullough, A. Katsuyama, I. Baci Hamilton, and W.I. Sundquist. 2011. ESCRT-III protein requirements for HIV-1 budding. *Cell Host Microbe*. 9:235-242.

Munshi, U.M., J. Kim, K. Nagashima, J.H. Hurley, and E.O. Freed. 2007. An Alix fragment potently inhibits HIV-1 budding: characterization of binding to retroviral YPXL late domains. *J Biol Chem*. 282:3847-3855.

Muranyi, W., S. Malkusch, B. Muller, M. Heilemann, and H.G. Krausslich. 2013. Super-resolution microscopy reveals specific recruitment of HIV-1 envelope proteins to viral assembly sites dependent on the envelope C-terminal tail. *PLoS Pathog*. 9:e1003198.

Nabhan, J.F., R. Hu, R.S. Oh, S.N. Cohen, and Q. Lu. 2012. Formation and release of arrestin domain-containing protein 1-mediated microvesicles (ARMMs) at plasma membrane by recruitment of TSG101 protein. *Proc Natl Acad Sci U S A*. 109:4146-4151.

NACA. 2010. Progress report of the national response to the 2001 declaration of commitment on HIV and AIDS. Botswana Country Report 2010. Period 2008-2009. http://www.unaids.org/en/dataanalysis/knowyourresponse/countryprogressreports/2010countries.

Ndung'u, T., E. Sepako, M.F. McLane, F. Chand, K. Bedi, S. Gaseitsiwe, F. Doualla-Bell, T. Peter, I. Thior, S.M. Moyo, P.B. Gilbert, V.A. Novitsky, and M. Essex. 2006. HIV-1 subtype C in vitro growth and coreceptor utilization. *Virology*. 347:247-260.

Ndung'u, T., and R.A. Weiss. 2012. On HIV diversity. *AIDS*. 26:1255-1260.

Neil, S.J., T. Zang, and P.D. Bieniasz. 2008. Tetherin inhibits retrovirus release and is antagonized by HIV-1 Vpu. *Nature*. 451:425-430.

Nguyen, K.L., M. llano, H. Akari, E. Miyagi, E.M. Poeschla, K. Strebel, and S. Bour. 2004. Codon optimization of the HIV-1 vpu and vif genes stabilizes their mRNA and allows for highly efficient Rev-independent expression. *Virology*. 319:163-175.

Novitsky, V., and M. Essex. 2012. Using HIV viral load to guide treatment-for-prevention interventions. *Curr Opin HIV AIDS*. 7:117-124.

Novitsky, V., S. Lagakos, M. Herzig, C. Bonney, L. Kebaabetswe, R. Rossenkhan, D. Nkwe, L. Margolin, R. Musonda, S. Moyo, E. Woldegabriel, E. van Widenfelt, J. Makhema, and M. Essex. 2009. Evolution of proviral gp120 over the first year of HIV-1 subtype C infection. *Virology*. 383:47-59.

Novitsky, V., R. Wang, H. Bussmann, S. Lockman, M. Baum, R. Shapiro, I. Thior, C. Wester, C.W. Wester, A. Ogwu, A. Asmelash, R. Musonda, A. Campa, S. Moyo, E. van Widenfelt, M. Mine, C. Moffat, M. Mmalane, J. Makhema, R. Marlink, P. Gilbert, G.R. Seage, 3rd, V. DeGruttola, and M. Essex. 2010a. HIV-1 subtype C-infected individuals maintaining high viral load as potential targets for the "test-and-treat" approach to reduce HIV transmission. *PLoS One*. 5:e10148.

Novitsky, V., R. Wang, S. Lagakos, and M. Essex. 2010b. HIV-1 Subtype C Phylodynamics in the Global Epidemic. *Viruses*. 2:33-54.

Novitsky, V., C.W. Wester, V. DeGruttola, H. Bussmann, S. Gaseitsiwe, A. Thomas, S. Moyo, R. Musonda, E. Van Widenfelt, R.G. Marlink, and M. Essex. 2007. The reverse transcriptase 67N 70R 215Y genotype is the predominant TAM pathway associated with virologic failure among HIV type 1C-infected adults treated with ZDV/ddI-containing HAART in southern Africa. *AIDS Res Hum Retroviruses*. 23:868-878.

O'Brien, S.J., and G.W. Nelson. 2004. Human genes that limit AIDS. *Nat Genet*. 36:565-574.

O'Doherty, U., W.J. Swiggard, and M.H. Malim. 2000. Human immunodeficiency virus type 1 spinoculation enhances infection through virus binding. *J Virol*. 74:10074-10080.

Ochsenbauer, C., T.G. Edmonds, H. Ding, B.F. Keele, J. Decker, M.G. Salazar, J.F. Salazar-Gonzalez, R. Shattock, B.F. Haynes, G.M. Shaw, B.H. Hahn, and J.C. Kappes. 2012. Generation of transmitted/founder HIV-1 infectious molecular clones and characterization of their replication capacity in CD4 T lymphocytes and monocyte-derived macrophages. *J Virol*. 86:2715-2728.

Ono, A., S.D. Ablan, S.J. Lockett, K. Nagashima, and E.O. Freed. 2004. Phosphatidylinositol (4,5) bisphosphate regulates HIV-1 Gag targeting to the plasma membrane. *Proc Natl Acad Sci U S A*. 101:14889-14894.

Orenstein, J.M. 2007. Replication of HIV-1 in vivo and in vitro. *Ultrastruct Pathol*. 31:151-167.

Orenstein, J.M., M.S. Meltzer, T. Phipps, and H.E. Gendelman. 1988. Cytoplasmic assembly and accumulation of human immunodeficiency virus types 1 and 2 in recombinant human colony-stimulating factor-1-treated human monocytes: an ultrastructural study. *J Virol*. 62:2578-2586.

Pallesen, J. 2011. Structure of the HIV-1 5' untranslated region dimer alone and in complex with gold nanocolloids: support of a TAR-TAR-containing 5' dimer linkage site (DLS) and a 3' DIS-DIS-containing DLS. *Biochemistry*. 50:6170-6177.

Peeters, M., M. D'Arc, and E. Delaporte. 2014. Origin and diversity of human retroviruses. *AIDS Rev*. 16:23-34.

Pehlivanova, V.N., I.H. Tsoneva, and R.D. Tzoneva. 2012. Multiple effects of electroporation on the adhesive behaviour of breast cancer cells and fibroblasts. *Cancer Cell Int*. 12:9.

Pelchen-Matthews, A., S. Giese, P. Mlcochova, J. Turner, and M. Marsh. 2012. beta2 integrin adhesion complexes maintain the integrity of HIV-1 assembly compartments in primary macrophages. *Traffic*. 13:273-291.

Pelchen-Matthews, A., B. Kramer, and M. Marsh. 2003. Infectious HIV-1 assembles in late endosomes in primary macrophages. *J Cell Biol*. 162:443-455.

Pelchen-Matthews, A., and M. Marsh. 2007. Electron microscopy analysis of viral morphogenesis. *Methods Cell Biol*. 79:515-542.

Perelson, A.S., A.U. Neumann, M. Markowitz, J.M. Leonard, and D.D. Ho. 1996. HIV-1 dynamics in vivo: virion clearance rate, infected cell life-span, and viral generation time. *Science*. 271:1582-1586.

Pettit, S.C., J.C. Clemente, J.A. Jeung, B.M. Dunn, and A.H. Kaplan. 2005. Ordered processing of the human immunodeficiency virus type 1 GagPol precursor is influenced by the context of the embedded viral protease. *J Virol*. 79:10601-10607.

Pettit, S.C., M.D. Moody, R.S. Wehbie, A.H. Kaplan, P.V. Nantermet, C.A. Klein, and R. Swanstrom. 1994. The p2 domain of human immunodeficiency virus type 1 Gag regulates sequential proteolytic processing and is required to produce fully infectious virions. *J Virol*. 68:8017-8027.

Pincetic, A., and J. Leis. 2009. The Mechanism of Budding of Retroviruses From Cell Membranes. *Adv Virol*. 2009:6239691-6239699.

Platt, E.J., K. Wehrly, S.E. Kuhmann, B. Chesebro, and D. Kabat. 1998. Effects of CCR5 and CD4 cell surface concentrations on infections by macrophagetropic isolates of human immunodeficiency virus type 1. *J Virol*. 72:2855-2864.

Pornillos, O., S.L. Alam, D.R. Davis, and W.I. Sundquist. 2002. Structure of the Tsg101 UEV domain in complex with the PTAP motif of the HIV-1 p6 protein. *Nat Struct Biol*. 9:812-817.

Pornillos, O., D.S. Higginson, K.M. Stray, R.D. Fisher, J.E. Garrus, M. Payne, G.P. He, H.E. Wang, S.G. Morham, and W.I. Sundquist. 2003. HIV Gag mimics the Tsg101-recruiting activity of the human Hrs protein. *J Cell Biol*. 162:425-434.

Raposo, G., M. Moore, D. Innes, R. Leijendekker, A. Leigh-Brown, P. Benaroch, and H. Geuze. 2002. Human macrophages accumulate HIV-1 particles in MHC II compartments. *Traffic*. 3:718-729.

Raymond, C.K., I. Howald-Stevenson, C.A. Vater, and T.H. Stevens. 1992. Morphological classification of the yeast vacuolar protein sorting mutants: evidence for a prevacuolar compartment in class E vps mutants. *Mol Biol Cell*. 3:1389-1402.

Regoes, R.R., and S. Bonhoeffer. 2005. The HIV coreceptor switch: a population dynamical perspective. *Trends Microbiol*. 13:269-277.

Renjifo, B., and M. Essex. 2002. HIV-1 Subtypes and recombinants. *In* AIDS in Africa. M. Essex, S. Mboup, P.J. Kanki, R.G. Marlink, and S.D. Tlou, editors. Kluwer Academic Publishers, Secaucus, NJ, USA. 263-281.

Roxrud, I., H. Stenmark, and L. Malerod. 2010. ESCRT & Co. *Biol Cell*. 102:293-318.

Roy, N.H., J. Chan, M. Lambele, and M. Thali. 2013. Clustering and mobility of HIV-1 Env at viral assembly sites predict its propensity to induce cell-cell fusion. *J Virol*. 87:7516-7525.

Ruiz-Mateos, E., A. Pelchen-Matthews, M. Deneka, and M. Marsh. 2008. CD63 is not required for production of infectious human immunodeficiency virus type 1 in human macrophages. *J Virol*. 82:4751-4761.

Saad, J.S., J. Miller, J. Tai, A. Kim, R.H. Ghanam, and M.F. Summers. 2006a. Structural basis for targeting HIV-1 Gag proteins to the plasma membrane for virus assembly. *Proc Natl Acad Sci U S A*. 103:11364-11369.

Saad, M.D., Q. Aliev, B.A. Botros, J.K. Carr, P.J. Gomatos, Y. Nadai, A.A. Michael, Z. Nasibov, J.L. Sanchez, D.I. Brix, and K.C. Earhart. 2006b. Genetic forms of HIV Type 1 in the former Soviet Union dominate the epidemic in Azerbaijan. *AIDS Res Hum Retroviruses*. 22:796-800.

Samson, M., F. Libert, B.J. Doranz, J. Rucker, C. Liesnard, C.M. Farber, S. Saragosti, C. Lapoumeroulie, J. Cognaux, C. Forceille, G. Muyldermans, C. Verhofstede, G. Burtonboy, M. Georges, T. Imai, S. Rana, Y. Yi, R.J. Smyth, R.G. Collman, R.W. Doms, G. Vassart, and M. Parmentier. 1996. Resistance to HIV-1 infection in caucasian individuals bearing mutant alleles of the CCR-5 chemokine receptor gene. *Nature*. 382:722-725.

Samson, R.Y., and S.D. Bell. 2009. Ancient ESCRTs and the evolution of binary fission. *Trends Microbiol*. 17:507-513.

Sauter, M.M., A. Pelchen-Matthews, R. Bron, M. Marsh, C.C. LaBranche, P.J. Vance, J. Romano, B.S. Haggarty, T.K. Hart, W.M. Lee, and J.A. Hoxie. 1996. An internalization signal in the simian immunodeficiency virus transmembrane protein cytoplasmic domain modulates expression of envelope glycoproteins on the cell surface. *J Cell Biol*. 132:795-811.

Schiffner, T., Q.J. Sattentau, and C.J. Duncan. 2013. Cell-to-cell spread of HIV-1 and evasion of neutralizing antibodies. *Vaccine*. 31:5789-5797.

Schmidt, O., and D. Teis. 2012. The ESCRT machinery. *Curr Biol*. 22:R116-120.

Schneider, R., M. Campbell, G. Nasioulas, B.K. Felber, and G.N. Pavlakis. 1997. Inactivation of the human immunodeficiency virus type 1 inhibitory elements allows Rev-independent expression of Gag and Gag/protease and particle formation. *J Virol*. 71:4892-4903.

Schroff, R.W., M.S. Gottlieb, H.E. Prince, L.L. Chai, and J.L. Fahey. 1983. Immunological studies of homosexual men with immunodeficiency and Kaposi's sarcoma. *Clin Immunol Immunopathol*. 27:300-314.

Schwartz, S., M. Campbell, G. Nasioulas, J. Harrison, B.K. Felber, and G.N. Pavlakis. 1992a. Mutational inactivation of an inhibitory sequence in human immunodeficiency virus type 1 results in Rev-independent gag expression. *J Virol*. 66:7176-7182.

Schwartz, S., B.K. Felber, and G.N. Pavlakis. 1992b. Distinct RNA sequences in the gag region of human immunodeficiency virus type 1 decrease RNA stability and inhibit expression in the absence of Rev protein. *J Virol*. 66:150-159.

Seif, E., M. Niu, and L. Kleiman. 2013. Annealing to sequences within the primer binding site loop promotes an HIV-1 RNA conformation favoring RNA dimerization and packaging. *RNA*. 19:1384-1393.

Sette, P., J.A. Jadwin, V. Dussupt, N.F. Bello, and F. Bouamr. 2010. The ESCRT-associated protein Alix recruits the ubiquitin ligase Nedd4-1 to facilitate HIV-1 release through the LYPXnL L domain motif. *J Virol*. 84:8181-8192.

Shimauchi, T., and V. Piguet. 2014. DC-T cell Virological Synapses and the Skin: Novel Perspectives in Dermatology. *Exp Dermatol*:doi: 10.1111/exd.12511.

Sidoti, A., R. D'Angelo, C. Rinaldi, G. De Luca, F. Pino, C. Salpietro, D.E. Giunta, F. Saltalamacchia, and A. Amato. 2005. Distribution of the mutated delta 32 allele of the CCR5 gene in a Sicilian population. *Int J Immunogenet*. 32:193-198.

Simon, V., and D.D. Ho. 2003. HIV-1 dynamics in vivo: implications for therapy. *Nat Rev Microbiol*. 1:181-190.

Skripkin, E., J.C. Paillart, R. Marquet, B. Ehresmann, and C. Ehresmann. 1994. Identification of the primary site of the human immunodeficiency virus type 1 RNA dimerization in vitro. *Proc Natl Acad Sci U S A*. 91:4945-4949.

Slagsvold, T., K. Pattni, L. Malerod, and H. Stenmark. 2006. Endosomal and non-endosomal functions of ESCRT proteins. *Trends Cell Biol*. 16:317-326.

Slot, J.W., and H.J. Geuze. 2007. Cryosectioning and immunolabeling. *Nat Protoc*. 2:2480-2491.

Stacey, K.J., I.L. Ross, and D.A. Hume. 1993. Electroporation and DNA-dependent cell death in murine macrophages. *Immunol Cell Biol*. 71 (Pt 2):75-85.

Stefani, F., L. Zhang, S. Taylor, J. Donovan, S. Rollinson, A. Doyotte, K. Brownhill, J. Bennion, S. Pickering-Brown, and P. Woodman. 2011. UBAP1 is a component of an endosome-specific ESCRT-I complex that is essential for MVB sorting. *Curr Biol*. 21:1245-1250.

Strack, B., A. Calistri, S. Craig, E. Popova, and H.G. Gottlinger. 2003. AIP1/ALIX is a binding partner for HIV-1 p6 and EIAV p9 functioning in virus budding. *Cell*. 114:689-699.

Stuchell, M.D., J.E. Garrus, B. Muller, K.M. Stray, S. Ghaffarian, R. McKinnon, H.G. Krausslich, S.G. Morham, and W.I. Sundquist. 2004. The human endosomal sorting complex required for transport (ESCRT-I) and its role in HIV-1 budding. *J Biol Chem*. 279:36059-36071.

Sundquist, W.I., and H.G. Krausslich. 2012. HIV-1 assembly, budding, and maturation. *Cold Spring Harb Perspect Med*. 2:a006924.

Tan, J., and Q.J. Sattentau. 2013. The HIV-1-containing macrophage compartment: a perfect cellular niche? *Trends Microbiol*. 21:405-412.

Tavassoli, A., Q. Lu, J. Gam, H. Pan, S.J. Benkovic, and S.N. Cohen. 2008. Inhibition of HIV budding by a genetically selected cyclic peptide targeting the Gag-TSG101 interaction. *ACS Chem Biol*. 3:757-764.

Tebit, D.M., and E.J. Arts. 2011. Tracking a century of global expansion and evolution of HIV to drive understanding and to combat disease. *Lancet Infect Dis*. 11:45-56.

Tedbury, P.R., and E.O. Freed. 2014. The role of matrix in HIV-1 envelope glycoprotein incorporation. *Trends Microbiol*. 22:372-378.

Teis, D., S. Saksena, B.L. Judson, and S.D. Emr. 2010. ESCRT-II coordinates the assembly of ESCRT-III filaments for cargo sorting and multivesicular body vesicle formation. *EMBO J*. 29:871-883.

Tourret, J., G. Deray, and C. Isnard-Bagnis. 2013. Tenofovir effect on the kidneys of HIV-infected patients: a double-edged sword? *J Am Soc Nephrol*. 24:1519-1527.

Tsunetsugu-Yokota, Y., and M. Muhsen. 2013. Development of human dendritic cells and their role in HIV infection: antiviral immunity versus HIV transmission. *Front Microbiol*. 4:178.

Turville, S.G., J.J. Santos, I. Frank, P.U. Cameron, J. Wilkinson, M. Miranda-Saksena, J. Dable, H. Stossel, N. Romani, M. Piatak, Jr., J.D. Lifson, M. Pope, and A.L. Cunningham. 2004. Immunodeficiency virus uptake, turnover, and 2-phase transfer in human dendritic cells. *Blood*. 103:2170-2179.

UNAIDS. 2014. The Gap Report, http://www.unaids.org/en/resources/documents/2014/name,97466,en.asp.

UNAIDS. December 2010. Global report : UNAIDS report on the global AIDS epidemic: 2010, Geneva, Switzerland.

UNAIDS. November 2013. Global report : UNAIDS report on the global AIDS epidemic: 2013. Joint United Nations Programme on HIV/AIDS, Geneva, Switzerland.

Usami, Y., S. Popov, and H.G. Gottlinger. 2007. Potent rescue of human immunodeficiency virus type 1 late domain mutants by ALIX/AIP1 depends on its CHMP4 binding site. *J Virol*. 81:6614-6622.

Van Engelenburg, S.B., G. Shtengel, P. Sengupta, K. Waki, M. Jarnik, S.D. Ablan, E.O. Freed, H.F. Hess, and J. Lippincott-Schwartz. 2014. Distribution of ESCRT machinery at HIV assembly sites reveals virus scaffolding of ESCRT subunits. *Science*. 343:653-656.

Venkatesh, S., and P.D. Bieniasz. 2013. Mechanism of HIV-1 virion entrapment by tetherin. *PLoS Pathog*. 9:e1003483.

Vlach, J., and J.S. Saad. 2013. Trio engagement via plasma membrane phospholipids and the myristoyl moiety governs HIV-1 matrix binding to bilayers. *Proc Natl Acad Sci U S A*. 110:3525-3530.

von Schwedler, U.K., M. Stuchell, B. Muller, D.M. Ward, H.Y. Chung, E. Morita, H.E. Wang, T. Davis, G.P. He, D.M. Cimbora, A. Scott, H.G. Krausslich, J. Kaplan, S.G. Morham, and W.I. Sundquist. 2003. The protein network of HIV budding. *Cell*. 114:701-713.

Votteler, J., E. Iavnilovitch, O. Fingrut, V. Shemesh, D. Taglicht, O. Erez, S. Sorgel, T. Walther, N. Bannert, U. Schubert, and Y. Reiss. 2009. Exploring the functional interaction between POSH and ALIX and the relevance to HIV-1 release. *BMC Biochem*. 10:12.

Votteler, J., and W.I. Sundquist. 2013. Virus budding and the ESCRT pathway. *Cell Host Microbe*. 14:232-241.

Wainberg, M.A. 2004. HIV-1 subtype distribution and the problem of drug resistance. *AIDS*. 18 Suppl 3:S63-68.

Waki, K., and E.O. Freed. 2010. Macrophages and Cell-Cell Spread of HIV-1. *Viruses*. 2:1603-1620.

Watanabe, S.M., M.H. Chen, M. Khan, L. Ehrlich, K.S. Kemal, B. Weiser, B. Shi, C. Chen, M. Powell, K. Anastos, H. Burger, and C.A. Carter. 2013. The S40 residue in HIV-1 Gag p6 impacts local and distal budding determinants, revealing additional late domain activities. *Retrovirology*. 10:143.

Watters, S.A., P. Mlcochova, and R.K. Gupta. 2013. Macrophages: the neglected barrier to eradication. *Curr Opin Infect Dis*. 26:561-566.

Watts, J.M., K.K. Dang, R.J. Gorelick, C.W. Leonard, J.W. Bess, Jr., R. Swanstrom, C.L. Burch, and K.M. Weeks. 2009. Architecture and secondary structure of an entire HIV-1 RNA genome. *Nature*. 460:711-716.

Wei, X., J.M. Decker, H. Liu, Z. Zhang, R.B. Arani, J.M. Kilby, M.S. Saag, X. Wu, G.M. Shaw, and J.C. Kappes. 2002. Emergence of resistant human immunodeficiency virus type 1 in patients receiving fusion inhibitor (T-20) monotherapy. *Antimicrob Agents Chemother*. 46:1896-1905.

Weiss, E.R., and H. Gottlinger. 2011. The role of cellular factors in promoting HIV budding. *J Mol Biol*. 410:525-533.

Welsch, S., F. Groot, H.G. Krausslich, O.T. Keppler, and Q.J. Sattentau. 2011. Architecture and regulation of the HIV-1 assembly and holding compartment in macrophages. *J Virol*. 85:7922-7927.

Welsch, S., O.T. Keppler, A. Habermann, I. Allespach, J. Krijnse-Locker, and H.G. Krausslich. 2007. HIV-1 buds predominantly at the plasma membrane of primary human macrophages. *PLoS Pathog*. 3:e36.

West, M.J. 2012. Introduction to stereology. *Cold Spring Harb Protoc*. 2012:top070623.

Wester, C.W., H. Bussmann, J. Koethe, C. Moffat, S. Vermund, M. Essex, and R.G. Marlink. 2009. Adult combination antiretroviral therapy in sub-Saharan Africa: lessons from Botswana and future challenges. *HIV Ther*. 3:501-526.

Wester, C.W., S.K. Eden, B.E. Shepherd, H. Bussmann, V. Novitsky, D.C. Samuels, S.L. Hendrickson, C.A. Winkler, S.J. O'Brien, M. Essex, R.T. D'Aquila, V. Degruttola, and R.G. Marlink. 2012. Risk factors for symptomatic hyperlactatemia and lactic acidosis among combination antiretroviral therapy-treated adults in botswana: results from a clinical trial. *AIDS research and human retroviruses*. 28:759-765.

Wester, C.W., A.M. Thomas, H. Bussmann, S. Moyo, J.M. Makhema, T. Gaolathe, V. Novitsky, M. Essex, V. deGruttola, and R.G. Marlink. 2010. Non-nucleoside reverse transcriptase inhibitor outcomes among combination antiretroviral therapy-treated adults in Botswana. *AIDS*. 24 Suppl 1:S27-36.

WHO. 2013. Consolidated guidelines on the use of antiretroviral drugs for treating and preventing HIV infection: Recommendations for a public health approach, Geneva, Switzerland.

Wilen, C.B., J.C. Tilton, and R.W. Doms. 2012. HIV: cell binding and entry. *Cold Spring Harb Perspect Med*. 2:a006866.

Wollert, T., D. Yang, X. Ren, H.H. Lee, Y.J. Im, and J.H. Hurley. 2009. The ESCRT machinery at a glance. *J Cell Sci*. 122:2163-2166.

Wu, L., and V.N. KewalRamani. 2006. Dendritic-cell interactions with HIV: infection and viral dissemination. *Nat Rev Immunol*. 6:859-868.

Yuan, X., X. Yu, T.H. Lee, and M. Essex. 1993. Mutations in the N-terminal region of human immunodeficiency virus type 1 matrix protein block intracellular transport of the Gag precursor. *J Virol*. 67:6387-6394.

Zhang, W.Y., P.M. Gaynor, and H.S. Kruth. 1997. Aggregated low density lipoprotein induces and enters surface-connected compartments of human monocyte-macrophages. Uptake occurs independently of the low density lipoprotein receptor. *J Biol Chem*. 272:31700-31706.

Zhou, W., L.J. Parent, J.W. Wills, and M.D. Resh. 1994. Identification of a membrane-binding domain within the amino-terminal region of human immunodeficiency virus type 1 Gag protein which interacts with acidic phospholipids. *J Virol*. 68:2556-2569.

8. Appendix

8.1 Analysis of Gag_{BaL} in different vector backgrounds

To test whether the lack of expression of the native Gag_{BaL} was due to the expression vector, I subcloned Gag_{BaL} from the pRK5 background into two alternative vectors, pcDNA3.1 and pcDNA3. The new constructs were tested in HEK 293T cells and analysed by WB. The pRK5Gag_{BaL} WT was used as a positive control for this experiment. Although the pRK5Gag_{BaL} was expressed efficiently, I could only see very weak bands of cell-associated Gag_{BaL} in pcDNA3.1 and pcDNA3; band intensities for the cell lysates were barely above background, even after over-exposure of the WB, and no bands were seen for the VLPs (Figure 7.1). Taken together, these data demonstrate that plasmid vector background does impact on the expression of native Gag_{BaL}, in addition to the AU content that makes Gag transcripts unstable.

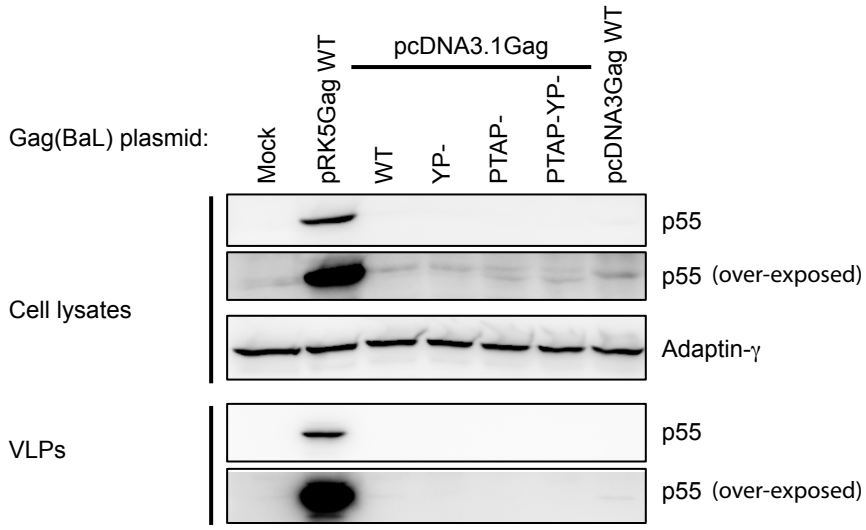

Figure 8.1: Biochemical analysis of Gag_{BaL} in different expression vectors.
HEK 293T cells were transfected with the indicated Gag_{BaL} plasmids, harbouring either WT or mutant Gag sequences. Transfected cells were incubated 24 hrs, harvested by pelleting VLPs through sucrose cushions and lysing cells in sample buffer. VLPs and cell lysates were analysed by WB. Membranes were incubated with anti-p24/55 or the loading control, adaptin-γ. Gag band signals for pCDNA3.1Gag and pCDNA3Gag were barely above background, after overexposing the WBs (Panels 2 and 5). Adaptin-γ was used as the loading control for the cell lysates.

8.2 Analysis of HIV-1 budding profiles in HEK 293T cells

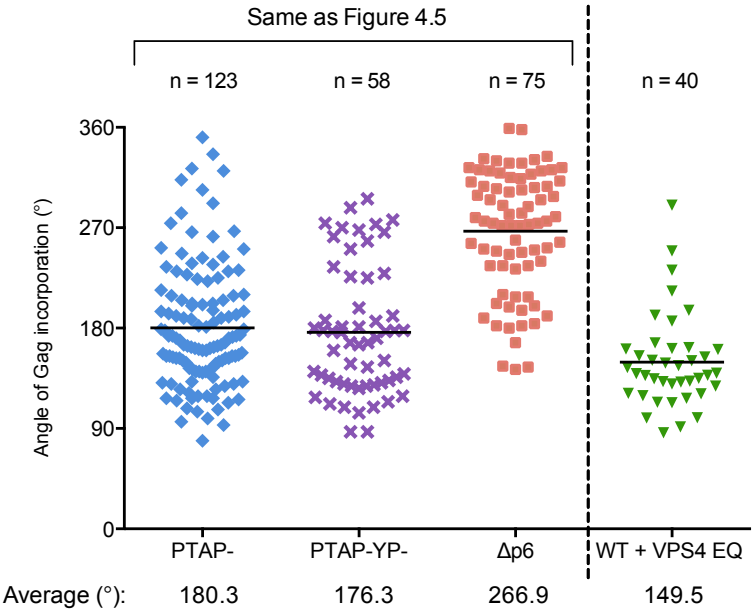

Figure 8.2: Comparison of budding profiles on HEK 293T cells.
The cells were transfected with the indicated HIV-1 R3A mutants or co-transfected with HIV-1 R3A WT and VPS4 EQ expression vectors. The average angles of Gag incorporation are shown below the graph.

The quantitative analysis of budding profiles for HIV-1 R3A mutants revealed that HIV-1 R3A PTAP^{-}YP^{-} and PTAP^{-} had shallower profiles compared to HIV-1 R3A Δp6 (Figure 4.5). As the dominant negative VPS4 EQ has been reported to disrupt virus release and produce arrested budding viruses (Garrus et al., 2001; von Schwedler et al., 2003), I wanted to examine the wild-type virus morphologies in the presence of VPS4 EQ, and compare them to morphologies for mutant viruses. To this end, HIV-1 R3A WT was co-expressed with GFP-VPS4 EQ in HEK 293T cells growing on gridded cover slips. Cells expressing GFP-VPS4 were located using light microscopy, and cover slip coordinates for the cells were recorded, so the same cells could be found at the electron microscope, and be assessed for HIV expression. Cells with the virus were imaged, and the morphologies of HIV-1 budding profiles were analysed as shown in Materials and Methods, Figure 2.7. These preliminary data show that, on average, budding profiles generated when HIV-1 R3A WT is co-expressed with VPS4 EQ are shallower than those for the mutants (PTAP^{-}YP^{-}, PTAP^{-}, Δp6) (Figure 7.2), suggesting that VPS4 may be involved early in the biogenesis of HIV particles.

8.3 Analysis of virus distribution in MDM: videos for IF data

Table 8.1: A list of videos on the enclosed CD.

The movies are on PowerPoint slides.

Video	Reference figures in Chapter 5	Description
1	5.1B	HIV-1 R3A WT virus in IPMC only
2	5.1E	HIV-1 R3A PTAP^{-}YP^{-} virus in IPMC only
3	5.2A	HIV-1 R3A WT virus in IPMC only
4	5.2B	HIV-1 R3A PTAP^{-}YP^{-} virus in IPMC only
5	5.2C	HIV-1 R3A PTAP^{-}YP^{-} virus on the cell surface
6	5.2D	HIV-1 R3A PTAP^{-}YP^{-} virus at the cell surface and IPMC
7-9	5.4	Using “3D Object Counter” to estimate fluorescence intensity